



Newcastle
University

Neuropathological and Molecular Studies in Alpers' Syndrome

Helen Judith Bogle B.Sc. (Hons)

A thesis submitted for the degree of Doctor of Philosophy

Wellcome Trust Centre for Mitochondrial Research

Institute for Ageing and Health

May 2014

Author's Declaration

This thesis is submitted to the degree of Doctor of Philosophy in the University of Newcastle. The research was performed in the Wellcome Trust Centre for Mitochondrial Research under the supervision of Professor D.M. Turnbull, Professor R.W. Taylor, and Dr R McFarland, and is my own work unless otherwise stated in the text.

I certify that none of the material offered in this thesis has been previously submitted by me for a degree or any other qualification at this or any other university.

Abstract

Mitochondrial disease is a significant burden on human health, at least 16.5 in 100,000 individuals are at risk of developing a mitochondrial DNA disorder (Schaefer et al., 2008). Early-onset mitochondrial disease affects young children and can have devastating consequences. One such disease, Alpers' syndrome, is a rare, autosomal recessive, early-onset neurological condition, which was first described in 1931 (Alpers 1931), characterised by refractory seizures, developmental delay, ataxia, visual abnormalities, and liver dysfunction and failure (Huttenlocher et al., 1976). It is primarily attributable to mutations in the gene *POLG* which encodes the only known polymerase to replicate mitochondrial DNA (Hance et al., 2005). *POLG* mutations lead to secondary defects of mitochondrial DNA (mtDNA), including deletion and depletion. There is a poor prognosis for patients diagnosed with Alpers' syndrome with no effective treatments currently available and little research into this rare condition.

The research presented here aims to understand the mechanisms leading to the neuropathological characteristics and clinical features in 12 patients with Alpers' syndrome and sex-/age-matched controls. Four brain areas were investigated; three areas frequently reported to show involvement in Alpers' syndrome and one area that is less frequently described. A battery of immunohistological stains and antibodies was used to assess the cohort. Neuropathological features identified and quantified included severe neuronal loss, widespread astrogliosis, reduced mitochondrial mass, white matter abnormalities, and microglial activation. The most severe neuropathology occurred in the posterior regions of the brain, yet all areas investigated exhibited pathology to different degrees. The expression of key respiratory chain proteins was quantified in neurons from different brain regions and revealed wide variation within and between individuals. There was a clear deficiency of complexes I and III in neurons, with a milder deficiency of complex IV. Assessment of mtDNA content in neurons revealed prominent mtDNA depletion, with a subset of neurons in older patients displaying high levels of mtDNA deletion.

This study shows clear evidence of respiratory chain deficiency of complexes I and III. This occurs most severely in the posterior region of the brain, correlating with more neuropathological changes in these regions. MtDNA depletion is a central feature of DNA damage in neurons likely driving the development of respiratory chain deficiency. These findings provide a clear insight into the mechanisms of respiratory chain deficiency leading to the neuropathology and clinical features in patients with Alpers' syndrome.

- Alpers, B. J. (1931). "Diffuse progressive degeneration of the gray matter of the cerebrum." Arch Neurol Psychiatry **25**: 469-505.
- Hance, N., M. I. Ekstrand and A. Trifunovic (2005). "Mitochondrial DNA polymerase gamma is essential for mammalian embryogenesis." Human Molecular Genetics **14**(13): 1775-1783.
- Huttenlocher, P. R., G. B. Solitare and G. Adams (1976). "Infantile diffuse cerebral degeneration with hepatic cirrhosis." Archives of Neurology **33**(3): 186-192.
- Schaefer, A. M., R. McFarland, E. L. Blakely, L. He, R. G. Whittaker, R. W. Taylor, P. F. Chinnery and D. M. Turnbull (2008). "Prevalence of mitochondrial DNA disease in adults." Annals of Neurology **63**(1): 35-39.

Acknowledgments

First and foremost, I would like to thank the patients involved in this study and their families. The generosity shown by the families in being a part of this study is greatly valued.

I would like to thank the project's sponsors: The Ryan Stanford Appeal and The Sir James Knott Trust. The Ryan Stanford Appeal has been an inspiration, in their optimism and in determination. Anne and Dave Stanford have worked tirelessly to ensure this project went ahead and maintain its funding, and without Ryan Stanford, none of this would have been possible in the first place.

I would like to thank everyone in the MRG for their help and advice and thank the NBTR for their help with samples and techniques. I would particularly like to thank my supervisors for all their support, encouragement and advice throughout this project, and thank Dr Evelyn Jaros for all her help with examining the slides and pathology discussions. A special 'thank you' goes to Dr Nichola Lax for all her support throughout this project, from beginning to end. She showed me incredible patience and practical help whenever it was needed, and I am extremely grateful. Being a part of the MRG has given me a lot of support and guidance, and the best thing about working with a group of scientists who love to bake – there is always a lot of cake!

Finally, I need to say a huge thank you to all my friends and family, who have shown me so much support and patience over the last three years. My mum and dad have been there at every step, supported me through the write-up period, and somehow been persuaded to proofread drafts of chapters as well. I am very grateful for their love and support. I cannot thank all my friends enough for the endless cups of coffee and for making me laugh through the tough times.

Table of Contents

Author's Declaration	i
Abstract.....	ii
Acknowledgments	iii
Table of Contents.....	iv
List of Figures	xii
List of Tables.....	xvi
Courses and Conferences Attended.....	xix
Publications.....	xx
Abbreviations	xxi
Chapter 1 Introduction	1
Mitochondria	1
1.1 Mitochondrial Structure	1
1.2 Mitochondrial Dynamics	4
1.2.1 Mitochondrial Fission and Fusion	4
1.2.1.1 Fission	4
1.2.1.2 Fusion.....	4
1.2.2 Mitochondrial Transport	6
1.3 Mitochondrial Function	7
1.3.1 Aerobic Respiration.....	7
1.3.1.1 Glycolysis	7
1.3.1.2 The Citric Acid Cycle.....	7
1.3.2 Oxidative Phosphorylation.....	8
1.3.2.1 The Electron Transport Chain	8
1.3.2.1.1 Complex I - NADH: Ubiquinone Oxidoreductase	11
1.3.2.1.2 Complex II - Succinate: Ubiquinone Oxidoreductase.....	13
1.3.2.1.3 Complex III - Ubiquinol Cytochrome c Reductase.....	14
1.3.2.1.4 Complex IV - Cytochrome c Oxidase.....	15
1.3.2.2 Complex V – ATP Synthase.....	16
1.3.2.3 Supercomplexes	18
1.3.3 Apoptosis	18
1.3.4 Reactive Oxygen Species	19

1.3.5	Calcium Dynamics	20
1.4	The Mitochondrial Genome	21
1.4.1	Mitochondrial DNA Replication.....	23
1.4.1.1	The 'Asynchronous Strand Displacement' Model	23
1.4.1.2	The 'Strand-Coupled Bidirectional Replication' Model.....	24
1.4.1.3	The 'RNA Incorporated Throughout the Lagging Strand (RITOLS)' Model	24
1.4.2	Transcription	25
1.4.3	Translation	26
1.5	Mitochondrial Genetics.....	27
1.5.1	Mitochondrial Inheritance	27
1.5.2	Heteroplasmy and the Threshold Effect	27
1.5.3	Clonal Expansion	30
1.5.4	Mitochondrial DNA Mutation Rates	31
1.5.5	Mitochondrial DNA Mutations.....	31
1.5.5.1	Point Mutations	32
1.5.5.2	Rearrangements	33
1.5.5.2.1	Duplications.....	33
1.5.5.2.2	MtDNA Deletions.....	33
1.5.5.3	MtDNA Depletion	34
1.6	Mitochondrial Disease.....	35
1.6.1	Mitochondrial Disease Prevalence	35
1.6.2	Mitochondrial Disease due to Nuclear Gene Mutations	35
1.6.2.1	Leigh Syndrome.....	36
1.6.2.2	Mitochondrial Neurogastrointestinal Encephalomyopathy (MNGIE)	36
1.6.3	Mitochondrial Disease due to Mitochondrial Gene Mutations	37
1.6.3.1	Mitochondrial Encephalomyopathy, Lactic Acidosis, and Stroke-Like Episodes (MELAS)	37
1.6.3.2	Myoclonic Epilepsy with Ragged Red Fibres (MERRF).....	37
1.6.3.3	Leber's Hereditary Optic Neuropathy (LHON).....	38
1.6.3.4	Maternally Inherited Leigh Syndrome.....	38
1.6.4	Complex Genetic Inheritance	39
1.6.4.1	Chronic Progressive External Ophthalmoplegia (cPEO)	39
1.7	Mitochondrial DNA Polymerase Gamma (POLG).....	40
1.7.1	Structure of POLG Polymerase.....	40
1.7.2	Functions of POLG	43

1.7.3	POLG Mutation Frequency.....	43
1.7.4	POLG Disorders.....	46
1.8	POLG Mouse Models.....	49
1.9	Alpers' Syndrome.....	51
1.9.1	Alternative Terms.....	52
1.9.2	Involvement of POLG in Alpers' Syndrome	53
1.9.2.1	Phenotype and Genotype	53
1.9.2.2	Common Mutations.....	54
1.9.2.2.1	p.Ala467Thr Mutation	56
1.9.2.2.2	p.Trp748Ser Mutation.....	56
1.9.2.2.3	p.Gly848Ser Mutation.....	57
1.9.3	Involvement of non-POLG genes in Alpers' Syndrome.....	57
1.9.4	Cells of the Central Nervous System.....	57
1.9.5	Affected Tissues	58
1.9.5.1	Central Nervous System Involvement.....	59
1.9.5.2	Neuropathology	59
1.9.5.3	Liver Involvement.....	61
1.9.5.4	Use of Sodium Valproate	61
1.9.6	Therapy.....	62
1.9.6.1	Anticonvulsant Drugs	62
1.9.6.2	Ketogenic Diet	62
1.9.6.3	Magnesium Therapy	63
1.9.6.4	Surgical Therapy.....	63
1.10	Aims of the Study.....	64
Chapter 2	Materials and Methods.....	65
2.1	Materials	65
2.1.1	Solutions	65
2.1.2	Chemicals	67
2.1.2.1	Histological Reagents	67
2.1.2.2	Polymerase Chain Reaction.....	69
2.1.2.3	Gel Electrophoresis.....	69
2.1.2.4	Sequencing and Pyrosequencing.....	70
2.1.3	Consumables	70
2.1.4	Equipment.....	71
2.2	Methods	73

2.2.1	Patient and Control Cohort.....	73
2.2.1.1	Patient 1	73
2.2.1.2	Patient 2	74
2.2.1.3	Patient 3	75
2.2.1.4	Patient 4	75
2.2.1.5	Patient 5	76
2.2.1.6	Patient 6	76
2.2.1.7	Patient 7	77
2.2.1.8	Patient 8	77
2.2.1.9	Patient 9	77
2.2.1.10	Patient 10	78
2.2.1.11	Patient 11	78
2.2.1.12	Patient 12	79
2.2.2	Definition of Alpers' Syndrome	80
2.2.3	Tissue Preparation	86
2.2.4	Neurohistopathological Methods in Staining FFPE Tissue	87
2.2.4.1	Rehydration of FFPE Tissue	87
2.2.4.2	Haematoxylin and Eosin Stain	87
2.2.4.3	Cresyl Fast Violet Stain.....	87
2.2.4.4	Loyez Silver Stain	88
2.2.4.5	Bielschowsky Silver Stain	88
2.2.5	Antibody Staining in FFPE Tissue.....	89
2.2.5.1	Respiratory Chain Antibody Staining.....	90
2.2.5.1.1	Complex I.....	91
2.2.5.1.2	Complex II.....	91
2.2.5.1.3	Complex III.....	91
2.2.5.1.4	Complex IV	91
2.2.6	Quantitative Methods	92
2.2.6.1	Neuronal Cell Counting.....	92
2.2.7	Semi-quantitative Methods.....	94
2.2.7.1	Myelin Quantification.....	94
2.2.7.2	Neuronal Cell Loss Quantification	94
2.2.7.3	Astrogliosis Quantification.....	94
2.2.7.4	Microglial Activation Quantification.....	95
2.2.8	Sequential COX/SDH Staining in Frozen Tissue.....	95

2.2.8.1 Single Cell Isolation	96
2.2.9 Real-time PCR	96
2.2.10 Pyrosequencing PCR	97
2.2.11 DNA Sequencing	97
2.2.11.1 DNA Extraction	97
2.2.11.2 POLG Pyrosequencing	98
2.2.11.3 POLG Sequencing	100
2.2.12 Electron Microscopy	100
Chapter 3 Neuropathological Features of Patients with Alpers' Syndrome	101
3.1 Introduction	101
3.2 Aims	103
3.3 Methodological Approach	103
3.4 Results	105
3.4.1 Molecular Investigations of POLG	105
3.4.2 Patient Characteristics	108
3.4.3 Morphological Assessment of Tissue	108
3.4.3.1 Cerebellum	108
3.4.3.2 Occipital Lobe	112
3.4.3.3 Parietal Lobe	115
3.4.3.4 Basal Ganglia	118
3.4.4 Neuron Loss	121
3.4.4.1 Cerebellum	122
3.4.4.2 Occipital Lobe	129
3.4.4.3 Parietal Lobe	133
3.4.4.4 Basal Ganglia	137
3.4.5 Astrogliosis	140
3.4.5.1 Cerebellum	140
3.4.5.2 Occipital Lobe	143
3.4.5.3 Parietal Lobe	146
3.4.5.4 Basal Ganglia	149
3.4.6 Mitochondrial Localisation in Neurons	152
3.4.7 White Matter Abnormalities	157
3.4.8 Microglial Activation	162
3.5 Electron Microscopy	166
3.6 Discussion	171

3.6.1	Patient Variability	171
3.6.1.1	Patient 1	171
3.6.1.2	Patient 2	172
3.6.1.3	Patient 6	173
3.6.1.4	Stillbirth Patient 5.....	173
3.6.1.5	Patient 12	174
3.6.2	Within-group Variation.....	175
3.6.3	Inter-group Variation	176
3.6.4	The Project's Findings in the Context of the Literature	177
3.6.4.1	Areas of Pathology	177
3.6.4.2	Neuron Loss	178
3.6.4.3	Astrogliosis	179
3.6.4.4	Mitochondrial Localisation	179
3.6.4.5	White Matter Abnormalities.....	180
3.6.4.6	Microglial Activation.....	180
3.6.4.7	Electron Microscopy	181
3.6.5	Novel Findings	182
3.7	Future Work	183
Chapter 4	Respiratory Chain Deficiency in Patients with Alpers' Syndrome.....	184
4.1	Introduction	184
4.2	Aims.....	185
4.3	Methodological Approach.....	186
4.4	Results.....	187
4.4.1	Staining Quantification	187
4.4.2	Cerebellum	189
4.4.2.1	Purkinje Cells	189
4.4.2.1.1	Complex I – NADH: Ubiquinone Oxidoreductase	189
4.4.2.1.2	Complex II – Succinate: Ubiquinone Oxidoreductase.....	193
4.4.2.1.3	Complex III – Ubiquinol Cytochrome c Reductase.....	196
4.4.2.1.4	Complex IV – Cytochrome c Oxidase.....	199
4.4.2.2	Dentate Nucleus.....	203
4.4.2.2.1	Complex I – NADH: Ubiquinone Oxidoreductase	203
4.4.2.2.2	Complex II – Succinate: Ubiquinone Oxidoreductase.....	206
4.4.2.2.3	Complex III – Ubiquinol Cytochrome c Reductase.....	208
4.4.2.2.4	Complex IV – Cytochrome c Oxidase.....	211

4.4.3	Occipital Lobe	216
4.4.3.1	Pyramidal Neurons of Layer V	216
4.4.3.1.1	Complex I – NADH: Ubiquinone Oxidoreductase	216
4.4.3.1.2	Complex II – Succinate: Ubiquinone Oxidoreductase	219
4.4.3.1.3	Complex III – Ubiquinol Cytochrome c Reductase	221
4.4.3.1.4	Complex IV – Cytochrome c Oxidase	224
4.4.4	Parietal Lobe	229
4.4.4.1	Pyramidal Neurons of Layer V	229
4.4.4.1.1	Complex I – NADH: Ubiquinone Oxidoreductase	229
4.4.4.1.2	Complex II – Succinate: Ubiquinone Oxidoreductase	232
4.4.4.1.3	Complex III – Ubiquinol Cytochrome c Reductase	235
4.4.4.1.4	Complex IV – Cytochrome c Oxidase	238
4.4.5	Basal Ganglia	243
4.4.5.1	Caudate, Putamen, and Globus Pallidus	243
4.4.5.1.1	Complex I – NADH: Ubiquinone Oxidoreductase	243
4.4.5.1.2	Complex II – Succinate: Ubiquinone Oxidoreductase	246
4.4.5.1.3	Complex III – Ubiquinol Cytochrome c Reductase	249
4.4.5.1.4	Complex IV – Cytochrome c Oxidase	252
4.4.6	Respiratory Chain Deficiency in Glial Cells	260
4.4.6.1	Patient 2	260
4.4.6.2	Patient 6	262
4.5	Discussion	264
4.5.1	Respiratory Chain Deficiency In Relation to Neuropathology	264
4.5.2	Respiratory Chain Deficiency in Neurons	265
4.5.2.1	Complex I	265
4.5.2.2	Complex II	266
4.5.2.3	Complex III	267
4.5.2.4	Complex IV	267
4.5.2.5	Patient Variability	268
4.5.2.6	Within-group Variation	269
4.5.2.7	Inter-group Variation	269
4.5.3	Respiratory Chain Deficiency in Glial Cells	270
4.5.4	The Project's Findings in the Context of the Literature	271
4.5.5	Novel Findings	277
4.6	Future Work	278

Chapter 5	Mitochondrial DNA Deletion and Depletion in Alpers' Syndrome	279
5.1	Introduction	279
5.2	Aims	280
5.3	Methodological Approach	280
5.3.1	Patients and Controls	280
5.3.2	SDH Histochemistry	281
5.3.3	Real-time PCR	281
5.3.4	Statistical Testing	282
5.4	Results	282
5.4.1	Mitochondrial DNA Deletion	282
5.4.1.1	Young Adult Patients – Single Histochemistry	282
5.4.1.2	Young Adult Patients – Sequential Histochemistry	285
5.4.1.3	Young Child Patient	288
5.4.2	Mitochondrial DNA Depletion	289
5.4.2.1	Young Adult Patients	289
5.4.2.2	Young Child Patient	294
5.5	Discussion	297
5.5.1	Inter-group Variation	297
5.5.2	COX-Positive and COX-Deficient Neurons	298
5.5.3	The Project's Findings in the Context of the Literature	298
5.5.4	Novel Findings	300
5.6	Future Work	301
Chapter 6	Final Discussion	302
6.1	Introduction	302
6.2	Major Findings	303
6.2.1	Neuropathological Features	303
6.2.2	Respiratory Chain Deficiency	304
6.2.4	MtDNA Deletion and Depletion	306
6.3	Strengths and Limitations	306
6.5	Future Work	308
6.6	Conclusions	309
References	310

List of Figures

Figure 1.1. The structure of a mitochondrion.	3
Figure 1.2. Mitochondrial fission and fusion.....	5
Figure 1.3. The mitochondrial respiratory chain.....	10
Figure 1.4. Image of the respiratory chain complex I.....	12
Figure 1.5. Image of the respiratory chain complex II.....	13
Figure 1.6. Image of the respiratory chain complex III.....	14
Figure 1.7. Image of the respiratory chain complex IV.....	15
Figure 1.8. Image of complex V (ATP synthase).....	17
Figure 1.9. The mitochondrial genome.....	22
Figure 1.10. Homoplasmy and heteroplasmy.....	29
Figure 1.11. Structure of POLG.....	42
Figure 1.12. Mutations in POLG.....	45
Figure 1.13. Mutations in POLG leading to Alpers' syndrome.....	55
Figure 1.14. MRI images (T2-FLAIR) showing occipital lobe and thalamic lesions during disease progression.....	60
Figure 2.1. Reference spaces for quantification of neuronal cells.....	93
Figure 3.1. Image of an agarose gel showing no amplification of <i>POLG</i> exons.....	106
Figure 3.2. Neurodegenerative abnormalities in the cerebellum.....	110
Figure 3.3. Microvacuolation in the occipital lobe.....	113
Figure 3.4. Microvacuolation in the parietal lobe.....	116
Figure 3.5. Microvacuolation in the caudate of the basal ganglia.....	119
Figure 3.6. Neuron loss in the cerebellum.....	124
Figure 3.7. Average number of Purkinje cells per length of cell layer (mm) in the cerebellum of patients and controls.....	125
Figure 3.8. Average number of Purkinje cells per length of cell layer (mm) in the cerebellum of a stillbirth and a fetal control.....	126
Figure 3.9. Neuron loss in the occipital lobe.....	130
Figure 3.10. Neuron loss in the occipital lobe of patients and controls.....	132
Figure 3.11. Neuron loss in the parietal lobe.....	134
Figure 3.12. Neuron loss in the parietal lobe of patients and controls.....	136
Figure 3.13. Neuron loss in the putamen of the basal ganglia.....	138
Figure 3.14. Bergmann glia of the cerebellum.....	141
Figure 3.15. Astrogliosis in the occipital lobe.....	144
Figure 3.16. Astrogliosis in the parietal lobe.....	147
Figure 3.17. Astrogliosis in the basal ganglia.....	150

Figure 3.18. Mitochondrial localisation.	154
Figure 3.19. Myelin abnormalities.....	159
Figure 3.20. Microglial activation.	164
Figure 3.21. TEM images of formalin-fixed tissue taken at 2600X.	167
Figure 3.22. TEM images of formalin-fixed tissue taken at 19,000X.	168
Figure 3.23. TEM images of formalin-fixed tissue taken at 34,000X.	169
Figure 4.1. Semi-quantitative scale of antibody staining in neurons.....	188
Figure 4.2. Staining with antibodies for complex I in the Purkinje cells of the cerebellum.	191
Figure 4.3. Staining with antibodies for complex II in the Purkinje cells of the cerebellum.	194
Figure 4.4. Staining with antibodies for complex III Rieske subunit in the Purkinje cells of the cerebellum.....	197
Figure 4.5. Staining with antibodies for complex IV subunit I in Purkinje cells of the cerebellum.	200
Figure 4.6. Staining with antibodies for complex IV subunit IV in Purkinje cells of the cerebellum.	201
Figure 4.7. Staining with antibodies for complex I in neurons of the dentate nucleus in the cerebellum.....	204
Figure 4.8. Staining with antibodies for complex II in neurons of the dentate nucleus in the cerebellum.....	207
Figure 4.9. Staining with antibodies for complex III Rieske subunit in neurons of the dentate nucleus in the cerebellum.....	209
Figure 4.10. Staining with antibodies for complex IV subunit I in neurons of the dentate nucleus in the cerebellum.....	212
Figure 4.11. Staining with antibodies for complex IV subunit IV in neurons of the dentate nucleus in the cerebellum.....	213
Figure 4.12. Staining with antibodies for complex I in the pyramidal neurons of the occipital lobe.	217
Figure 4.13. Staining with antibodies for complex II in the pyramidal neurons of the occipital lobe.	220
Figure 4.14. Staining with antibodies for complex III Rieske subunit in the pyramidal neurons of the occipital lobe.....	222
Figure 4.15. Staining with antibodies for complex IV subunit I in pyramidal neurons of the occipital lobe.	225

Figure 4.16. Staining with antibodies for complex IV subunit IV in pyramidal neurons of the occipital lobe.	226
Figure 4.17. Staining with antibodies for complex I in the pyramidal neurons of the parietal lobe.	230
Figure 4.18. Staining with antibodies for complex II in the pyramidal neurons of the parietal lobe.	233
Figure 4.19. Staining with antibodies for complex III Rieske subunit in the pyramidal neurons of the parietal lobe.	236
Figure 4.20. Staining with antibodies for complex IV subunit I in pyramidal neurons of the parietal lobe.	239
Figure 4.21. Staining with antibodies for complex IV subunit IV in pyramidal neurons of the parietal lobe.	240
Figure 4.22. Staining with antibodies for complex I in neurons of the basal ganglia.	244
Figure 4.23. Staining with antibodies for complex II in neurons of the basal ganglia.	247
Figure 4.24. Staining with antibodies for complex III Rieske subunit in neurons of the basal ganglia.	250
Figure 4.25. Staining with antibodies for complex IV subunit I in neurons of the basal ganglia.	253
Figure 4.26. Staining with antibodies for complex IV subunit IV in neurons of the basal ganglia.	254
Figure 4.27. Respiratory chain deficiency within glial cells in the parietal lobe of Patient 2.	261
Figure 4.28. Respiratory chain deficiency within glial cells in the parietal lobe of Patient 6.	263
Figure 5.1. <i>MT-ND4</i> deletions in frontal lobe of Patient 3 and Controls 3 and 4.	283
Figure 5.2. <i>MT-ND4</i> deletions in Patient 4 and Controls 3 and 4.	284
Figure 5.3. <i>MT-ND4</i> deletions in Patient 4 taken from slides with sequential COX/SDH histochemistry.	286
Figure 5.4. <i>MT-ND4</i> deletions in Patient 4 taken from slides with sequential COX/SDH histochemistry from the basal ganglia.	287
Figure 5.5. <i>MT-ND4</i> deletions in Patient 12 and Control 9.	288
Figure 5.6. MtDNA copy number in frontal lobe of Patient 3 and Controls 3 and 4.	290
Figure 5.7. MtDNA copy number in parietal lobe of Patient 4 and Controls 3 and 4.	291
Figure 5.8. MtDNA copy number in frontal lobe of Patient 4 and Controls 3 and 4.	292
Figure 5.9. MtDNA copy number in temporal lobe of Patient 4 and Controls 3 and 4.	293
Figure 5.10. MtDNA copy number in occipital lobe Patient 12 and Control 9.	294

Figure 5.11. MtDNA copy number in parietal lobe Patient 12 and Control 9.295
Figure 5.12. MtDNA copy number in the putamen of the basal ganglia from Patient 12
and Control 9.296

List of Tables

Table 1.1. Table of the nuclear and mitochondrial location of genes coding for subunits of the mitochondrial respiratory chain in humans.....	9
Table 1.2. Disorders arising from POLG mutations.	48
Table 2.1. Clinical details for the patients.	83
Table 2.2. Neuropathological details of the patients and controls used in this study....	85
Table 2.3. Antibodies used for immunohistochemistry in FFPE brain tissue.	89
Table 2.4. Antibodies used to visualise mitochondrial respiratory chain proteins, using immunohistochemistry, in FFPE brain tissue.....	90
Table 2.5. Primer sequences used for <i>MT-ND1</i> and <i>MT-ND4</i> in real-time PCR.....	96
Table 2.6. Primer sequences used to amplify DNA mutation regions from the gene <i>POLG</i> for pyrosequencing.	99
Table 2.7. Primer sequences used to amplify exons from the gene <i>POLG</i> containing the mutation, for pyrosequencing.	99
Table 3.1. Details of the patients used in the study of neuropathological features.	104
Table 3.2. A list of <i>POLG</i> mutations sequenced in Patient 12 and in the sibling of Patient 5.....	107
Table 3.3. Summary of neuropathology in the cerebellum.....	111
Table 3.4. Summary of neuropathology in the occipital lobe.....	114
Table 3.5. Summary of neuropathology in the parietal lobe.....	117
Table 3.6. Summary of neuropathology in the basal ganglia.	120
Table 3.7. Calculation of Purkinje cell loss in the cerebellum.....	127
Table 3.8. Summary of neuron loss in the cerebellum.....	128
Table 3.9. Summary of neuron loss in the occipital lobe.....	131
Table 3.10. Summary of neuron loss in the parietal lobe.	135
Table 3.11. Summary of neuron loss in the basal ganglia.	139
Table 3.12. Summary of Bergmann glia of the cerebellum.	142
Table 3.13. Summary of astrogliosis in the occipital lobe.	145
Table 3.14. Summary of astrogliosis in the parietal lobe.....	148
Table 3.15. Summary of astrogliosis in basal ganglia.	151
Table 3.16. Summary of mitochondrial density and localisation in the cerebellum.....	155
Table 3.17. Summary of mitochondrial density and localisation in the occipital lobe, parietal lobe, and basal ganglia.....	156
Table 3.18. Myelin quantification in the cerebellum.	160
Table 3.19. Myelin quantification in the occipital lobe, parietal lobe, and basal ganglia.	161

Table 3.20. Summary of microglial activation.	165
Table 3.21. Summary of EM structure counts in patient and controls.	170
Table 4.1. Details of the patients used in the study of respiratory chain deficiency.	186
Table 4.2. Table of complex I deficiency in Purkinje cells of the cerebellum.	192
Table 4.3. Table of complex II deficiency in Purkinje cells of the cerebellum.	195
Table 4.4. Table of complex III deficiency in Purkinje cells of the cerebellum.	198
Table 4.5. Table of complex IV deficiency in Purkinje cells of the cerebellum.	202
Table 4.6. Table of complex I deficiency in neurons of the dentate nucleus in the cerebellum.	205
Table 4.7. Table of complex III deficiency in neurons of the dentate nucleus in the cerebellum.	210
Table 4.8. Table of complex IV deficiency in neurons of the dentate nucleus in the cerebellum.	214
Table 4.9. Summary of respiratory chain deficiency in the cerebellum.	215
Table 4.10. Table of complex I deficiency in the pyramidal neurons of the occipital lobe.	218
Table 4.11. Table of complex III deficiency in the pyramidal neurons of the occipital lobe.	223
Table 4.12. Table of complex IV deficiency in the pyramidal neurons of the occipital lobe.	227
Table 4.13. Summary of respiratory chain deficiency in the occipital lobe.	228
Table 4.14. Table of complex I deficiency in the pyramidal neurons of the parietal lobe.	231
Table 4.15. Table of complex II deficiency in the pyramidal neurons of the parietal lobe.	234
Table 4.16. Table of complex III deficiency in the pyramidal neurons of the parietal lobe.	237
Table 4.17. Table of complex IV deficiency in the pyramidal neurons of the parietal lobe.	241
Table 4.18. Summary of respiratory chain deficiency in the parietal lobe.	242
Table 4.19. Table of complex I deficiency in the basal ganglia.	245
Table 4.20. Table of complex II deficiency in the basal ganglia.	248
Table 4.21. Table of complex III deficiency in the basal ganglia.	251
Table 4.22. Table of complex IV deficiency in the basal ganglia.	255
Table 4.23. Summary of respiratory chain deficiency in the basal ganglia.	256
Table 4.24. Summary of respiratory chain deficiency in all brain areas.	258

Table 4.25. Published studies of respiratory chain investigations in patients with Alpers' syndrome.....275

Table 5.1. Details of the patients and controls used in the study of mtDNA abnormalities.....280

Courses and Conferences Attended

November 2010 North East Postgraduate Conference, Newcastle University

January 2011 British Neuropathological Society, Institute of Child Health, University College London

July 2011 Human Brain Anatomy Course, University College London

October 2011 North East Postgraduate Conference, Newcastle University. Presented a poster entitled 'Neuropathological changes in Alpers' syndrome: A mitochondrial DNA replication disorder'. **Awarded 'Best Poster' Prize.**

January 2012 British Neuropathological Society, Institute of Child Health, University College London. Presented a poster entitled 'Neuropathological changes in Alpers' syndrome: A mitochondrial DNA replication disorder'.

January 2012 IAH/IHS Postgraduate Research Conference, Newcastle University. Presented a poster entitled 'Neuropathological changes in Alpers' syndrome: A mitochondrial DNA replication disorder' (as for BNS 2012 conference).

June 2012 10th European Congress of Neuropathology, Edinburgh. Presented a poster entitled 'Neuropathological changes in Alpers' syndrome'.

October 2012 North East Postgraduate Conference, Newcastle University. Presented a talk entitled 'Alpers' Syndrome: A Mitochondrial DNA Replication Disorder'.

December 2012 Abcam 'Mitochondria and the Central Nervous System' Conference, London. Presented a poster entitled 'Neuropathological changes in Alpers' syndrome' (as for Edinburgh 2012 conference).

January 2013 IAH/IGM Postgraduate Research Conference, Newcastle University. Presented a poster entitled 'Neuropathological changes in Alpers' syndrome' (as for Edinburgh 2012 conference).

February 2013 Keystone Conference – New Frontiers in Neurodegenerative Research/Neurogenesis, Santa Fe, New Mexico, USA. Presented a poster entitled 'Neuropathological changes and mtDNA defects in Alpers' syndrome'.

March 2013 British Neuropathological Society, Institute of Child Health, University College London. Presented a poster entitled 'Neuropathological changes and mtDNA defects in Alpers' syndrome' (as for Keystone 2013 conference).

Publications

Bogle H, Lax NZ, Jaros E, McFarland R, Taylor RW, Turnbull DM. Understanding the neurodegenerative changes underpinning Alpers' syndrome: a clinical, genetic and pathological study. *Manuscript in preparation.*

Abbreviations

A – adenine

ACTH – adrenocorticotrophic hormone

ADP – adenosine diphosphate

adPEO – autosomal dominant progressive external ophthalmoplegia

arPEO – autosomal recessive progressive external ophthalmoplegia

AID – accessory interacting subdomain

AIF – apoptosis-inducing factor

ANT1 – adenine nucleotide translocase 1

AP endonuclease – apurinic/apyrimidinic endonuclease

ATP – adenosine-5'-triphosphate

bp – base pair

C – cytosine

CI-19 – complex I subunit 19

CI-20 – complex I subunit 20

CI-30 – complex I subunit 30

CI-39 – complex I subunit 39

CFV – cresyl fast violet

CNP – 2',3'-cyclic-nucleotide 3'-phosphodiesterase

CNS – central nervous system

COX – cytochrome *c* oxidase

cPEO – chronic progressive external ophthalmoplegia

CsCl – caesium chloride

Ct – threshold cycle

CT Scan – computerised tomography scan

DAB – 3, 3'-diaminobenzidine

D-loop – displacement loop

DEPC – diethylpyrocarbonate

DNA – deoxyribonucleic acid

dNMP – deoxynucleoside monophosphate

dNTP – deoxyribonucleotide

dRP lyase – deoxyribose phosphate lyase

EDTA – ethylenediaminetetraacetic acid

EEG Scan – electroencephalography scan

EM – electron microscopy

ER – endoplasmic reticulum

ERG – electroretinography

ETC – electron transport chain

F₁F_o-ATPase – ATP synthase

FADH₂ – reduced flavin adenine dinucleotide

FARS2 – mitochondrial phenylalanyl transfer RNA synthetase

FFPE – formalin-fixed paraffin embedded

G – guanine

g – gram

GABA – gamma-aminobutyric acid

GFAP – glial fibrillary acidic protein

GRACILE syndrome – growth retardation, amino aciduria, cholestasis, iron overload, lactic acidosis, and early death

H strand – heavy strand

H⁺ – hydrogen ion

H&E – haematoxylin and eosin

H₂O – water

H₂O₂ – hydrogen peroxide

HCl – hydrochloric acid

IP – intrinsic processivity subdomain

iPSC – induced pluripotent stem cell

kDa – kilodalton

L strand – light strand

LHON – Leber's hereditary optic neuropathy

M – molar

MBP – myelin basic protein

MCHS – myocerebrohepatopathy spectrum disorders

MCU – mitochondrial calcium uniporter

MELAS – mitochondrial encephalomyopathy, lactic acidosis, and stroke-like episodes

MEMSA – myoclonic epilepsy myopathy sensory ataxia

MERRF – myoclonic epilepsy with ragged red fibres

MIRAS – mitochondrial recessive ataxia syndrome

ml – millilitre

MMR – measles, mumps and rubella vaccination

MNGIE – mitochondrial neurogastrointestinal encephalomyopathy

MR spectroscopy – magnetic resonance spectroscopy

MRI – magnetic resonance imaging

mRNA – messenger RNA

MSCAE – mitochondrial spinocerebellar ataxia and epilepsy

mtDNA – mitochondrial DNA

mtSSB – mitochondrial single strand binding protein

NADH – reduced nicotinamide adenine dinucleotide

NARP – neuropathy, ataxia, and retinitis pigmentosa

NBT – nitro blue tetrazolium

nDNA – nuclear DNA

ng – nanogram

NMDA – N-methyl-D-aspartate receptor

O₂ – oxygen

O_H – origin of heavy strand replication

O_L – origin of light strand replication

OPA1 – optic atrophy 1

OXPPOS – oxidative phosphorylation

P⁺ – phosphate ion

PARK2 – E3-ubiquitin ligase

PBS – phosphate buffered saline

PCR – polymerase chain reaction

PEN – polyethylene naphthalate

PEO – progressive external ophthalmoplegia

PINK1 – PTEN-induced putative kinase 1

PMS – phenazine methosulphate

PNDC – progressive neuronal degeneration of childhood

POLG – mitochondrial polymerase gamma

PTEN – phosphatase and tensin homolog

Q – ubiquinone

QH₂ – ubiquinol

RNA – ribonucleic acid

ROS – reactive oxygen species

rRNA – ribosomal RNA

SCAE – spinocerebellar ataxia with epilepsy

SANDO – sensory ataxic neuropathy with dysarthria and ophthalmoplegia

SDH – succinate dehydrogenase

SNP – single nucleotide polymorphism

SSBP1 – single strand binding protein

T – thymidine

TAE – tris acetate-EDTA

TBS – tris buffered saline

TBST – tris buffered saline tween

TEM – transmission electron microscopy

TFAM – mitochondrial transcription factor alpha

TIM – translocase of the inner membrane protein complex

T_m – melting temperature

TNF – tumour necrosis factor

TOM – translocase of the outer membrane protein complex

tRNA – transfer RNA

UV – ultraviolet

VDAC – voltage-dependent anion channel

w/w – weight for weight

Ψ_m – membrane potential

μl – microlitre

μm – micrometre

Chapter 1 Introduction

Mitochondria

The word 'mitochondrion' comes from the Greek roots *mito* for 'thread' and *chondrion* for 'small grain', and is a reference to the shape of the mitochondria and to the size of the mitochondria relative to the host cell.

It is a commonly held view that mitochondria arose from the free-living alpha-proteobacteria which were engulfed by another cell in the environment, most probably an archaeal cell, to give rise to all the eukaryotic cells we see today (Margulis 1975). This contributed to the formation of the endosymbiotic theory of eukaryote evolution. Some eukaryotes do not possess mitochondria, such as the diplomonads, but it is thought that events in which these cells lost their mitochondria occurred separately.

Other mitochondria-like organelles can be found in eukaryotic and prokaryotic cells. Hydrogenosomes and mitosomes are double-membraned organelles related to mitochondria. Hydrogenosomes have been shown to produce adenosine-5'-triphosphate (ATP) with hydrogen production as a by-product (Lindmark and Muller 1973) and in some species hydrogenosomes may even contain their own genome (Akhmanova et al., 1998). Mitosomes do not produce ATP, though there is conflicting evidence over whether mitosomes do in fact contain their own DNA (Tovar et al., 1999; Léon-Avila and Tovar 2004).

1.1 Mitochondrial Structure

Mitochondria are traditionally considered to be oval-shaped organelles, comprised of a relatively permeable outer membrane, intermembrane space, selectively permeable inner membrane, and a matrix (Figure 1.1).

The outer membrane is flexible compared to a eukaryotic cell's cytoplasmic membrane, as the mitochondrial outer membrane does not contain sterols. This can be visualised through live cell imaging which shows mitochondria moving through the cytoplasm, changing their shape and branching off (Martz et al., 1984). The mitochondria may take on different morphologies, becoming elongated or corkscrew-shaped, or construct and deconstruct networks through fission and fusion, which can be seen in the cells of different tissues or even in the same cell. Mitochondrial fission and fusion enable a fine control over the number and size of the mitochondrial population of the cell, allowing for a rapid response to physiological stresses. The outer membrane contains enzymes

and membrane transport proteins such as porins, which act as channels to allow passive diffusion of medium sized molecules.

The intermembrane space is the space between the inner and outer membranes where ions and molecules pass into and out of the mitochondrion. Protons are pumped into this space by the electron transport chain complexes to maintain the mitochondrial membrane potential and to create the proton gradient needed for ATP production (see section 1.2.2 '*Oxidative Phosphorylation*').

In comparison, the inner membrane is selectively permeable to small, uncharged molecules such as water and oxygen which diffuse across it at a rate relative to the membrane's surface area. It increases its surface area by forming invaginations called cristae, which may form through the interactions between the inner and outer membrane, the actions of ATP synthase (Strauss et al., 2008), and through the involvement of OPA1 (Amutha et al., 2004). The mitochondrial DNA (mtDNA) molecules are attached to the matrix side of the inner membrane, while the complexes of the respiratory chain and ANT translocator, which facilitates ATP export from the matrix, are embedded in the inner membrane (Gautheron 1984). The density of the cristae is directly proportional to the energy demands of the cell as it is the site of oxidative phosphorylation and energy production.

The matrix contains the mtDNA attached to the inner membrane and RNA, and it is where the citric acid cycle (Krebs Cycle) takes place under aerobic conditions.

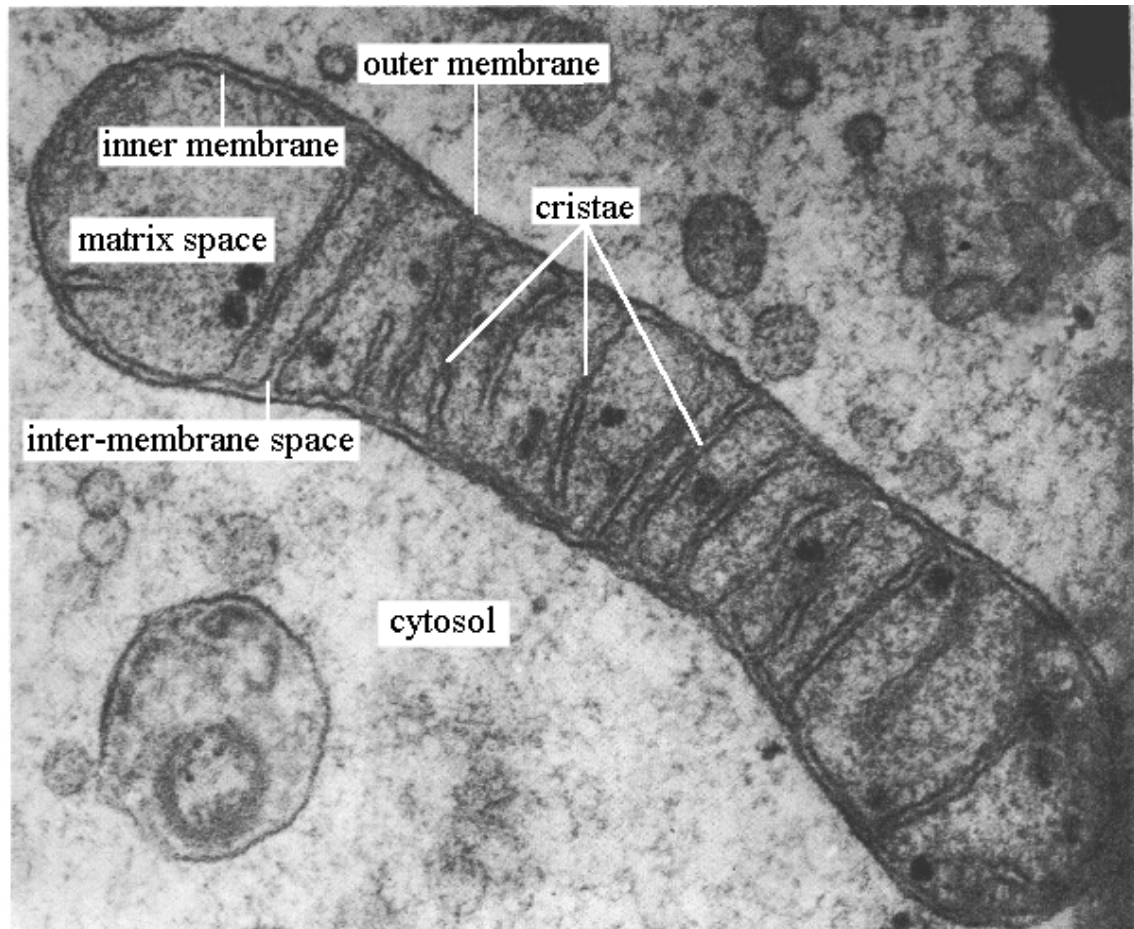


Figure 1.1. The structure of a mitochondrion.

Mitochondria consist of a double membrane with an intermembrane space in-between. The inner membrane forms the folded cristae where the electron transport chain is found and encloses the matrix, where the mtDNA, RNA and enzymes of the citric acid cycle are found.

Image taken from <http://www.bmb.leeds.ac.uk/illingworth/6form/mito.gif>

1.2 Mitochondrial Dynamics

1.2.1 Mitochondrial Fission and Fusion

The mitochondrial population inside a cell is dynamic and can increase or decrease in number when necessary. They form a changeable, interconnected network which can quickly react to the requirements of the cell. Fission and fusion play important roles in cell development and normal cellular functioning and are well regulated processes.

1.2.1.1 Fission

Mitochondrial fission is the splitting of a single mitochondrion into two mitochondria (Figure 1.2). Under times of stress, increased levels of ATP may be required by the cell and the act of fission allows for an increase in the number of mitochondria available for ATP production. Fission and mtDNA replication are coordinated so that each daughter mitochondrion receives an adequate number of copies of the mitochondrial genome.

A key protein involved in fission is Dynamin Related Protein 1 (Drp1). Drp1 is recruited by the membrane-bound protein hFis1 during fission to allow the splitting of the mitochondrial membranes, through the splitting of clathrin-coated pits. The function of Drp1 is regulated by two other proteins; hFis1 and Mff1 (Otera et al., 2010). Mitofusin 2 (Mfn2) is known to link mitochondria to the endoplasmic reticulum (ER), which becomes a place where Drp1 complexes form and mitochondrial fission occurs (Friedman et al., 2011).

Fission is thought to be regulated by endophilin B (Karbowski et al., 2004) and the sumoylation of Drp1 (Harder et al., 2004) but the exact mechanism has not yet been completely explained.

1.2.1.2 Fusion

Mitochondrial fusion is the merging of two or more mitochondria into a single mitochondrion (Figure 1.2). This may happen many times to form a large network of mitochondria merged together. Fusion is a mechanism for sharing mitochondrial proteins and genomes, which may rescue a subset of mitochondria that are deficient in certain key proteins or certain genes.

Mitofusin 1 and 2 (Mfn1 and Mfn2) are known to be involved in the fusion of the mitochondrial outer membranes (Koshiba et al., 2004) while OPA1 is known to be involved in the fusion of the mitochondrial inner membranes (Cipolat et al., 2004).

There are known to be different isoforms of OPA1 and these may allow for a greater regulation of fusion (Song et al., 2007).

When mitochondrial fusion is impaired, or the genes involved are affected, it can result in disease; it is known that defects in Mfn2 can cause Charcot-Marie-Tooth 2A (Züchner et al., 2004) and defects in OPA1 can cause Autosomal Dominant Optic Atrophy (Delettre et al., 2000; Ferraris et al., 2008).

Mitochondrial fusion has been reported to have a protective role in neurons of the cerebellum (Chen et al., 2007). This makes clear the central role fusion plays in the health of a mitochondrial population.

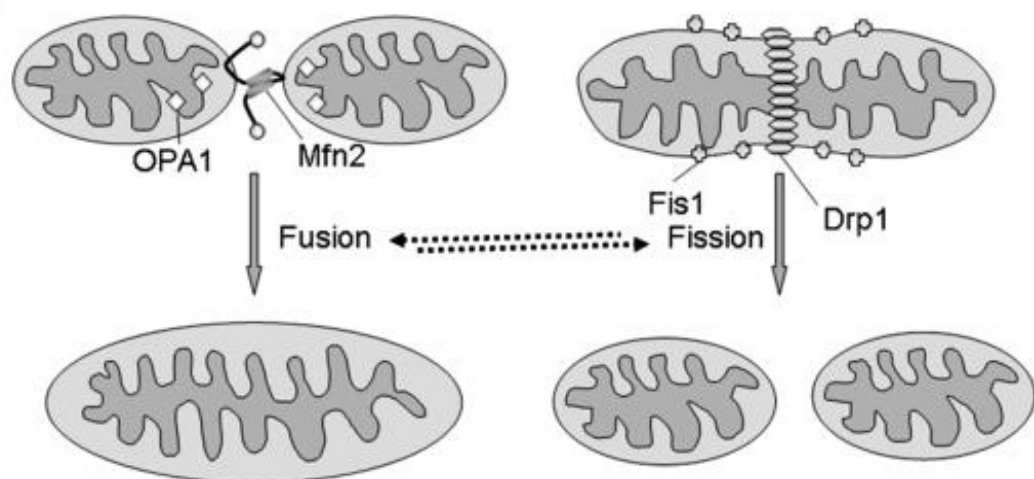


Figure 1.2. Mitochondrial fission and fusion.

Fission and fusion of the mitochondria is a constant process, allowing fine control over the mitochondrial population. Mitochondrial fusion is demonstrated on the left of the image. OPA1 and Mfn2 play a key role in the fusion of the inner and outer membranes respectively. Mitochondrial fission is demonstrated on the right of the image. Fis1 and Drp1 facilitate the splitting of the mitochondrial membranes. Image taken and modified from Palaniyandi et al., (2010).

1.2.2 Mitochondrial Transport

Mitochondria are motile organelles, moving throughout the cytoplasm of a cell to provide energy where it is required. Neurons are relatively large cells with an obvious polarity; they have a cell soma at one extremity and a cell synapse at the other extremity, connected by a long, thin axon. Mitochondria must travel between these sites to maintain a healthy functioning of the neuron, providing energy and buffering calcium levels.

This is achieved through a process known as axonal transport. Mitochondria can move in a bidirectional manner along a neuronal axon. They may travel in an anterograde movement from the cell soma to the synapse to provide energy to this highly dynamic site. The mitochondria may move in a retrograde movement from the synapse to the cell soma in order to be degraded and recycled. This occurs once the mitochondria have become depolarised and they are recycled as part of a normal and healthy cell functioning. Microtubule motor proteins aid mitochondrial transport, with kinesin motors allowing mitochondrial movement in an anterograde manner (Nangaku et al., 1994) and dynein motors allowing mitochondrial movement in a retrograde manner (Hirokawa et al., 1990).

It is known that depolarised mitochondria may cluster around the cell nucleus prior to degradation by mitophagy. This may occur in healthy cells as part of the normal turnover of mitochondria; mutations in dynein have been shown to reduce perinuclear clustering of defective mitochondria in fibroblast cells from mice (Eschbach et al., 2013). However, increased perinuclear clustering and movement of mitochondria away from the cell periphery is reported to occur after the disruption of the dynein complex in HeLa cells (Varadi et al., 2004). The mechanisms involved in coordinating mitochondrial transport and degradation are not well understood and are an area under current investigation.

1.3 Mitochondrial Function

Mitochondria have a diverse range of functions within the cell which include energy generation, calcium dynamics, production of reactive oxygen species, and control over whether the cell enters the apoptotic pathway.

1.3.1 Aerobic Respiration

Mitochondria are the main sites of aerobic cellular respiration within eukaryotic cells, producing ATP as a source of energy for both the mitochondrion and the cell. Different stages of the process take place in various parts of the mitochondrion and the cell. For each molecule of glucose that enters glycolysis and undergoes aerobic respiration 38 molecules of ATP are produced, though in reality fewer molecules are in fact available due to the energetic costs of actively transporting substrates required for aerobic respiration into the mitochondria.

1.3.1.1 Glycolysis

The first step in the process of respiration is glycolysis; a form of anaerobic respiration which takes place in the cytosol of the eukaryotic cell. One molecule of glucose ($C_6H_{12}O_6$) splits to produce two molecules of pyruvate (CH_3COCOO^-), forming many intermediate molecules in the process and producing a net gain of two ATP molecules. In actuality, four ATP molecules are produced by glycolysis though two are in fact consumed in order to add phosphate groups to the glucose molecule during the initial reactions. Pyruvate may be subject to anaerobic conditions forming lactate, or aerobic conditions during the citric acid cycle which is mentioned in greater detail in the next section. Although anaerobic respiration does not produce as great a quantity of ATP as oxidative phosphorylation (Pfeiffer et al., 2001), it does produce it 100 times faster than aerobic respiration (oxidative phosphorylation), which has a significant advantage in the muscle tissue where rapid energy increase can be vital.

1.3.1.2 The Citric Acid Cycle

The second step in the process of respiration is the citric acid cycle (also known as the Krebs Cycle) which takes place in the matrix of the mitochondria. Pyruvate molecules produced during glycolysis (see section 1.2.1.1 'Glycolysis' above) are oxidised to acetyl coenzyme-A and then enter an 8 enzyme cycle, producing intermediates including citrate, succinate, fumarate, and malate. During the production of these intermediates, NADH and $FADH_2$ are generated and subsequently used as substrates

in oxidative phosphorylation while water and carbon dioxide are produced as end products.

1.3.2 Oxidative Phosphorylation

Oxidative phosphorylation is the process by which ATP is produced using the respiratory chain complexes, found on the inner mitochondrial membrane. Production of ATP can be controlled through a negative feedback mechanism, with increasing levels of ATP inhibiting further ATP production (Reeves and Hall 1973).

There are four complexes that make up the electron transport chain (ETC) as well two electron carriers; complex I-IV with electron carriers ubiquinone and cytochrome *c* (Figure 1.3). As electrons flow along the four complexes of the ETC, hydrogen ions are produced which are pumped into the intermembrane space by complexes I, III, and IV. As the hydrogen ions accumulate they create a proton-motive force. This proton-motive force was first described in the chemiosmotic hypothesis (Mitchell 1961) and is harnessed by complex V (ATP synthase). As the hydrogen ions move down their electrochemical gradient they cause complex V to rotate, combining adenosine diphosphate (ADP) and a phosphate ion (P^+) to generate ATP.

Chemicals termed 'uncouplers' can act to allow the hydrogen ions to leak back across the inner membrane and flow down their concentration gradient without passing through complex V. This inefficiency may appear a wasteful action yet it can, under certain circumstances, be beneficial to the organism in the generation of heat (Rial and Nicholls 1984). This form of non-shivering thermogenesis can be used as an alternative to using ATP for the muscle contractions of shivering.

1.3.2.1 The Electron Transport Chain

The electron transport chain (ETC) is a group of multi-subunit protein complexes embedded in the inner mitochondrial membrane. There are five complexes in total, four comprising the ETC and the addition of complex V (ATP synthase) forming the mitochondrial respiratory chain (Figure 1.3). The most important property of the ETC is its capacity to permit oxidation-reduction reactions to occur in complex I-IV. This happens due to the iron-sulphur groups within the complexes (Page et al., 1999). The mitochondrial respiratory chain is encoded by both nuclear and mitochondrial genes (Table 1.1). The five complexes form larger supercomplexes which allow for greater efficiency of the mitochondrial respiratory chain, increasing the stability of the complexes and providing some protection from oxidative stress. Supercomplexes may

also play a role in shaping the inner mitochondrial membrane (Vonck and Schäfer 2009).

	Alternative name of the complex	Subunits encoded by nuclear genes	Subunits encoded by mitochondrial genes
Complex I	NADH dehydrogenase	37	7 (ND1-ND6, ND4L)
Complex II	Succinate dehydrogenase	4	0
Complex III	Ubiquinol cytochrome <i>c</i> reductase	10	1 (Cytochrome <i>b</i>)
Complex IV	Cytochrome <i>c</i> oxidase	11	3 (COX I-III)
Complex V	ATP synthase	17	2 (ATP6, ATP8)

Table 1.1. Table of the nuclear and mitochondrial location of genes coding for subunits of the mitochondrial respiratory chain in humans.

All 13 polypeptides encoded by the mitochondrial genome are represented in the table.

NADH and FADH₂, generated by the citric acid cycle, are the initial substrates of the ETC which are oxidised by complex I and complex II. Electrons donated by these substrates are passed along the ETC allowing hydrogen ions to be pumped across the inner membrane and into the intermembrane space. Both complex I and complex II pass electrons to an electron carrier called ubiquinone. Complex III receives these electrons from ubiquinone and passes the electrons to another carrier, cytochrome *c*. Cytochrome *c* then passes the electrons to complex IV, at which the electrons react with oxygen (O₂) and hydrogen ions (H⁺) to produce water.

The process of ATP production using the respiratory chain was first proposed in 1961 (Mitchell 1961) but their enzyme systems were first deduced much earlier, in 1948 (Hogeboom et al., 1948). Since that time, the individual complexes of the respiratory chain have been investigated and characterised, with their role in human disease the current topic of research.

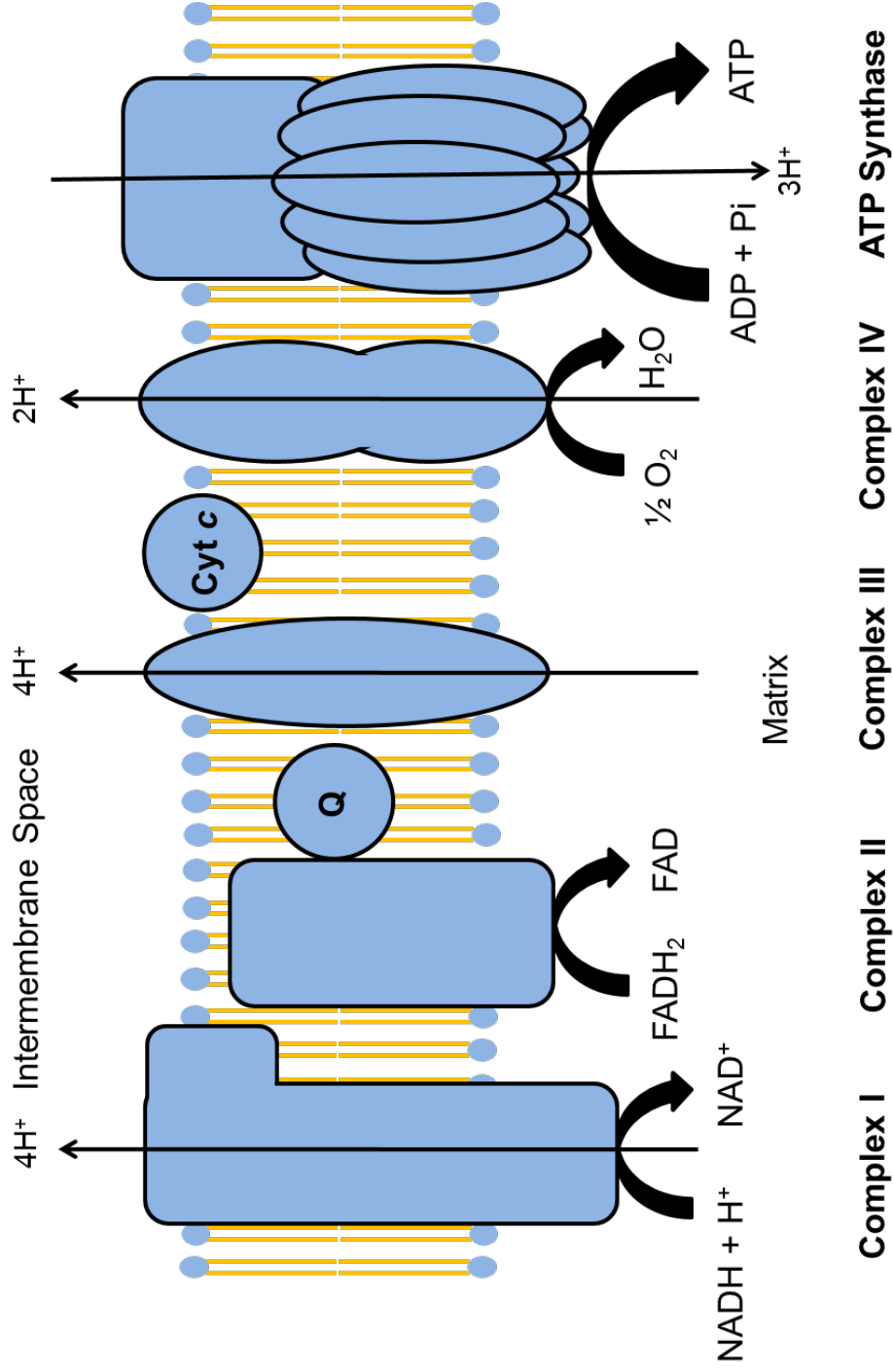


Figure 1.3. The mitochondrial respiratory chain.

The four complexes of the ETC and ATP synthase are shown in the inner mitochondrial membrane.

Key: Q=ubiquinone, Cyt c=cytochrome c, H^+ =hydrogen ion, O_2 =oxygen, ADP=adenosine diphosphate, P_i =phosphate ion

1.3.2.1.1 Complex I - NADH: Ubiquinone Oxidoreductase

Complex I, NADH: ubiquinone oxidoreductase, is the largest of all of the five complexes in the OXPHOS system and produces much of the proton-motive force required for ATP synthesis. It functions to catalyse the oxidation of NADH to NAD⁺ and the simultaneous reduction of the electron carrier ubiquinone (Q) to ubiquinol (QH₂). This results in the movement of two electrons from NADH to ubiquinone, forming ubiquinol which is later oxidised by complex III. As the translocation of electrons occurs, four hydrogen ions are pumped across the inner membrane into the intermembrane space; it is this build-up of hydrogen ions that will create the electrochemical gradient that allows the production of ATP.

A 1MDa protein, it consists of at least 44 subunits; 37 subunits encoded by nuclear genes and 7 subunits encoded by mitochondrial genes (Anderson et al., 1981). There are 14 'core' subunits that perform the redox reactions; 7 of these are encoded from mitochondrial DNA (*ND1-6, ND4L*) and 7 from nuclear DNA (*NDUFS1-3, NDUFS7-8, NDUFV1-2*). The other subunits act to stabilise this large complex. The complex takes on an L-shaped conformation, with the hydrophobic arm spanning the entire plasma membrane and the hydrophilic arm extending into the mitochondrial matrix (Figure 1.4). The hydrophilic domain is the part of the protein that catalyses the redox reactions, transferring electrons from its iron-sulphur clusters to the electron carrier ubiquinone (Q) to reduce it to ubiquinol (QH₂). The hydrophobic domain attaches the complex to the inner membrane.

The assembly of complex I requires 11 assembly factors, all encoded from nuclear DNA. Little is known about its process of assembly but it is thought that assembly progresses through intermediate stages (Antonicka et al., 2003), with the core subunits being assembled first, as opposed to the assembly of single subunits sequentially. It is thought that the hydrophobic membrane arm is assembled first, with other subunits assembling together and then attaching onto the arm (Vogel et al., 2007).

Defects in complex I are the most commonly noted defects in mitochondrial disease (Darin et al., 2001) but may be underdiagnosed due to their heterogeneous clinical signs and potential for normal lactate levels (Kirby et al., 1999). The intricacy and size of this complex makes issues with subunit availability or subunit assembly more likely to occur than with other complexes.

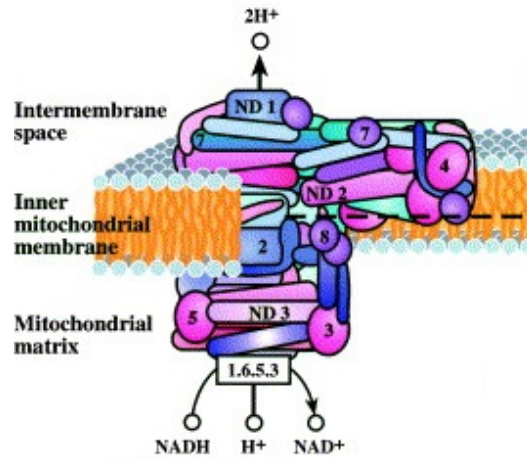


Figure 1.4. Image of the respiratory chain complex I.

The L-shaped complex is shown with labelled subunits. ND1-3 shown are mitochondrially-encoded subunits. Image taken and modified from Mandavilli et al., (2002).

1.3.2.1.2 Complex II - Succinate: Ubiquinone Oxidoreductase

Complex II, succinate: ubiquinone oxidoreductase partially spans the inner mitochondrial membrane. It contains a hydrophobic domain within the plasma membrane and a hydrophilic domain that interacts with the mitochondrial matrix (Figure 1.5). This complex plays a role in both the electron transport chain and the citric acid cycle, catalysing the simultaneous oxidation of succinate to fumarate and the reduction of ubiquinone (Q) to ubiquinol (QH₂). Hydrogen ions are not transported into the intermembrane space by this complex and so it does not contribute directly to the electrochemical gradient that enables the generation of ATP.

Complex II is a 127.5kDa protein made up of 4 subunits, all of which are encoded by the nuclear genome. The subunits are labelled A, B, C, and D and play a functionally distinct role within the complex. Subunit A is a flavoprotein to which succinate is able to bind. Subunit B is an iron-sulphur protein to which electrons are passed from subunit A, and like subunit A is hydrophilic and can interact outside of the plasma membrane. Subunits C and D are hydrophobic proteins within the plasma membrane, containing a bound haem group, anchoring the complex in the inner membrane and transferring electrons to ubiquinone (Sun et al., 2005).

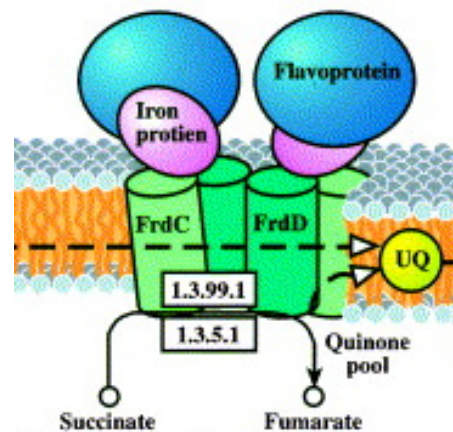


Figure 1.5. Image of the respiratory chain complex II.

The complex is shown with labelled subunits. The electron carrier ubiquinone is shown as yellow circled UQ. Electrons pass from complex II to ubiquinone. Hydrophilic subunit A is shown as a flavoprotein and subunit B is shown as an iron protein. Hydrophobic subunit C and subunit D are shown within the membrane as FrdC and FrdD. Image taken and modified from Mandavilli et al., (2002).

1.3.2.1.3 Complex III - Ubiquinol Cytochrome c Reductase

Complex III, ubiquinol cytochrome c reductase, functions to catalyse the oxidation of ubiquinol (QH₂) and the simultaneous reduction of cytochrome c (Baum et al., 1967), both carrier molecules in the ETC. Four hydrogen ions are pumped across the inner membrane, into the intermembrane space to be harnessed by the proton-motive force and produce ATP.

This complex is a 248kDa protein made up of 11 subunits (Figure 1.6); 10 subunits are encoded by nuclear genes and one subunit, cytochrome b, is encoded by mitochondrial genes. Three of the eleven subunits that make up this complex have prosthetic groups attached; the iron-sulphur protein (Rieske subunit), cytochrome c₁, and cytochrome b with two haem groups attached: b_L and b_H.

During electron transfer, two electrons are transferred from ubiquinol to the Rieske subunit and the cytochrome b_L haem. In the first reaction, the Rieske subunit becomes reduced and it oscillates, facilitating electron transfer to cytochrome c₁. In the second reaction, an electron transfers from the cytochrome b_L haem to the b_H haem, both reactions releasing hydrogen ions and increasing the proton-motive force.

The 'core' subunits of complex III facilitate the assembly of the complex through stable intermediate assembly stages. The full assembly of complex III requires 2 assembly factors, both encoded from nuclear DNA (Smith et al., 2012).

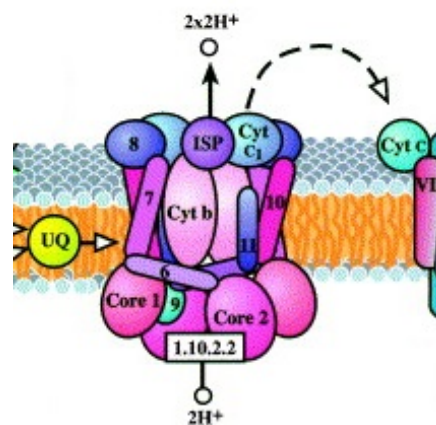


Figure 1.6. Image of the respiratory chain complex III.

The third complex is shown with labelled subunits. The electron carrier ubiquinone is shown as yellow circled UQ. Electrons pass from ubiquinone, to complex III, and to the next electron carrier, cytochrome c, shown as aquamarine circled Cyt c. The mitochondrially-encoded subunit cytochrome b is shown at the centre of the complex. Image taken and modified from Mandavilli et al., (2002).

1.3.2.1.4 Complex IV - Cytochrome c Oxidase

Complex IV, cytochrome c oxidase, functions to catalyse the oxidation of cytochrome c and production of water by combining electrons with molecular oxygen and hydrogen ions. During this reaction, two hydrogen ions are moved across the inner membrane, into the intermembrane space which increases the proton-motive force.

This complex is a 204kDa protein made up of several metal prosthetic sites and 14 subunits; 11 subunits are encoded by nuclear genes, 3 subunits, COX I-III, are encoded by mitochondrial genes. COX I and COX II make up the catalytic core of the subunit, containing two haem groups (a and a₃) and two copper groups (cu_A and cu_B) which allow electron transfer and oxygen reduction. Little is known about the enzymatic role of COX III subunit. Complex IV exists as a dimer to allow for functional efficiency, and it is the final complex in the ETC and the terminal electron acceptor (Figure 1.7).

The assembly of complex IV occurs on both sides of the inner membrane and requires 18 assembly factors, all encoded from nuclear DNA (Mick et al., 2011). It is suggested that mitochondrially-encoded COX I is directly linked to the assembly and plays a central role in the association of the other subunits, including COX II and COX III.

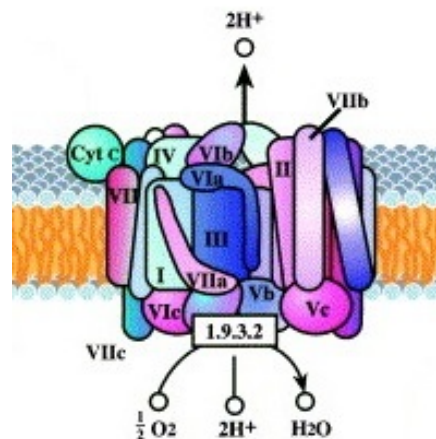


Figure 1.7. Image of the respiratory chain complex IV.

The final complex of the electron transport chain is shown with labelled subunits. Mitochondrially-encoded subunits COX I, II, and III are labelled in the centre of the complex. The electron carrier cytochrome c is shown as aquamarine circled Cyt c. Electrons pass from cytochrome c to complex IV where they are combined with molecular oxygen and hydrogen ions to form water. Image taken and modified from Mandavilli et al., (2002).

1.3.2.2 Complex V – ATP Synthase

Complex V, ATP synthase, is made up of 19 subunits; 17 subunits are encoded by nuclear genes, 2 subunits are encoded by mitochondrial genes *ATP6* and *ATP8*. It is the final protein of the OXPHOS system. Human ATP synthase is also termed F₁F_o-ATPase named after the two functional domains of the complex; the F₁ domain, which contains the functional portion of the complex that synthesises ATP using the electrochemical gradient produced by the mitochondrial respiratory chain, and the F_o domain, embedded in the inner membrane (Figure 1.8).

Complex V has an intricate structure comprising two functional domains made up of many subunits. The F₁ domain is made up of three copies of subunits α and β , and a single copy of subunits γ , δ and ϵ . These subunits form the functional parts of the complex: subunits α and β form the knob, and subunits γ , δ and ϵ form the rod (Figure 1.8). The membrane-bound F_o domain is made up of a subunit-c ring which forms the functional rotor (Figure 1.8). It also consists of a single copy of subunits a, b, d, F₆, and OSCP which form the stator. There are four further additional subunits which associate with the F_o domain, including subunit a and subunit A6L encoded by the mitochondrial genes *ATP6* and *ATP8* (Anderson et al., 1981).

The synthesis of ATP from ADP and phosphate is performed by the F₁ domain, powered by the movement of hydrogen ions (the proton-motive force) that had been generated by the electron transport chain. The movement of hydrogen ions down its electrochemical gradient causes the subunit-c ring to rotate (Cox et al., 1984). This causes the rod subunits of F₁ domain to also rotate, in particular the γ subunit, and a flow of protons through subunit α , through the subunit-c ring and into the mitochondrial matrix. Rotation of the γ subunit provides energy for ATP synthesis, which occurs due to a binding-change mechanism in the subunits (Boyer 1975). Each binding site on the three β subunits undergoes three conformational changes to bind ADP, phosphate, and then release the formed ATP molecule. Binding of the ADP and phosphate occurs in the open conformational state which causes a rotation of the α and β subunits by 120°. Formation of ATP occurs in the tight conformational state with the release of a molecule of ATP from the loose conformational state and a return to the ability to bind another ADP and phosphate molecule.

The assembly of complex V begins by attachment of the membrane-bound subunit-c ring. The F₁ domain will then attach to this and finally the stator arm, before dimerization of two fully assembled complexes (Jonckheere et al., 2012). Full assembly

requires 4 assembly factors, all encoded from nuclear DNA (Wang et al., 2001). Complex V mutations and assembly abnormalities have been implicated in mitochondrial disease (De Meirleir et al., 2004; Mayr et al., 2010; Jonckheere et al., 2013) but the incidence may be higher than reported as this complex is seldom investigated and not a regular candidate for genetic analysis.

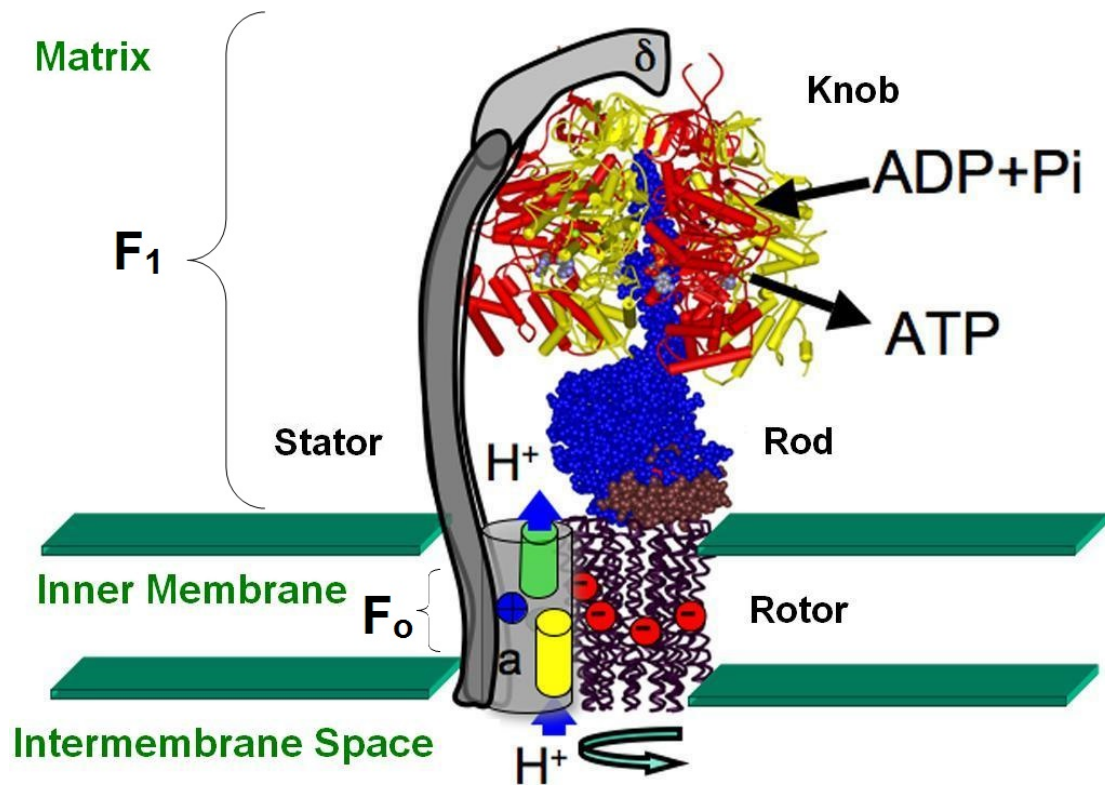


Figure 1.8. Image of complex V (ATP synthase).

Complex V of the OXPHOS system is shown. The F₁ domain comprises the part of the complex that synthesises ATP from ADP. The F_o domain anchors the complex to the inner membrane and channels hydrogen ions through. Image taken and modified from Nakamoto et al., (2008).

1.3.2.3 Supercomplexes

The mitochondrial respiratory chain is often shown as individual, unlinked complexes in the mitochondrial inner membrane, electron carriers allowing the movement of electrons between them. However, it has now been shown that the complexes come together to form functionally intact supercomplexes (Schägger and Pfeiffer 2000; Vonck and Schäfer 2009), which have also been termed respirasomes due to their functional respiration (Acín-Pérez et al., 2008).

Complex I, a large and unstable protein, has been found to associate with both complex III and complex IV within the supercomplex, ensuring it remains stable (Acín-Pérez et al., 2004; Diaz et al., 2006). It has been reported that any disruption between complex I and complex III may increase reactive oxygen species (ROS) production (Maranzana et al., 2013) confirming the stabilising effect that other complexes have upon complex I and the beneficial properties of the supercomplex.

In addition to a respiratory role, the supercomplexes may also be involved in shaping the cristae of the inner mitochondrial membrane through their presence on narrow cristae of the inner membrane (Vogel et al., 2006). In addition, supercomplexes allow for substrate channelling (Bianchi et al., 2004).

1.3.3 Apoptosis

Apoptosis is the programmed cell death that occurs naturally in multicellular organisms. It is a controlled death of the entire cell as opposed to the two other forms of cell death; necrosis, where cell injury results in premature cell death; and autophagy, which is the controlled degradation of cellular components. Apoptotic cell death is a natural process initiated by either extracellular or intracellular signals. The general process of apoptosis involves the blebbing of the cell membrane, cell shrinkage, condensation of chromosomes, and nuclear fragmentation. There is typically no inflammation of surrounding tissue or strong osmotic reaction involved. It is a process that has evolved to allow for the removal of individual damaged cells from a multicellular organism, so that the organism may survive and reproduce.

There are two main pathways of apoptosis that lead to downstream modifications of structural proteins. The extracellular pathway is initiated by cell surface receptors while the intracellular pathway involves the mitochondria (Zamzami et al., 1995). Both the extracellular and intracellular pathways activate caspases which then go on to activate

pro-apoptotic proteins in a cascade reaction that can result in many activated proteins from many times fewer caspase proteins.

The extracellular pathway is mediated by membrane-bound proteins of the tumour necrosis factor (TNF) receptor family such as FAS or TNFR1, termed 'death receptors', on the cell's surface. For example, immune system cells may produce the FAS ligand which binds to the FAS death receptor protein on the cell's surface. Once bound, these receptors can bind to intracellular adaptor proteins that can activate caspase-8 molecules. There is a downstream cascade reaction resulting in apoptosis of the cell.

The intracellular pathway is mediated by the release of cytochrome *c* from the mitochondria (Liu et al., 1996). The cytochrome *c* is released into the cytosol and there it binds to and activates APAF-1 protein. This induces the assembly of an apoptosome which when it binds to caspase-9, promotes the activation of caspase-3 and apoptosis of the cell. The intracellular pathway is controlled by proteins from the Bcl-2 family; when Bcl-2 or Bcl-X_L are inhibited, other pro-apoptotic members of the protein family such as BAX and BAK can promote the permeabilisation of the outer mitochondrial membrane and the release of cytochrome *c*. Apoptosis-inducing factor (AIF) is also released from mitochondria to promote apoptosis (Susin et al., 1999) in a system that is caspase-independent and instead causes DNA fragmentation (Susin et al., 2000).

Apoptotic pathways have many check points to allow apoptosis to halt before it reaches a certain point, beyond which apoptosis is irreversible. In addition to these, it has been reported that OPA1 can protect the cell from apoptosis by keeping junctions in the cristae tight to prevent the release of cytochrome *c* (Frezza et al., 2006).

1.3.4 *Reactive Oxygen Species*

Reactive oxygen species (ROS) are reactive molecules that have an oxygen atom with a 'free radical' pair of electrons attached to it. This makes the oxygen molecule many times more likely to bind to other molecules in the cell, oxidising molecules, and potentially disrupting cellular systems. ROS found in the cell include hydrogen peroxide (H₂O₂), the superoxide radical (O₂⁻) and the hydroxyl radical (.OH). Complexes I and III are the main producers of ROS in the mitochondria (Chen et al., 2003). Complex I releases ROS across the inner membrane unidirectionally into the matrix only, while complex III releases ROS across both sides of the inner membrane, into both the matrix and the intermembrane space (Muller et al., 2004).

ROS may play a key role in cellular signalling, functioning in the control of smooth muscle tone, ventilation, and autophagy. However, highly increased levels of free radicals can lead to damage to mtDNA, due to the close proximity of the mtDNA to the electron transport chain of the inner membrane where the free radicals are formed. ROS cause damage which contributes to the ageing process, apoptosis, and *de novo* mtDNA mutations and the rate of ROS production may in fact increase under states of physiological stress, including hypoxia and ischemia (Becker et al., 1999; Kevin et al., 2003).

1.3.5 Calcium Dynamics

Free calcium in the cell is required for many cellular processes, including control of the citric acid cycle, and for signal transduction. Cellular homeostasis of calcium levels is required and both the endoplasmic reticulum (ER) and mitochondria perform this important function to avoid any damage to the cell.

Mitochondria have the ability to sequester calcium. This is very important as the calcium concentration increases to potentially damaging levels inside the cell. High levels of calcium, per mg of protein, can be sequestered with mitochondrial function still intact (Rossi and Lehninger 1964). This is achieved by the mitochondrial calcium uniporter (MCU) protein on the inner mitochondrial membrane, which allows for the influx of calcium into the mitochondria (Deluca and Engstrom 1961). It is dependent upon mitochondrial membrane potential to function, which in turn is driven by the respiratory chain, as opposed to ATP-dependent active transport. The outer membrane is permeable to calcium through a class of porin channels, voltage-dependent anion channels (VDAC), that allow medium-sized molecules to pass through. As calcium enters the mitochondria through VDAC channels in the outer membrane and the MCU in the inner membrane, it has been hypothesised through computational assessments that at least two distinct classes of calcium buffer may exist in the mitochondria (Bazil et al., 2012).

The mechanism by which large amounts of calcium are taken up and stored is not well understood and is an active topic of research.

1.4 The Mitochondrial Genome

The genome of the human mitochondrion was fully sequenced in 1981; it is a circular molecule of 16,569Kb in length and coding for a total of 37 genes (Anderson et al., 1981) (Figure 1.9). The two strands of mtDNA are made up of different proportions of purine and pyrimidine bases thus giving them different buoyancies in CsCl density gradients, thus earning them the names heavy strand (H strand) and light strand (L strand). The 37 genes (28 on the H strand and 9 on the L strand) code for 13 polypeptide genes, 2 rRNA genes and 22 tRNA genes; there are two tRNA leucine and two tRNA serine genes that each recognise a different mRNA codon. The polypeptide genes contain no introns and its largest non-coding region is the displacement loop (D-loop), which is the origin of replication on the H strand of mtDNA. A third strand of DNA holds the double stranded DNA apart, and enables replication to begin.

All other proteins which make up the mitochondria and their metabolic processes are encoded by nuclear genes. These products enter the mitochondria, facilitated by a mitochondrial import signal. This includes the protein machinery required for mtDNA replication, transcription, and translation. The mitochondrial genome is able to replicate independently of the cell cycle (relaxed replication) and can excise misincorporated bases through the proof-reading ability of the polymerase.

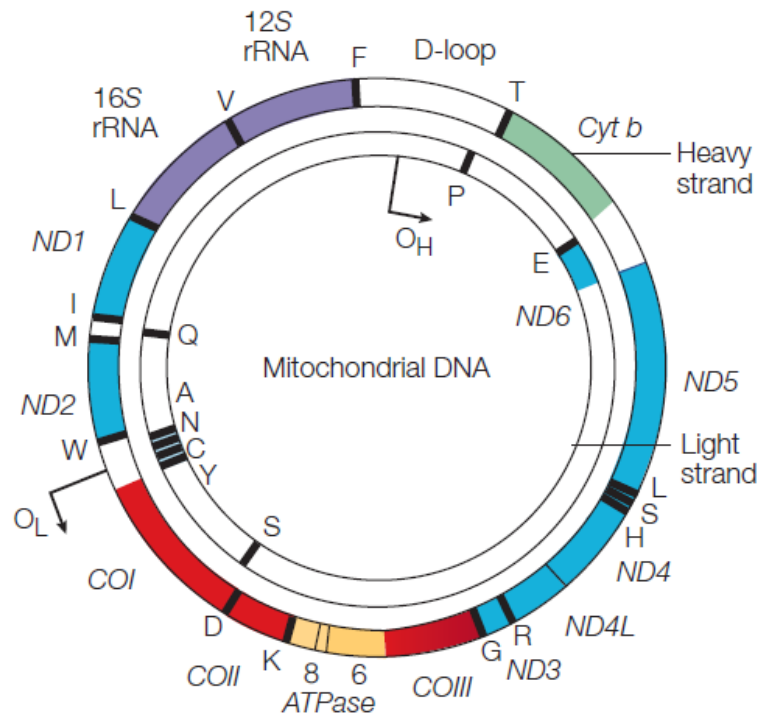


Figure 1.9. The mitochondrial genome.

The mitochondrial genome is a 16,569 base-pair circular, double-stranded molecule. There is both a heavy strand and a light strand composed of different proportions of purine and pyrimidine bases. These strands have their own origins of replication shown on the image: O_H on the heavy strand and O_L on the light strand. There are 37 genes; 22 tRNAs (black), 2 rRNAs (purple), and 13 polypeptides which consist of 7 subunits of complex I (blue), 1 subunit of complex III (green), 3 subunits of complex IV (red), and 2 subunits of complex V (orange). The displacement loop (D-loop) is the initiation site of replication of the H strand and of transcription.

Used by kind permission of Professor Robert Taylor, Newcastle University.

1.4.1 Mitochondrial DNA Replication

Mitochondria contain their own DNA (Nass and Nass 1963) and it is replicated independently of the cell cycle by a unique DNA polymerase, encoded by the nuclear gene *POLG* (Hance et al., 2005). Many other proteins are involved in the process of replication which are encoded by nuclear genes and transported into the mitochondria. These include Twinkle, a helicase that unwinds double-stranded DNA to single-stranded DNA; TFAM, a mitochondrial transcription factor A that functions in promoter activation; and single-stranded binding proteins which stabilise single strand portions of mtDNA. Topoisomerases may also be involved in order to reverse any supercoiling of the genome and allow the necessary enzymes and polymerases to attach to the DNA. Mutations in genes involved in DNA replication, transcription and translation can lead to mutations in mtDNA, decreased mtDNA content, and decreased oxidative phosphorylation leading to mitochondrial disease.

Three different models of mtDNA replication have been put forward to describe how replication of the mitochondrial genome may proceed on both the heavy strand (H strand) and light strand (L strand) of mtDNA. These models are termed the 'asynchronous strand displacement' model (Robberson and Clayton 1972; Clayton 1982), the 'strand-coupled bidirectional replication' model (Holt et al., 2000), and the 'RNA incorporated throughout the lagging strand (RITOLS)' model (Yang et al., 2002; Yasukawa et al., 2006). A further, rare intermediate form of mtDNA replication has been noted in adult human heart, skeletal muscle, and placenta involving the replication of many mtDNA molecules linked by a four-way Holliday junction termed an 'X-spike' (Kajander et al., 2001).

1.4.1.1 The 'Asynchronous Strand Displacement' Model

This model for mtDNA replication proposed that covalently-closed circular molecules are formed through a process of displacement replication (Robberson and Clayton 1972). Replication is initiated at the D-loop region on the H strand (O_H) and proceeds in a clockwise fashion. The L strand is dissociated from the H strand during replication and almost two thirds of the H strand is replicated until the origin of replication on the L strand (O_L) is then exposed. This allows replication to be initiated in the opposite direction on the L strand until the entire strand is replicated (Clayton 1982). The strands are covalently closed once replication is complete to form a circular molecule, and they dissociate from the template strand.

1.4.1.2 The 'Strand-Coupled Bidirectional Replication' Model

This model for mtDNA replication states that replication is initiated at the D-loop region (O_H) on the H strand in a clockwise fashion, followed shortly afterwards by replication initiation on the L strand in the opposite direction. Both the leading and lagging strands are replicated at the same time in a bidirectional fashion. The L strand is not replicated as a single chain however; it is replicated in short segments termed Okazaki fragments. The strands are covalently closed and they dissociate from the template strands (Holt et al., 2000).

It was considered that this 'strand-coupled bidirectional replication' model may occur in cells that are under steady-state conditions, whereas the 'asynchronous strand displacement' model may occur in cells where accelerated mtDNA replication may be advantageous (Fish et al., 2004).

1.4.1.3 The 'RNA Incorporated Throughout the Lagging Strand (RITOLS)' Model

This model agrees with the 'strand-coupled bidirectional replication' model that replication is initiated at the D-loop region (O_H) on the H strand in a clockwise fashion, followed by replication on the L strand. However, this model proposed that the lagging strand is replicated through segments of RNA that are first incorporated onto the leading strand, later replaced by DNA (Yang et al., 2002; Yasukawa et al., 2006). Using two-dimensional agarose gel electrophoresis, it was shown that RNA was not only used to initiate the short DNA Okazaki fragments on the lagging strand, but that RNA could in fact extend across an entire strand of mtDNA (Yasukawa et al., 2006). Transmission electron microscopy (TEM) and immunopurification has further corroborated the evidence of large regions of RNA on one of the replicating mtDNA strands (Pohjoismäki et al., 2010) and the use of interstrand cross-linking techniques has shown these DNA/RNA hybrid tracts present in living tissue prior to study methodology and that they are not due to adventitious factors (Reyes et al., 2013). It has been suggested that mature RNA transcripts that are already present in the matrix may hybridise to the lagging strand as DNA synthesis of the leading strand occurs in a 'bootlace mechanism', where the RNA strand is not continuous (Reyes et al., 2013).

1.4.2 Transcription

Transcription of mitochondrial genes is a complex process requiring all proteins involved to be imported into the mitochondria. Efficient transcription of mitochondrial genes is vital to the production of ATP. Key components of transcription are mitochondrial RNA polymerase (POLRMT), TFAM, Twinkle helicase, SSBP1, TFB2M and MTERF1.

Transcription occurs on each strand of the mtDNA, with a large polycistronic RNA molecule being synthesised. On the L strand this is initiated from the light-strand promoter, LSP, while on the H strand this is initiated from two promoters, HSP1 and HSP2 (Montoya et al., 1982). This large RNA transcript is then processed to produce individual mRNA, tRNA, and rRNA molecules, with each mRNA and rRNA transcript bordered by at least one tRNA transcript. These tRNA transcripts are thought to be a key substrate in the mechanism of RNA processing, known as the 'tRNA punctuation model' (Ojala et al., 1981).

POLRMT is the mitochondrial RNA polymerase which synthesises the mRNA transcripts of mitochondrial genes. The gene shows high sequence homology to the genes of RNA polymerases found in yeast and to the C-terminal region of the RNA polymerase in bacteriophages (Tiranti et al., 1997). It was considered to interact with both mitochondrial transcription factors TFB1M and TFB2M to enhance transcription (Rantanen et al., 2003) though more recently TFB1M has been reported to function as the primary 12S rRNA methyltransferase for the biogenesis of the 28S ribosomal subunit (Cotney et al., 2007; Metodiev et al., 2009). *TFAM* encodes the mitochondrial transcription factor A protein which facilitates mitochondrial promoter recognition and initiation of transcription through structural changes to the DNA, allowing POLRMT to bind and begin transcription. Twinkle helicase protein uncoils the mtDNA and single strand binding protein (SSBP1) maintains the uncoiled state of the mtDNA to allow for TFAM protein to interact with the DNA. MTERF1 acts to terminate transcription through binding to a short region at the 3'-end of the tRNA leucine^(UUR) gene (Kruse et al., 1989) and the clarification of other termination sites is under investigation.

1.4.3 Translation

Translation of processed mitochondrial RNA transcripts requires the action of mitoribosomes, in addition to aminoacyl-tRNA synthetases and methionyl-tRNA transformylase which are essential to the production of charged tRNA molecules that are able to produce a peptide strand. Mitoribosomes are made up of 81 nuclear-encoded proteins and two mitochondrially-encoded rRNAs. The 28S small subunit is made up of 12S RNA and 33 proteins, and the 39S large subunit is made up of 16S RNA and 48 proteins (Anderson et al., 1981; Smits et al., 2007). These nuclear-encoded proteins are directed into the mitochondrial matrix via protein complexes known as translocase of the outer membrane (TOM) proteins and translocase of the inner membrane (TIM) proteins.

Translation of RNA transcripts occurs on the mitoribosome in the separate stages of initiation, elongation, and termination of the synthesised strand. Initiation is performed by two initiation factors: mtIF1 and mtIF3 (Koc and Spremulli 2002) which recognise the codons AUG, AUA and AUU. They act to allow assembly of the initiation complex which ensures the start codon of the RNA transcript is bound to the peptidyl site (P-site) of the mitoribosome where peptide elongation is instigated. The elongation step of translation is tightly controlled by nuclear factors mtEFTu, mtEFTs, mtEFG1 and mtEFG2. It is proposed that termination of the peptide is by mitochondrial release factor 1a (mtRF1a) (Zhang and Spremulli 1998) which recognises stop codons at the acceptor site and terminates further translation to allow detachment of the protein (Soleimanpour-Lichaei et al., 2007).

The codons AGA and AGG conventionally encode arginine in the human genome but human mitoribosomes do not recognise these codons. It was considered that they may act as translation termination codons in addition to the termination codons UAA and UAG. However, mitoribosomes do not recognise the AGA and AGG codons as termination codons and this can induce -1 frameshift mutations caused by stalling of the mitoribosomes. The frameshift mutation then allows the mitoribosome to recognise a UAA or UAG codon and subsequently mitochondrial release factors are able to terminate and release the peptide (Temperley et al., 2010).

1.5 Mitochondrial Genetics

The genetics of mitochondria are exceptionally different to the genetics of their host eukaryotic cell. Many of their unique traits are described in the following sections.

1.5.1 Mitochondrial Inheritance

Uniparental inheritance of mitochondria is found in most animals, plants and fungi, when the fusion of gametes from two donors occurs. Mitochondrial inheritance is usually from the maternal donor, although famous exceptions to this rule exist, including mussels (*Mytilus edulis*) (Hoeh et al., 1991) and fruit flies (*Drosophila*) (Kondo et al., 1992; Wolff et al., 2013), where a mixed inheritance of mtDNA has been demonstrated from both the maternal and paternal donors. In mammals, there is normally a strict maternal inheritance of mtDNA to the offspring, although exceptions here have been documented in humans (Schwartz and Vissing 2002) and mice (Gyllensten et al., 1991).

This uniparental inheritance is thought to prevent a mixed and competing population of mtDNA genomes in the cell. It has been noted in rodents that when mtDNA from both parents enter the oocyte, the paternal population is eliminated (Shalgi et al., 1994). This prevents the transmission of deleterious mitochondrial genome mutations by preventing cytoplasmic mixing of different mitochondrial populations (Hastings 1992; Hurst 1996). A deleterious mutation could spread throughout the mitochondrial population if it has a replication advantage, even if it is harmful to the host. Uniparental inheritance may have evolved to prevent deleterious mutations spreading throughout the entire host population and as a result, allow a greater efficiency of oxidative phosphorylation.

1.5.2 Heteroplasmy and the Threshold Effect

Mitochondria contain multiple copies of their genome which replicate independently of the cell cycle (relaxed replication) (Bogenhagen and Clayton 1977). Heteroplasmy (“heterogeneity of the cytoplasm”) describes the state of mixed populations of mitochondria with different genomes within a tissue. Homoplasmy describes the state in which the mitochondria in the tissue will have identical genomes but as mtDNA accumulates mutations throughout an individual's lifetime (Wallace 1992) this leads to populations of mitochondria with varying oxidative phosphorylation capacities (Figure 1.10).

Mutations can occur in a single DNA molecule in a variety of ways, as *de novo* events or through the action of mutated proteins such as POLG, and mutations may be propagated to be found in a higher proportion of mtDNA molecules. The mtDNA turnover of a cell has been estimated to have a half-life of between 6 days in cardiac cells and 31 days in the brain cells of rats (Gross et al., 1969) but recent investigations suggest the turnover may be much faster; 1.83 days in hepatocytes of mice (Miwa et al., 2008). With quick mtDNA replacement happening in cells, it is important to understand the mechanisms by which a mutation may reach high levels in a cell.

Clonal expansion of mtDNA mutations can explain how mutations are propagated in cell populations (Nekhaeva et al., 2002). Segregation of mutations at different proportions in the cell's progeny can result in a mutation being propagated at higher levels in some daughter progeny and then the subsequent effect of random genetic drift may lead to fixation of a mutation over time.

In this way, mtDNA mutations can expand to be found at very high levels and may lead to impaired oxidative phosphorylation and disease (Moslemi et al., 1998). This high level is termed the 'threshold level' (Sciaccio et al., 1994). Once the amount of mtDNA with a mutation reaches a threshold value of between 70% - 90% (Rossignol et al., 2003), the cell may start to show the signs of impaired oxidative phosphorylation. However, the exact threshold level may be dependent on where in the mitochondrial genome the mutation occurs; whether structural subunits or core functional subunits are affected. Heteroplasmy of mutations in structural subunits will typically have a lower threshold level than mutations in tRNA genes due to their link with ATP production.

It is currently unknown how mitochondria with impaired function accumulate in the cell, and it is a current topic of research in the fields of ageing and neurodegenerative disease.

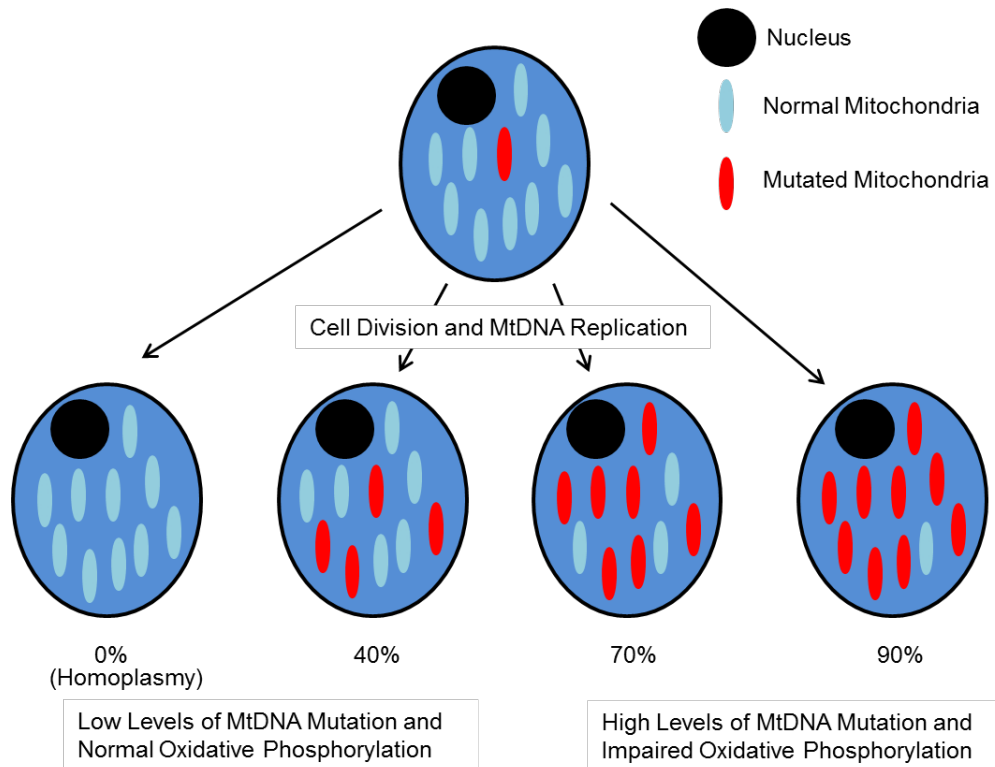


Figure 1.10. Homoplasmy and heteroplasmy.

Following cell division and mtDNA replication, the distribution of normal and mutated mitochondria may differ. Mitochondria segregate randomly into daughter cells and replicate. Some cells may exhibit homoplasmy, having all mitochondria with identical genomes. Other cells may exhibit heteroplasmy, having mitochondria with different genomes, some of which may contain mutations. Low levels of heteroplasmy do not usually affect the functions of the mitochondria. High levels of heteroplasmy can result in impaired oxidative phosphorylation, once a threshold level is reached, leading to signs of mitochondrial disease. Light blue mitochondria represent those containing wild type mtDNA. Red mitochondria represent those containing mutated mtDNA.

1.5.3 Clonal Expansion

Clonal expansion is the process by which mutations and deletions in the mtDNA can be expanded and the mutated mtDNA passed on to daughter mitochondria. This is a common process happening in normal tissues at the average rate of one expanded mtDNA point mutation per cell (Nekhaeva et al., 2002) but once the heteroplasmy threshold has been reached, impaired oxidative phosphorylation may lead to a clinical disease phenotype (Moslemi et al., 1998). If the mutation in question is not deleterious, it may form part of the natural genetic variation in an individual.

There have been a number of theories to explain how clonal expansion may lead to accumulation of mutated mtDNA molecules in multiple cells of a tissue. It has been proposed that a faster replication of small mtDNA molecules that contain deletions could lead to the accumulation of these mutated molecules (Wallace 1992). However this theory has been disregarded as mtDNA replication is not rate-limiting and there are long stages in-between mtDNA replication events (Shadel and Clayton 1997). The 'Vicious Cycle' hypothesis suggests that as mtDNA is more sensitive to damage by free radicals, more mtDNA mutations will occur (Bandy and Davison 1990). In tissues with a high oxygen consumption, such as the brain, there are high levels of mtDNA mutations (Arnheim and Cortopassi 1992). Therefore, there are more initial mtDNA mutations and a greater probability of a proportion of these reaching the threshold level. The 'survival of the slowest' hypothesis (De Grey 1997) is linked to the 'free radical hypothesis of ageing' first proposed in 1956 (Harman 1956). This early hypothesis stated that the damage inflicted on molecules by free radicals will result in the effect of ageing. This was later refined to include mitochondria as the main producers of free radicals. The 'survival of the slowest' hypothesis takes this further to state that those mitochondria with impaired oxidative phosphorylation will be subject to less degradation as their production of free radicals is slower. However, this theory is not considered to be consistent with known theories of mitochondrial fission and fusion and the preferential degradation of dysfunctional mitochondria (Kim and Lemasters 2011).

The most satisfactory theory currently being investigated is the theory of random genetic drift, whereby a mutation may reach very high levels or very low levels due to stochastic events (Chinnery and Samuels 1999; Elson et al., 2001). Computational modelling has shown that mutation loads can increase to levels seen in human biological samples due to random genetic drift alone through relaxed replication (Elson et al., 2001). However, random genetic drift is not a general explanation because in computer simulations with short-lived animals the results do not match the observed

heteroplasmy levels (Kowald and Kirkwood 2013). Random genetic drift may not represent a stand-alone theory and other mechanisms may be at work in other animal species.

1.5.4 *Mitochondrial DNA Mutation Rates*

The mitochondrial genome is a circular construct attached to the inner mitochondrial membrane. This makes it prone to damage by free radicals produced by the inner membrane's mitochondrial respiratory chain by their proximity to each other. It has been estimated that the mtDNA mutation rate in higher primates is ten times higher than for single-copy nuclear DNA, using cleavage mapping with restriction endonucleases (Brown et al., 1979). This higher mutation rate may be contributed to by the fact that the mitochondrial genome is not protected by histone proteins and does not contain introns (Margulis 1975) as well as the high error rate of the sole mitochondrial DNA polymerase, POLG (Kunkel and Loeb 1981). To counter this, the polymerase has DNA proof-reading abilities and the mitochondria have a DNA repair system that can repair damaged sections of mtDNA. It is thought this could occur by base excision repair (Pinz and Bogenhagen 1998).

The rate of mtDNA mutation accumulation depends upon the type of mutation and its location in the mitochondrial genome. The mutation rate is not equal for all areas of the mitochondrial genome and in areas of high percentages of purine bases there is a greater rate of mutation. This unequal mutation rate has been used in slower mutating regions, such as the D-loop control region of the mtDNA, for phylogenetic analyses and studies into sequence divergence (Richards et al., 2000; Howell et al., 2003).

1.5.5 *Mitochondrial DNA Mutations*

MtDNA mutations may occur sporadically in an individual or they may be inherited through the maternal germ cell line. These mutations can be associated with defective oxidative phosphorylation, ageing and neurodegeneration. There are different types of mutation that may occur in the mitochondrial genome; these include point mutations, rearrangements and deletions. In addition, the total copy number of mtDNA can be depleted within the cell and may itself lead to clinical disease.

1.5.5.1 Point Mutations

Point mutations are single base changes in the DNA sequence. These mutations may be described as synonymous, resulting in the same amino acid being translated despite a genetic alteration or as non-synonymous, with a genetic mutation resulting in a different amino acid being translated. Synonymous mutations are possible due to the redundancy of the genetic code and its property of different codons coding for the same amino acid, and also owing to the ability of a tRNA molecule to allow 'wobble' in the third base of the anti-codon matching to the codon.

The alteration of a single base can lead to amino acid substitution and changes to the protein's conformation, resulting in loss of function. For example, various mtDNA point mutations can cause mitochondrial encephalomyopathy, lactic acidosis, and stroke-like episodes (MELAS), a devastating, multisystemic illness that will be later described in section 1.6.3.1 '*Mitochondrial Encephalomyopathy, Lactic Acidosis, and Stroke-Like Episodes (MELAS)*'. MELAS is an example of genetic heterogeneity and the capability of different mutations in different genes to result in clinically similar symptoms.

Currently there are over 20 mutations reported in different mitochondrial genes leading to MELAS. Examples include the common single point mutation m.3243A>G in the tRNA leucine^(*UUR*) gene (*MT-TL1*) (Goto et al., 1990) and recently a case of MELAS in a 35-year-old woman which was reported due to the pathogenic point mutation m.6597C>A in the *MT-COI* gene (Lamperti et al., 2012).

Myoclonic epilepsy with ragged red fibres (MERRF) is a rare condition that will be later described in section 1.6.3.2 '*Myoclonic Epilepsy with Ragged Red Fibres (MERRF)*'.

The eponymous 'ragged red fibres' are due to damaged mitochondria aggregating in the subsarcolemmal region of the muscle fibres, which can be visualised as red clumps when stained with modified Gömöri trichrome stain. As in MELAS, there is a genetic heterogeneity in MERRF with mutations in different mitochondrial genes giving rise to clinically similar symptoms. The most common single point mutation m.8344A>G in the tRNA lysine gene (*MT-TK*) (Shoffner et al., 1990) occurs in 80-90% of cases and the mutations m.8356T>C and m.8363G>A occur in most other reported cases. However novel mutations such as m.661G>A in tRNA phenylalanine (Mancuso et al., 2004) demonstrate the clinical overlap that can occur between mutations in different genes.

In addition to point mutations in tRNA genes, mutations in protein-coding mitochondrial genes have been reported. These include the mutation m.8993T>G in complex V, leading to symptoms of neuropathy, ataxia, and retinitis pigmentosa (NARP) (Holt et

al., 1990) and the mutations m.11778G>A, m.3460G>A, and m.14484T>C in complex I leading to Leber's hereditary optic neuropathy (LHON) (Wallace et al., 1988; Howell et al., 1991; Johns et al., 1992).

1.5.5.2 Rearrangements

Mitochondrial rearrangements are sporadic and can include several genes. The types of rearrangement that can occur include large-scale deletions, microdeletions, and duplications.

1.5.5.2.1 Duplications

Mitochondrial DNA duplications have been associated with disease, with the first reported duplication being implicated in a mitochondrial disease in 1989 (Poulton et al., 1989). MtDNA duplications have been associated with Kearns-Sayre syndrome (Poulton et al., 1994; Fromenty et al., 1997), mitochondrial myopathy (Brockington et al., 1993), and diabetes mellitus (Ballinger et al., 1994).

It has been suggested that both duplications and deletions on mtDNA molecules are part of the same process, and that duplications are an intermediate stage in the formation of a deletion (Poulton et al., 1993). This is supported by the observation that both duplication and deletion rearrangements can occur at the same time in the same patient (Manfredi et al., 1997; Kajander et al., 2000), though this relationship is still not clear and warrants further investigation.

1.5.5.2.2 MtDNA Deletions

Deletions found in mtDNA may be of two forms; microdeletions of <5bp, or large-scale deletions encompassing many genes. Both can result in mitochondrial disease depending on the exact size and location of the deletion. MtDNA deletions have been implicated in many mitochondrial diseases and in ageing, with post-mitotic tissues accumulating deletions over time leading to impaired oxidative phosphorylation. It has been noted that post-mitotic tissues with high oxygen consumption, such as the brain and skeletal muscle, acquire higher levels of mtDNA deletion (Arnheim and Cortopassi 1992) and that different areas of the brain may have different levels of deletion (Soong et al., 1992).

Deletions have been reported in association with disease and ageing. In the major arc of the mitochondrial genome there is a 5Kb section that can often be found to harbour deletions (Hayakawa et al., 1992). A deletion over 5Kb section can encompass many

genes, including tRNAs and those that code for subunits of complex I and complex IV that are vital to the function of the mitochondrial respiratory chain.

MtDNA deletions have been reported in numerous disorders including Kearns-Sayre syndrome (Zeviani et al., 1988) and adPEO (Van Goethem et al., 2001) in the form of single deletions thought to have occurred sporadically. In addition, mtDNA deletions have been associated with ageing. Both mtDNA deletions and duplications, as well as tissue mosaicism of these rearrangements, have been observed in human ageing (Kovalenko et al., 1998).

1.5.5.3 MtDNA Depletion

MtDNA depletion is caused by a quantitative loss of mtDNA content leading to impaired oxidative phosphorylation in affected tissues due to insufficient production of the core respiratory chain components.

MtDNA depletion is often caused by nuclear gene defects in the replication machinery (*POLG*, *c10orf2*) and in mtDNA maintenance genes (*TYMP*, *TK2*, *SUCLA2*, *SUCLG1*, *RRM2B*, *DGUOK*, *ANT1*). These mutations may result in fewer replicated mtDNA molecules, or a lower dNTP pool of one or more dNTPs so that there is limited availability for incorporation during mtDNA replication.

MtDNA depletion syndromes often occur in early life and can be described in four different categories: myopathic syndromes, encephalopathic syndromes, hepatocerebral syndromes, and neurogastrointestinal syndromes. However, clinical disorders may be placed in overlapping categories. Mutations in genes of the replication machinery such as *POLG* have been reported to result in mtDNA depletion in Alpers' syndrome (Naviaux et al., 1999) through replication stalling. Mutations in genes involved in mtDNA maintenance such as *ANT1* can lead to mtDNA depletion in adPEO (Napoli et al., 2001). Mutations in *TYMP* can lead to MNGIE (Nishino et al., 1999), as can mutations in *RRM2B* (Shaibani et al., 2009).

Treatments and therapies of mtDNA depletion are usually symptomatic. Experimental studies have shown a rescue of cells with mtDNA depletion with the addition of excess dNTPs (Cámara et al., 2013) or the addition of deoxynucleoside monophosphates (dNMP) to cell culture medium (Bulst et al., 2009). Addition of inhibitors of dNTP catabolism may be another possible therapy. A greater understanding of the structural and functional consequences of mutations upon these genes is essential to realising their full effect in mtDNA depletion syndromes.

1.6 Mitochondrial Disease

Mitochondrial diseases may be sporadic, with a single proband in a family, or there may be demonstrable familial inheritance with a clear pattern of inheritance. The first human mitochondrial disease was described by Luft in 1962, of a patient suffering from severe hypermetabolism with increased perspiration, polydipsia, polyphagia, a decrease in body weight, and muscle weakness (Luft et al., 1962). Since then, there have been hundreds of different mitochondrial diseases described in the scientific literature. These may be described as a primary mtDNA disease if the condition is due to a mutation or deletion of the mtDNA, or a secondary mtDNA disease if the condition is due to a mutation or deletion of a nuclear gene which has a direct effect on mtDNA maintenance.

1.6.1 Mitochondrial Disease Prevalence

Mitochondrial disorders are an underdiagnosed group of diseases that create a significant burden of disease upon the population. The prevalence of these disorders is difficult to determine accurately due to the wide range of symptoms and gene mutations, but it has been estimated that at least one in every two hundred healthy members of the population harbours a pathogenic mitochondrial mutation (Elliott et al., 2008). A study of the North-East of England showed that 9.2 individuals in 100,000 people had a manifest mitochondrial disease while 16.5 individuals in 100,000 were at risk of developing one (Schaefer et al., 2008). In both studies, the most common mutation found was the m.3243A>G mtDNA mutation which can lead to MELAS.

Mitochondrial disease is a relatively new branch of disorders and further research into the prevalence of mitochondrial disease in different populations is needed to increase our understanding.

1.6.2 Mitochondrial Disease due to Nuclear Gene Mutations

Mitochondrial diseases are genetic disorders affecting mitochondrial metabolism. Many proteins that are required for mitochondrial function are encoded by nuclear genes. Mutations in these genes can give rise to abnormal proteins and when the proteins are imported into the mitochondria, that protein may be dysfunctional and affect mitochondrial processes, manifesting as signs of mitochondrial disease. It is important that rigorous research is carried out to demonstrate whether any mutations discovered are actually pathogenic, or if they are merely part of natural genomic variation. The most common disorders arising from mutations in nuclear genes are discussed below.

1.6.2.1 Leigh Syndrome

Leigh syndrome (subacute necrotising encephalopathy) is an early-onset neurodegenerative disease with brainstem and basal ganglia dysfunction, first described by neuropathologist Dr Archibald Denis Leigh in 1951 (Leigh 1951). Most patients present in infancy with failure to thrive, hypotonia and developmental delay. Involvement of the brainstem and basal ganglia is particularly characteristic and often leads to dystonia, dysphagia, ptosis or abnormal eye movements and breathing difficulties (Finsterer 2008). Other clinical features may include developmental regression, ataxia and seizures.

There is a range of mutations in many genes reported to lead to Leigh syndrome, with the pattern of inheritance appearing to be complex. Mutations in the nuclear gene *SURF1* have been reported to lead to a Leigh's syndrome phenotype with autosomal recessive inheritance (Tiranti et al., 1998; Zhu et al., 1998). *SURF1* encodes one of a large number of assembly factors of complex IV, which is required to maintain the structure of complex IV. Loss of complex IV will lead to isolated complex IV deficiency and a reduced OXPHOS capacity.

1.6.2.2 Mitochondrial Neurogastrointestinal Encephalomyopathy (MNGIE)

Mitochondrial neurogastrointestinal encephalomyopathy (MNGIE) is an autosomal recessive disorder clinically presenting with gastrointestinal dysmotility, cachexia, ophthalmoplegia, sensorimotor neuropathy, and leukoencephalopathy.

Mutations in the gene encoding thymidine phosphorylase (*TYMP*) have been frequently implicated in MNGIE (Hirano et al., 1998; Nishino et al., 1999; Suh et al., 2013).

Thymidine phosphorylase plays a key role in the nucleotide salvage pathway of mtDNA and loss of function of this gene can lead to an imbalance in the dNTP pool, causing mtDNA instability, mtDNA deletions and mtDNA depletion. Mutations in another gene, *RRM2B*, encoding ribonucleotide reductase have also been purported to be the genetic cause of MNGIE in a patient with normal levels of thymidine (Shaibani et al., 2009).

1.6.3 Mitochondrial Disease due to Mitochondrial Gene Mutations

Mitochondrial disease may arise due to mutations in genes of the mitochondrial genome. There are 37 genes encoded by the mitochondrial genome, coding for essential subunits of the respiratory chain, tRNAs, and rRNAs. The disorders arising from mutations in mitochondrial genes are discussed below.

1.6.3.1 Mitochondrial Encephalomyopathy, Lactic Acidosis, and Stroke-Like Episodes (MELAS)

Mitochondrial encephalomyopathy, lactic acidosis, and stroke-like episodes (MELAS) is a common mitochondrial condition associated with muscle pain, fatigue, migraine, epilepsy, and stroke-like episodes leading to dementia. There are currently over 20 mutations in different mitochondrial genes leading to MELAS reported on the MITOMAP mitochondrial genome database website

(<http://www.mitomap.org/MITOMAP>).

The most common single point mutation is m.3243A>G in the tRNA leucine^(UUR) gene (*MT-TL1*) (Goto et al., 1990) which is the genetic basis of the condition in the majority of cases. As further research into mitochondrial disease continues, novel mutations are being reported in cases of MELAS. The point mutation m.6597C>A in the *MT-COI* gene for complex IV subunit I has been reported (Lamperti et al., 2012) and the point mutation m.12299A>C which had not previously been described in MELAS in the tRNA leucine^(CUN) gene (Abu-Amro et al., 2006).

MELAS is an example of a disorder with genetic heterogeneity and as further cases are investigated, the understanding of the genetic basis of MELAS will broaden.

1.6.3.2 Myoclonic Epilepsy with Ragged Red Fibres (MERRF)

Myoclonic epilepsy with ragged red fibres (MERRF) leads to muscle fatigue, myoclonic epilepsy, exercise intolerance, and hearing loss (Fukuhara et al., 1980). A modified Gömöri trichrome stain may be used to visualise ragged red fibres. These are damaged mitochondria that aggregate in the subsarcolemmal region of the muscle fibre.

The most frequent mutation associated with MERRF is a single point mutation at m.8344A>G in the tRNA lysine gene (*MT-TK*) (Shoffner et al., 1990; Noer et al., 1991). It occurs in 80-90% of cases, with the other mutations m.8356T>C and m.8363G>A occurring in most other reported cases (Silvestri et al., 1992; Ozawa et al., 1997). In

addition to the common mutations, a novel mutation has been reported in the tRNA phenylalanine gene, m.661G>A (Mancuso et al., 2004).

1.6.3.3 Leber's Hereditary Optic Neuropathy (LHON)

Leber's hereditary optic neuropathy (LHON) is characterised by a bilateral loss of central vision due to retinal ganglion cell degeneration and retinal microangiopathy, with some patients displaying dystonia or cardiac dysrhythmia. Some patients may also display the cardiac pre-excitation condition of Wolff-Parkinson-White syndrome (Nikoskelainen et al., 1994; Finsterer et al., 2001). There is a teenage-onset to late-onset of symptoms with incomplete penetrance of the disorder, with symptoms occurring in ~50% of males and ~10% of females with the mutation (Harding et al., 1995; Riordan-Eva et al., 1995). Symptoms are predominantly reported in males harbouring a mutation at close to 100% homoplasmy, though females may also demonstrate a mutation close to 100% homoplasmy but may be asymptomatic. There is currently no test to accurately determine which patients with a mutation will display the LHON phenotype.

There are 3 primary mutations in the mitochondrially-encoded subunits of complex I which have been reported to cause LHON; m.3460G>A in *MT-ND1* (Howell et al., 1991), m.11778G>A in *MT-ND4* (Wallace et al., 1988), and m.14484T>C in *MT-ND6* (Johns et al., 1992), all affecting complex I which account for the genetic defect in the majority of cases. Many rarer mutations have been reported to cause LHON, all located in the mitochondrial complex I genes (Achilli et al., 2012; Caporali et al., 2013). These mutations are commonly reported at, or close to, 100% homoplasmy in patients, though not all patients will display the clinical signs.

1.6.3.4 Maternally Inherited Leigh Syndrome

Leigh syndrome is an early-onset neurodegenerative disease that has been described previously (see section 1.5.2.1 'Leigh Syndrome'). There is a range of mutations in many genes reported to lead to Leigh syndrome, with the pattern of inheritance appearing to be complex. Maternal inheritance of Leigh's syndrome occurs if the mutation is present in a mitochondrial gene, as mtDNA is maternally inherited. Point mutations in the mitochondrial gene *MT-ATP6* account for a large proportion of cases of maternally inherited Leigh syndrome and high levels of heteroplasmy are required to result in disease symptoms (Tatuch et al., 1992).

1.6.4 Complex Genetic Inheritance

The inheritance of mitochondrial disease can be complex and a single mitochondrial disorder may have multiple modes of inheritance. Leigh syndrome may be maternally inherited through mutations in the mitochondrial gene *MT-ATP6* or mitochondrial tRNA genes, may have autosomal recessive inheritance, or may display an X-linked Mendelian inheritance through pyruvate dehydrogenase deficiency due to mutations in the *PDHA1* gene (Rahman et al., 1996). Some of these modes of inheritance in Leigh syndrome have been described previously in this thesis (see sections 1.5.2.1 'Leigh Syndrome' and 1.5.3.4 'Maternally Inherited Leigh Syndrome').

1.6.4.1 Chronic Progressive External Ophthalmoplegia (cPEO)

Chronic progressive external ophthalmoplegia (cPEO) is a late-onset disorder that may be diagnosed as a single condition or diagnosed in association with another disorder. It is characterised by bilateral ptosis, ophthalmoplegia, and muscle weakness (Laforêt et al., 1995) with additional signs that may include neurological involvement. It is often seen in association with other disorders and is assessed as part of a wider range of symptoms. Both single large-scale deletions and secondary mtDNA deletions due to mutations in *POLG* and *c10orf2* may lead to cPEO.

Single large-scale mtDNA deletions in muscle tissue have been previously described in patients with cPEO (Holt et al., 1988; Moraes et al., 1989). Mutations in nuclear genes which are involved in mtDNA replication and repair can lead to multiple mtDNA deletions. MtDNA replication genes, including *c10orf2* (Twinkle) (Lewis et al., 2002), *POLG* (Van Goethem et al., 2001), and *ANT1* (Kaukonen et al., 2000) have been implicated in cPEO. Rare mutations in *POLG2* have been described which may be responsible for a small percentage of PEO cases in adults (Longley et al., 2006; Walter et al., 2010).

Mutations in tRNA genes have also been implicated as the cause of the disease (Gupta et al., 1995; Laforêt et al., 1995) which highlights the range of genetic defects that may correlate with the same clinical signs.

1.7 Mitochondrial DNA Polymerase Gamma (POLG)

Mitochondrial DNA polymerase gamma (POLG) is the only known DNA polymerase to replicate mtDNA in mammals and is essential for embryonic development (Hance et al., 2005). It comprises a large catalytic subunit and two smaller beta subunits. The large catalytic subunit is encoded by the nuclear gene *POLG*, located on chromosome 15q25 (Walker et al., 1997), which comprises 23 exons and is 21Kb long.

Like the catalytic subunit, the accessory subunit has also been shown to be essential for mammalian embryogenesis and at least one functional copy of the gene must be present for embryonic development (Humble et al., 2013). The smaller beta subunits are encoded by the nuclear gene *POLG2* located on chromosome 17q23 comprising 8 exons. Pathogenic mutations in the catalytic subunit *POLG* may be either dominant or recessive and are a major cause of mitochondrial disease, displaying a heterogeneous range of disease phenotypes.

1.7.1 Structure of POLG Polymerase

Human POLG polymerase was first cloned, sequenced and characterised using cDNA to sequence the gene and polyclonal antibodies to verify the findings (Ropp and Copeland 1996). It is comprised of two different subunits: a 140kDa catalytic α subunit encoded by the gene *POLG* and a 55kDa accessory β subunit encoded by the gene *POLG2*. These form a heterotrimer made up of one catalytic (α) subunit and two accessory (β) subunits to form the functional holoenzyme (Yakubovskaya et al., 2006) (Figure 1.11).

Both accessory subunits bind together and bind asymmetrically to one face of the catalytic subunit, where they position the accessory interacting subdomain (AID) of the catalytic subunit to bind to DNA. Through examining the crystal structure of the POLG holoenzyme, it has been shown that one of the accessory subunits interacts with the spacer/linker domain of the catalytic α subunit to bind both accessory subunits there (Lee et al., 2009).

The accessory subunits are processivity factors that enhance the function of the catalytic subunit and increase substrate binding (Carrodeguas et al., 1999). They can also confer resistance to N-ethylmaleimide (Lim et al., 1999) which can inhibit polymerase activity. Each of the accessory subunits has been found to have a slightly different function in the holoenzyme, with the proximal accessory subunit allowing

better interaction with the DNA strand, and the distal accessory subunit increasing the DNA replication rate (Lee et al., 2010).

They also have a novel function to other polymerase processivity factors. In addition to accelerating the polymerisation rate, they are thought to suppress exonuclease activity to possibly allow for a more stable polymerase conformation (Johnson and Johnson 2001). This will decrease the fidelity of the polymerase, as the catalytic subunit will extend a mismatched primer to homopolynucleotide sequences more frequently with the presence of the accessory subunit (Longley et al., 2001).

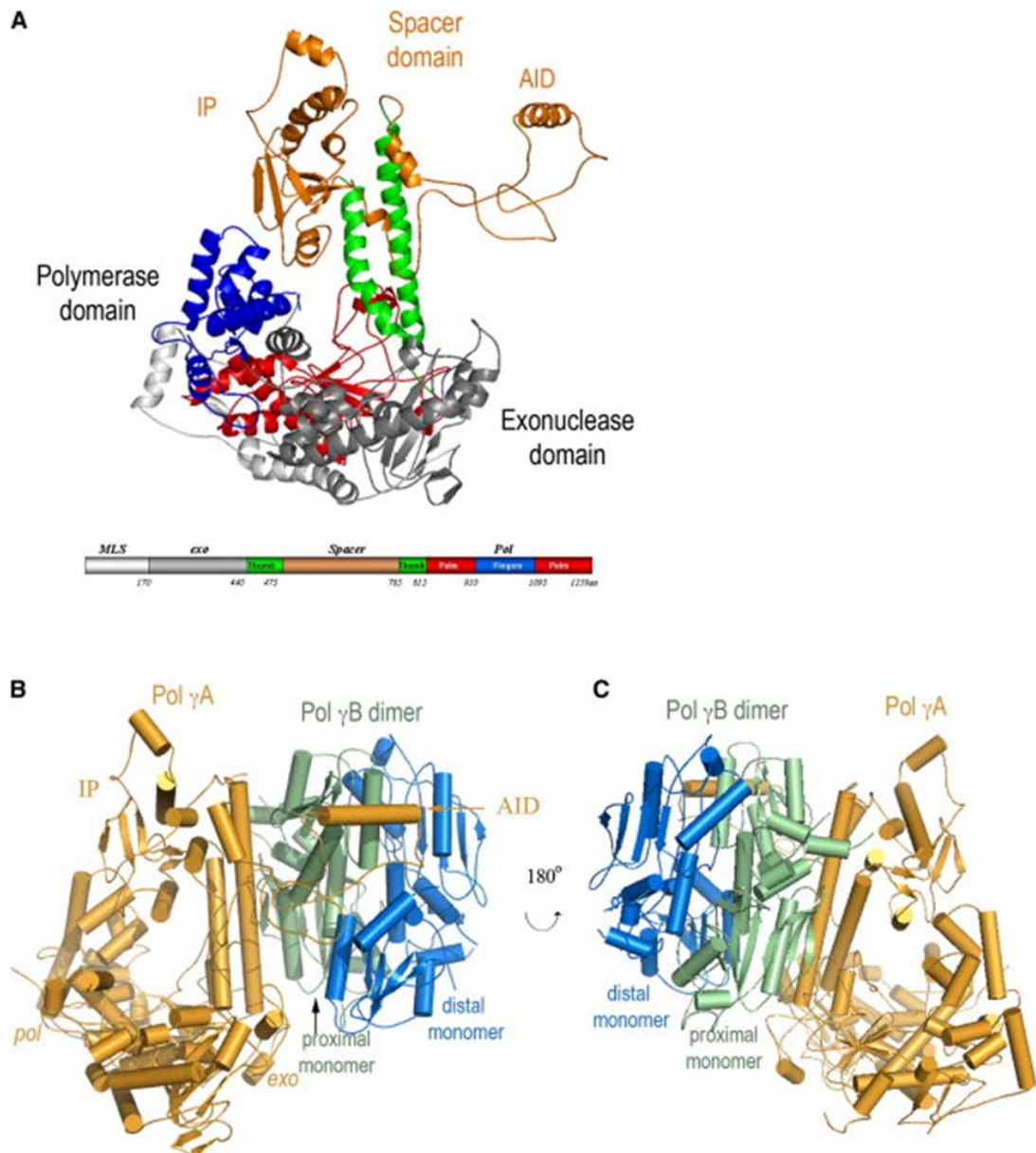


Figure 1.11. Structure of POLG.

Image A shows the structure of POLG polymerase and the gene, and the location of the exonuclease, spacer, and polymerase domains in their relation to the polymerase. AID refers to the accessory interacting subdomain and IP refers to the intrinsic processivity subdomain. Images B and C show POLG in association with the proximal and distal POLG2 subunits, forming the functional heterotrimer. Image taken from Lee et al., (2009).

1.7.2 Functions of POLG

POLG polymerase is a type A DNA polymerase that can perform a range of functions. Its primary function is 5'-3' DNA-synthesising activity and in addition to replicating DNA, it also plays a role in 3'-5' base excision repair and has 5'-dRP lyase activity for excision repair. Base excision repair is thought to be the only mechanism of DNA repair to occur in mitochondria requiring POLG and mtDNA ligase (Pinz and Bogenhagen 1998). This mechanism repairs single base lesions; the base is excised leaving an abasic site and a new base is incorporated by POLG. A mitochondrial AP endonuclease creates a nick in the phosphodiester backbone of the DNA to allow incorporation of the new base while mitochondrial DNA ligase repairs the phosphodiester bonds after repair. The 5'-dRP lyase activity of POLG can remove the 5'-dRP molecule left by the AP endonuclease cleavage during base excision.

The different functions are performed by the three distinct domains of the catalytic subunit of the polymerase. The N-terminal domain contains an exonuclease region which has 3'-5' base-excision repair activity to remove misincorporated bases. There is a linker/spacer region considered to be involved in binding the catalytic (α) subunit to the accessory (β) subunits, and a C-terminal polymerase region with 5'-3' DNA-synthesising activity. Based upon molecular and computer modelling data, it has been suggested that there are five distinct and functional domains of the polymerase where recessive mutations can occur and may result in disease (Euro et al., 2011).

Understanding the effect that pathogenic mutations have upon the function of POLG is essential to unravelling the full effect of a mutation in the heterogeneous group of mitochondrial diseases.

1.7.3 POLG Mutation Frequency

Pathogenic mutations in the *POLG* gene regularly occur in the linker or polymerase regions and this may affect the way the catalytic subunit and accessory subunit bind or how the polymerase binds to the substrate. There have been over 230 mutations listed on The Human DNA Polymerase Gamma Mutation Database (<http://tools.niehs.nih.gov/polq/>) (Figure 1.12). There are 3 common pathogenic mutations in *POLG* that are often seen in patients with a heterogeneous range of symptoms, from severe, early-onset conditions, to milder, adult-onset symptoms; p.Ala467Thr, p.Trp748Ser and p.Gly848Ser.

A study to investigate *POLG* gene mutations in patients from around Europe examined 38 cases of *POLG* disease and sequenced the *POLG* gene in each. They reported that the most common mutation in children was the p.Ala467Thr mutation (Horvath et al., 2006). A Dutch patient cohort of 37 cases with *POLG* mutations reported that the p.Ala467Thr mutation occurred 23 times in 74 alleles in 15 patients, occurring in 31% of all alleles. Two hundred controls were tested and the p.Ala467Thr mutation was not seen (Blok et al., 2009). After analysing intronic SNPs and polymorphic dinucleotide markers flanking the *POLG* gene, it is suggested that founder effects for the p.Ala467Thr mutation have led to its frequency in different populations (Hakonen et al., 2007).

The carrier frequency of the p.Trp748Ser mutation in *cis* with the p.Glu1143Gly mutation in the Finnish population was reported to be 1:125 in patients diagnosed with mitochondrial recessive ataxia syndrome (MIRAS), due to a founder effect (Hakonen et al., 2005). That is a frequency of 1:62,500 for homozygotes for the p.Trp748Ser mutation from Finland (Uusimaa et al., 2008). Subsequently, founder effects have also been identified for the p.Trp748Ser mutation in patients diagnosed with Alpers' syndrome and MIRAS in Australian and New Zealand populations (Hakonen et al., 2007).

A Chinese cohort of 265 patients with adult-onset ataxia was investigated for the p.Ala467Thr and p.Trp748Ser mutations. Interestingly, no mutations were reported in any of the patients, suggesting that these mutations are rare causes of adult-onset ataxia in Taiwan (Lee et al., 2007) and that population genetics are important to consider when searching for pathogenic mutations.

There has been very little data published on the frequency of a third common *POLG* mutation, p.Gly848Ser. Many case studies report it as a recessive mutation in patients but population studies have not yet been fully conducted. Data on the population frequency of *POLG* mutations is an expanding field, though more investigation is needed into the frequency of other common mutations to further understand the impact of pathogenic mutations upon the population.

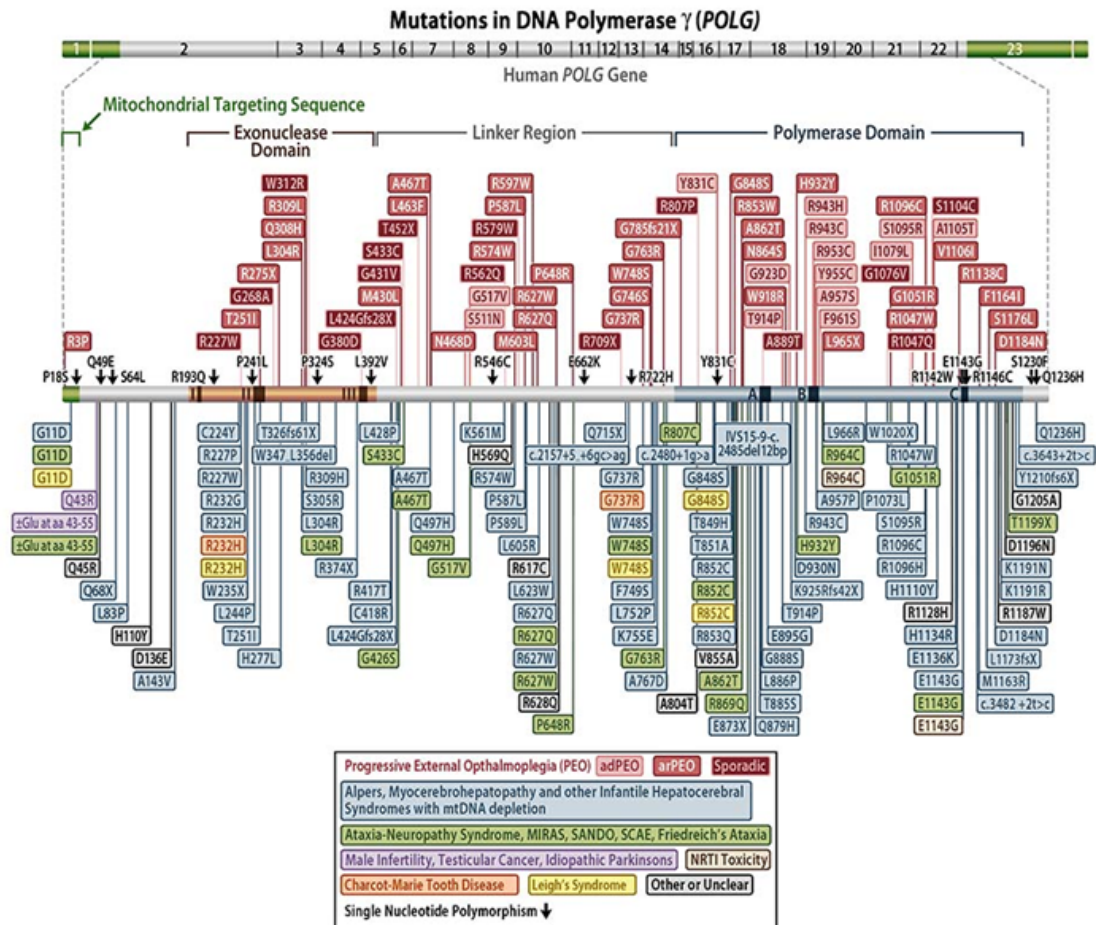


Figure 1.12. Mutations in POLG.

Mutations in POLG have been associated with a heterogeneous range of disorders. Image taken from The Human DNA Polymerase Gamma Mutation Database at <http://tools.niehs.nih.gov/polg/>. Database accessed 31-03-2014.

1.7.4 *POLG Disorders*

Mutations in *POLG* can lead to a large, heterogeneous group of disorders, each displaying a varied phenotype and age of onset (Table 1.2). These may include disorders on the myocerebrohepatopathy (MCHS) spectrum, such as Alpers' syndrome which is mentioned in further detail in section 1.9 '*Alpers' Syndrome*', and myoclonic epilepsy myopathy sensory ataxia (MEMSA) spectrum. As further research is carried out, mutations in *POLG* are found to be the genetic cause of a growing number of conditions. *POLG* mutations may be reported in a small number of patients diagnosed with a condition but it is vital to recognise this phenotypic spectrum in order to understand the underlying mechanism of manifestation of mitochondrial disease in different patients.

Both dominant and recessive mutations in *POLG* can lead to clinical signs of mitochondrial disease. An example of a condition that may be due to either dominant or recessive *POLG* mutations is PEO; autosomal dominant PEO (adPEO) is due to dominant mutations (Van Goethem et al., 2001; Graziewicz et al., 2004) and displays the phenotype of ophthalmoplegia and ptosis which may cosegregate with other conditions (Luoma et al., 2004), while all other forms of PEO are due to recessive mutations (arPEO) and may display more severe symptoms than in adPEO (Van Goethem et al., 2001; Van Goethem et al., 2003). When arPEO is associated with additional symptoms, such as neurological or multisystem abnormalities, it is termed PEO+. PEO has been previously described in detail in section 1.6.4.1 '*Chronic progressive external ophthalmoplegia (cPEO)*'.

The role of *POLG* mutations in some conditions is under investigation. In some cases of male infertility it has been suggested that *POLG* mutations may be the underlying cause. There have been published reports of microsatellite repeat size leading to sperm quality defects (Rovio et al., 2001; Baklouti-Gargouri et al., 2012). However, this is disputed and other studies have reported that there is no correlation between the *POLG* CAG microsatellite and male infertility (Rani et al., 2009; Poongothai 2013). The suggestion that mutations in *POLG* may lead to male infertility is still unclear. Mutations in *POLG* have also been reported to affect female fertility. Premature ovarian failure (POF) has been associated with *POLG* mutations in patients with premature menopause. POF has been reported in association with other disorders such as PEO and parkinsonism (Luoma et al., 2004). The mutation p.Tyr955Cys has been reported to segregate with POF, PEO and mtDNA depletion in the same family lineage (Pagnamenta et al., 2006).

Where two recessive mutations cannot be found in *POLG*, other forms of genetic rearrangement may account for a disease which increases the range of known *POLG* mutations that may lead to disease. The use of quantitative multiplex PCR with short fluorescent fragments to detect large-scale deletions in patients can be employed to search for alternative aetiology. A large-scale deletion of part of intron 21 and exon 22 in *POLG* was detected in a patient diagnosed with Alpers' syndrome using this technique (Rouzier et al., 2013).

There have been two reported findings of Leigh syndrome due to *POLG* mutations (Naess et al., 2009; Taanman et al., 2009). The spectrum and overlap of possible phenotypes is important and is highlighted in a report of a patient initially diagnosed on the myocerebrohepatopathy (MCHS) spectrum, which then evolved into an Alpers' syndrome-like phenotype with neuropathology typical of Leigh syndrome (Scalais et al., 2012). The possible involvement of *POLG* in Leigh syndrome is an area of investigation.

It is currently unclear why it should be that combinations of mutations common to more than one disease should produce such varied phenotypes.

Disorder	Clinical Phenotype	Early/Late Onset	Reported Mutations*	Publication
Alpers' Syndrome	Refractory seizures; psychomotor regression; ataxia; liver failure	Early-onset	p.Ala467Thr; p.Trp748Ser; p.Gly848Ser	(Naviaux and Nguyen 2004)
Ataxia-Neuropathy	Ataxia; loss of sensation	Early to late-onset	p.Pro765Thr	(Bostan et al., 2012)
Charcot-Marie Tooth Disease	Muscle wasting; loss of sensation	Early-adult to late-onset	p.Arg232His; p.Gly737Arg	(Harrower et al., 2008)
Friedreich's Ataxia	Ataxia; muscle weakness; dysarthria; scoliosis	Early-adult to late-onset	CAG repeats	(Heidari et al., 2008)
Leigh Syndrome	Seizures; ataxia; ophthalmoplegia	Early-onset	p.Arg232His; p.Trp748Ser; p.Gly848Ser; p.Arg852Cys	(Naess et al., 2009; Taanman et al., 2009)
MIRAS	Ataxia; epilepsy; ophthalmoplegia	Early to early-adult onset	p.Ala467Thr; p.Trp748Ser; p.Gln467His	(Winterthun et al., 2005)
MSCAE	Ataxia; epilepsy	Early to teenage onset	p.Thr419Pro; p.Trp748Ser	(Hinnell et al., 2012)
Parkinsonism	Tremor; hypokinesia; postural rigidity and instability	Early to late-onset	p.Ala1105Thr; p.Asn468Asp; p.Tyr955Cys	(Luoma et al., 2004)
adPEO	Ophthalmoplegia; ptosis	Late-onset	p.Tyr955Cys; p.Arg943His; p.Gly923Asp; p.Ala957Ser	(Van Goethem et al., 2001; Graziewicz et al., 2004)
arPEO	Ophthalmoplegia; ptosis	Late-onset	p.Ala467Thr; p.Leu304Arg; p.Arg627Trp	(Van Goethem et al., 2001; Van Goethem et al., 2003)
POF	Premature menopause	Late-onset	p.Tyr955Cys	(Pagnamenta et al., 2006)
SANDO	Dysarthria; ophthalmoplegia; ptosis	Teenage-Late-onset	p.Ala467Thr	(McHugh et al., 2010)
Testicular Cancer	Tumours	Late-onset	CAG repeats	(Nowak et al., 2005)

Table 1.2. Disorders arising from POLG mutations.

MIRAS= mitochondrial recessive ataxia syndrome, MSCAE= mitochondrial spinocerebellar ataxia and epilepsy, adPEO=autosomal dominant progressive external ophthalmoplegia, arPEO=autosomal recessive progressive external ophthalmoplegia, POF=premature ovarian failure, SANDO= sensory ataxic neuropathy with dysarthria and ophthalmoplegia. *= this is not an exhaustive list, for some conditions only the most common mutations have been listed.

1.8 POLG Mouse Models

There have been many mouse models produced to investigate mtDNA disease and its progression: transmitochondrial models (Mito-Mice), models of nuclear gene modifications that affect mitochondrial DNA maintenance (*ANT* models, *POLG* models, *TFAM* models, *c10orf2* models), and models of increased mtDNA copy by overexpression of a mtDNA maintenance gene (*TFAM*, *TK2*). These models display a variety of phenotypes which can resemble human disease, and which can allow investigations into mechanisms of mitochondrial disease that are currently unknown.

POLG is the only known polymerase to replicate mtDNA and impaired functioning due to mutations can introduce mtDNA deletions and depletion, leading to a range of disorders. Many mouse models have been created with different mutations in the three domains of *POLG* to allow studies into the many heterogeneous phenotypes that result from mutations in this gene.

A homozygous *POLG* $-/-$ mouse model was reported in which exon 3 was removed on both alleles of the gene through a beta-actin-*cre* system. This resulted in an embryonic lethal phenotype (Hance et al., 2005), proving the vital role this polymerase has in the cell.

The Mutator mouse model, a homozygous p.Asp257Ala knock-in model expressing a proof-reading-deficient version of *POLG*, was reported. The expression of the defective polymerase resulted in mtDNA mutations and an ageing phenotype, including weight loss, kyphosis, alopecia, anaemia, osteoporosis, and heart enlargement (Trifunovic et al., 2004). The ageing phenotype has been further explored through the mechanisms of age-related hearing loss, using this model. Mutator model mice showing accelerated ageing and hearing loss through degeneration of hair cells, spiral ganglion cells and stria vascularis of the cochlear duct, also showed increased mtDNA mutation rates (Yamasoba et al., 2007). In a following paper, they reported that the accumulation of mtDNA mutations may cause transcriptional alterations and increased apoptosis of cells leading to hearing loss (Someya et al., 2008). Ageing in relation to skeletal muscle

loss (sarcopenia) has been investigated using the Mutator mouse model. Reports showed a different protein expression profile in model mice and increased mitochondrial fission and autophagy compared to control mice, that contributes to sarcopenia (Joseph et al., 2013).

Tissue-specific transgenic mouse models have been genetically engineered to more closely resemble a disease phenotype. A heterozygote p.Asp181Ala transgenic mouse model was reported with a point mutation in the proofreading exonuclease domain of *POLG* which was expressed solely in cardiac tissue. The model showed an increased frequency of mtDNA mutations and deletions with normal mtDNA replication with an enlarged heart (Zhang et al., 2000). A subsequent study used a similar heterozygote p.Asp181Ala model to express defective *POLG* in the brain in order to look into cPEO, and found mood disorder-like symptoms and increased mtDNA mutations in neurons (Kasahara et al., 2006).

A heterozygous p.Tyr955Cys *POLG* transgenic mouse model was used to investigate chronic progressive external ophthalmoplegia (cPEO). This is a common mutation found in cPEO (Van Goethem et al., 2001). The *POLG* polymerase was overexpressed in the heart and cardiac cells showed mtDNA depletion, a reduction in mtDNA replication, and oxidative stress (Lewis et al., 2007).

POLG mouse models will further our understanding of disease progression and the effects of mutations on post-mitotic cells. The use of Cre-Lox recombination systems and use of specific promoters within the models allows for defective protein expression in specific cell types. This creates a level of control not previously known, tailoring the model's use to a tissue-type of interest. However, this technique is limited because it is not applicable to many *POLG* disorders. Many of the mouse models mentioned previously match an ageing phenotype and may be used successfully in investigations into the effects of ageing. When investigating disorders such as Alpers' syndrome, there is no mouse model with a matching phenotype.

1.9 Alpers' Syndrome

Alpers' syndrome is a rare autosomal recessive hepatocerebral disorder. The majority of patients present with symptoms in early childhood that include refractory epilepsy, developmental delay, ataxia, cortical visual abnormalities and subsequently a rapidly occurring neurological decline with a poor prognosis. Liver dysfunction and failure often occurs and in some cases it is considered to be linked to the use of the anti-epileptic drug, sodium valproate. The syndrome is caused by mutations in the mitochondrial DNA polymerase gamma gene, *POLG* (Naviaux et al., 1999), with the p.Ala467Thr, p.Trp748Ser, and p.Gly848Ser mutations being commonly noted and have become part of routine diagnostic testing when investigating *POLG* disorders. However there are emerging reports of patients displaying clinical variability in both the age of onset and gene involvement.

The syndrome was first described in 1931 through the work of Dr Bernard Alpers (Alpers 1931) and was later characterised to include involvement of the liver by Dr Peter Huttenlocher and colleagues (Huttenlocher et al., 1976). This is a rare disorder with The National Institute of Neurologic Disorders and Strokes estimating the incidence of Alpers' syndrome at 1/100,000 (Mangalat et al., 2012) (<http://www.ninds.nih.gov/disorders/alpersdisease/alpersdisease.htm>) and the preschool incidence being reported as 1/51,000 (Darin et al., 2001).

Neuropathological investigations of Alpers' syndrome have revealed neuronal cell loss, spongiosis and astrogliosis (Harding et al., 1995; Wiltshire et al., 2008) in both the cerebellum and cerebral cortex. White matter abnormalities have been infrequently reported as a pathological sign (Simonati et al., 2003b; Bao et al., 2008) but are an important consideration. Analysis of the mitochondrial respiratory chain has shown a reduced capacity for OXPHOS and a tissue specificity of this defect; liver shows this reduced capacity (Schaller et al., 2011), while skeletal muscle can show either a reduced capacity (Delarue et al., 2000) or normal results (Wiltshire et al., 2008). To date, there have been no reports in the literature of respiratory chain investigations in neurons of the brain in patients with Alpers' syndrome.

1.9.1 *Alternative Terms*

Alpers' syndrome (OMIM 203700) is also known by its alternative terms Alpers-Huttenlocher syndrome, progressive neuronal degeneration of childhood (PNDC), and progressive infantile poliodystrophy.

The term Alpers-Huttenlocher syndrome encompasses the clinical characterisation of patients by Dr Bernard Alpers and Dr Peter Huttenlocher. It is a term that has come to mean an Alpers' syndrome phenotype with involvement of the liver. Efforts to compare diagnostic techniques and genetic analyses between Alpers' syndrome and Alpers-Huttenlocher syndrome showed there are no important differences between the terms, and they should be used to describe the same condition (Harding 1990).

Progressive neuronal degeneration of childhood (PNDC) is a term used to describe what was seen in patients with the phenotype of Alpers' syndrome (Boyd et al., 1986; Harding et al., 1986; Egger et al., 1987; Harding 1990; Harding et al., 1995; Simonati et al., 2003a). Its use has endured until recent years and is used as a synonym of Alpers' syndrome. A similar term to PNDC had previously been used in the literature; 'diffuse cerebral degeneration' (Blackwood et al., 1963). The term PNDC should be considered synonymous with Alpers' syndrome and Alpers-Huttenlocher syndrome.

Progressive infantile poliodystrophy is a lesser used term used to report a patient described with Alpers' syndrome (Prick et al., 1982). An intermediate term of Alpers progressive infantile neuronal poliodystrophy has been used with the suggestion of naming an acute neonatal form of Alpers' syndrome as "Alpers' syndrome type 1" (Frydman et al., 1993). This did not become a commonly used term.

These alternative terms for Alpers' syndrome most likely arose at a time when the characterisation of Alpers' syndrome was becoming more commonly reported. They should not immediately be confused for separate neurological conditions but care should be taken when considering these cases in the current definition of Alpers' Syndrome. The recording of a single term to refer to this disorder should be used to minimise confusion.

1.9.2 *Involvement of POLG in Alpers' Syndrome*

The main mechanism behind the mtDNA defects in Alpers' syndrome is known to be caused by mutations in the nuclear gene *POLG* (Naviaux and Nguyen 2004). The first publication of a patient with Alpers' syndrome which linked mtDNA copy number with reduced activity of the *POLG* showed a severe mtDNA depletion with undetectable levels of polymerase activity (Naviaux et al., 1999). The assay used to detect the activity of the polymerase was the most sensitive assay available and tested on tissue homogenate from both liver and skeletal muscle. MtDNA copy number was assessed by a dual-label, slot-blot method, based on a previous method using dot blots hybridised with a radioactively-labelled mtDNA probe and a reference radioactively-labelled nDNA probe and the ratio measured (Poulton et al., 1995). Electron transport chain and citrate synthase assays showed a reduction in the activity of all complexes. This was the first molecular-based explanation of the mtDNA depletion in a patient with Alpers' syndrome.

With a better understanding of the clinical signs of Alpers' syndrome and widely-available genetic testing, reports of alternative genetic causes have been published. These alternative causes are discussed in greater detail in section 1.9.3 '*Involvement of non-POLG genes in Alpers' Syndrome*'. Mutations in *POLG* continue to be the most widely reported genetic defect in patients diagnosed with Alpers' syndrome. *POLG* disorders lead to a wide, heterogeneous range of clinical symptoms and understanding the effects of these mutations is vital.

1.9.2.1 *Phenotype and Genotype*

The genotype of an individual is expressed as the phenotype, modified by epigenetic factors such as the environment. In patients with the same *POLG* mutations, the onset and progression of disease can vary and there is no obvious and proven association between the genotype and clinical signs of *POLG* disease. The common mutation p.Ala467Thr can occur in a range of disorders; from severe paediatric disease that includes Alpers' syndrome (Nguyen et al., 2005) to milder late-onset disease that includes cPEO (Van Goethem et al., 2003).

It has been reported that there is an effect on survival time depending on the *POLG* mutation in patients with Alpers' syndrome; compound heterozygotes for the p.Ala467Thr /p.Trp748Ser mutations had a lower survival rate when compared to patients homozygous for either the p.Ala467Thr or p.Trp748Ser mutations (Tzoulis et al., 2006). Further observations have been reported that homozygous p.Ala467Thr

mutations occur more frequently in late-onset Alpers' syndrome (Naviaux and Nguyen 2004; Nguyen et al., 2006; Blok et al., 2009).

In addition, patients with a similar phenotype may in fact have different *POLG* mutations or even mutations in different genes. This highlights the heterogeneous phenotypes of *POLG* disease and the difficulty in creating discrete phenotypes based on genotype. There has been no persuasive argument to fully explain how mutations in a single gene can give rise to a number of heterogeneous phenotypes.

1.9.2.2 Common Mutations

There are currently over 230 mutations in *POLG* listed on the freely accessible database, The Human DNA Polymerase Gamma Mutation Database. This is available at <http://tools.niehs.nih.gov/polg/> and lists mutations in all 3 domains of *POLG*, including the mutations causing Alpers' syndrome (Figure 1.12). Any discrepancies between the mutations listed in Figure 1.13 and the current database may occur due to the fact that The Human DNA Polymerase Gamma Mutation Database is being constantly updated as research findings are reported. It is an important yet difficult task to prove that a mutation in the *POLG* gene is actually pathogenic and contributes to the disease phenotype. In the following sections, the common mutations found in *POLG* in the linker and polymerase regions are described. There are currently no commonly reported mutations associated with Alpers' syndrome in the exonuclease region, though they can occur in this domain in patients with Alpers' syndrome. Exonuclease mutations have been reported with high frequencies of mtDNA mutations owing to infidelity of DNA replication (Del Bo et al., 2003).

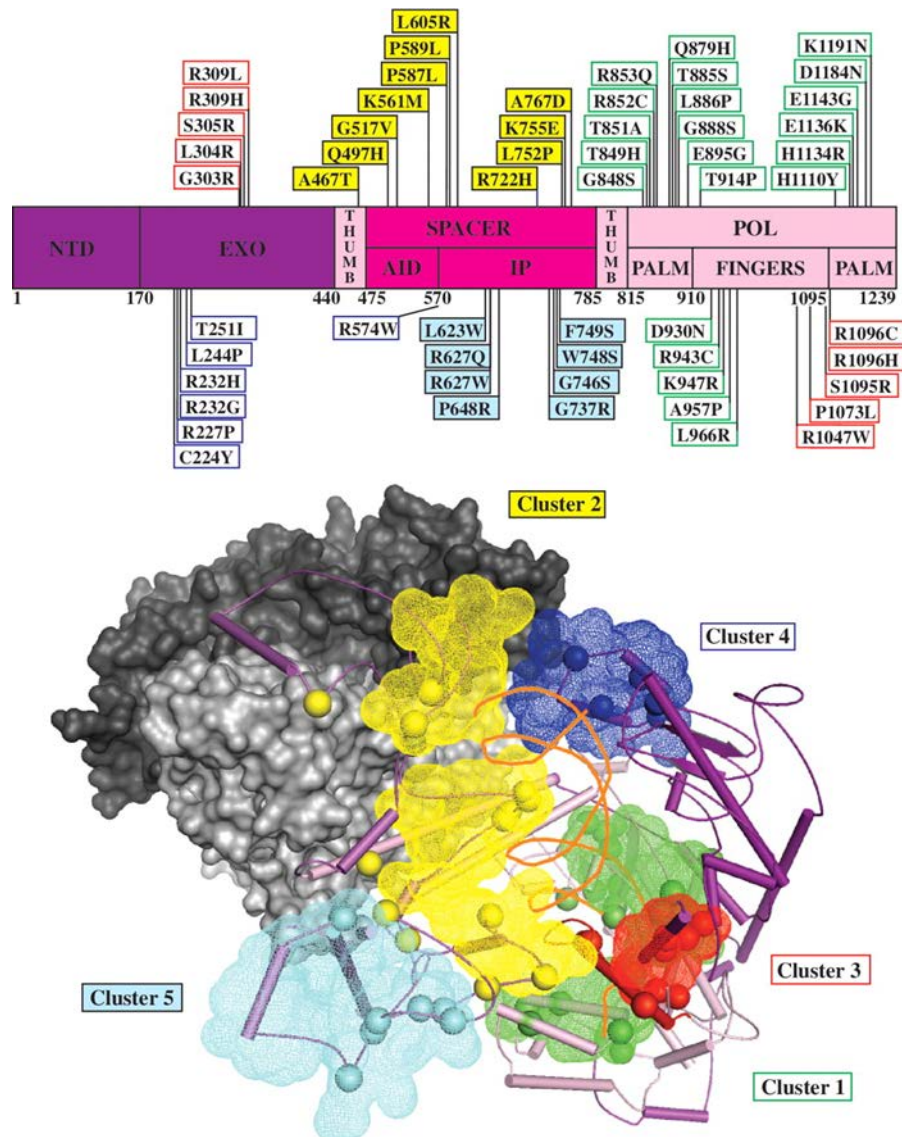


Figure 1.13. Mutations in *POLG* leading to Alpers' syndrome.

Top image depicts *POLG* gene showing the three main domains; the exonuclease domain, spacer region, and polymerase domain. The positions of mutations implicated in Alpers' syndrome are indicated and the colour of the box surrounding the mutation text refers to their inclusion in a cluster, depicted in the bottom image. NTD refers to the N-terminal domain, AID refers to the accessory interacting subdomain, IP refers to the intrinsic processivity subdomain. Bottom image illustrates *POLG* polymerase and its suggested five functional cluster groups. Image taken from Euro et al., (2011).

1.9.2.2.1 p.Ala467Thr Mutation

The p.Ala467Thr mutation is found in the linker/spacer domain of the *POLG* gene. This mutation is the most commonly reported and is implicated in a wide range of *POLG* disorders. This heterogeneity and phenotype overlap has led to suggestions that *POLG* disorders, including Alpers' syndrome, are a continuum of symptoms and not discrete phenotypes (Neeve et al., 2012).

This is considered to be the most common mutation associated with Alpers' syndrome. In a cohort of 15 patients and 20 published cases sequenced, the p.Ala467Thr mutation was the most frequent, on its own or in *trans* with other mutations (Nguyen et al., 2006).

In vitro assays of *POLG* protein with the p.Ala467Thr mutation showed that this mutation resulted in a polymerase with roughly 4% of the wild-type polymerase activity. The catalytic subunit failed to interact with the accessory subunit and so exhibited low processivity of DNA synthesis (Chan et al., 2005). This disruption may lead to the mtDNA deletion and depletion that result from this *POLG* mutation.

1.9.2.2.2 p.Trp748Ser Mutation

The p.Trp748Ser mutation is found in the linker/spacer domain of the *POLG* gene and it is a frequently reported mutation in Alpers' syndrome. It is often found in *cis* with the mutation p.Glu1143Gly but it is not thought that this mutation plays a role in disease progression. Polymerase containing this mutation has been shown to exhibit low levels of activity, low processivity, and poor DNA-binding capabilities but in fact polymerase containing only the p.Glu1143Gly mutation was 1.4-fold more active than wild-type polymerase (Chan et al., 2006).

Monoallelic expression of the p.Trp748Ser allele in a patient hemizygous for *POLG*, led to a more severe phenotype than patients homozygous for the p.Trp748Ser mutation (Naess et al., 2012). It is not clear why this should be and highlights the need for further studies into the function of mutations and the full extent of their effects upon disease progression.

1.9.2.2.3 p.Gly848Ser Mutation

The p.Gly848Ser mutation is found in the polymerase domain of the *POLG* gene. Mutations in this domain have been shown to reduce polymerase activity by up to 99% depending on where the mutation is exactly in this region (Kasiviswanathan et al., 2009). It has also been suggested from cultured fibroblast cells that mutations in the polymerase or exonuclease regions result in more mtDNA depletion than when mutations occur in the linker region of the *POLG* gene (Ashley et al., 2008).

1.9.3 Involvement of non-POLG genes in Alpers' Syndrome

Full sequencing of *POLG* can show no pathogenic mutations despite the occurrence of the clinical signs of Alpers' syndrome (Nguyen et al., 2006). There have been recent publications reporting mutations in genes other than *POLG* may lead to an Alpers' syndrome-like phenotype. Mutations in *FARS2* (mitochondrial phenylalanyl transfer RNA synthetase) has been implicated in some cases of Alpers' syndrome (Elo et al., 2012). In addition to this, mutations in the gene coding for Twinkle helicase, *C10orf2*, have been found in cases with an Alpers-like phenotype (Hunter et al., 2011).

It is expected that further reports will be published in future years and as the definition of Alpers' syndrome evolves and is redefined, so is our understanding of the underlying genetic causes.

1.9.4 Cells of the Central Nervous System

The architecture of the CNS is highly complex and is comprised of many different cell types. These primarily fall under the main categories of neuronal cells and glial cells, which include astrocytes, microglia, and oligodendrocytes. Glial cells are specialised, functioning in a specific role, for example microglia function in an immunological role in the CNS, and oligodendrocytes produce the myelin required to support and insulate neuronal axons and increase the rate of impulse conductivity. The brain is estimated to use 20% of body's energy sources for the production of ATP and its ATP requirements may fluctuate between different brain regions and under different physiological stresses. Mitochondria are required by each of these cell types for correct functioning. Mitochondrial dysfunction in glial cells has been studied less frequently than in neurons. A respiratory chain deficiency has been reported in astrocytes of patients with mitochondrial disease (Lax et al., 2012) and an abnormal mitochondrial morphology reported in activated microglial cells (Banati et al., 2004). In addition to the effect of mitochondrial dysfunction in neurons, mitochondrial dysfunction in astrocytes and microglia will be examined in this thesis.

1.9.5 Affected Tissues

It has been observed that there is a clear tissue-selectivity in Alpers' syndrome. Certain organs and tissues are more severely affected than others.

Published scientific literature on Alpers' syndrome frequently cites the brain and liver as the most severely affected organs. This is attributed to their highly ATP-dependent processes. Other organs are also involved to a lesser degree, including the pancreas, resulting in pancreatitis and diabetes mellitus, the nerves innervating the eyes causing blindness and ears causing deafness. Gastrointestinal pathology has also been reported (Kapur et al., 2011; Spiegler et al., 2011).

However, the literature has reported a mixed effect on skeletal muscle in patients with Alpers' syndrome. Reports of reduced respiratory chain activity in skeletal muscle (Naviaux et al., 1999) and reduced mtDNA levels (Uusimaa et al., 2008; Taanman et al., 2009; Scalais et al., 2012) have been published in the literature. There have also been reports of skeletal muscle being unaffected despite other tissues showing a respiratory chain or mtDNA abnormality and the patient receiving a clinical diagnosis of Alpers' syndrome. In a case report of two patients with Alpers' syndrome, mtDNA depletion was seen in the liver at 16% of the control value, but there was no difference in the skeletal muscle of both patients (Pronicka et al., 2011). A respiratory chain abnormality in muscle was seen in one of the patients for complex II and complex IV. A similar pattern of tissue specificity has been reported previously (Flemming et al., 2002; Simonati et al., 2003a; Simonati et al., 2003b; Wiltshire et al., 2008).

Investigations into the effect on mitochondrial structure, using electron microscopy (EM) on brain and muscle samples, have revealed an increase in the size and number of mitochondria in muscle, and the presence of globoid inclusions within the mitochondria (Nolte et al., 2013). Electron-dense inclusions have also been reported in liver and skeletal muscle in a patient with Alpers' syndrome (Mangalat et al., 2012).

In muscle, pathogenic changes may be ultrastructural and not become dysfunctional until later in disease progression. The symptoms caused by mitochondrial dysfunction in other tissue types may result in disease pathology that is more obvious than the changes in muscle. It is currently unclear why mutations in a nuclear gene do not equally affect all tissues that are similarly ATP-dependent.

1.9.5.1 Central Nervous System Involvement

The brain has a large involvement in Alpers' syndrome, requiring a large amount of ATP to function correctly and appropriately. When ATP production is impaired, the brain can be severely affected because the neurons may be selectively vulnerable to changing levels of ATP as they cannot produce ATP through the process of glycolysis.

MRI scans are frequently used to visualise the brain and can reveal areas of atrophy, oedema, inflammation or other abnormalities in patients. MR spectroscopy is associated with MRI scans and has been used to investigate the CNS of a patient diagnosed with Alpers' syndrome, revealing oedema and increased lactate levels which were interpreted as respiratory chain deficiency (Flemming et al., 2002).

Epilepsy, psychomotor regression, and cortical blindness are the key symptoms of Alpers' syndrome, which all stem from neuronal dysfunction. Epilepsy in these patients is often difficult to control and progressive. The posterior of the brain and the cerebellum are typically more severely affected than the anterior and central regions of the cerebrum.

1.9.5.2 Neuropathology

It is commonly reported that the grey matter of both the cerebrum and cerebellum is affected by neuronal cell loss, astrogliosis, and capillary proliferation (Harding 2008). In the cerebellum, it is the Purkinje cells that are noticeably depleted, accompanied by astrogliosis (Bergmann gliosis). Different areas of the brain are affected to varying degrees and can alter throughout disease progression, which can typically be identified using MRI scans and CT scans (Figure 1.14).

The cerebellum and posterior regions of the cerebrum, such as the occipital lobe, are often severely affected during the course of Alpers' syndrome (Harding et al., 1986; Khan et al., 2012). It is unclear why this occurs, a possibility is that these regions are more active and use large amounts of energy to function. A reduction in energy production may result in the neurons in posterior areas being detrimentally affected sooner than neurons in more anterior regions.

Neuron loss is a very commonly reported neuropathological aspect of Alpers' syndrome (Wiltshire et al., 2008; Scalais et al., 2012). It can cause many of the signs and symptoms that are seen in the patient, and create inconsistent signalling between connected areas of the brain. Other pathology such as astrogliosis is reported in the

literature (Harding et al., 1995; Wiltshire et al., 2008), however, it is very rarely quantified in patients.

White matter abnormalities are reported uncommonly in the literature (Harding et al., 1995; Simonati et al., 2003b; Bao et al., 2008). It is unclear how frequently white matter abnormalities occur and to what severity. These abnormalities may be due to primary loss of myelin or to secondary loss of myelin due to axonal loss.

Alpers' syndrome is considered to be a condition on a wide spectrum of *POLG* disorders. A case of Alpers' syndrome in a young patient with compound heterozygous p.Ala467Thr and p.Gly848Ser mutations was initially thought to resemble a condition on the myocerebrohepatopathy spectrum (Scalais et al., 2012). The neuropathology showed much necrosis and astrogliosis in the occipital lobe, neuron loss in the basal ganglia, and Purkinje cell loss in the cerebellum. In addition to the cerebellum and basal ganglia, the thalamus showed neuron loss and vacuolation which resembled the pathology of Leigh syndrome. This report highlights the wide range of neuropathology that can occur and the overlap between syndromes that we are beginning to recognise.

As the neurological aspects of Alpers' syndrome are often severe, a better understanding of the neuropathology and the pathological mechanisms is essential in order to improve the treatment of this syndrome. Genetic diagnosis of patients and their families is important as it gives a wider picture of the factors leading to Alpers' syndrome and ultimately allows medical professionals to inform 'at risk' individuals of their choices through genetic counselling.

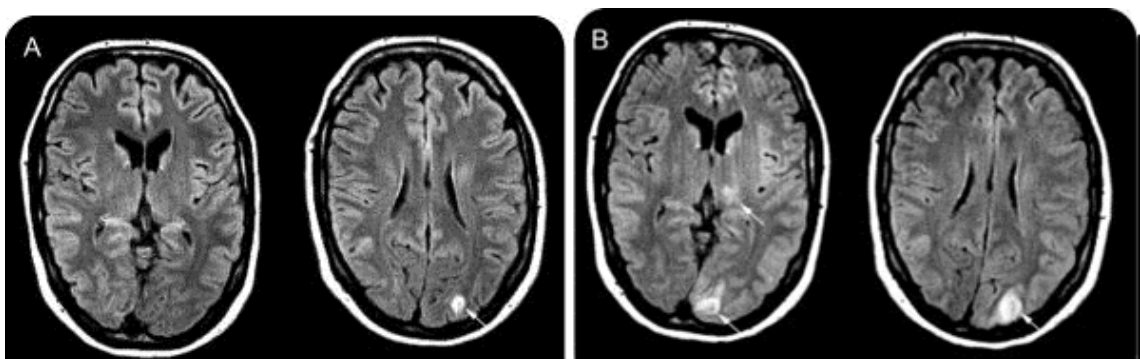


Figure 1.14. MRI images (T2-FLAIR) showing occipital lobe and thalamic lesions during disease progression

Image A is a T2-FLAIR MRI image taken on patient admission. There is a small hyperintense cortical lesion of the occipital lobe (arrowed). Image B is a T2-FLAIR MRI image taken during disease progression. There is a larger hyperintense cortical lesion of the occipital lobe (arrowed) and a smaller lesion of the thalamic region (arrowed). Images taken from Visser et al., (2010).

1.9.5.3 Liver Involvement

Liver dysfunction and failure is a common feature in Alpers' syndrome. Failure is often preceded by steatosis, hepatocyte cell dysfunction and dropout, bile duct proliferation, cholestasis, and immune cell infiltration. The first report of hypoglycaemia due to impaired glycogenolysis in a patient with Alpers' syndrome has been recently reported, with abnormal glycogen storage in the liver (Simon et al., 2013). This patient presented with glucosuria without any preceding neurological or developmental symptoms. Liver dysfunction often occurs in the later stages of Alpers' syndrome after initial symptoms of epilepsy and neurological abnormalities. However, the onset of liver complications is variable and there have been reports of liver dysfunction and failure occurring before the onset of epilepsy (Egger et al., 1987).

1.9.5.4 Use of Sodium Valproate

Sodium valproate is a solid compound formed from the addition of liquid valproic acid to a base chemical. Its primary use is as an anti-convulsant drug and as a mood stabiliser.

Its use as an anti-epileptic drug for patients with mitochondrial disease is not recommended, as it has been reported that it can inhibit fatty acid oxidation in the mitochondria (Eyer et al., 2005) and inhibit oxidative phosphorylation leading to hepatotoxicity (Horvath et al., 2006) and the precipitation of liver failure (Bicknese et al., 1992). Nevertheless, the mechanisms behind how this leads to adverse effects, in the liver in particular, are unclear. Cases have been described in the literature where liver abnormalities were present before sodium valproate was given to the patients (Ferrari et al., 2005; Uusimaa et al., 2008), which could suggest that sodium valproate may quicken the onset of pre-existing liver failure in some patients. When liver dysfunction has been diagnosed prior to a correct diagnosis, liver transplants have occasionally been performed on Alpers' syndrome patients. However, these transplants have been unsuccessful at preventing the course of the syndrome owing to the involvement of seizures (Delarue et al., 2000; Kayihan et al., 2000). A report of a reversal of sodium valproate toxicity has been published after cessation of the drug in a child with four heterozygous mutations in *POLG*, two of which were the common p.Ala467Thr and p.Trp748Ser mutations often associated with Alpers' syndrome (McFarland et al., 2008). The presence of an additional two mutations in *POLG*, the p.Gln879His and p.Thr885Ser mutations, may have influenced this unusual outcome.

Sodium valproate is commonly prescribed in a clinical setting to control epileptic seizures. It has been often recommended that testing for *POLG* disorders, and in particular Alpers' syndrome, should be carried out before administering sodium valproate in order to prevent side effects (Saneto et al., 2010). This should be applied to all mitochondrial disorders.

1.9.6 Therapy

There are currently no existing treatments for Alpers' syndrome, with relief and support in the form of symptomatic therapies. This section will discuss the current available therapies for patients with Alpers' syndrome.

1.9.6.1 Anticonvulsant Drugs

Seizures are the most common sign in Alpers' syndrome. Seizures are usually refractory and do not consistently respond to the anticonvulsant drugs usually used in treatment, such as phenytoin, carbamazepine, and levetiracetam. Use of this medication may result in temporary benefits but this does not last and a decline in health rapidly transpires.

Sodium valproate is an anticonvulsant drug once commonly used to treat all seizures but more recent observations have led to the call for it not to be used where mitochondrial disease is suspected in the patient (Saneto et al., 2010). This was previously discussed further in section 1.9.5.3 '*Use of Sodium Valproate*'.

1.9.6.2 Ketogenic Diet

A ketogenic diet is occasionally used in the treatment of refractory epilepsy in children. It consists of a high fat, low carbohydrate diet. The ratio of fat to carbohydrate varies and is roughly of 4 parts fat to one part each protein and carbohydrate. There have been a range of reported effects due to this diet.

A beneficial effect in a young patient with Alpers' syndrome was reported, with twitching of the left hand stopping completely after commencing the diet, a remarkable improvement of electroencephalogram (EEG) tests, and a cessation of seizures for seven months (Joshi et al., 2009). However, reduced compliance with the diet and an infection led to a recurrence of seizures which could not be controlled. A separate study of 32 infants with intractable epilepsy though not diagnosed with Alpers' syndrome, were placed on a ketogenic diet and resulted in over 50% of the patients having a >50% reduction in seizure frequency, and the diet was considered a safe

treatment for infant patients with intractable epilepsy (Nordli Jr et al., 2001). However, Wiltshire *et al.*, reported that the ketogenic diet had no effect in their Alpers' syndrome patient (Wiltshire et al., 2008).

Though mechanisms have been discussed for why this diet may work as an effective treatment, these remain speculative. Further trial of the ketogenic diet as a treatment option is required. It may provide relief to some patients and should remain an option for families.

1.9.6.3 Magnesium Therapy

Magnesium therapy has been used to effectively control seizures in conditions such as eclampsia (Roy et al., 2013). It has also been reported to have had a positive effect in two patients with Alpers' syndrome (Visser et al., 2011). In one patient, seizures stopped completely upon administration of magnesium and did not return, though unfortunately further complications led to multi-organ failure. The second patient showed improvement of paresis and dysphagia, and improved EEG after extubation. Unfortunately seizures continued in this patient.

Magnesium therapy is not a widely used treatment and further studies into the efficacy of this treatment are required. The mechanisms through which magnesium therapy may act are unclear, though it is speculated that it may act through an antagonistic effect on N-methyl-D-aspartate (NMDA) receptors, blocking calcium influx (Hallak 1998).

1.9.6.4 Surgical Therapy

Functional hemispherectomy has been described as a possible treatment for refractory seizures in patients with Alpers' syndrome. This was performed in a four-year-old patient and halted seizures and improved quality of life for two months (Lupashko et al., 2011). Further research is needed into the benefits of hemispherectomy in patients with Alpers' syndrome, to assess whether it can be beneficial as an option to manage the refractory seizures seen with the condition.

1.10 Aims of the Study

The aims of this study are to understand the correlation between and the mechanism leading to the key neurological signs and degenerative changes in post-mortem brain tissue. This will be achieved through:

1. The characterisation of the neuropathology of patients diagnosed with Alpers' syndrome, in comparison with age-/sex-matched controls. A quantitative approach will be taken to assess the grey and white matter for a range of characteristics, including neuron loss, astrogliosis, and white matter abnormalities.
2. Achieving a genetic diagnosis in patients where one was not available.
3. Determining the respiratory chain deficiency in patients diagnosed with Alpers' syndrome, in comparison with matched controls. Complexes I to IV will be assessed in the cohort of patients, through the use of immunohistochemistry, to investigate any deficiencies or partial deficiencies in neurons.
4. Assessing the mtDNA in single neurons and whether there is DNA damage. Both mtDNA deletion and mtDNA depletion are assessed separately to investigate which may be the more prominent feature.

- Abu-Amero, K. K., P. T. Ozand and H. Al-Dhalaan (2006). "Novel mitochondrial DNA transversion mutation in transfer ribonucleic acid for leucine 2 (CUN) in a patient with the clinical features of MELAS." Journal of Child Neurology **21**(11): 971-972.
- Achilli, A., L. Iommarini, A. Olivieri, M. Pala, B. Hooshiar Kashani, P. Reynier, C. La Morgia, M. L. Valentino, R. Liguori, F. Pizza, P. Barboni, F. Sadun, A. M. de Negri, M. Zeviani, H. Dollfus, A. Moulignier, G. Ducos, C. Orssaud, D. Bonneau, V. Procaccio, B. Leo-Kottler, S. Fauser, B. Wissinger, P. Amati-Bonneau, A. Torroni and V. Carelli (2012). "Rare primary mitochondrial DNA mutations and probable synergistic variants in leber's hereditary optic neuropathy." PLoS ONE **7**(8).
- Acín-Pérez, R., M. P. Bayona-Bafaluy, P. Fernández-Silva, R. Moreno-Loshuertos, A. Pérez-Martos, C. Bruno, C. T. Moraes and J. A. Enríquez (2004). "Respiratory complex III is required to maintain complex I in mammalian mitochondria." Molecular Cell **13**(6): 805-815.
- Acín-Pérez, R., P. Fernández-Silva, M. L. Peleato, A. Pérez-Martos and J. A. Enriquez (2008). "Respiratory Active Mitochondrial Supercomplexes." Molecular Cell **32**(4): 529-539.
- Akhmanova, A., F. Voncken, T. Van Alen, A. Van Hoek, B. Boxma, G. Vogels, M. Veenhuis and J. H. P. Hackstein (1998). "A hydrogenosome with a genome [7]." Nature **396**(6711): 527-528.
- Alpers, B. J. (1931). "Diffuse progressive degeneration of the gray matter of the cerebrum." Arch Neurol Psychiatry **25**: 469-505.
- Amutha, B., D. M. Gordon, Y. Gu and D. Pain (2004). "A novel role of Mgm1p, a dynamin-related GTPase, in ATP synthase assembly and cristae formation/maintenance." Biochemical Journal **381**(1): 19-23.
- Anderson, S., A. T. Bankier and B. G. Barrell (1981). "Sequence and organization of the human mitochondrial genome." Nature **290**(5806): 457-465.
- Antonicka, H., I. Ogilvie, T. Taivassalo, R. P. Anitori, R. G. Haller, J. Vissing, N. G. Kennaway and E. A. Shoubridge (2003). "Identification and Characterization of a Common Set of Complex I Assembly Intermediates in Mitochondria from Patients with Complex I Deficiency." Journal of Biological Chemistry **278**(44): 43081-43088.
- Arnheim, N. and G. Cortopassi (1992). "Deleterious mitochondrial DNA mutations accumulate in aging human tissues." Mutation Research - DNAging Genetic Instability and Aging **275**(3-6): 157-167.
- Ashley, N., A. O'Rourke, C. Smith, S. Adams, V. Gowda, M. Zeviani, G. K. Brown, C. Fratter and J. Poulton (2008). "Depletion of mitochondrial DNA in fibroblast cultures from patients with POLG1 mutations is a

- consequence of catalytic mutations." Human Molecular Genetics **17**(16): 2496-2506.
- Baklouti-Gargouri, S., M. Ghorbel, N. Chakroun, A. Sellami, F. Fakhfakh and L. Ammar-Keskes (2012). "The CAG repeat polymorphism of mitochondrial polymerase gamma (POLG) is associated with male infertility in Tunisia." Andrologia **44**(SUPPL.1): 68-73.
- Ballinger, S. W., J. M. Shoffner, S. Gebhart, D. A. Koontz and D. C. Wallace (1994). "Mitochondrial diabetes revisited [1]." Nature Genetics **7**(4): 458-459.
- Banati, R. B., R. Egensperger, A. Maassen, G. Hager, G. W. Kreutzberg and M. B. Graeber (2004). "Mitochondria in activated microglia in vitro." Journal of Neurocytology **33**(5): 535-541.
- Bandy, B. and A. J. Davison (1990). "Mitochondrial mutations may increase oxidative stress: Implications for carcinogenesis and aging?" Free Radical Biology and Medicine **8**(6): 523-539.
- Bao, X., Y. Wu, L. J. C. Wong, Y. Zhang, H. Xiong, P. C. Chou, C. K. Truong, Y. Jiang, J. Qin, Y. Yuan, Q. Lin and X. Wu (2008). "Alpers syndrome with prominent white matter changes." Brain and Development **30**(4): 295-300.
- Baum, H., J. C. Rieske, H. I. Silman and S. H. Lipton (1967). "On the mechanism of electron transfer in complex iii of the electron transfer chain." Proc Natl Acad Sci U S A. **57**(3): 798-805.
- Bazil, J. N., C. A. Blomeyer, R. K. Pradhan, A. K. S. Camara and R. K. Dash (2012). "Modeling the calcium sequestration system in isolated guinea pig cardiac mitochondria." Journal of Bioenergetics and Biomembranes: 1-12.
- Becker, L. B., T. L. Vanden Hoek, Z. H. Shao, C. Q. Li and P. T. Schumacker (1999). "Generation of superoxide in cardiomyocytes during ischemia before reperfusion." American Journal of Physiology - Heart and Circulatory Physiology **277**(6 46-6): H2240-H2246.
- Bianchi, C., M. L. Genova, G. P. Castelli and G. Lenaz (2004). "The mitochondrial respiratory chain is partially organized in a supercomplex assembly: Kinetic evidence using flux control analysis." Journal of Biological Chemistry **279**(35): 36562-36569.
- Bicknese, A. R., W. May, W. F. Hickey and W. E. Dodson (1992). "Early childhood hepatocerebral degeneration misdiagnosed as valproate hepatotoxicity." Annals of Neurology **32**(6): 767-775.
- Blackwood, W., P. H. Buxton, J. N. Cumings, D. J. Robertson and S. M. Tucker (1963). "Diffuse cerebral degeneration in infancy (Alpers' disease)." Archives of Disease in Childhood **38**: 193-204.

- Blok, M. J., B. J. Van Den Bosch, E. Jongen, A. Hendrickx, C. E. De Die-Smulders, J. E. Hoogendijk, E. Brusse, M. De Visser, B. T. Poll-The, J. Bierau, I. F. De Coo and H. J. Smeets (2009). "The unfolding clinical spectrum of POLG mutations." Journal of Medical Genetics **46**(11): 776-785.
- Bogenhagen, D. and D. A. Clayton (1977). "Mouse I cell mitochondrial DNA molecules are selected randomly for replication throughout the cell cycle." Cell **11**(4): 719-727.
- Bostan, A., G. Glibert, B. Dachy and B. Dan (2012). "Novel mutation in spacer region of POLG associated with ataxia neuropathy spectrum and gastroparesis." Autonomic Neuroscience: Basic and Clinical **170**(1-2): 70-72.
- Boyd, S. G., A. Harden, J. Egger and G. Pampiglione (1986). "Progressive neuronal degeneration of childhood with liver disease ('Alpers' disease): Characteristic neurophysiological features." Neuropediatrics **17**(2): 75-80.
- Boyer, P. D. (1975). "A model for conformational coupling of membrane potential and proton translocation to ATP synthesis and to active transport." FEBS Letters **58**(1-2): 1-6.
- Brockington, M., M. G. Sweeney, S. R. Hammans, J. A. Morgan-Hughes and A. E. Harding (1993). "A tandem duplication in the D-loop of human mitochondrial DNA is associated with deletions in mitochondrial myopathies." Nature Genetics **4**(1): 67-71.
- Brown, W. M., M. George Jr and A. C. Wilson (1979). "Rapid evolution of animal mitochondrial DNA." Proceedings of the National Academy of Sciences of the United States of America **76**(4): 1967-1971.
- Bulst, S., A. Abicht, E. Holinski-Feder, S. Müller-Ziermann, U. Koehler, C. Thirion, M. C. Walter, J. D. Stewart, P. F. Chinnery, H. Lochmüller and R. Horvath (2009). "In vitro supplementation with dAMP/dGMP leads to partial restoration of mtDNA levels in mitochondrial depletion syndromes." Human Molecular Genetics **18**(9): 1590-1599.
- Cámara, Y., E. González-Vioque, M. Scarpelli, J. Torres-Torronteras, A. Caballero, M. Hirano and R. Martí (2013). "Administration of deoxyribonucleosides or inhibition of their catabolism as a pharmacological approach for mitochondrial DNA depletion syndrome." Human Molecular Genetics.
- Caporali, L., A. M. Ghelli, L. Iommarini, A. Maresca, M. L. Valentino, C. La Morgia, R. Liguori, C. Zanna, P. Barboni, V. De Nardo, A. Martinuzzi, G. Rizzo, C. Tonon, R. Lodi, M. A. Calvaruso, M. Cappelletti, A. M. Porcelli, A. Achilli, M. Pala, A. Torroni and V. Carelli (2013). "Cybrid studies establish the causal link between the mtDNA m.3890G>A/MT-ND1

- mutation and optic atrophy with bilateral brainstem lesions." Biochimica et Biophysica Acta - Molecular Basis of Disease **1832**(3): 445-452.
- Carrodeguas, J. A., R. Kobayashi, S. E. Lim, W. C. Copeland and D. F. Bogenhagen (1999). "The accessory subunit of *Xenopus laevis* mitochondrial DNA polymerase γ increases processivity of the catalytic subunit of human DNA polymerase γ and is related to class II aminoacyl-tRNA synthetases." Molecular and Cellular Biology **19**(6): 4039-4046.
- Chan, S. S. L., M. J. Longley and W. C. Copeland (2005). "The common A467T mutation in the human mitochondrial DNA polymerase (POLG) compromises catalytic efficiency and interaction with the accessory subunit." Journal of Biological Chemistry **280**(36): 31341-31346.
- Chan, S. S. L., M. J. Longley and W. C. Copeland (2006). "Modulation of the W748S mutation in DNA polymerase γ by the E1143G polymorphism in mitochondrial disorders." Human Molecular Genetics **15**(23): 3473-3483.
- Chen, H., J. M. McCaffery and D. C. Chan (2007). "Mitochondrial Fusion Protects against Neurodegeneration in the Cerebellum." Cell **130**(3): 548-562.
- Chen, Q., E. J. Vazquez, S. Moghaddas, C. L. Hoppel and E. J. Lesnfsky (2003). "Production of reactive oxygen species by mitochondria: Central role of complex III." Journal of Biological Chemistry **278**(38): 36027-36031.
- Chinnery, P. F. and D. C. Samuels (1999). "Relaxed replication of mtDNA: A model with implications for the expression of disease." American Journal of Human Genetics **64**(4): 1158-1165.
- Cipolat, S., O. M. De Brito, B. Dal Zilio and L. Scorrano (2004). "OPA1 requires mitofusin 1 to promote mitochondrial fusion." Proceedings of the National Academy of Sciences of the United States of America **101**(45): 15927-15932.
- Clayton, D. A. (1982). "Replication of animal mitochondrial DNA." Cell **28**(4): 693-705.
- Cotney, J., Z. Wang and G. S. Shadel (2007). "Relative abundance of the human mitochondrial transcription system and distinct roles for h-mtTFB1 and h-mtTFB2 in mitochondrial biogenesis and gene expression." Nucleic Acids Research **35**(12): 4042-4054.
- Cox, G. B., D. A. Jans, A. L. Fimmel, F. Gibson and L. Hatch (1984). "Hypothesis. The mechanism of ATP synthase. Conformational change by rotation of the beta-subunit." Biochim Biophys Acta **17**: 201-208.
- Darin, N., A. Oldfors, A. R. Moslemi, E. Holme and M. Tulinius (2001). "The incidence of mitochondrial encephalomyopathies in childhood: Clinical

- features and morphological, biochemical, and DNA abnormalities." Annals of Neurology **49**(3): 377-383.
- De Grey, A. D. N. J. (1997). "A proposed refinement of the mitochondrial free radical theory of aging." BioEssays **19**(2): 161-166.
- De Meirleir, L., S. Seneca, W. Lissens, I. De Clercq, F. Eyskens, E. Gerlo, J. Smet and R. Van Coster (2004). "Respiratory chain complex V deficiency due to a mutation in the assembly gene ATP12." Journal of Medical Genetics **41**(2): 120-124.
- Del Bo, R., A. Bordoni, M. Sciacco, A. Di Fonzo, S. Galbiati, M. Crimi, N. Bresolin and G. P. Comi (2003). "Remarkable infidelity of polymerase γ A associated with mutations in POLG1 exonuclease domain." Neurology **61**(7): 903-908.
- Delarue, A., O. Paut, J. M. Guys, M. F. Montfort, V. Lethel, B. Roquelaure, J. F. Pellissier, J. Sarles and J. Camboulives (2000). "Inappropriate liver transplantation in a child with Alpers-Huttenlocher syndrome misdiagnosed as valproate-induced acute liver failure." Pediatric Transplantation **4**(1): 67-71.
- Delettre, C., G. Lenaers, J. M. Griffoin, N. Gigarel, C. Lorenzo, P. Belenguer, L. Pelloquin, J. Grosgeorge, C. Turc-Carel, E. Perret, C. Astarie-Dequeker, L. Lasquelles, B. Arnaud, B. Ducommun, J. Kaplan and C. P. Hamel (2000). "Nuclear gene OPA1, encoding a mitochondrial dynamin-related protein, is mutated in dominant optic atrophy." Nature Genetics **26**(2): 207-210.
- Deluca, H. F. and G. W. Engstrom (1961). "Calcium uptake by rat kidney mitochondria." Proceedings of the National Academy of Sciences of the United States of America **47**: 1744-1750.
- Diaz, F., H. Fukui, S. Garcia and C. T. Moraes (2006). "Cytochrome c oxidase is required for the assembly/stability of respiratory complex I in mouse fibroblasts." Molecular and Cellular Biology **26**(13): 4872-4881.
- Egger, J., B. N. Harding, S. G. Boyd, J. Wilson and M. Erdohazi (1987). "Progressive neuronal degeneration of childhood (PNDC) with liver disease." Clinical Pediatrics **26**(4): 167-173.
- Elliott, H. R., D. C. Samuels, J. A. Eden, C. L. Relton and P. F. Chinnery (2008). "Pathogenic Mitochondrial DNA Mutations Are Common in the General Population." American Journal of Human Genetics **83**(2): 254-260.
- Elo, J. M., S. S. Yadavalli, L. Euro, P. Isohanni, A. Götz, C. J. Carroll, L. Valanne, F. S. Alkuraya, J. Uusimaa, A. Paetau, E. M. Caruso, H. Pihko, M. Ibba, H. Tynismaa and A. Suomalainen (2012). "Mitochondrial phenylalanyl-trna synthetase mutations underlie fatal infantile alpers encephalopathy." Human Molecular Genetics **21**(20): 4521-4529.

- Elson, J. L., D. C. Samuels, D. M. Turnbull and P. F. Chinnery (2001). "Random intracellular drift explains the clonal expansion of mitochondrial DNA mutations with age." *American Journal of Human Genetics* **68**(3): 802-806.
- Eschbach, J., J. Sinniger, J. Bouitbir, A. Fergani, A. I. Schlagowski, J. Zoll, B. Geny, F. René, Y. Larmet, V. Marion, R. H. Baloh, M. B. Harms, M. E. Shy, N. Messadeq, P. Weydt, J. P. Loeffler, A. C. Ludolph and L. Dupuis (2013). "Dynein mutations associated with hereditary motor neuropathies impair mitochondrial morphology and function with age." *Neurobiology of Disease* **58**: 220-230.
- Euro, L., G. A. Farnum, E. Palin, A. Suomalainen and L. S. Kaguni (2011). "Clustering of Alpers disease mutations and catalytic defects in biochemical variants reveal new features of molecular mechanism of the human mitochondrial replicase, Pol γ ." *Nucleic Acids Research* **39**(21): 9072-9084.
- Eyer, F., N. Felgenhauer, K. Gempel, W. Steimer, K. D. Gerbitz and T. Zilker (2005). "Acute valproate poisoning: Pharmacokinetics, alteration in fatty acid metabolism, and changes during therapy." *Journal of Clinical Psychopharmacology* **25**(4): 376-380.
- Ferrari, G., E. Lamantea, A. Donati, M. Filosto, E. Briem, F. Carrara, R. Parini, A. Simonati, R. Sanier and M. Zeviani (2005). "Infantile hepatocerebral syndromes associated with mutations in the mitochondrial DNA polymerase- γ A." *Brain* **128**(4): 723-731.
- Ferraris, S., S. Clark, E. Garelli, G. Davidzon, S. A. Moore, R. H. Kardon, R. J. Bienstock, M. J. Longley, M. Mancuso, P. Ríos Gutiérrez, M. Hirano, W. C. Copeland and S. DiMauro (2008). "Progressive external ophthalmoplegia and vision and hearing loss in a patient with mutations in POLG2 and OPA1." *Archives of Neurology* **65**(1): 125-131.
- Finsterer, J. (2008). "Leigh and Leigh-Like Syndrome in Children and Adults." *Pediatric Neurology* **39**(4): 223-235.
- Finsterer, J., C. Stöllberger, W. Kopsa and M. Jaksch (2001). "Wolff-Parkinson-White syndrome and isolated left ventricular abnormal trabeculation as a manifestation of Leber's hereditary optic neuropathy." *Canadian Journal of Cardiology* **17**(4): 464-466.
- Fish, J., N. Raule and G. Attardi (2004). "Discovery of a major D-loop replication origin reveals two modes of human mtDNA synthesis." *Science* **306**(5704): 2098-2101.
- Flemming, K., S. Ulmer, B. Duisberg, A. Hahn and O. Jansen (2002). "MR spectroscopic findings in a case of Alpers-Huttenlocher syndrome." *American Journal of Neuroradiology* **23**(8): 1421-1423.

- Frezza, C., S. Cipolat, O. Martins de Brito, M. Micaroni, G. V. Beznoussenko, T. Rudka, D. Bartoli, R. S. Polishuck, N. N. Danial, B. De Strooper and L. Scorrano (2006). "OPA1 Controls Apoptotic Cristae Remodeling Independently from Mitochondrial Fusion." Cell **126**(1): 177-189.
- Friedman, J. R., L. L. Lackner, M. West, J. R. DiBenedetto, J. Nunnari and G. K. Voeltz (2011). "ER tubules mark sites of mitochondrial division." Science **334**(6054): 358-362.
- Fromenty, B., R. Carrozzo, S. Shanske and E. A. Schon (1997). "High proportions of mtDNA duplications in patients with Kearns-Sayre syndrome occur in the heart." American Journal of Medical Genetics **71**(4): 443-452.
- Frydman, M., E. Jager-Roman, L. DeVries, G. Stoltenburg-Didinger, M. Nussinovitch and L. Sirota (1993). "Alpers progressive infantile neuronal poliodystrophy: An acute neonatal form with findings of the fetal akinesia syndrome." American Journal of Medical Genetics **47**(1): 31-36.
- Fukuhara, N., S. Tokiguchi, K. Shirakawa and T. Tsubaki (1980). "Myoclonus epilepsy associated with ragged-red fibres (mitochondrial abnormalities): Disease entity or a syndrome? Light- and electron-microscopic studies of two cases and review of literature." Journal of the Neurological Sciences **47**(1): 117-133.
- Gautheron, D. C. (1984). "Mitochondrial oxidative phosphorylation and respiratory chain: Review." Journal of Inherited Metabolic Disease **7**(SUPPL. 1): 57-61.
- Goto, Y.-i., I. Nonaka and S. Horai (1990). "A mutation in the tRNA^{Leu}(UUR) gene associated with the MELAS subgroup of mitochondrial encephalomyopathies." Nature **348**(6302): 651-653.
- Graziewicz, M. A., M. J. Longley, R. J. Bienstock, M. Zeviani and W. C. Copeland (2004). "Structure-function defects of human mitochondrial DNA polymerase in autosomal dominant progressive external ophthalmoplegia." Nature Structural and Molecular Biology **11**(8): 770-776.
- Gross, N. J., G. S. Getz and M. Rabinowitz (1969). "Apparent turnover of mitochondrial deoxyribonucleic acid and mitochondrial phospholipids in the tissues of the rat." Journal of Biological Chemistry **244**(6): 1552-1562.
- Gupta, S. R., M. Brigell, M. Gujrati and J. M. Lee (1995). "Supranuclear eye movement dysfunction in mitochondrial myopathy with tRNA(LEU) mutation." Journal of Neuro-Ophthalmology **15**(1): 20-25.
- Gyllenstein, U., D. Wharton, A. Josefsson and A. C. Wilson (1991). "Paternal inheritance of mitochondrial DNA in mice." Nature **352**(6332): 255-257.

- Hakonen, A. H., G. Davidzon, R. Salemi, L. A. Bindoff, G. Van Goethem, S. DiMauro, D. R. Thorburn and A. Suomalainen (2007). "Abundance of the POLG disease mutations in Europe, Australia, New Zealand, and the United States explained by single ancient European founders." European Journal of Human Genetics **15**(7): 779-783.
- Hakonen, A. H., S. Heiskanen, V. Juvonen, I. Lappalainen, P. T. Luoma, M. Rantamäki, G. Van Goethem, A. Löfgren, P. Hackman, A. Paetau, S. Kaakkola, K. Majamaa, T. Varilo, B. Udd, H. Kääriäinen, L. A. Bindoff and A. Suomalainen (2005). "Mitochondrial DNA polymerase W748S mutation: A common cause of autosomal recessive ataxia with ancient European origin." American Journal of Human Genetics **77**(3): 430-441.
- Hallak, M. (1998). "Effect of parenteral magnesium sulfate administration on excitatory amino acid receptors in the rat brain." Magnesium Research **11**(2): 117-131.
- Hance, N., M. I. Ekstrand and A. Trifunovic (2005). "Mitochondrial DNA polymerase gamma is essential for mammalian embryogenesis." Human Molecular Genetics **14**(13): 1775-1783.
- Harder, Z., R. Zunino and H. McBride (2004). "Sumo1 conjugates mitochondrial substrates and participates in mitochondrial fission." Current Biology **14**(4): 340-345.
- Harding, A. E., M. G. Sweeney, G. G. Govan and P. Riordan-Eva (1995). "Pedigree analysis in Leber hereditary optic neuropathy families with a pathogenic mtDNA mutation." American Journal of Human Genetics **57**(1): 77-86.
- Harding, B. N. (1990). "Progressive neuronal degeneration of childhood with liver disease (Alpers-Huttenlocher Syndrome): A personal review." Journal of Child Neurology **5**(4): 273-287.
- Harding, B. N., N. Alsanjari, S. J. M. Smith, C. M. Wiles, D. Thrush, D. H. Miller, F. Scaravilli and A. E. Harding (1995). "Progressive neuronal degeneration of childhood with liver disease (Alpers' disease) presenting in young adults." Journal of Neurology Neurosurgery and Psychiatry **58**(3): 320-325.
- Harding, B. N., J. Egger, B. Portmann and M. Erdohazi (1986). "Progressive neuronal degeneration of childhood with liver disease: A pathological study." Brain **109**(1): 181-206.
- Harding, B. N., Surtees, R.A.H (2008). Metabolic and neurodegenerative disease of childhood. Greenfield's neuropathology volume 1 Eighth Edition. S. Love, Louis, D.N., Ellison, D.W. London, UK, Hodder Arnold. **1**: 481 – 514.
- Harman, D. (1956). "Aging: a theory based on free radical and radiation chemistry." Journal of gerontology **11**(3): 298-300.

- Harrower, T., J. D. Stewart, G. Hudson, H. Houlden, G. Warner, D. G. O'Donovan, L. J. Findlay, R. W. Taylor, R. De Silva and P. F. Chinnery (2008). "POLG1 mutations manifesting as autosomal recessive axonal Charcot-Marie-Tooth disease." Archives of Neurology **65**(1): 133-136.
- Hastings, I. M. (1992). "Population genetic aspects of deleterious cytoplasmic genomes and their effect on the evolution of sexual reproduction." Genetical Research **59**(3): 215-225.
- Hayakawa, M., K. Hattori, S. Sugiyama and T. Ozawa (1992). "Age-associated oxygen damage and mutations in mitochondrial DNA in human hearts." Biochemical and Biophysical Research Communications **189**(2): 979-985.
- Heidari, M. M., M. Houshmand, S. Hosseinkhani, S. Nafissi, B. Scheiber-Mojdehkar and M. Khatami (2008). "Association between trinucleotide CAG repeats of the DNA polymerase gene (POLG) with age of onset of Iranian Friedreich's ataxia patients." Neurological Sciences **29**(6): 489-493.
- Hinnell, C., S. Haider, S. Delamont, C. Clough, N. Hadzic and M. Samuel (2012). "Dystonia in mitochondrial spinocerebellar ataxia and epilepsy syndrome associated with novel recessive POLG mutations." Movement Disorders **27**(1): 162-163.
- Hirano, M., J. Garcia-de-Yebenes, A. C. Jones, I. Nishino, S. DiMauro, J. R. Carlo, A. N. Bender, A. F. Hahn, L. M. Salberg, D. E. Weeks and T. G. Nygaard (1998). "Mitochondrial neurogastrointestinal encephalomyopathy syndrome maps to chromosome 22q13.32-qter." American Journal of Human Genetics **63**(2): 526-533.
- Hirokawa, N., R. Sato-Yoshitake, T. Yoshida and T. Kawashima (1990). "Brain dynein (MAP1C) localizes on both anterogradely and retrogradely transported membranous organelles in vivo." Journal of Cell Biology **111**(3): 1027-1037.
- Hoeh, W. R., K. H. Blakley and W. M. Brown (1991). "Heteroplasmy suggests limited biparental inheritance of mytilus mitochondrial DNA." Science **251**(5000): 1488-1490.
- Hogeboom, G. H., W. C. Schneider and G. E. Pallade (1948). "Cytochemical studies of mammalian tissues; isolation of intact mitochondria from rat liver; some biochemical properties of mitochondria and submicroscopic particulate material." The Journal of biological chemistry **172**(2): 619-635.
- Holt, I. J., A. E. Harding and J. A. Morgan-Hughes (1988). "Deletions of muscle mitochondrial DNA in patients with mitochondrial myopathies." Nature **331**(6158): 717-719.

- Holt, I. J., A. E. Harding, R. K. H. Petty and J. A. Morgan-Hughes (1990). "A new mitochondrial disease associated with mitochondrial DNA heteroplasmy." *American Journal of Human Genetics* **46**(3): 428-433.
- Holt, I. J., H. E. Lorimer and H. T. Jacobs (2000). "Coupled leading- and lagging-strand synthesis of mammalian mitochondrial DNA." *Cell* **100**(5): 515-524.
- Horvath, R., G. Hudson, G. Ferrari, N. Fütterer, S. Ahola, E. Lamantea, H. Prokisch, H. Lochmüller, R. McFarland, V. Ramesh, T. Klopstock, P. Freisinger, F. Salvi, J. A. Mayr, R. Santer, M. Tesarova, J. Zeman, B. Udd, R. W. Taylor, D. Turnbull, M. Hanna, D. Fialho, A. Suomalainen, M. Zeviani and P. F. Chinnery (2006). "Phenotypic spectrum associated with mutations of the mitochondrial polymerase γ gene." *Brain* **129**(7): 1674-1684.
- Howell, N., L. A. Bindoff, D. A. McCullough, I. Kubacka, J. Poulton, D. Mackey, L. Taylor and D. M. Turnbull (1991). "Leber hereditary optic neuropathy: Identification of the same mitochondrial NDI mutation in six pedigrees." *American Journal of Human Genetics* **49**(5): 939-950.
- Howell, N., C. B. Smejkal, D. A. Mackey, P. F. Chinnery, D. M. Turnbull and C. Herrstadt (2003). "The pedigree rate of sequence divergence in the human mitochondrial genome: There is a difference between phylogenetic and pedigree rates." *American Journal of Human Genetics* **72**(3): 659-670.
- Humble, M. M., M. J. Young, J. F. Foley, A. R. Pandiri, G. S. Travlos and W. C. Copeland (2013). "Polg2 is essential for mammalian embryogenesis and is required for mtDNA maintenance." *Human Molecular Genetics* **22**(5): 1017-1025.
- Hunter, M. F., H. Peters, R. Salemi, D. Thorburn and M. T. MacKay (2011). "Alpers syndrome with mutations in POLG: Clinical and investigative features." *Pediatric Neurology* **45**(5): 311-318.
- Hurst, L. D. (1996). "Why are There Only Two Sexes?" *Proceedings of the Royal Society of London. Series B: Biological Sciences* **263**(1369): 415-422.
- Huttenlocher, P. R., G. B. Solitare and G. Adams (1976). "Infantile diffuse cerebral degeneration with hepatic cirrhosis." *Archives of Neurology* **33**(3): 186-192.
- Johns, D. R., M. J. Neufeld and R. D. Park (1992). "An ND-6 mitochondrial DNA mutation associated with Leber hereditary optic neuropathy." *Biochemical and Biophysical Research Communications* **187**(3): 1551-1557.

- Johnson, A. A. and K. A. Johnson (2001). "Exonuclease Proofreading by Human Mitochondrial DNA Polymerase." Journal of Biological Chemistry **276**(41): 38097-38107.
- Jonckheere, A. I., G. Herma Renkema, M. Bras, L. P. Van Den Heuvel, A. Hoischen, C. Gilissen, S. B. Nabuurs, M. A. Huynen, M. C. De Vries, J. A. M. Smeitink and R. J. T. Rodenburg (2013). "A complex v ATP5A1 defect causes fatal neonatal mitochondrial encephalopathy." Brain **136**(5): 1544-1554.
- Jonckheere, A. I., J. A. M. Smeitink and R. J. T. Rodenburg (2012). "Mitochondrial ATP synthase: Architecture, function and pathology." Journal of Inherited Metabolic Disease **35**(2): 211-225.
- Joseph, A. M., P. J. Adihetty, N. R. Wawrzyniak, S. E. Wohlgemuth, A. Picca, G. C. Kujoth, T. A. Prolla and C. Leeuwenburgh (2013). "Dysregulation of Mitochondrial Quality Control Processes Contribute to Sarcopenia in a Mouse Model of Premature Aging." PLoS ONE **8**(7).
- Joshi, C. N., C. R. Greenberg, A. A. Mhanni and M. S. Salman (2009). "Ketogenic Diet in Alpers-Huttenlocher Syndrome." Pediatric Neurology **40**(4): 314-316.
- Kajander, O. A., P. J. Karhunen, I. J. Holt and H. T. Jacobs (2001). "Prominent mitochondrial DNA recombination intermediates in human heart muscle." EMBO Reports **2**(11): 1007-1012.
- Kajander, O. A., A. T. Rovio, K. Majamaa, J. Poulton, J. N. Spelbrink, I. J. Holt, P. J. Karhunen and H. T. Jacobs (2000). "Human mtDNA sublimons resemble rearranged mitochondrial genomes found in pathological states." Human Molecular Genetics **9**(19): 2821-2835.
- Kapur, R. P., C. Fligner, B. Maghsoodi and R. Jaffe (2011). "Gastrointestinal neuromuscular pathology in alpers disease." American Journal of Surgical Pathology **35**(5): 714-722.
- Karbowski, M., S. Y. Jeong and R. J. Youle (2004). "Endophilin B1 is required for the maintenance of mitochondrial morphology." Journal of Cell Biology **166**(7): 1027-1039.
- Kasahara, T., M. Kubota, T. Miyauchi, Y. Noda, A. Mouri, T. Nabeshima and T. Kato (2006). "Mice with neuron-specific accumulation of mitochondrial DNA mutations show mood disorder-like phenotypes." Molecular Psychiatry **11**(6): 577-593.
- Kasiviswanathan, R., M. J. Longley, S. S. L. Chan and W. C. Copeland (2009). "Disease mutations in the human mitochondrial DNA polymerase thumb subdomain impart severe defects in mitochondrial DNA replication." Journal of Biological Chemistry **284**(29): 19501-19510.

- Kaukonen, J., J. K. Juselius, V. Tiranti, A. Kyttala, M. Zeviani, G. P. Comi, S. Keranen, L. Peltonen and A. Suomalainen (2000). "Role of adenine nucleotide translocator 1 in mtDNA maintenance." Science **289**(5480): 782-785.
- Kayihan, N., I. Nennesmo, B. G. Ericzon and A. NÄ©meth (2000). "Fatal deterioration of neurological disease after orthotopic liver transplantation for valproic acid-induced liver damage." Pediatric Transplantation **4**(3): 211-214.
- Kevin, L. G., A. K. S. Camara, M. L. Riess, E. Novalija and D. F. Stowe (2003). "Ischemic preconditioning alters real-time measure of O₂ radicals in intact hearts with ischemia and reperfusion." American Journal of Physiology - Heart and Circulatory Physiology **284**(2 53-2): H566-H574.
- Khan, A., C. Trevenen, X. C. Wei, H. B. Sarnat, E. Payne and A. Kirton (2012). "Alpers syndrome: The natural history of a case highlighting neuroimaging, neuropathology, and fat metabolism." Journal of Child Neurology **27**(5): 636-640.
- Kim, I. and J. J. Lemasters (2011). "Mitophagy selectively degrades individual damaged mitochondria after photoirradiation." Antioxidants and Redox Signaling **14**(10): 1919-1928.
- Kirby, D. M., M. Crawford, M. A. Cleary, H. H. M. Dahl, X. Dennett and D. Thorburn (1999). "Respiratory chain complex I deficiency: An underdiagnosed energy generation disorder." Neurology **52**(6): 1255-1264.
- Koc, E. C. and L. L. Spremulli (2002). "Identification of mammalian mitochondrial translational initiation factor 3 and examination of its role in initiation complex formation with natural mRNAs." Journal of Biological Chemistry **277**(38): 35541-35549.
- Kondo, R., E. T. Matsuura and S. I. Chigusa (1992). "Further observation of paternal transmission of drosophila mitochondrial DNA by PCR selective amplification method." Genetical Research **59**(2): 81-84.
- Koshiba, T., S. A. Detmer, J. T. Kaiser, H. Chen, J. M. McCaffery and D. C. Chan (2004). "Structural basis of mitochondrial tethering by mitofusin complexes." Science **305**(5685): 858-862.
- Kovalenko, S. A., G. Kopsidas, J. Kelso, F. Rosenfeldt and A. W. Linnane (1998). Tissue-specific distribution of multiple mitochondrial DNA rearrangements during human aging. **854**: 171-181.
- Kowald, A. and T. B. L. Kirkwood (2013). "Mitochondrial mutations and aging: random drift is insufficient to explain the accumulation of mitochondrial deletion mutants in short-lived animals." Aging Cell **12**(4): 728-731.

- Kruse, B., N. Narasimhan and G. Attardi (1989). "Termination of transcription in human mitochondria: Identification and purification of a DNA binding protein factor that promotes termination." Cell **58**(2): 391-397.
- Kunkel, T. A. and L. A. Loeb (1981). "Fidelity of mammalian DNA polymerases." Science **213**(4509): 765-767.
- Laforêt, P., A. Lombès, B. Eymard, C. Danan, M. Chevally, A. Rouche, P. Frachon and M. Fardeau (1995). "Chronic progressive external ophthalmoplegia with ragged-red fibers: Clinical, morphological and genetic investigations in 43 patients." Neuromuscular Disorders **5**(5): 399-413.
- Lamperti, C., D. Diodato, E. Lamantea, F. Carrara, D. Ghezzi, P. Mereghetti, R. Rizzi and M. Zeviani (2012). "MELAS-like encephalomyopathy caused by a new pathogenic mutation in the mitochondrial DNA encoded cytochrome c oxidase subunit I." Neuromuscular Disorders **22**(11): 990-994.
- Lax, N. Z., P. D. Hepplewhite, A. K. Reeve, V. Nesbitt, R. McFarland, E. Jaros, R. W. Taylor and D. M. Turnbull (2012). "Cerebellar ataxia in patients with mitochondrial DNA disease: A molecular clinicopathological study." Journal of Neuropathology and Experimental Neurology **71**(2): 148-161.
- Lee, Y. C., Y. C. Lu, M. H. Chang and B. W. Soong (2007). "Common mitochondrial DNA and POLG1 mutations are rare in the Chinese patients with adult-onset ataxia on Taiwan." Journal of the Neurological Sciences **254**(1-2): 65-68.
- Lee, Y. S., W. D. Kennedy and Y. W. Yin (2009). "Structural Insight into Processive Human Mitochondrial DNA Synthesis and Disease-Related Polymerase Mutations." Cell **139**(2): 312-324.
- Lee, Y. S., S. Lee, B. Demeler, I. J. Molineux, K. A. Johnson and Y. W. Yin (2010). "Each monomer of the dimeric accessory protein for human mitochondrial DNA polymerase has a distinct role in conferring processivity." Journal of Biological Chemistry **285**(2): 1490-1499.
- Leigh, D. (1951). "Subacute necrotizing encephalomyelopathy in an infant." Journal of neurology, neurosurgery, and psychiatry **14**(3): 216-221.
- Léon-Avila, G. and J. Tovar (2004). "Mitosomes of *Entamoeba histolytica* are abundant mitochondrion-related remnant organelles that lack a detectable organellar genome." Microbiology **150**(5): 1245-1250.
- Lewis, S., W. Hutchison, D. Thyagarajan and H. H. M. Dahl (2002). "Clinical and molecular features of adPEO due to mutations in the Twinkle gene." Journal of the Neurological Sciences **201**(1-2): 39-44.

- Lewis, W., B. J. Day, J. J. Kohler, S. H. Hosseini, S. S. L. Chan, E. C. Green, C. P. Haase, E. S. Keebaugh, R. Long, T. Ludaway, R. Russ, J. Steltzer, N. Tioleco, R. Santoianni and W. C. Copeland (2007). "Decreased mtDNA, oxidative stress, cardiomyopathy, and death from transgenic cardiac targeted human mutant polymerase γ ." Laboratory Investigation **87**(4): 326-335.
- Lim, S. E., M. J. Longley and W. C. Copeland (1999). "The mitochondrial p55 accessory subunit of human DNA polymerase γ enhances DNA binding, promotes processive DNA synthesis, and confers N-ethylmaleimide resistance." Journal of Biological Chemistry **274**(53): 38197-38203.
- Lindmark, D. G. and M. Muller (1973). "Hydrogenosome, a cytoplasmic organelle of the anaerobic flagellate *Tritrichomonas foetus*, and its role in pyruvate metabolism." Journal of Biological Chemistry **248**(22): 7724-7728.
- Liu, X., C. N. Kim, J. Yang, R. Jemmerson and X. Wang (1996). "Induction of apoptotic program in cell-free extracts: Requirement for dATP and cytochrome c." Cell **86**(1): 147-157.
- Longley, M. J., S. Clark, C. Y. W. Man, G. Hudson, S. E. Durham, R. W. Taylor, S. Nightingale, D. M. Turnbull, W. C. Copeland and P. F. Chinnery (2006). "Mutant POLG2 disrupts DNA polymerase γ subunits and causes progressive external ophthalmoplegia." American Journal of Human Genetics **78**(6): 1026-1034.
- Longley, M. J., D. Nguyen, T. A. Kunkel and W. C. Copeland (2001). "The Fidelity of Human DNA Polymerase γ with and without Exonucleolytic Proofreading and the p55 Accessory Subunit." Journal of Biological Chemistry **276**(42): 38555-38562.
- Luft, R., D. Ikkos, G. Palmieri, L. Ernster and B. Afzelius (1962). "A case of severe hypermetabolism of nonthyroid origin with a defect in." The Journal of clinical investigation **41**: 1776-1804.
- Luoma, P., A. Melberg, J. O. Rinne, J. A. Kaukonen, N. N. Nupponen, R. M. Chalmers, P. A. Oldfors, I. Rautakorpi, P. L. Peltonen, P. K. Majamaa, H. Somer and A. Suomalainen (2004). "Parkinsonism, premature menopause, and mitochondrial DNA polymerase γ mutations: Clinical and molecular genetic study." Lancet **364**(9437): 875-882.
- Lupashko, S., S. Malik, D. Donahue, A. Hernandez and M. S. Perry (2011). "Palliative functional hemispherectomy for treatment of refractory status epilepticus associated with Alpers' disease." Child's Nervous System **27**(8): 1321-1323.
- Mancuso, M., M. Filosto, V. K. Mootha, A. Rocchi, S. Pistolesi, L. Murri, S. DiMauro and G. Siciliano (2004). "A novel mitochondrial tRNAPhe mutation causes MERRF syndrome." Neurology **62**(11): 2119-2121.

- Mandavilli, B. S., J. H. Santos and B. Van Houten (2002). "Mitochondrial DNA repair and aging." Mutat Res **509**(1-2): 127-151.
- Manfredi, G., T. Vu, E. Bonilla, E. A. Schon, S. Dimauro, E. Arnaudo, L. Zhang, L. P. Rowland and M. Hirano (1997). "Association of myopathy with large-scale mitochondrial DNA duplications and deletions: Which is pathogenic?" Annals of Neurology **42**(2): 180-188.
- Mangalat, N., N. Tatevian, M. Bhattacharjee and J. M. Rhoads (2012). "Alpers syndrome: An unusual etiology of failure to thrive." Ultrastructural Pathology **36**(4): 219-221.
- Maranzana, E., G. Barbero, A. I. Falasca, G. Lenaz and M. L. Genova (2013). "Mitochondrial respiratory supercomplex association limits production of reactive oxygen species from Complex I." Antioxidants and Redox Signaling.
- Margulis, L. (1975). "Symbiotic theory of the origin of eukaryotic organelles; criteria for proof." Symposia of the Society for Experimental Biology(29): 21-38.
- Martz, D., R. J. Lasek, S. T. Brady and R. D. Allen (1984). "Mitochondrial motility in axons: membranous organelles may interact with the force generating system through multiple surface binding sites." Cell Motility **4**(2): 89-101.
- Mayr, J. A., V. Havlíčková, F. Zimmermann, I. Magler, V. Kaplanová, P. Ješina, A. Pecinová, H. Nůsková, J. Koch, W. Sperl and J. Houštěk (2010). "Mitochondrial ATP synthase deficiency due to a mutation in the ATP5E gene for the F1 ϵ subunit." Human Molecular Genetics **19**(17): 3430-3439.
- McFarland, R., G. Hudson, R. W. Taylor, S. H. Green, S. Hodges, P. J. McKiernan, P. F. Chinnery and V. Ramesh (2008). "Reversible valproate hepatotoxicity due to mutations in mitochondrial DNA polymerase γ (POLG1)." Archives of Disease in Childhood **93**(2): 151-153.
- McHugh, J. C., R. Lonergan, R. Howley, K. O'Rourke, R. W. Taylor, M. Farrell, M. Hutchinson and S. Connolly (2010). "Sensory ataxic neuropathy dysarthria and ophthalmoparesis (SANDO) in a sibling pair with a homozygous p.a467T POLG mutation." Muscle and Nerve **41**(2): 265-269.
- Metodiev, M. D., N. Lesko, C. B. Park, Y. Cámara, Y. Shi, R. Wibom, K. Hultenby, C. M. Gustafsson and N. G. Larsson (2009). "Methylation of 12S rRNA Is Necessary for In Vivo Stability of the Small Subunit of the Mammalian Mitochondrial Ribosome." Cell Metabolism **9**(4): 386-397.
- Mick, D. U., T. D. Fox and P. Rehling (2011). "Inventory control: Cytochrome c oxidase assembly regulates mitochondrial translation." Nature Reviews Molecular Cell Biology **12**(1): 14-20.

- Mitchell, P. (1961). "Coupling of phosphorylation to electron and hydrogen transfer by a chemi-osmotic type of mechanism." Nature **191**(4784): 144-148.
- Miwa, S., C. Lawless and T. Von Zglinicki (2008). "Mitochondrial turnover in liver is fast in vivo and is accelerated by dietary restriction: Application of a simple dynamic model." Aging Cell **7**(6): 920-923.
- Montoya, J., T. Christianson, D. Levens, M. Rabinowitz and G. Attardi (1982). "Identification of initiation sites for heavy-strand and light-strand transcription in human mitochondrial DNA." Proceedings of the National Academy of Sciences of the United States of America **79**(23 I): 7195-7199.
- Moraes, C. T., S. DiMauro, M. Zeviani, A. Lombes, S. Shanske, A. F. Miranda, H. Nakase, E. Bonilla, L. C. Werneck, S. Servidei, I. Nonaka, Y. Koga, A. J. Spiro, A. K. W. Brownell, B. Schmidt, D. L. Schotland, M. Zupanc and D. C. DeVivo (1989). "Mitochondrial DNA deletions in progressive external ophthalmoplegia and Kearne-Sayre syndrome." New England Journal of Medicine **320**(20): 1293-1299.
- Moslemi, A. R., M. Tulinius, E. Holme and A. Oldfors (1998). "Threshold expression of the tRNA(Lys) A8344G mutation in single muscle fibres." Neuromuscular Disorders **8**(5): 345-349.
- Muller, F. L., Y. Liu and H. Van Remmen (2004). "Complex III releases superoxide to both sides of the inner mitochondrial membrane." Journal of Biological Chemistry **279**(47): 49064-49073.
- Naess, K., M. Barbaro, H. Bruhn, R. Wibom, I. Nennesmo, U. von Döbeln, N. G. Larsson, A. Nemeth and N. Lesko (2012). "Complete deletion of a *POLG1* allele in a patient with Alpers syndrome." JIMD Reports **4**: 67-73.
- Naess, K., C. Freyer, H. Bruhn, R. Wibom, G. Malm, I. Nennesmo, U. von Döbeln and N. G. Larsson (2009). "MtDNA mutations are a common cause of severe disease phenotypes in children with Leigh syndrome." Biochimica et Biophysica Acta - Bioenergetics **1787**(5): 484-490.
- Nakamoto, R. K., J. A. Baylis Scanlon and M. K. Al-Shawi (2008). "The rotary mechanism of the ATP synthase." Archives of Biochemistry and Biophysics **476**(1): 43-50.
- Nangaku, M., R. Sato-Yoshitake, Y. Okada, Y. Noda, R. Takemura, H. Yamazaki and N. Hirokawa (1994). "KIF1B, a novel microtubule plus end-directed monomeric motor protein for transport of mitochondria." Cell **79**(7): 1209-1220.
- Napoli, L., A. Bordoni, M. Zeviani, G. M. Hadjigeorgiou, M. Sciacco, V. Tiranti, A. Terentiu, M. Moggio, A. Papadimitriou, G. Scarlato and G. P. Comi

- (2001). "A novel missense adenine nucleotide translocator-1 gene mutation in a greek adPEO family." Neurology **57**(12): 2295-2298.
- Nass, M. M. and S. Nass (1963). "INTRAMITOCHONDRIAL FIBERS WITH DNA CHARACTERISTICS. I. FIXATION AND." The Journal of cell biology **19**: 593-611.
- Naviaux, R. K. and K. V. Nguyen (2004). "POLG Mutations Associated with Alpers' Syndrome and Mitochondrial DNA Depletion." Annals of Neurology **55**(5): 706-712.
- Naviaux, R. K., W. L. Nyhan, B. A. Barshop, J. Poulton, D. Markusic, N. C. Karpinski and R. H. Haas (1999). "Mitochondrial DNA polymerase γ deficiency and mtDNA depletion in a child with Alpers' syndrome." Annals of Neurology **45**(1): 54-58.
- Neeve, V. C. M., D. C. Samuels, L. A. Bindoff, B. Van Den Bosch, G. Van Goethem, H. Smeets, A. Lombès, C. Jardel, M. Hirano, S. Dimauro, M. De Vries, J. Smeitink, B. W. Smits, I. F. M. De Coo, C. Saft, T. Klopstock, B. C. Keiling, B. Czermin, A. Abicht, H. Lochmüller, G. Hudson, G. G. Gorman, D. M. Turnbull, R. W. Taylor, E. Holinski-Feder, P. F. Chinnery and R. Horvath (2012). "What is influencing the phenotype of the common homozygous polymerase- γ mutation p.Ala467Thr?" Brain **135**(12): 3614-3626.
- Nekhaeva, E., N. D. Bodyak, Y. Kravtsov, S. B. McGrath, N. J. Van Orsouw, A. Pluzhnikov, J. Y. Wei, J. Vijg and K. Khrapko (2002). "Clonally expanded mtDNA point mutations are abundant in individual cells of human tissues." Proceedings of the National Academy of Sciences of the United States of America **99**(8): 5521-5526.
- Nguyen, K. V., E. Østergaard, S. Holst Ravn, T. Balslev, E. Rubæk Danielsen, A. Vardag, P. J. McKiernan, G. Gray and R. K. Naviaux (2005). "POLG mutations in Alpers syndrome." Neurology **65**(9): 1493-1495.
- Nguyen, K. V., F. S. Sharief, S. S. L. Chan, W. C. Copeland and R. K. Naviaux (2006). "Molecular diagnosis of Alpers syndrome." Journal of Hepatology **45**(1): 108-116.
- Nikoskelainen, E. K., M. L. Savontaus, K. Huoponen, K. Antila and J. Hartiala (1994). "Pre-excitation syndrome in Leber's hereditary optic neuropathy." Lancet **344**(8926): 857-858.
- Nishino, I., A. Spinazzola and M. Hirano (1999). "Thymidine phosphorylase gene mutations in MNGIE, a human mitochondrial disorder." Science **283**(5402): 689-692.
- Noer, A. S., H. Sudoyo, P. Lertrit, D. Thyagarajan, P. Utthanaphol, R. Kapsa, E. Byrne and S. Marzuki (1991). "A tRNA(Lys) mutation in the mtDNA is the causal genetic lesion underlying myoclonic epilepsy and ragged-red fiber (MERRF) syndrome." Am J Hum Genet **49**(4): 715-722.

- Nolte, K. W., S. Trepels-Kottek, D. Honnef, J. Weis, C. G. Bien, A. van Baalen, K. Ritter, B. Czermin, S. Rudnik-Schöneborn, N. Wagner and M. Häusler (2013). "Early muscle and brain ultrastructural changes in polymerase gamma 1-related encephalomyopathy." Neuropathology **33**(1): 59-67.
- Nordli Jr, D. R., M. M. Kuroda, J. Carroll, D. Y. Koenigsberger, L. J. Hirsch, H. J. Bruner, W. T. Seidel and D. C. De Vivo (2001). "Experience with the ketogenic diet in infants." Pediatrics **108**(1): 129-133.
- Nowak, R., R. Zub, I. Skoneczna, K. Sikora and M. Ligaj (2005). "CAG repeat polymorphism in the DNA polymerase γ gene in a Polish population: An association with testicular cancer risk [5]." Annals of Oncology **16**(7): 1211-1212.
- Ojala, D., J. Montoya and G. Attardi (1981). "tRNA punctuation model of RNA processing in human mitochondria." Nature **290**(5806): 470-474.
- Otera, H., C. Wang, M. M. Cleland, K. Setoguchi, S. Yokota, R. J. Youle and K. Mihara (2010). "Mff is an essential factor for mitochondrial recruitment of Drp1 during mitochondrial fission in mammalian cells." Journal of Cell Biology **191**(6): 1141-1158.
- Ozawa, M., I. Nishino, S. Horai, I. Nonaka and Y. I. Goto (1997). "Myoclonus epilepsy associated with ragged-red fibers: A G-to-A mutation at nucleotide pair 8363 in mitochondrial tRNA(Lys) in two families." Muscle and Nerve **20**(3): 271-278.
- Page, C. C., C. C. Moser, X. Chen and P. L. Dutton (1999). "Natural engineering principles of electron tunnelling in biological oxidation-reduction." Nature **402**(6757): 47-52.
- Pagnamenta, A. T., J. W. Taanman, C. J. Wilson, N. E. Anderson, R. Marotta, A. J. Duncan, M. Bitner-Glindzicz, R. W. Taylor, A. Laskowski, D. R. Thorburn and S. Rahman (2006). "Dominant inheritance of premature ovarian failure associated with mutant mitochondrial DNA polymerase gamma." Human Reproduction **21**(10): 2467-2473.
- Palaniyandi, S. S., X. Qi, G. Yogalingam, J. C. B. Ferreira and D. Mochly-Rosen (2010). "Regulation of mitochondrial processes: A target for heart failure." Drug Discovery Today: Disease Mechanisms **7**(2): e95-e102.
- Pfeiffer, T., S. Schuster and S. Bonhoeffer (2001). "Cooperation and competition in the evolution of ATP-producing pathways." Science **292**(5516): 504-507.
- Pinz, K. G. and D. F. Bogenhagen (1998). "Efficient repair of abasic sites in DNA by mitochondrial enzymes." Molecular and Cellular Biology **18**(3): 1257-1265.
- Pohjoismäki, J. L. O., J. B. Holmes, S. R. Wood, M. Y. Yang, T. Yasukawa, A. Reyes, L. J. Bailey, T. J. Cluett, S. Goffart, S. Willcox, R. E. Rigby, A. P.

- Jackson, J. N. Spelbrink, J. D. Griffith, R. J. Crouch, H. T. Jacobs and I. J. Holt (2010). "Mammalian mitochondrial DNA replication intermediates are essentially duplex but contain extensive tracts of RNA/DNA hybrid." Journal of Molecular Biology **397**(5): 1144-1155.
- Poongothai, J. (2013). "Mitochondrial DNA polymerase gamma gene polymorphism is not associated with male infertility." Journal of Assisted Reproduction and Genetics: 1-6.
- Poulton, J., M. E. Deadman, L. Bindoff, K. Morten, J. Land and G. Brown (1993). "Families of mtDNA re-arrangements can be detected in patients with mtDNA deletions: duplications may be a transient intermediate form." Human Molecular Genetics **2**(1): 23-30.
- Poulton, J., M. E. Deadman and R. M. Gardiner (1989). "Duplications of mitochondrial DNA in mitochondrial myopathy." Lancet **1**(8632): 236-240.
- Poulton, J., K. J. Morten, K. Weber, G. K. Brown and L. Bindoff (1994). "Are duplications of mitochondrial DNA characteristic of Kearns-Sayre syndrome?" Human Molecular Genetics **3**(6): 947-951.
- Poulton, J., C. Sewry, C. G. Potter, T. Bougeron, D. Chretien, F. A. Wijburg, K. J. Morten and G. Brown (1995). "Variation in mitochondrial DNA levels in muscle from normal controls. Is depletion of mtDNA in patients with mitochondrial myopathy a distinct clinical syndrome?" Journal of Inherited Metabolic Disease **18**(1): 4-20.
- Prick, M. J. J., F. J. M. Gabreels, W. O. Renier, J. M. Trijbels, J. L. Willems, A. J. Janssen, J. L. Slooff, J. A. Geelen and J. P. de Jager (1982). "Progressive infantile poliodystrophy (Alpers' disease) with a defect in citric acid cycle activity in liver and fibroblasts." Neuropediatrics **13**(2): 108-111.
- Pronicka, E., A. Weglewska-Jurkiewicz, M. Pronicki, J. Sykut-Cegielska, P. Kowalski, M. Pajdowska, I. Jankowska, K. Kotulska, P. Kaliciński, J. Jakóbkiewicz-Banecka and G. Węgrzyn (2011). "Drug-resistant epilepsy and fulminant valproate liver toxicity. Alpers-Huttenlocher syndrome in two children confirmed post mortem by identification of p.W748S mutation in POLG gene." Medical Science Monitor **17**(4): 203-209.
- Rahman, S., R. B. Blok, H. H. M. Dahl, D. M. Danks, D. M. Kirby, C. W. Chow, J. Christodoulou and D. R. Thorburn (1996). "Leigh syndrome: Clinical features and biochemical and DNA abnormalities." Annals of Neurology **39**(3): 343-351.
- Rani, D. S., S. J. Carlus, J. Poongothai, A. Jyothi, K. Pavani, N. J. Gupta, A. G. Reddy, M. M. Rajan, K. Rao, B. Chakravarty, L. Singh and K. Thangaraj (2009). "CAG repeat variation in the mtDNA polymerase γ is not associated with oligoasthenozoospermia." International Journal of Andrology **32**(6): 647-655.

- Rantanen, A., M. Gaspari, M. Falkenberg, C. M. Gustafsson and N. G. Larsson (2003). "Characterization of the mouse genes for mitochondrial transcription factors B1 and B2." Mammalian Genome **14**(1): 1-6.
- Reeves, S. G. and D. O. Hall (1973). "The stoichiometry (ATP/2e ratio) of non cyclic photophosphorylation in isolated spinach chloroplasts." Biochimica et Biophysica Acta **314**(1): 66-78.
- Reyes, A., L. Kazak, S. R. Wood, T. Yasukawa, H. T. Jacobs and I. J. Holt (2013). "Mitochondrial DNA replication proceeds via a 'bootlace' mechanism involving the incorporation of processed transcripts." Nucleic Acids Research **41**(11): 5837-5850.
- Rial, E. and D. G. Nicholls (1984). "The mitochondrial uncoupling protein from guinea-pig brown adipose tissue. Synchronous increase in structural and functional parameters during cold-adaptation." Biochemical Journal **222**(3): 685-693.
- Richards, M., V. Macaulay, E. Hickey, E. Vega, B. Sykes, V. Guida, C. Rengo, D. Sellitto, F. Cruciani, T. Kivisild, R. Villems, M. Thomas, S. Rychkov, O. Rychkov, Y. Rychkov, M. Golge, D. Dimitrov, E. Hill, D. Bradley, V. Romano, F. Cali, G. Vona, A. Demaine, S. Papiha, C. Triantaphyllidis, G. Stefanescu, J. Hatina, M. Belledi, A. Di Rienzo, A. Novelletto, A. Oppenheim, S. Norby, N. Al-Zaheri, S. Santachiara-Benerecetti, R. Scozzari, A. Torroni and H. J. Bandelt (2000). "Tracing European founder lineages in the Near Eastern mtDNA pool." American Journal of Human Genetics **67**(5): 1251-1276.
- Riordan-Eva, P., M. D. Sanders, G. G. Govan, M. G. Sweeney, J. Da Costa and A. E. Harding (1995). "The clinical features of Leber's hereditary optic neuropathy defined by the presence of a pathogenic mitochondrial DNA mutation." Brain **118**(2): 319-337.
- Robberson, D. L. and D. A. Clayton (1972). "Replication of mitochondrial DNA in mouse L cells and their thymidine kinase - derivatives: displacement replication on a covalently-closed circular template." Proceedings of the National Academy of Sciences of the United States of America **69**(12): 3810-3814.
- Ropp, P. A. and W. C. Copeland (1996). "Cloning and characterization of the human mitochondrial DNA polymerase, DNA polymerase gamma." Genomics **36**(3): 449-458.
- Rossi, C. S. and A. L. Lehninger (1964). "STOICHIOMETRY OF RESPIRATORY STIMULATION, ACCUMULATION OF CA⁺⁺ AND." The Journal of biological chemistry **239**: 3971-3980.
- Rossignol, R., B. Faustin, C. Rocher, M. Malgat, J. P. Mazat and T. Letellier (2003). "Mitochondrial threshold effects." Biochemical Journal **370**(3): 751-762.

- Rouzier, C., A. Chaussenot, V. Serre, K. Fragaki, S. Bannwarth, S. Ait-El-Mkadem, S. Attarian, E. Kaphan, A. Cano, E. Delmont, S. Sacconi, B. M. de Camaret, M. Rio, A. S. Lebre, C. Jardel, R. Deschamps, C. Richelme, J. Pouget, B. Chabrol and V. Paquis-Flucklinger (2013). "Quantitative multiplex PCR of short fluorescent fragments for the detection of large intragenic POLG rearrangements in a large French cohort." European Journal of Human Genetics.
- Rovio, A. T., D. R. Marchington, S. Donat, H. C. Schuppe, J. Abel, E. Fritsche, D. J. Elliott, P. Laippala, A. L. Ahola, D. McNay, R. F. Harrison, B. Hughes, T. Barrett, D. M. D. Bailey, D. Mehmet, A. M. Jequier, T. B. Hargreave, S. H. Kao, J. M. Cummins, D. E. Barton, H. J. Cooke, Y. H. Wei, L. Wichmann, J. Poulton and H. T. Jacobs (2001). "Mutations at the mitochondrial DNA polymerase (POLG) locus associated with male infertility." Nature Genetics **29**(3): 261-262.
- Roy, J., J. K. Mitra and A. Pal (2013). "Magnesium sulphate versus phenytoin in eclampsia - Maternal and foetal outcome - A comparative study." Australasian Medical Journal **6**(9): 483-495.
- Saneto, R. P., I. C. Lee, M. K. Koenig, X. Bao, S. W. Weng, R. K. Naviaux and L. J. C. Wong (2010). "POLG DNA testing as an emerging standard of care before instituting valproic acid therapy for pediatric seizure disorders." Seizure **19**(3): 140-146.
- Scalais, E., B. Francois, P. Schlessler, R. Stevens, C. Nuttin, J. J. Martin, R. Van Coster, S. Seneca, F. Roels, G. Van Goethem, A. Löfgren and L. De Meirleir (2012). "Polymerase gamma deficiency (POLG): Clinical course in a child with a two stage evolution from infantile myocerebrohepatopathy spectrum to an Alpers syndrome and neuropathological findings of Leigh's encephalopathy." European Journal of Paediatric Neurology **16**(5): 542-548.
- Schaefer, A. M., R. McFarland, E. L. Blakely, L. He, R. G. Whittaker, R. W. Taylor, P. F. Chinnery and D. M. Turnbull (2008). "Prevalence of mitochondrial DNA disease in adults." Annals of Neurology **63**(1): 35-39.
- Schägger, H. and K. Pfeiffer (2000). "Supercomplexes in the respiratory chains of yeast and mammalian mitochondria." EMBO Journal **19**(8): 1777-1783.
- Schaller, A., D. Hahn, C. B. Jackson, I. Kern, C. Chardot, D. C. Belli, S. Gallati and J. Nuoffer (2011). "Molecular and biochemical characterisation of a novel mutation in POLG associated with Alpers syndrome." BMC Neurology **11**.
- Schwartz, M. and J. Vissing (2002). "Paternal inheritance of mitochondrial DNA." New England Journal of Medicine **347**(8): 576-580.
- Sciacco, M., E. Bonilla, E. A. Schon, S. DiMauro and C. T. Moraes (1994). "Distribution of wild-type and common deletion forms of mtDNA in normal

- and respiration-deficient muscle fibers from patients with mitochondrial myopathy." Human Molecular Genetics **3**(1): 13-19.
- Shadel, G. S. and D. A. Clayton (1997). Mitochondrial DNA maintenance in vertebrates. **66**: 409-436.
- Shaibani, A., O. A. Shchelochkov, S. Zhang, P. Katsonis, O. Lichtarge, L. J. Wong and M. Shinawi (2009). "Mitochondrial neurogastrointestinal encephalopathy due to mutations in RRM2B." Archives of Neurology **66**(8): 1028-1032.
- Shalgi, R., A. Magnus, R. Jones and D. M. Phillips (1994). "Fate of sperm organelles during early embryogenesis in the rat." Molecular Reproduction and Development **37**(3): 264-271.
- Shoffner, J. M., M. T. Lott, A. M. S. Lezza, P. Seibel, S. W. Ballinger and D. C. Wallace (1990). "Myoclonic Epilepsy and Ragged-Red Fiber Disease (MERRF) is associated with a mitochondrial DNA tRNALys mutation." Cell **61**(6): 931-937.
- Silvestri, G., C. T. Moraes, S. Shanske, S. J. Oh and S. DiMauro (1992). "A new mtDNA mutation in the tRNA(Lys) gene associated with myoclonic epilepsy and ragged-red fibers (MERRF)." Am J Hum Genet **51**(6): 1213-1217.
- Simon, M., R. Chang, D. Bali, L.-J. Wong, Y. Peng and J. Abdenur (2013). *Abnormalities in Glycogen Metabolism in a Patient with Alpers' Syndrome Presenting with Hypoglycemia*, Springer Berlin Heidelberg: 1-7.
- Simonati, A., M. Filosto, C. Savio, G. Tomelleri, P. Tonin, B. Dalla Bernardina and N. Rizzuto (2003a). "Features of cell death in brain and liver, the target tissues of progressive neuronal degeneration of childhood with liver disease (Alpers-Huttenlocher disease)." Acta Neuropathologica **106**(1): 57-65.
- Simonati, A., M. Filosto, G. Tomelleri, C. Savio, P. Tonin, A. Polo and N. Rizzuto (2003b). "Central-peripheral sensory axonopathy in a juvenile case of Alpers-Huttenlocher disease." Journal of Neurology **250**(6): 702-706.
- Smith, P. M., J. L. Fox and D. R. Winge (2012). "Reprint of: Biogenesis of the cytochrome bc1 complex and role of assembly factors." Biochimica et Biophysica Acta - Bioenergetics **1817**(6): 872-882.
- Smits, P., J. A. M. Smeitink, L. P. van den Heuvel, M. A. Huynen and T. J. G. Ettema (2007). "Reconstructing the evolution of the mitochondrial ribosomal proteome." Nucleic Acids Research **35**(14): 4686-4703.
- Soleimanpour-Lichaei, H. R., I. Kühn, M. Gaisne, J. F. Passos, M. Wydro, J. Rorbach, R. Temperley, N. Bonnefoy, W. Tate, R. Lightowlers and Z.

- Chrzanowska-Lightowlers (2007). "mtRF1a Is a Human Mitochondrial Translation Release Factor Decoding the Major Termination Codons UAA and UAG." Molecular Cell **27**(5): 745-757.
- Someya, S., T. Yamasoba, G. C. Kujoth, T. D. Pugh, R. Weindruch, M. Tanokura and T. A. Prolla (2008). "The role of mtDNA mutations in the pathogenesis of age-related hearing loss in mice carrying a mutator DNA polymerase γ ." Neurobiology of Aging **29**(7): 1080-1092.
- Song, Z., H. Chen, M. Fiket, C. Alexander and D. C. Chan (2007). "OPA1 processing controls mitochondrial fusion and is regulated by mRNA splicing, membrane potential, and Yme1L." Journal of Cell Biology **178**(5): 749-755.
- Soong, N. W., D. R. Hinton, G. Cortopassi and N. Arnheim (1992). "Mosaicism for a specific somatic mitochondrial DNA mutation in adult human brain." Nature Genetics **2**(4): 318-323.
- Spiegler, J., I. Stefanova, Y. Hellenbroich and J. Sperner (2011). "Bowel obstruction in patients with Alpers-Huttenlocher syndrome." Neuropediatrics **42**(5): 194-196.
- Strauss, M., G. Hofhaus, R. R. Schröder and W. Kühlbrandt (2008). "Dimer ribbons of ATP synthase shape the inner mitochondrial membrane." EMBO Journal **27**(7): 1154-1160.
- Suh, B. C., H. N. Jeong, B. S. Yoon, J. H. Park, H. J. Kim, S. W. Park, J. H. Hwang, B. O. Choi and K. W. Chung (2013). "Compound heterozygous mutations of TYMP as underlying causes of mitochondrial neurogastrointestinal encephalomyopathy (MNGIE)." Molecular Medicine Reports **8**(1): 17-22.
- Sun, F., X. Huo, Y. Zhai, A. Wang, J. Xu, D. Su, M. Bartlam and Z. Rao (2005). "Crystal structure of mitochondrial respiratory membrane protein Complex II." Cell **121**(7): 1043-1057.
- Susin, S. A., E. Daugas, L. Ravagnan, K. Samejima, N. Zamzami, M. Loeffler, P. Costantini, K. F. Ferri, T. Irinopoulou, M. C. Prévost, G. Brothers, T. W. Mak, J. Penninger, W. C. Earnshaw and G. Kroemer (2000). "Two distinct pathways leading to nuclear apoptosis." Journal of Experimental Medicine **192**(4): 571-579.
- Susin, S. A., H. K. Lorenzo, N. Zamzami, I. Marzo, B. E. Snow, G. M. Brothers, J. Mangion, E. Jacotot, P. Costantini, M. Loeffler, N. Larochette, D. R. Goodlett, R. Aebersold, D. P. Siderovski, J. M. Penninger and G. Kroemer (1999). "Molecular characterization of mitochondrial apoptosis-inducing factor." Nature **397**(6718): 441-446.
- Taanman, J. W., S. Rahman, A. T. Pagnamenta, A. A. M. Morris, M. Bitner-Glindzicz, N. I. Wolf, J. V. Leonard, P. T. Clayton and A. H. V. Schapira

- (2009). "Analysis of mutant DNA polymerase γ in patients with mitochondrial DNA depletion." Human Mutation **30**(2): 248-254.
- Tatuch, Y., J. Christodoulou, A. Feigenbaum, J. T. R. Clarke, J. Wherret, C. Smith, N. Rudd, R. Petrova-Benedict and B. H. Robinson (1992). "Heteroplasmic mtDNA mutation (T→G) at 8993 can cause Leigh disease when the percentage of abnormal mtDNA is high." American Journal of Human Genetics **50**(4): 852-858.
- Temperley, R., R. Richter, S. Dennerlein, R. N. Lightowlers and Z. M. Chrzanowska-Lightowlers (2010). "Hungry codons promote frameshifting in human mitochondrial ribosomes." Science **327**(5963): 301.
- Tiranti, V., K. Hoernagel, R. Carrozzo, C. Calimberti, M. Munaro, M. Granatiero, L. Zelante, P. Gasparini, R. Marzella, M. Rocchi, M. Pilar Bayona-Bafaluy, J. A. Enriquez, G. Uziel, E. Bertini, C. Dionisi-Vici, B. Franco, T. Meitinger and M. Zeviani (1998). "Mutations of SURF-1 in Leigh disease associated with cytochrome C oxidase deficiency." American Journal of Human Genetics **63**(6): 1609-1621.
- Tiranti, V., A. Savoia, F. Forti, M. F. D'Apolito, M. Centra, M. Rocchi and M. Zeviani (1997). "Identification of the gene encoding the human mitochondrial RNA polymerase (h-mtRPOL) by cyberscreening of the Expressed Sequence Tags database." Human Molecular Genetics **6**(4): 615-625.
- Tovar, J., A. Fischer and C. G. Clark (1999). "The mitosome, a novel organelle related to mitochondria in the amitochondrial parasite *Entamoeba histolytica*." Molecular Microbiology **32**(5): 1013-1021.
- Trifunovic, A., A. Wredenberg, M. Falkenberg, J. N. Spelbrink, A. T. Rovio, C. E. Bruder, M. Bohlooly-Y, S. Gidlöf, A. Oldfors, R. Wibom, J. Törnell, H. T. Jacobs and N. G. Larsson (2004). "Premature ageing in mice expressing defective mitochondrial DNA polymerase." Nature **429**(6990): 417-423.
- Tzoulis, C., B. A. Engelsen, W. Telstad, J. Aasly, M. Zeviani, S. Winterthun, G. Ferrari, J. H. Aarseth and L. A. Bindoff (2006). "The spectrum of clinical disease caused by the A467T and W748S POLG mutations: A study of 26 cases." Brain **129**(7): 1685-1692.
- Uusimaa, J., R. Hinttala, H. Rantala, M. Päivärinta, R. Herva, M. Röttä, H. Soini, J. S. Moilanen, A. M. Remes, I. E. Hassinen and K. Majamaa (2008). "Homozygous W748S mutation in the POLG1 gene in patients with juvenile-onset Alpers syndrome and status epilepticus." Epilepsia **49**(6): 1038-1045.
- Van Goethem, G., B. Dermaut, A. Löfgren, J. J. Martin and C. Van Broeckhoven (2001). "Mutation of POLG is associated with progressive external ophthalmoplegia characterized by mtDNA deletions." Nature Genetics **28**(3): 211-212.

- Van Goethem, G., J. J. Martin, B. Dermaut, A. Löfgren, A. Wibail, D. Ververken, P. Tack, I. Dehaene, M. Van Zandijcke, M. Moonen, C. Ceuterick, P. De Jonghe and C. Van Broeckhoven (2003). "Recessive POLG mutations presenting with sensory and ataxic neuropathy in compound heterozygote patients with progressive external ophthalmoplegia." Neuromuscular Disorders **13**(2): 133-142.
- Varadi, A., L. I. Johnson-Cadwell, V. Cirulli, Y. Yoon, V. J. Allan and G. A. Rutter (2004). "Cytoplasmic dynein regulates the subcellular distribution of mitochondria by controlling the recruitment of the fission factor dynamin-related protein-1." Journal of Cell Science **117**(19): 4389-4400.
- Visser, N. A., K. P. J. Braun, F. S. S. Leijten, O. van Nieuwenhuizen, J. H. J. Wokke and W. M. van den Bergh (2011). "Magnesium treatment for patients with refractory status epilepticus due to POLG1-mutations." Journal of Neurology: 1-5.
- Visser, N. A., K. P. J. Braun, W. M. Van Den Bergh, F. S. S. Leijten, C. R. B. Willems, L. Ramos, B. J. C. Van Den Bosch, H. J. M. Smeets and J. H. J. Wokke (2010). "Juvenile-onset alpers syndrome: Interpreting MRI findings." Neurology **74**(15): 1231-1233.
- Vogel, F., C. Bornhövd, W. Neupert and A. S. Reichert (2006). "Dynamic subcompartmentalization of the mitochondrial inner membrane." Journal of Cell Biology **175**(2): 237-247.
- Vogel, R. O., J. A. M. Smeitink and L. G. J. Nijtmans (2007). "Human mitochondrial complex I assembly: A dynamic and versatile process." Biochimica et Biophysica Acta - Bioenergetics **1767**(10): 1215-1227.
- Vonck, J. and E. Schäfer (2009). "Supramolecular organization of protein complexes in the mitochondrial inner membrane." Biochimica et Biophysica Acta - Molecular Cell Research **1793**(1): 117-124.
- Walker, R. L., P. Anziano and P. S. Meltzer (1997). "A PAC containing the human mitochondrial DNA polymerase gamma gene (POLG) maps to chromosome 15q25." Genomics **40**(2): 376-378.
- Wallace, D. C. (1992). "Mitochondrial genetics: A paradigm for aging and degenerative diseases?" Science **256**(5057): 628-632.
- Wallace, D. C., G. Singh, M. T. Lott, J. A. Hodge, G. T. Schurr, A. M. S. Lezza, L. J. Elsas li and E. K. Nikoskelainen (1988). "Mitochondrial DNA mutation associated with Leber's hereditary optic neuropathy." Science **242**(4884): 1427-1430.
- Walter, M. C., B. Czermin, S. Muller-Ziermann, S. Bulst, J. D. Stewart, G. Hudson, P. Schneiderat, A. Abicht, E. Holinski-Feder, H. Lochmüller, P. F. Chinnery, T. Klopstock and R. Horvath (2010). "Late-onset ptosis and

- myopathy in a patient with a heterozygous insertion in POLG2." Journal of Neurology **257**(9): 1517-1523.
- Wang, Z. G., P. S. White and S. H. Ackerman (2001). "Atp11p and Atp12p are Assembly Factors for the F1-ATPase in Human Mitochondria." Journal of Biological Chemistry **276**(33): 30773-30778.
- Wiltshire, E., G. Davidzon, S. Dimauro, H. O. Akman, L. Sadleir, L. Haas, J. Zuccollo, A. McEwen and D. R. Thorburn (2008). "Juvenile Alpers disease." Archives of Neurology **65**(1): 121-124.
- Winterthun, S., G. Ferrari, L. He, R. W. Taylor, M. Zeviani, D. M. Turnbull, B. A. Engelsens, G. Moen and L. A. Bindoff (2005). "Autosomal recessive mitochondrial ataxic syndrome due to mitochondrial polymerase γ mutations." Neurology **64**(7): 1204-1208.
- Wolff, J. N., M. Nafisnia, P. Sutovsky and J. W. O. Ballard (2013). "Paternal transmission of mitochondrial DNA as an integral part of mitochondrial inheritance in metapopulations of *Drosophila simulans*." Heredity **110**(1): 57-62.
- Yakubovskaya, E., Z. Chen, J. A. Carrodeguas, C. Kisker and D. F. Bogenhagen (2006). "Functional human mitochondrial DNA polymerase γ forms a heterotrimer." Journal of Biological Chemistry **281**(1): 374-382.
- Yamasoba, T., S. Someya, C. Yamada, R. Weindruch, T. A. Prolla and M. Tanokura (2007). "Role of mitochondrial dysfunction and mitochondrial DNA mutations in age-related hearing loss." Hearing Research **226**(1-2): 185-193.
- Yang, M. Y., M. Bowmaker, A. Reyes, L. Vergani, P. Angeli, E. Gringeri, H. T. Jacobs and I. J. Holt (2002). "Biased incorporation of ribonucleotides on the mitochondrial L-strand accounts for apparent strand-asymmetric DNA replication." Cell **111**(4): 495-505.
- Yasukawa, T., A. Reyes, T. J. Cluett, M. Y. Yang, M. Bowmaker, H. T. Jacobs and I. J. Holt (2006). "Replication of vertebrate mitochondrial DNA entails transient ribonucleotide incorporation throughout the lagging strand." EMBO Journal **25**(22): 5358-5371.
- Zamzami, N., P. Marchetti, M. Castedo, D. Decaudin, A. Macho, T. Hirsch, S. A. Susin, P. X. Petit, B. Mignotte and G. Kroemer (1995). "Sequential reduction of mitochondrial transmembrane potential and generation of reactive oxygen species in early programmed cell death." Journal of Experimental Medicine **182**(2): 367-377.
- Zeviani, M., C. T. Moraes, S. DiMauro, H. Nakase, E. Bonilla, E. A. Schon and L. P. Rowland (1988). "Deletions of mitochondrial DNA in Kearns-Sayre syndrome." Neurology **38**(9): 1339-1346.

- Zhang, D., J. L. Mott, S. W. Chang, G. Denniger, Z. Feng and H. P. Zassenhaus (2000). "Construction of transgenic mice with tissue-specific acceleration of mitochondrial DNA mutagenesis." Genomics **69**(2): 151-161.
- Zhang, Y. and L. L. Spremulli (1998). "Identification and cloning of human mitochondrial translational release factor 1 and the ribosome recycling factor." Biochimica et Biophysica Acta - Gene Structure and Expression **1443**(1-2): 245-250.
- Zhu, Z., J. Yao, T. Johns, K. Fu, I. De Bie, C. Macmillan, A. P. Cuthbert, R. F. Newbold, J. C. Wang, M. Chevrette, G. K. Brown, R. M. Brown and E. A. Shoubridge (1998). "SURF1, encoding a factor involved in the biogenesis of cytochrome c oxidase, is mutated in Leigh syndrome." Nature Genetics **20**(4): 337-343.
- Züchner, S., I. V. Mersiyanova, M. Muglia, N. Bissar-Tadmouri, J. Rochelle, E. L. Dadali, M. Zappia, E. Nelis, A. Patitucci, J. Senderek, Y. Parman, O. Evgrafov, P. De Jonghe, Y. Takahashi, S. Tsuji, M. A. Pericak-Vance, A. Quattrone, E. Battologlu, A. V. Polyakov, V. Timmerman, J. M. Schröder and J. M. Vance (2004). "Mutations in the mitochondrial GTPase mitofusin 2 cause Charcot-Marie-Tooth neuropathy type 2A." Nature Genetics **36**(5): 449-451.

Chapter 2 Materials and Methods

2.1 Materials

This section will detail all materials used during this project.

2.1.1 Solutions

Citrate Buffer 0.01M, pH6.0	2.94g Sodium citrate
	1 Litre Deionised water
Developer Solution	7.4ml Formaldehyde 40%
	50µl Nitric acid
	0.5g Citric acid
	100ml Deionised water
DNA Loading Buffer	0.125g Bromophenol blue
	0.125g Xylene Cyanol
	15ml Glycerol
	35ml Deionised water
EDTA 0.001M, pH8.0	0.416g EDTA
	1 Litre Deionised water
Eosin Solution	10g Eosin Yellowish
	0.25g Phloxine B
	0.25g Erythrosin B
	1 Litre of 20% ethanol in tap water
	Filter before use

Haematoxylin Solution	1g Haematoxylin powder
	10ml Ethanol
	90ml Deionised water
	2ml Saturated lithium carbonate
Iron Alum 4%	4g Ammonium iron(III) sulphate dodecahydrate
	100ml Deionised water
Lysis Buffer	50µl Tris-HCl
	250µl 1% Tween [®]
	5µl Proteinase K
	195µl DEPC-treated water
Phosphate Buffered Saline (PBS)	One tablet dissolved in
	100ml deionised water
Scott's Tap Water	2g Sodium bicarbonate
	20g Magnesium sulphate
	1 Litre tap water
	A few crystals of thymol
Tris Buffered Saline (TBS) pH7.4	1.2g Trisma base
	17g Sodium chloride
	2 Litres Deionised water
TBST with Tween [®] pH7.4	1.2g Trisma base
	17g Sodium chloride
	1ml Tween [®]

2 Litres Deionised water

2.1.2 Chemicals

2.1.2.1 Histological Reagents

Acetic Acid Analar	BDH
Ammonia Analar	BDH
Ammonium Iron(III) Sulphate Dodecahydrate	Sigma
Calcium Chloride	Sigma
Catalase	Sigma
Citric Acid	Fisher Scientific
Cresyl Violet Acetate	Sigma
Cytochrome c	Sigma
3, 3' Diaminobenzidine Tetrahydrochloride (DAB) tablets and liquid	Sigma
DPX™ Mountant	CellPath
EDTA	USB
Eosin Yellowish	Raymond Lamb
Ethanol Analar	Fisher Scientific
Ethidium Bromide	Sigma
Erythrosin B	Raymond Lamb
Formaldehyde Solution	Sigma
Gold Chloride (Sodium Chloroaurate)	Sigma
Haematoxylin Powder	Fisher Scientific
Haematoxylin Liquid (Meyer's)	Fisher Scientific
Histoclear™	National Diagnostics

Hydrochloric Acid ~37%	Fisher Scientific
Hydrogen Peroxide 30% (w/w)	Sigma
Lithium Carbonate	BDH
Magnesium Sulphate	Sigma
Nitric Acid	BDH
Nitro Blue Tetrazolium	Sigma
Phenazine Methosulphate	Sigma
Phloxine B	Raymond Lamb
Phosphate Buffered Saline (PBS) Tablets	Oxoid
Proteinase K	Invitrogen
Silver Nitrate Analar	VWR
Sodium Azide	Sigma
Sodium Acetate	BDH
Sodium Bicarbonate	Sigma
Sodium Chloride	Sigma
Sodium Citrate Analar	VWR
Sodium Hydroxide Analar	VWR
Sodium Succinate	Sigma
Sodium Thiosulphate Analar	BDH
Thymol	Sigma
Trypsin	Sigma
Trisma Base	Sigma

Tween [®] 20	Sigma
-----------------------	-------

2.1.2.2 Polymerase Chain Reaction

Deoxynucleotide Triphosphates	Roalab
-------------------------------	--------

DEPC-treated Water	Ambion
--------------------	--------

GoTaq [®] Polymerase	Promega
-------------------------------	---------

GoTaq [®] Hot Start Polymerase	Promega
-----------------------------------------	---------

Magnesium Chloride	Promega
--------------------	---------

5X GoTaq [®] PCR Buffer	Promega
----------------------------------	---------

5X GoTaq [®] Flexi PCR Buffer	Promega
----------------------------------------	---------

TaqMan [®] TAMRA [™] ND1/ND4 Probes	Applied Biosystems
-------------------------------------------------------	--------------------

TaqMan [®] Universal PCR Mastermix	Applied Biosystems
---------------------------------------------	--------------------

2.1.2.3 Gel Electrophoresis

Agarose Powder	Bioline
----------------	---------

Bromophenol Blue	Sigma
------------------	-------

1Kb DNA Ladder	Norgen
----------------	--------

GelRed [™] Nucleic Acid Stain	Biotium
----------------------------------------	---------

Glycerol	Sigma
----------	-------

Tris Acetate-EDTA (TAE) Buffer	Sigma
--------------------------------	-------

Xylene Cyanol	VWR
---------------	-----

2.1.2.4 Sequencing and Pyrosequencing

BigDye Terminator v3.1 Cycle Sequencing Kit	Applied Biosystems
DMSO	Sigma
ExoSAP-IT	GE Healthcare
HiDi	Applied Biosystems
PyroGold Reagents	Qiagen

2.1.3 Consumables

0.2ml Thin-Walled PCR Tubes	Thermo Scientific
0.5ml PCR Tubes	Thermo Scientific
1.5ml Eppendorf Tubes	Thermo Scientific
2.0ml Eppendorf Tubes	Thermo Scientific
Aluminium Foil	VWR
Coverslips (22X20mm, 22X32mm, 22X40mm, 22X50mm)	CellPath
Coverslips HiQA (37X58mm, 48X64mm)	CellPath
NucleoSpin [®] Tissue Preparations	Macherey-Nagel
Medical Tissue	Kimberly-Clark
Microscope Slides (mega, supa mega 1.0-1.2mm, 76X26X1.0-1.2mm)	CellPath
Microscope Slides, SuperFrost [®] (76X26X1.0mm)	VWR
Microtome blades MX35 Premier	Thermo Scientific
PCR Plates (real-time PCR)	Starlabs
PCR Plate Seals (real-time PCR)	Starlabs
Pipette Tips (10ml, 20ml, 200ml, 1000ml)	Starlabs

Polyethylene naphthalate (PEN) Membrane Slides	Leica
Slide Racks	CellPath
Sliderite 5 Mailer™	CellPath
Weigh Boats	Fisher Scientific

2.1.4 Equipment

Alamut™ Software	Interactive Biosoftware
Antigen Retrieval Unit	A. Menarini Diagnostics
ABI 3100 Genetic Analyser	Applied Biosystems
Autoclave	Astell
Balance, Adventurer™	Ohaus
Centrifuge 3-15	Sigma
Centrifuge C5418	Eppendorf
Centrifuge PCV2400	Grant-Bio
Cryostat OTF	Bright
Dry Heat Block	Techne
Electrophoresis Power Supply	Cleaver Scientific Ltd
Electrophoresis Power Supply	Amersham Pharmacia Biotech
EZ1® Advanced Workstation	Qiagen
Incubator (35°C)	Thermo Scientific
Incubator (60°C)	Genlab
Microtome HM325	Microm
Nanodrop ND-1000 Spectrophotometer	Labtech International

Olympus BX51 Microscope	Olympus
Palm MicroBeam Laser Microdissection Microscope and Software	Zeiss
PCR Machines	Applied Biosystems
PCR Machines (real-time PCR)	Applied Biosystems
pH Meter 3510	Jenway
Pipettes (2 μ l, 10 μ l, 20 μ l, 200 μ l, 1000 μ l)	Gilson
PyroMark Q24	Qiagen
QIAmp DNA Mini Kit	Qiagen
Stereoinvestigator Software	MBF Bioscience
Tweezers	CellPath
UV Biological Hood	Bioair Instruments
UV Gel Imaging System, ChemiDoc MP	Bio-Rad
UV Gel Imaging Software, Image Lab 4.1	Bio-Rad
Zeiss Imaging System and software	Zeiss

2.2 Methods

This section will detail all methods followed during this project.

2.2.1 Patient and Control Cohort

The patients that were included in this study all had a clinical diagnosis of Alpers' syndrome or Alpers-like syndrome. Patients fulfilled the criteria for Alpers' syndrome based upon the presentation of defined features. These criteria are explained fully in section 2.2.2 '*Definition of Alpers' Syndrome*'. The diagnosis given by the clinician and the presence of seizures and ataxia symptoms noted in the medical notes were used for inclusion of patients in the study. Patient 4 was diagnosed with mitochondrial disease due to a *POLG* mutation. This patient was the oldest patient in the cohort at 24 years at the time of death. Patient details are summarised in Table 2.1. *POLG* mutations are stated where known. However, the full sequencing data was not available to me.

Where possible, controls were used that were age-matched and sex-matched to the patients. Patient and control neuropathology details are summarised in Table 2.2.

Patient material was obtained from a number of sources. The Newcastle Brain Tissue Resource (NBTR) provided formalin-fixed, paraffin-embedded (FFPE), frozen, and formalin-fixed tissue for Patients 1, 2, 4-6 and 12. The Institute of Neurology, University of Vienna, Austria provided FFPE tissues for Patients 7-11. The University of Bonn, Germany provided frozen tissue for Patient 3. Due to the rarity of the disease and the sensitive nature of the patient age, it was extremely difficult to obtain both patient and age-matched control tissue. A number of centres were approached to request tissue; centres that responded positively had one or two possible cases of Alpers' syndrome. In order to visualise mitochondrial antibodies, it was desirable that possible cases had FFPE tissue blocks that had been fixed in formalin for less than 6 months. This made the acquisition of suitable tissue a challenging task.

The following patient histories are taken from clinician's reports written at the time.

2.2.1.1 Patient 1

Patient 1 was the first child of non-consanguineous parents and was born after an uneventful pregnancy. There was a family history of epilepsy on the mother's side.

She presented at hospital at 11 months old with continuous right focal seizures which were treated with the anticonvulsants diazepam and then sodium valproate. After a few

months with no seizures, they restarted following her MMR (measles, mumps and rubella) vaccination, and her development regressed as she stopped weight bearing or crawling. At 13 months old, she became drowsy, irritable, jaundiced, anorexic, and lost weight. The jaundice was accompanied by clinical evidence of abnormal clotting (easy bruising and bleeding gums), enterohepatic obstruction (dark urine and pale stools), and hypoproteinaemia (oedema).

She was admitted to Newcastle General Hospital with encephalopathy and required ventilation. She had hypoglycaemia and abnormal liver function tests: bilirubin 113, alkaline phosphatase 243, alanine transaminase 189, albumin 31 and ammonia 70. She also exhibited coagulopathy: prothrombin >200, partial thromboplastin >180, fibrinogen <0.1, platelets 60, haemoglobin 8.9, and white cell count 6.6. In view of this she was transferred to Birmingham Children's Liver Unit to be considered for liver transplant. A repeat CT scan at Birmingham showed mild generalised cerebral atrophy with a low attenuation area in the right frontal lobe.

She was diagnosed with Alpers' syndrome and she returned to Newcastle General Hospital for terminal care. She died aged 14 months due to hepatic failure.

Molecular genetic investigations confirmed the patient was compound heterozygous for the p.Ala467Thr and p.Gly848Ser POLG mutations. Diagnostic biochemical investigations in muscle showed 50% reduced activity for complex I and 25% reduced activity for other complexes when compared to normal controls. Histochemistry revealed 20% COX-negative fibres in muscle.

2.2.1.2 Patient 2

Patient 2 was the first child of the family, with a clinically normal younger sister.

He had normal development until 17 months of age when following a day of vomiting, fever and drowsiness he had a prolonged seizure that evolved into status epilepticus. A right hemiparesis resolved but hemianopia continued. An EEG some months later was normal. A subsequent seizure occurred at 19 months of age associated with a convergent squint and left-sided neurological defects, and once again there was spontaneous recovery with speech and motor functions returning to normal. Hemianopia continued. CT scan showed atrophy in left posterior region and EEG scan showed deterioration. The following month there was a similar readmission with visual loss. Patient was discharged on a ketogenic diet and with anticonvulsants that included sodium valproate. A couple of months later the patient's condition deteriorated and he

became floppy, his feeding deteriorated and he was excessively drowsy. A respiratory chain disorder was suspected as the patient's condition continued to deteriorate and he became unable to walk, had poor vision and had seizures in the right upper limbs. He died aged 27 months due to pulmonary haemorrhage and respiratory failure.

Molecular genetic investigations confirmed the patient was compound heterozygous for the p.Ala467Thr and p.Thr914Pro POLG mutations. A case report of this patient was published describing clinical course and a partial deficiency of cytochrome c oxidase in muscle and activity of this enzyme was less than 30% of the mean control value (Morris et al., 1996).

2.2.1.3 Patient 3

This patient had clinical signs of epilepsy partialis continua, and sodium valproate-induced liver failure. He died at 17 years old.

Molecular genetic investigations confirmed the patient was homozygous for the p.Ala467Thr POLG mutation and clinical investigations showed COX-negative fibres in muscle and COX-negative areas in liver samples. Decreased complex I and complex IV enzyme activities in skeletal muscle were noted. Mitochondrial DNA deletion and depletion of copy number were seen in skeletal muscle, brain and liver samples (Zsurka et al., 2008).

2.2.1.4 Patient 4

Patient 4 had a normal childhood development. She first developed seizures at 20 years old, at which time she was 22 weeks pregnant. The seizures were very difficult to control with treatment and investigations showed high levels of urinary copper. She had ataxia and uncoordinated eye movements. CT scan was normal and a lumbar puncture showed normal CSF results.

Seizures continued and an EEG scan showed a diffuse abnormality, while an MRI scan showed three abnormal areas in the grey and white matter which suggested ischaemic changes. Her condition deteriorated and she developed striking eye movement abnormalities with impairment of her upgaze and horizontal gaze. A repeat MRI scan showed new ischaemic changes in the grey and white matter of the brain.

There was a brief period of improvement in her condition when she was started on Dexamethasone, but her condition once again deteriorated and she was found to have signs of osteoporosis when she fell and fractured her femur. Her condition showed a

further decline with progressive ataxia with epilepsy and paraparesis with clonic jerks with a reduced level of consciousness.

She died at 24 years old. Molecular genetic investigations confirmed the patient was heterozygous for the p.Ala467Thr and p.Trp748Ser POLG mutations.

2.2.1.5 Patient 5

Patient 5 died intrauterine at 34 weeks gestation. However, the size and weight of the patient suggested death at 36-38 weeks, suggesting the patient may have been older than 34 weeks. The mother was 31 years old with insulin-dependent diabetes. She presented with decreased fetal movements and intrauterine death was confirmed by an ultrasound scan.

This patient was included in the study as a sibling had shown signs of a progressive neurological disorder, and this sibling had previously been confirmed as having the pathological POLG mutation p.Ala467Thr, as well as the single nucleotide polymorphism p.Glu1143Gly (Craig et al., 2007). POLG sequencing carried out during this project also found the sibling carried the p.Asp1219Glu mutation, which has unknown pathogenicity. Patient 5 is considered as having a possible *POLG* defect.

2.2.1.6 Patient 6

This patient first presented to hospital at 16 years old with headache, double vision and photophobia. The next day she developed weakness in the left arm with left-sided twitching, and epilepsy developed which was initially controlled with diazepam and later with sodium valproate. A CT scan was normal but left-sided hemiplegia continued and epilepsy reoccurred.

Epilepsy persisted and a later CT scan showed ventricular dilation. She was admitted to hospital once again for left-sided seizures when she was thought to be about 10 weeks pregnant. Seizures were extremely difficult to control and it was decided that the pregnancy should be terminated unless the seizures could be managed.

After pregnancy termination, the seizures continued but were less severe. Local oedema of the larynx resulted in intubation. Her seizures continued and the patient remained unconscious with brief periods of responsiveness. This condition persisted until death from cardiac arrest at the age of 18 years old.

A brother survived into later life but suffered neurological problems. The brother had previously been confirmed as having the pathological POLG mutations p.Trp748Ser and p.Arg1096Cys.

2.2.1.7 Patient 7

She suffered epileptic seizures until death at 2.5 months old. There is very limited data for this patient from the Institute of Neurology, University of Austria, Vienna, and there was no conclusive diagnosis.

2.2.1.8 Patient 8

Patient 8 was the second child of the family; a sister had previously died at 4 months of age after a similar clinical course.

At birth, he suffered a 20 minute bradycardia with apnoea, generalised cyanosis, and required resuscitation. He was diagnosed with infant respiratory distress syndrome and apnoeic episodes occurred which were eventually identified as a consequence of epileptic seizures.

At 2 months old, he had problems swallowing, cyanosis, and epileptic seizures with episodes of apnoea. A CT scan showed symmetrical hydrocephalus. At 5 months old, he showed hypotonia, had no gaze fixation, and was developmentally similar to a one month old baby. He died at 5.5 months old during an epileptic seizure due to heart and respiratory failure. There was no conclusive diagnosis

2.2.1.9 Patient 9

This patient suffered epileptic seizures during the first few months of life, which presented as rhythmic jerks of the upper body and periorbital muscles. An EEG showed hypersarrhythmia and she was put on hydrocortisone therapy.

Epileptic seizures continued to be resistant to anticonvulsants and she developed a generalised tremor with subsequent vomiting and fatigue. Seizures were also followed by episodes of apnoea and a loss of consciousness.

She died at 6.5 months old from respiratory failure during an epileptic seizure. An autopsy revealed focal interstitial pneumonia and bilateral pleural emphysema.

2.2.1.10 Patient 10

Patient 10 was born by caesarean section after a normal pregnancy.

At 4 months old, his parents noticed a weak response to outside stimuli with no interest in toys, a rapid fatigue, and difficulties with drinking. He developed a stereotypical mouth movement with spasms of the upper and lower extremities.

At the age of 9 months, he had no head or trunk control, no gripping, no lifting of the body, and extremely variable muscle tone. At 11 months old, he showed strabismus of the eyes, no gaze fixation, and showed the movement coordination of a 3 month old baby.

An EEG showed hypsarrhythmia. Adrenocorticotrophic hormone (ACTH) therapy was started but was halted after 4 weeks due to high blood pressure, tachycardia, and fever. An acute neurological deficit appeared and the patient contracted pneumonia. Penicillin and IV therapy was started but the patient died at 13 months of age due to pneumonia in all lung lobes, hydropericardium, and liver steatosis.

2.2.1.11 Patient 11

This patient was the second child of the family with a clinically unaffected older sister. Birth and development were normal in the first 6 months of life, but then became delayed, with scar-like skin lesions appearing on the trunk of the body. As the patient started kindergarten, it was apparent that she was developmentally behind her peers and displayed a wide-based, wavy gait. Albinism was suspected due to her light hair and eye colour.

At 5 years old, she had an acute episode of crying, vomiting and nausea, and a loss of consciousness. Within hours, left-sided jerking began in the face and arm and she was admitted to hospital. After being discharged from hospital, another episode of nausea, vomiting, and jerks on alternating sides of the body occurred. Her vision became impaired and she developed pneumonia which resulted in readmission to hospital. A neurological examination revealed impaired consciousness, right-sided spastic paresis, continuous focal jerks in upper right extremities, increased tendon reflexes, clonic muscle contractions in the lower extremities, and a tremor. An EEG showed asymmetric dysrhythmia in the brain with dominant delta activity in the fronto-parietal region and slow spike-wave variants in the occipital lobe.

At 6 years old, she was completely blind and could not speak and within a further 6 months was deaf and required tube-feeding. She died at 7 years of age.

The original account is described in a publication by Jellinger and Seitelberger (Jellinger and Seitelberger 1970).

2.2.1.12 Patient 12

Patient 12 was the first child of the family from a normal pregnancy and birth. A younger brother was clinically normal.

His parents noted that he had had fever, cough, and coryzal (catarrhal inflammation) symptoms. At 5 years old, he then developed headaches and visual hallucination of colours in front of his eyes and his parents called for an ambulance. Following an episode of irritability and vacant staring his conscious level deteriorated. His eyes deviated to the left and drowsiness increased until intubation and ventilation were required. CSF pressure was normal with glucose 3.7mmol/l. On arrival at hospital, he showed left-sided convulsions and EEG showed a right posterior focal status epilepticus. Seizures were treated with Thiopentone but were not well controlled. He showed a left-sided weakness and a left-sided homonymous hemianopia.

Subsequently, spasmodic jerks developed particularly in the ankle. The optic discs were pale with a 'salt and pepper' appearance of the retina but an electroretinography (ERG) was normal. Extensive investigations were performed, including metabolic and immunological, but all were within normal limits and there was no evidence of a viral infection. A muscle biopsy showed no evidence of a mitochondrial dysfunction and the complexes of the respiratory chain were normal with a possible lowering of complex IV.

The patient's consciousness gradually diminished and there were multiple left-sided myoclonic foci of the face and arm. Pupils were large and unresponsive with small pale optic discs. There were upper motor neurone signs in both upper and lower limbs, increased tone, hyperreflexia, and a moderate bilateral ankle clonus. Patient 12 died at home at the age of 6 years old due to bronchopneumonia.

POLG sequencing carried out in this project did not find the patient to carry a pathogenic mutation.

2.2.2 Definition of Alpers' Syndrome

Defining the condition of Alpers' syndrome is a difficult task and requires evidence from multiple assessments; assessment in the clinic or hospital, neurophysiological assessments that include EEG scan to evaluate brainwaves, neuroimaging including MRI scans, and neuropathological assessment attained post-mortem. The typical clinical course is a developmental delay followed by the explosive onset of intractable epilepsy during infancy (Harding et al., 1986), though they may occur in early adulthood. The seizures may be of variable type including epilepsia partialis continua, multifocal myoclonus, and/or status epilepticus. A developmental regression usually follows, accompanied by visual impairment, hypotonia, ataxia and/or hemiplegia. Impairment of liver function and eventual liver failure often occurs in patients and the onset of liver failure may be quickened by the use of the antiepileptic medication, sodium valproate. EEG investigations may show abnormal discharges, with high amplitude slow waves and low amplitude polyspikes in the occipital lobe. MRI scans may show areas of oedema and of both localised and generalised cortical and white matter degeneration. Genetic confirmation of the presence of two recessive mutations in the gene *POLG* can aid in diagnosis, but confirmed mutations are not essential as patients have been reported with mutations in genes other than *POLG*.

The patients in this cohort were defined as having Alpers' syndrome based on the presence of two or more features of 1) intractable epilepsy, 2) a visual impairment including hemianopia, hallucinations or cortical blindness, and 3) either ataxia, hemiplegia or hypotonia.

The patients in this cohort that fulfilled the criteria of Alpers' syndrome with a comprehensive clinical background were Patients 1, 2, 4, 6, 11, and 12. It was not possible to ascertain further clinical details regarding Patient 3, though this patient was considered to have had Alpers' syndrome due to a recent clinical diagnosis and biochemical investigations reported in a recent publication. Patient 5 was included in the project because signs of a mitochondrial disorder with *POLG* mutations were documented in the sibling. Patients 7-10 did not fit the criteria though they all resembled an Alpers' syndrome-like phenotype. There is little clinical information on these patients which made it difficult to determine a diagnosis.

Patients 7-10 most likely had a primary mitochondrial disorder with an Alpers'-like phenotype, though there is insufficient clinical data to support a more accurate diagnosis. Patient 7 and Patient 9 displayed intractable seizures but no further symptoms of visual abnormalities or signs of ataxia, hemiplegia or hypotonia. Patient 8 and Patient 10 do show further clinical signs compatible with an Alpers'-like phenotype, though are not conclusive. Patient 9 and Patient 10 show atypical symptoms not associated with Alpers' syndrome, such as hypsarrhythmia on an EEG scan.

Patient	Sex	Age at onset	Age at death	Primary clinical features									Reported POLG mutation	Affected sibling	
				Fever	Headache	Vomiting	Drowsiness/ rapid fatigue	Hypotonia/ ataxia/ hemiplegia	Hemianopia	Visual Problems	Liver Failure	Seizures / Status Epilepticus			
	F	11m	14m			+	+	+				+	+	p.Ala467Thr; p.Gly848Ser	None
	M	17m	27m	+		+	+	+	+		+	+	+	p.Ala467Thr; p.Thr914Pro	Unaffected sister
	M	-	17y									+	+	p.Ala467Thr; p.Ala467Thr	Unknown
	F	20y	24y		+			+			+		+	p.Ala467Thr; p.Trp748Ser	Unknown
	M	-	ID 34weeks											N/A	One sister p.Ala467Thr; p.Glu1143Gly p.Asp1219Glu
	F	16y	18y		+	+		+			+	+	+	N/A	One brother p.Trp748Ser; p.Arg1096Cys
	F	-	2.5m										+	N/A	None
	M	2m	5.5m					+					+	N/A	Affected sister
	F	1m	6.5m			+	+						+	N/A	None

Patient	Sex	Age at onset	Age at death	Primary clinical features									Reported POLG mutation	Affected sibling	
				Fever	Headache	Vomiting	Drowsiness/ rapid fatigue	Hypotonia/ ataxia/ hemiplegia	Hemianopia	Visual Problems	Liver Failure	Seizures / Status Epilepticus			
	M	4m	13m				+	+			+	+	+	N/A	None
	F	6m	7y			+		+			+		+	N/A	Unaffected sister
	M	5y	6y	+	+		+	+	+		+		+	None	Unaffected brother

Table 2.1. Clinical details for the patients.

Clinical information for patients including: sex, age at onset, age at death, primary clinical features, reported POLG mutation, affected sibling.

^a was used to investigate mitochondrial respiratory chain complexes due to short formalin-fixation time.

^b frozen tissue used to assess mtDNA copy number and mtDNA deletion.

Key: ID= intrauterine death, N/A=data not available

	Category	Sex	Age at death	PMI (hours)	Length of fixation	Cause of death
	Patient	F	14m	12	1m	Hepatic failure
	Patient	M	27m	12	5weeks	Pulmonary haemorrhage and respiratory failure
	Patient	M	17y	12	N/A	Unknown
	Patient	F	24y	83	N/A	Unknown
	Patient	M	ID 34weeks	72	13y	Unknown
	Patient	F	18y	24	2m	Cardiac arrest
	Patient	F	2.5m	Unknown	Unknown	Unknown
	Patient	M	5.5m	Unknown	Unknown	Cardiac and respiratory failure
	Patient	F	6.5m	Unknown	Unknown	Respiratory failure
	Patient	M	13m	Unknown	Unknown	Pneumonia
	Patient	F	7y	Unknown	Unknown	Unknown
	Patient	M	6y	36	1m and 14y	Pneumonia
	Control	F	13m	72	2-4weeks	Occipital porencephaly
	Control	M	2y	Unknown	25y	Electrocution
	Control	M	19y	48	N/A	Motor cycle accident
	Control	M	27y	Unknown	N/A	Suicide by hanging
	Control	F	49days	24	4m	Premature rupture of the membranes with signs of neuromuscular disease
	Control	F	19y	5	18m	Overdose
	Control	F	18y	24	6m	Overdose
	Control	M	14m	72	2m	Tumours in thalamus and left occipital
	Control	F	6y	40	N/A	Road traffic accident
	Control	F	59y	19	2.5m	Carcinoma

	Category	Sex	Age at death	PMI (hours)	Length of fixation	Cause of death
	Control	M	8y	11	17y	Undiagnosed familial neurodegenerative disorder, suspected to be X-linked
	Control	M	51y	16	15y	Cardiac arrest

Table 2.2. Neuropathological details of the patients and controls used in this study.

Key: ID=intrauterine death; N/A=data not available

2.2.3 Tissue Preparation

Human brain tissue from Patient 1, 2, 4-6, and 12 was obtained from the Newcastle Brain Tissue Resource (NBTR). Brain tissue obtained from Patient 7 -11 was obtained from the University of Austria, Vienna. Brain tissue obtained from Patient 3 was obtained from the University of Bonn, Germany. Ethical approval was given for this project, ethical approval number 'Newcastle and North Tyneside Local Research Ethics Committees 2002/205'.

This study examined four areas of the brain. Three of these areas were previously reported to exhibit pathology in patients with Alpers' syndrome; occipital lobe, parietal lobe, and cerebellum. The basal ganglia was less frequently reported to exhibit pathology in the literature.

Tissue that had been fixed in formalin for 6 months or less was desired for use with mitochondrial antibodies, due to fixation in formalin masking the antigens and a possible risk of false negative results. Tissue fixed for longer periods of time was used for histological staining.

FFPE human brain tissue was sectioned at room temperature using a microtome. Sections were cut at 5µm, 10µm, or 20µm thickness dependent upon which stain or antibody was to be used. Sections were placed in a water bath and then mounted onto glass slides (subbed or SuperFrost® slides) of the appropriate size. Sections were kept inside a 37°C oven for 3-5 days to ensure the sections had adhered well to the slides.

Frozen human brain tissue was sectioned at -25°C using a cryostat. Sections were cut at 10µm or 20µm thickness and mounted straight onto glass slides or polyethylene naphthalate (PEN) membrane slides, respectively. Sections were dried at room temperature for one hour and stored at -80°C until required.

2.2.4 Neurohistopathological Methods in Staining FFPE Tissue

A number of histopathological stains were used to visualise specific tissue components in FFPE tissue, as detailed previously (Lax et al., 2012).

2.2.4.1 Rehydration of FFPE Tissue

Before each histological method was carried out, FFPE tissue sections were put in the 60°C incubator for 20 minutes to melt the paraffin on the sections. Sections were deparaffinised in HistoClear™ and rehydrated in an ethanol gradient for 5 minutes in each pot (100%, 100%, 95%, 70% ethanol) and finally in deionised water.

2.2.4.2 Haematoxylin and Eosin Stain

A haematoxylin and eosin stain was used to assess general cellular morphology. 5µm-thick sections of tissue were used. Sections were rehydrated as described in 2.2.3.1 *Rehydration of FFPE Tissue*. Meyer's haematoxylin was used for 5 minutes to stain the nuclei and then the sections were rinsed in tap water. Scott's Tap Water Substitute was used for 2 minutes to provide rapid blueing of the nuclei before a rinse in tap water. A counterstain of alcohol eosin was used for 4 minutes to stain eosinophilic structures pink, e.g. cytoplasm, and the sections were rinsed in tap water. The slides were then dehydrated in a separate ethanol gradient to the gradient previously used (100%, 100%, 95%, 70% ethanol), cleared in two changes of HistoClear™ and then mounted with a suitable coverslip using DPX mountant.

2.2.4.3 Cresyl Fast Violet Stain

Cresyl fast violet (CFV) stain was used to assess neuronal populations, through the staining of nissl substances in the neurons and cellular nuclei. 20µm-thick sections of tissue were used. Sections were rehydrated as described in 2.2.3.1 *Rehydration of FFPE Tissue*. Sections were placed in 1% acid alcohol for 5 minutes and then rinsed in 4 changes of deionised water. The sections were then incubated in the CFV working solution at 60°C for 15 minutes and rinsed in deionised water. They were then placed in 95% ethanol to differentiate the neurons from the background tissue stain. The slides were then dehydrated in a separate ethanol gradient to the gradient previously used (100%, 100%, 95%, 70% ethanol), cleared in two changes of HistoClear™ and then mounted with a suitable coverslip using DPX mountant.

2.2.4.4 Loyez Silver Stain

Loyez silver stain was used to assess myelin density in the white matter. 20µm-thick sections of tissue were used. Sections were rehydrated as described in 2.2.3.1 *Rehydration of FFPE Tissue*. Sections were placed in a 4% iron alum mordant for 6 hours at room temperature. Sections were then washed in 5 changes of deionised water before staining in haematoxylin solution overnight at room temperature. The next day, sections were washed in deionised water. The slides were then dehydrated in a separate ethanol gradient to the gradient previously used (100%, 100%, 95%, 70% ethanol), cleared in two changes of HistoClear™ and then mounted with a suitable coverslip using DPX mountant.

2.2.4.5 Bielschowsky Silver Stain

Bielschowsky silver stain was used to visualise nerve fibres and axons in the white matter. 10µm-thick sections of tissue were used. Prior to beginning the protocol, all glassware to be used was washed with 50% nitric acid and all glassware and solutions were refrigerated. Sections were rehydrated as described in 2.2.3.1 *Rehydration of FFPE Tissue*.

Sections were placed in 10% silver nitrate in the fridge in complete darkness for 20 minutes and then rinsed in deionised water. An ammoniacal silver solution was made by adding concentrated ammonia (25%) drop by drop to the silver solution until the precipitate disappears. This was performed under the fume hood and the sections were placed in this solution in the fridge in complete darkness for 20 minutes. The sections were then placed in 1% ammonia solution for 5 minutes. To 100ml of the ammoniacal solution, 0.5ml of Developer Solution was added and the sections placed in this solution for 10-20 minutes, then rinsed in deionised water. Throughout this time, the sections were checked macroscopically for a change in colour to tan brown. The sections were placed in a solution of 15ml 0.2% gold chloride diluted in 100ml deionised water, for less than one minute. Then sections were rinsed in deionised water. Sections were fixed in 5% sodium thiosulphate for 5 minutes and then rinsed under tap water.

The slides were then dehydrated in a separate ethanol gradient to the gradient previously used (100%, 100%, 95%, 70% ethanol), cleared in two changes of HistoClear™ and then mounted with a suitable coverslip using DPX mountant.

2.2.5 Antibody Staining in FFPE Tissue

FFPE tissue was stained with antibodies to assess the different cell types and mitochondrial localisation (Table 2.3). Tissue that had been fixed in formalin for 6 months or less was used, as a longer fixation time gave weak staining and the risk of false negative results. The length of formalin fixation did not appear to have an effect when using porin, so porin was stained and assessed in all tissues available.

CD68	Lysosomal membrane protein on microglia	0.1% trypsin and 0.1% calcium chloride in TBS, 37°C, 15 minutes	1:350	Dako	M0876
GFAP	Glial fibrillary acidic protein	0.01M citrate buffer, pH 6.0, microwave, 10 minutes	1:15,000	Dako	Z0334
Porin	VDAC1	1mmol EDTA, pH 8.0, high pressure decloaker unit	1:10,000	MitoSciences	MSA03

Table 2.3. Antibodies used for immunohistochemistry in FFPE brain tissue.

2.2.5.1 Respiratory Chain Antibody Staining

Antibodies were used for various subunits of the mitochondrial respiratory chain to allow for assessment of the integrity and expression of the electron transfer chain proteins in neurons (Table 2.4).

Complex I subunit NDUFA13	Complex I subunit 19kDa	1mmol EDTA, pH 8.0, high pressure decloaker unit	1:3,000	MitoSciences	MS103
Complex I subunit NDUFB8	Complex I subunit 20kDa	1mmol EDTA, pH 8.0, high pressure decloaker unit	1:300	MitoSciences	MS105
Complex I subunit NDUFS3	Complex I subunit 30kDa	1mmol EDTA, pH 8.0, high pressure decloaker unit	1:1,000	MitoSciences	MS110
Complex I subunit NDUFA9	Complex I subunit 39kDa	1mmol EDTA, pH 8.0, high pressure decloaker unit	1:100	MitoSciences	MS111
Complex II subunit 70kDa Fp	Complex II subunit 70kDa	1mmol EDTA, pH 8.0, high pressure decloaker unit	1:4,000	MitoSciences	MS204
Complex III subunit Rieske	Complex III subunit Rieske	1mmol EDTA, pH 8.0, high pressure decloaker unit	1:1,500	MitoSciences	MS305
Complex IV subunit I	Complex IV subunit I	1mmol EDTA, pH 8.0, high pressure decloaker unit	1:10,000	MitoSciences	MS404
Complex IV subunit IV	Complex IV subunit IV	1mmol EDTA, pH 8.0, high pressure decloaker unit	1:8,000	MitoSciences	MS408

Table 2.4. Antibodies used to visualise mitochondrial respiratory chain proteins, using immunohistochemistry, in FFPE brain tissue.

2.2.5.1.1 *Complex I*

These antibodies bind to NADH: ubiquinone oxidoreductase, the first complex in the mitochondrial ETC. Four different antibodies were used to four subunits of complex I; these were CI-19 (*NDUFA13*), CI-20 (*NDUFB8*), CI-30 (*NDUFS3*), and CI-39 (*NDUFA9*). Each of these subunits is nuclear-encoded. They antibodies were chosen as there are currently no mitochondrially-encoded antibodies available suitable for this method. These particular four antibodies were used due to their importance to the function of complex I. CI-19 and CI-30 are thought to be involved in the catalytic functions of this complex with CI-30 being one of the core subunits, while CI-20 and CI-39 are known to play a role in mitochondrial disease.

2.2.5.1.2 *Complex II*

This antibody binds to succinate: ubiquinone oxidoreductase, the second complex in the mitochondrial ETC. Electrons may enter the ETC at complex I or at complex II and continue to flow along the respiratory chain.

2.2.5.1.3 *Complex III*

This antibody for the Rieske subunit binds to the iron sulphur protein within ubiquinol cytochrome *c* reductase, the third complex in the mitochondrial ETC. The Rieske subunit is nuclear-encoded.

2.2.5.1.4 *Complex IV*

This antibody binds to cytochrome *c* oxidase, the fourth complex in the mitochondrial ETC. Two different antibodies were used; these were for subunit I and subunit IV. Subunit I is encoded by a mitochondrial gene while subunit IV is encoded by a nuclear gene.

2.2.6 Quantitative Methods

2.2.6.1 Neuronal Cell Counting

Tissue sections from patients and controls were stained with cresyl fast violet (CFV) stain to visualise the neurons. The Olympus BX51 microscope together with StereoInvestigator software was used to count the neurons. A neuron was defined as a cell that was intensely stained with CFV nissl stain and had a visible nucleus and nucleolus.

Three sections of tissue of 20 μ m each were taken from each brain area and stained with CFV stain, with an interval of 60 μ m between each section. Neurons were counted on each slide to give an indication of neuronal cell density through the tissue. This method is based upon previous quantitative methods for counting neurons (Lax et al., 2012). Within the cerebellum, neurons were counted in both the superior and inferior regions where available. In the superior region, the anterior crescentic and ala centralis regions were sampled. In the inferior region, the tonsilla, biventer, posterior inferior, posterior superior and posterior crescentic were sampled. Focal loss of Purkinje cells was investigated; areas of the cerebellum known to show neuron loss in one patient were sampled in all patients and the controls.

Reference spaces were randomly sampled on each slide; 21 spaces of 0.8mm² at X10 magnification in the cerebellum, and 5 columns of 1mm² each spanning the six cellular layers at X100 magnification in the occipital and parietal lobes (Figure 2.1). Within the 1mm² columns, every visible neuron was counted in layers I-VI. A total area of 5mm² was counted per slide, and a total area of 15mm² was counted per patient over the three slides. Within each 0.8mm² reference space, Purkinje cells were counted in the cerebellum. A total area of 16.8mm² was counted per slide and a total area of 50.4mm² was counted per patient over the three slides. The area of this reference space in the cerebellum correlates with the field of vision at X10 magnification, an optimal magnification in order to identify Purkinje cells. The coefficient of variation was calculated for each patient and control to assess the dispersion of data points around the mean value and so assess the accuracy of neuronal cell counting in each patient and control.

The length of the single-cell-deep layer of Purkinje cells was taken in order to calculate the density of Purkinje cells. The total area and perimeter of the entire tissue section on the slide was also taken in order to be aware of the section area examined in reference

to the entire tissue section. Section length was used rather than section volume in order to calculate neuron loss for all brain areas. Section volume is commonly used for tissue stereological approaches to calculation of cell loss. The use of stereological methods requires a large thickness of tissue to be used for accurate measurements. The rarity of the disease and difficulty in obtaining suitable tissue samples made the use of large volumes of tissue as part of the calculation unsatisfactory.

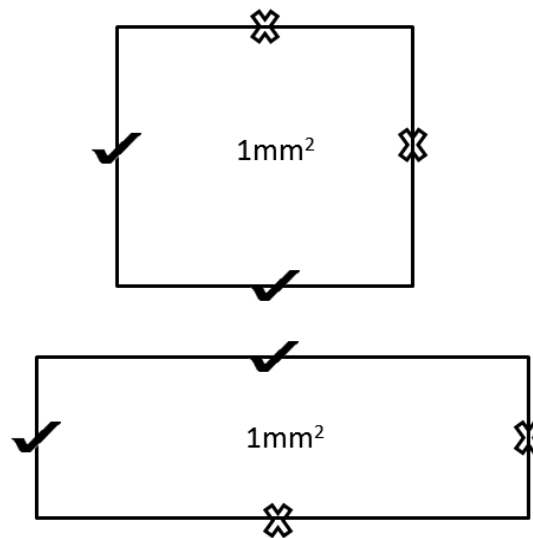


Figure 2.1. Reference spaces for quantification of neuronal cells.

Reference spaces were used to count neurons in the cortical layers. According to stereological conventions, only neurons that were touching two of the four sides of the spaces were counted. Neuronal bodies touching or crossing the sides with a tick were counted; neuronal bodies touching or crossing the sides with a cross were not counted.

2.2.7 *Semi-quantitative Methods*

2.2.7.1 *Myelin Quantification*

Tissue sections from patients and controls were stained with Loyez silver stain to visualise myelin. The tissue section from each patient was assessed and assigned a score based upon the density of myelin judged to be intact, when compared to a suitable control. The method was based upon a previous semi-quantitative method for assessing myelin density (Smallwood et al., 2012).

Images were taken for all brain areas at X10 magnification with the Olympus BX51 microscope. They were assessed semi-quantitatively using the scale 0=complete myelin loss, 1=marked loss of myelin staining, 2=slight pallor of myelin staining, 3=good myelin staining equivalent to controls, for assessment.

2.2.7.2 *Neuronal Cell Loss Quantification*

Tissue sections from patients and controls were stained with cresyl fast violet stain to visualise the neurons of the dentate nucleus. These neurons were assessed semi-quantitatively. The Olympus BX51 microscope was used to view the neurons.

Neuron loss was assessed semi-quantitatively using the scale -/+ /++ /+++ to describe any pathological changes. The scale is defined (-) no change, (+) mild neuron loss, (++) moderate neuron loss, and (+++) severe neuron loss.

2.2.7.3 *Astrogliosis Quantification*

Tissue sections from patients and controls were stained with GFAP antibody to visualise reactive astrocytes. The Olympus BX51 microscope was used to view the astrocytes.

They were assessed semi-quantitatively using the scale -/+ /++ /+++ to describe any pathological changes. The scale is defined (-) no change, (+) mild astrogliosis, (++) moderate astrogliosis, and (+++) severe astrogliosis.

2.2.7.4 Microglial Activation Quantification

Tissue sections from patients and controls were stained with CD68 antibody to visualise macrophages and activated microglial cells. The Olympus BX51 microscope was used to view the cells.

They were assessed semi-quantitatively using the scale -/+/++/+++ to describe any pathological changes. The scale is defined (-) no change, (+) mild increase, (++) moderate increase, and (+++) severe increase in CD68-positive cells.

2.2.8 Sequential COX/SDH Staining in Frozen Tissue

Slides were defrosted for at least one hour at room temperature. Sequential staining was performed to assess complex IV activity using cytochrome c (COX) incubation medium, and to assess complex II activity using succinate dehydrogenase (SDH) incubation medium.

The COX incubation medium was made by adding 200µl cytochrome c to 800µl 3, 3' diaminobenzidine tetrahydrochloride (DAB) and then a small amount of catalase (20µg/ml). The eppendorf was vortexed and centrifuged briefly. 50-100µl medium was added to tissue sections to cover them and they were incubated at 37°C for 50 minutes. After incubation, the sections were washed twice in phosphate-buffered saline (PBS) for 5 minutes each time.

The SDH incubation medium contains a substance that is sensitive to light, so the tube was wrapped in foil first. To 800µl nitro blue tetrazolium (NBT) was added 100µl sodium succinate, 100µl phenazine methosulphate (PMS, light-sensitive), and 10µl sodium azide.

Any excess PBS was wiped from the slides and 50-100µl medium was added to tissue sections to cover them. They were incubated at 37°C for 45 minutes. After incubation, the sections were washed twice in PBS for 5 minutes each time.

The slides were then dehydrated in an ethanol gradient (70%, 95%, 100%, 100%) with the final 100% ethanol being for 10 minutes. PEN slides were then left to dry for an hour at room temperature. Glass slides were taken through two changes of Histoclear™ and mounted with a suitable coverslip using DPX mountant.

2.2.8.1 Single Cell Isolation

Single neurons were taken from PEN membrane slides which were subjected to sequential COX/SDH histochemistry or single SDH histochemistry. Samples were defrosted for one hour at room temperature before single neurons were laser-capture microdissected directly into 15µl of buffer sitting in the cap of a sterile 0.5ml PCR tube. The Palm MicroBeam Laser Microdissection microscope from Zeiss was used for laser-capture microdissection.

2.2.9 Real-time PCR

Real-time polymerase chain reaction (PCR) was performed on DNA extracted from frozen human tissue as previously described (Krishnan et al., 2007). All reactions were set up under a UV hood and used DEPC-treated water and pipettes that had been under the UV hood for 30 minutes prior to PCR set up.

Reactions were set up in a 20µl volume which consisted of 5.8µl DEPC-treated water, 10µl TaqMan® Universal Mastermix, 0.4µl 5µM ND1 probe, 0.4µl 5µM ND4 probe, 0.6µl 10µM ND1 forward primer, 0.6µl 10µM ND1 reverse primer, 0.6µl 10µM ND4 forward primer, 0.6µl 10µM ND4 reverse primer, and 1µl standard DNA or 4µl DNA lysate from single neurons. Primer sequences are shown in Table 2.5.

MT-ND1	Forward	5'-CCCTAAAACCCGCCACATCT
	Reverse	5'-GAGCGATGGTGAGAGCTAAGGT
	VIC- labelled probe	5'-CCATCACCCCTCTACATCACCGCCC
MT-ND4	Forward	5'-CCATTCTCCTCCTATCCCTCAAC
	Reverse	5'-CACAATCTGATGTTTTGGTTAAACTATATTT
	FAM-labelled probe	5'-CCGACATCATTACCGGGTTTTCTCTTG

Table 2.5. Primer sequences used for *MT-ND1* and *MT-ND4* in real-time PCR.

2.2.10 Pyrosequencing PCR

Pyrosequencing PCR was performed on DNA extracted from frozen human tissue or FFPE human tissue. All reactions were set up under a UV hood and used DEPC-treated water and pipettes that had been under the UV hood for 30 minutes prior to PCR set up.

Reactions were set up in a 25µl volume which consisted of 10.8µl DEPC-treated water, 5µl GoTaq[®] Flexi buffer, 3µl MgCl₂, 2.5µl 10mM dNTPs, 1.25µl forward primer, 1.25µl reverse primer, 0.2µl 5U/µl GoTaq[®] HotStart polymerase, and 1µl DNA. DNA from a positive control that contained the one of the mutations and DNA from a wildtype control, which did not contain the mutations, were used to check the efficacy of the PCR.

Either the forward or reverse primers were biotinylated, which resulted in a biotinylated PCR product in one direction. If the forward primer was biotinylated, the reverse sequence strand was used for pyrosequencing.

2.2.11 DNA Sequencing

DNA was extracted from 9 patients and 1 patient sibling. The other patient sibling had eluted DNA available. Attempts were made to elucidate any mutations in the *POLG* gene. The following sections describe this.

2.2.11.1 DNA Extraction

DNA was extracted from FFPE tissue in patients where a *POLG* diagnosis had not been confirmed. The NucleoSpin[®] Tissue Preparation kit obtained from Macherey-Nagel was used and protocol followed as outlined below. Alternative systems of extraction were also used. A silica column-based method with the QIAmp DNA Mini Kit and the EZ1[®] Advanced Workstation, both from Qiagen, were additionally used on separate occasions during the optimisation of extracting DNA from FFPE tissue.

Sections of tissue were cut on the microtome. A new blade was used for each separate patient tissue block and gloves were changed between each block. The knife holder and tweezers were cleaned with HistoClear[™], 10% bleach, and then 70% ethanol in order to reduce cross contamination. A clean piece of medical tissue was used over the eppendorf cap when opening, to prevent contamination between eppendorf tubes (Greer et al., 1994).

Ten tissue sections of 20µm thickness were taken and deparaffinised in two changes of HistoClear™ at 56°C for 20 minutes. The tissue was rehydrated in two changes each of 100%, 95%, 70% ethanol and finally ultrapure water. Between each of the changes the eppendorf tubes containing the tissue were spun at 11,000g for three minutes to ensure the tissue was at the bottom of the tube and there would be minimal loss when changing the supernatant. The tubes were then left open at 37°C on the heat block to allow for the evaporation of residual ethanol. 80µl of buffer T1 and 8µl proteinase K were added to each tube, the tubes vortexed, and incubated at 56°C for 16 hours in the dry heat block. An increased incubation time can reverse cross-linkages between DNA and protein and increase PCR amplifiable DNA yield (Gilbert et al., 2007).

The next day, 80µl of Buffer 3 from the NucleoSpin® Tissue Preparation kit was added to the tissue then the samples were vortexed and incubated at 70°C for 5 minutes. 80µl of 100% ethanol was then added and the samples mixed by inverting and they were centrifuged briefly. The tissue lysates were transferred to a NucleoSpin® Tissue XS column and centrifuged at 11,000g for 1 minute. It has been suggested that a silica column-based extraction method is beneficial to DNA extraction from FFPE tissue (Gilbert et al., 2007). The flow through was discarded and two washes with 50ul Buffer B5 was applied to each column and centrifuged at 11,000 g for 1 minute. The DNA was then eluted with 20ul Buffer BE to each membrane and centrifuged at 11,000 g for 1 min. Residual ethanol removed by incubating the eluted DNA fraction in the open tube at 90°C for 5 minutes, on the heat block.

The DNA samples were tested on the nanodrop ND-1000 spectrophotometer to check DNA concentration, and check for any contaminants, and then stored at -20°C until needed.

2.2.11.2 *POLG* Pyrosequencing

DNA from 7 patients (Patients 5-11) was used in order to pyrosequence for the 3 most common *POLG* mutations; p.Ala467Thr, p.Trp748Ser, and p.Gly848Ser. The primers used to amplify the nuclear DNA sequence for the mutation in *POLG* are shown in Table 2.6. During the optimisation process, a first round of PCR was used to amplify the *POLG* exon containing the mutation, in order to create more initial template for subsequent PCR. The primers used to amplify the nuclear DNA sequence for the exon containing the mutation are shown in Table 2.7.

Pyrosequencing was performed using PyroMark Gold Q24 Reagents and according to the standard protocol, available from Qiagen. The biotinylated products were extracted from the mixture using the Instrument and read using the PyroMark Q24 machine, Qiagen. Then the results were analysed using the PyroMark Q24 software.

c.1399G>A p.Ala467Thr	Forward	5'-CCAGCGGGAGATGAAGAA	171bp	60°C
	(biotinylated)			
	Reverse	5'-TACAGAGCCAGTCCACTAGGG		
	Sequencing	5'-GGCAGGCATCATTGG		
c.2243G>C p.Trp748Ser	Forward	5'-CTCACAGACTGCCCGTGGT	142bp	60°C
	Reverse	5'-CAGGACAGGCCATGACCC		
	(biotinylated)			
	Sequencing	5'-ACATCCCTGGCTGCT		
c.2542G>A p.Gly848Ser	Forward	5'-CTGCCCAAGTGGTGACT	106bp	60°C
	Reverse	5'-AGGGGCCAGAGGTACAGAG		
	(biotinylated)			
	Sequencing	5'-CAAGTGGTGACTGCC		

Table 2.6. Primer sequences used to amplify DNA mutation regions from the gene *POLG* for pyrosequencing.

Exon 7 p.Ala467Thr	Forward	5'- TGAAAACGACGGCCAGTATGGG ATGATATTGTTCCCATTT	536bp	59°C
	Reverse	5'- CAGGAAACAGCTATGACCAGTCC ACTAGGGCAGGGCTA		
Exon 13 p.Trp748Ser	Forward	5'- TGAAAACGACGGCCAGTACAGT TTCAGGCCCTTTTCC	378bp	59°C
	Reverse	5'- CAGGAAACAGCTATGACCTGTGC CTGAAATCACACTCTG		
Exon 15+16 p.Gly848Ser	Forward	5'- TGAAAACGACGGCCAGTAGTGA GGCTGGGTAATGGAG	544bp	59°C
	Reverse	5'- CAGGAAACAGCTATGACCCAGGG TCCTTTTCATGATCC		

Table 2.7. Primer sequences used to amplify exons from the gene *POLG* containing the mutation, for pyrosequencing.

2.2.11.3 POLG Sequencing

DNA from one patient and one patient sibling (Patient 12 and the sibling of Patient 5) was used in order to sequence the entire *POLG* gene.

2.2.12 Electron Microscopy

Transmission electron microscopy (TEM) was performed on patient and control fixed tissues. Formalin-fixed brain tissue was taken from control 10, control 11, and Patient 12. This tissue had been fixed in formalin that was buffered with marble chips for between 14 to 17 years.

A small piece of tissue, ~1mm x 1mm, was dissected and first fixed in 2% glutaraldehyde in 0.1M sodium cacodylate buffer, then post fixed in 1% osmium tetroxide to make the tissue electron dense. The tissue was then dehydrated through a series of graded acetones and embedded in epoxy resin at 60°C. 70nm sections were cut and stained with uranyl acetate and lead citrate to give contrast to the image. A Philips CM100 transmission electron microscope was used to view the stained sections. All fixing, staining, and cutting of tissues were carried out by staff at the Electron Microscopy Research Services, Newcastle Biomedicine Core Scientific Facilities, Newcastle University. All images were taken at these facilities. Method adapted from Hogan *et al.*, (Hogan et al., 2009).

Sets of images were taken at various magnifications, depending upon the structure being visualised; 2600X to view cellular structure, 19,000X to view mitochondria, and 32,000X to view internal mitochondrial structure. Images were systematically and randomly sampled, maintaining a constant distant between each image. Images were then anonymised and randomly chosen for structures to be counted. Appropriate structures for each magnification were counted and analysed. Cellular nuclei and mitochondria must have a complete and intact membrane to be counted. At least 50% of the structure must be within the image to be counted, in order to be certain of its identification. Cellular nuclei and mitochondria were not counted if they were contained within a blood vessel structure. There must be visible cristae or remnants of cristae within a structure for it to be positively identified as a mitochondrion.

- Craig, K., G. Ferrari, W. Tiangyou, G. Hudson, C. Gellera, M. Zeviani and P. F. Chinnery (2007). "The A467T and W748S POLG substitutions are a rare cause of adult-onset ataxia in Europe [1]." Brain **130**(4).
- Gilbert, M. T., T. Haselkorn, M. Bunce, J. J. Sanchez, S. B. Lucas, L. D. Jewell, E. Van Marck and M. Worobey (2007). "The isolation of nucleic acids from fixed, paraffin-embedded tissues-which methods are useful when?" PloS one **2**(6).
- Greer, C. E., C. M. Wheeler and M. M. Manos (1994). "Sample preparation and PCR amplification from paraffin-embedded tissues." PCR Methods and Applications **3**(6): S113-S122.
- Harding, B. N., J. Egger, B. Portmann and M. Erdohazi (1986). "Progressive neuronal degeneration of childhood with liver disease: A pathological study." Brain **109**(1): 181-206.
- Hogan, V., K. White, J. Edgar, A. McGill, S. Karim, M. McLaughlin, I. Griffiths, D. Turnbull and P. Nichols (2009). "Increase in mitochondrial density within axons and supporting cells in response to demyelination in the Plp1 mouse model." Journal of Neuroscience Research **87**(2): 452-459.
- Jellinger, K. and F. Seitelberger (1970). "Spongy glio-neuronal dystrophy in infancy and childhood." Acta Neuropathologica **16**(2): 125-140.
- Krishnan, K. J., A. Bender, R. W. Taylor and D. M. Turnbull (2007). "A multiplex real-time PCR method to detect and quantify mitochondrial DNA deletions in individual cells." Analytical Biochemistry **370**(1): 127-129.
- Lax, N. Z., P. D. Hepplewhite, A. K. Reeve, V. Nesbitt, R. McFarland, E. Jaros, R. W. Taylor and D. M. Turnbull (2012). "Cerebellar ataxia in patients with mitochondrial DNA disease: A molecular clinicopathological study." Journal of Neuropathology and Experimental Neurology **71**(2): 148-161.
- Morris, A. A. M., R. Singh-Kler, R. H. Perry, P. D. Griffiths, A. D. Burt, W. Chee Pian, D. Gardner-Medwin and D. M. Turnbull (1996). "Respiratory chain dysfunction in progressive neuronal degeneration of childhood with liver disease." Journal of Child Neurology **11**(5): 417-419.

Smallwood, A., A. Oulhaj, C. Joachim, S. Christie, C. Sloan, A. D. Smith and M. Esiri (2012). "Cerebral subcortical small vessel disease and its relation to cognition in elderly subjects: A pathological study in the Oxford Project to Investigate Memory and Ageing (OPTIMA) cohort." Neuropathology and Applied Neurobiology **38**(4): 337-343.

Zsurka, G., M. Baron, J. D. Stewart, C. Kornblum, M. Bös, R. Sassen, R. W. Taylor, C. E. Elger, P. F. Chinnery and W. S. Kunz (2008). "Clonally expanded mitochondrial DNA mutations in epileptic individuals with mutated DNA polymerase γ ." Journal of Neuropathology and Experimental Neurology **67**(9): 857-866.

Chapter 3 Neuropathological Features of Patients with Alpers' Syndrome

3.1 Introduction

Alpers' syndrome is an autosomal recessive, early-onset disease often caused by mutations in *POLG*, primarily affecting the CNS and liver. Clinical features include refractory seizures, developmental delay, ataxia, visual abnormalities, and liver dysfunction and failure. There are over 230 *POLG* mutations, both dominant and recessive, listed on the National Institute of Environmental Health Sciences (NIEHS) website (<http://tools.niehs.nih.gov/polg/>). Many of these mutations are considered to be pathogenic and can lead to a heterogeneous group of symptoms, ranging from those which are mild with a late-onset, to symptoms which are severe with an early-onset. Alpers' syndrome is attributed to the presence of two recessive mutations in *POLG* and many different allele mutations have been reported to be pathological. The three most common mutations found in patients with Alpers' syndrome are the p.Ala467Thr mutation and the p.Trp748Ser mutation, found in the linker domain, and the p.Gly848Ser mutation, found in the polymerase domain of the gene. The p.Ala467Thr mutation is seen in around 40% of the mutations occurring in Alpers' syndrome (Nguyen et al., 2006).

Patients clinically diagnosed with Alpers' syndrome have a severe, early-onset phenotype that can be caused by a range of mutations in *POLG*. Mutations in *POLG* are the cause of 95% of the reported cases of Alpers' syndrome but there have been documented cases of clinical Alpers' syndrome where no mutation in *POLG* was present (Sofou et al., 2012). Genetic studies have been performed in patients without a mutation in *POLG* and subsequently, mutations in *FARS2* (Elo et al., 2012) and Twinkle have been reported in patients with the clinical signs of Alpers' syndrome (Hunter et al., 2011).

It is known that the Alpers' syndrome phenotype may manifest in patients of a wider age range than had been previously described in the literature, with late-teenage patients developing the clinical signs and harbouring two recessive *POLG* mutations (Wiltshire et al., 2008; Visser et al., 2011). The broadened age range was taken into account when forming the cohort and is reflected in the age range of the included patients (0 years – 24 years).

The posterior of the brain shows the most severe pathology in patients (Uusimaa et al., 2008; Khan et al., 2012). As a consequence, many key symptoms of Alpers' syndrome are most likely the result of damage to these regions: pathology to the cerebellum is associated with nystagmus and ataxia, while pathology to the occipital lobe is associated with impaired vision and visual abnormalities. Pathology in other regions of the cerebrum and the deep grey nuclei has been reported less frequently (Wiltshire et al., 2008; Cardenas and Amato 2010).

The neuropathological investigations in this study centre on four regions of the brain in the cohort: the cerebellum, occipital lobe, parietal lobe, and basal ganglia. The former two regions have been highly implicated in the neuropathology of the condition. Pathology of the latter two regions has been documented less frequently in the literature and these are areas of interest to this study. I investigated the morphology of the tissue (microvacuolation, capillary proliferation, and microinfarcts), neuronal cell loss, astrogliosis, microglial activation, and white matter abnormalities (myelin loss and axonal abnormalities). These criteria are commonly used to assess patient tissue, and aid neuropathologists in making a diagnosis.

This chapter examines many neuropathological aspects in a large cohort of patients with clinically diagnosed Alpers' syndrome. The literature on Alpers' syndrome contains many case reviews of one or two patients, written in isolation of other cases, while this cohort brings together many patients across a large age range with known and unknown *POLG* mutations. A poor prognosis is given for patients with Alpers' syndrome, increasing the importance of further investigations into the condition.

3.2 Aims

The patients were categorised into groups depending on the availability of a genetic diagnosis: evidence of two recessive *POLG* mutations, no genetic diagnosis possible due to no suitable DNA being available, no mutation in *POLG*, and a single stillbirth with *POLG* mutations identified in a sibling. The aims of this work are:

1. To achieve a genetic diagnosis in patients where one is not confirmed.
2. To correlate the neuropathology with severe clinical signs in the patients.
3. To quantitatively and semi-quantitatively assess the neuropathological characteristics in the brains of patients clinically diagnosed with Alpers' syndrome, and compare the findings to those of controls. The neuropathological characteristics studied gave information on the severity of pathology in the brain; these characteristics were the degree of atrophy, microvacuolation, neuron loss, astrogliosis, mitochondrial localisation, white matter changes, and microglial activation.
4. To investigate the differences in the neuropathology between the patient groups.

3.3 Methodological Approach

Ten patients were assessed for neuropathological characteristics (Table 3.1). Histological stains and antibodies were used to identify cells and cellular structures of interest. Standard protocols were followed for staining and antigen retrieval and the antibody dilutions used are listed in *Chapter 2 Materials and Methods, 2.2.3 'Neurohistopathological Methods in Staining FFPE Tissue'* and *2.2.4 'Antibody Staining in FFPE Tissue'*.

A battery of histological stains and antibodies were used to fully investigate the pathology: haematoxylin and eosin stain, cresyl fast violet stain, GFAP, porin, Loyez silver stain, Bielschowsky silver stain, and CD68. These are detailed below, using images to describe the pathology seen in the brain tissue of patients.

Patient	Age at Death	Sex	POLG Mutation
1	14 months	F	p.Ala467Thr; p.Gly848Ser
2	27 months	M	p.Ala467Thr; p.Thr914Pro
6	18 years	F	A sibling with p.Trp748Ser; p.Arg1096Cys
5	ID at 34 weeks	M	A sibling with p.Ala467Thr; p.Glu1143Gly; p.Asp1219Glu
7	2.5 months	F	Unknown
8	5.5 months	M	Unknown
9	6.5 months	F	Unknown
10	13 months	M	Unknown
11	7 years	F	Unknown
12	6 years	M	None

Table 3.1. Details of the patients used in the study of neuropathological features.

Key: ID= intrauterine death

3.4 Results

3.4.1 Molecular Investigations of *POLG*

DNA was extracted from the FFPE tissues from six patients, Patients 5-11, using a number of different methods described in *Chapter 2 Methods and Materials, 2.2.10.1 'DNA Extraction'*. It was then tested for DNA concentration and any contaminants present using the Nanodrop ND-1000 Spectrophotometer. A quantity of DNA in the range 1.1 ng/μl to 217.6 ng/μl appeared to be present but subsequent PCR reactions using primers for the three common mutations and their exons (see *Chapter 2 Methods and Materials, 2.2.10.1 'POLG Pyrosequencing'*) did not yield positive results (Figure 3.1). This may have been attributable to contaminants of a 260/230 absorption spectrum, including carbohydrate, organic chemicals, or solvents. This value should be in the range 2.0-2.2 but was frequently seen as negative values. Many different extraction methods were used, all ensuring full evaporation of any ethanol present in the sample before commencing with subsequent steps. This did not improve PCR amplification of the DNA sample.

Patient 5 and Patient 6 each had a sibling with known *POLG* mutations (Table 3.1). The reasons for the stillbirth of Patient 5 are not clear but Patient 6 was known to have presented with features of a *POLG* disorder. It was assumed that both these patients carried one or more of the same *POLG* mutations as their respective sibling. The data from the siblings were useful as only FFPE blocks of brain tissue were available for Patient 5 and Patient 6. Patients 7-11 are historical cases, diagnosed in the 1970s and 1980s when a genetic diagnosis in Alpers' syndrome was not considered; suitable material is no longer available to establish a genetic diagnosis.

Patient 12 in the cohort did not have a reported *POLG* mutation in DNA extracted from frozen muscle tissue. The gene *POLG* was sequenced as described in *Chapter 2 Methods and Materials, 2.2.10.3 'POLG Sequencing'* and was also later submitted for whole exome sequencing. This has identified a potential candidate gene although substantial further work, outside the remit of this thesis, is required to establish a link between the genetic defect and cellular respiration.

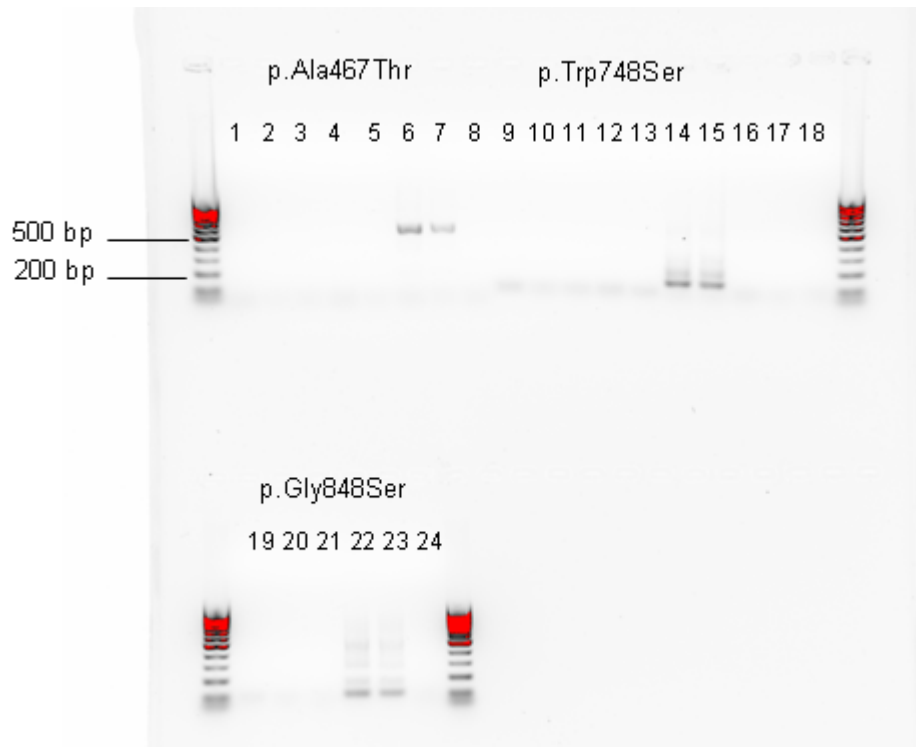


Figure 3.1. Image of an agarose gel showing no amplification of *POLG* exons.

The figure shows an image of a 1% agarose gel with 1Kb ladder, the bands are visualised with GelRed™. DNA had been extracted using the NucleoSpin® Tissue Preparation Kit (Macherey-Nagel). Two rounds of PCR performed using primers for the three common mutations and their exons. Lanes 1-5, 9-13, and 17-21 are repeated with extracted DNA from fixed tissue from Patients 7-11. A positive, wildtype, and negative control (water) were also tested. Lanes 1-8 are tested for the p.Ala467Thr mutation, lanes 9-16 are tested for the p.Trp748Ser mutation, and lanes 17-24 are tested for the p.Gly848Ser mutation. The positive control (lanes 6, 14, and 22) and wildtype DNA (lanes 7, 15, and 23) show positive for bands of amplified DNA. The negative control (lanes 8, 16, and 24) is clear, showing there is no contamination.

All introns and exons of *POLG* were sequenced in both Patient 12 and the female sibling of Patient 5. In Patient 12, seven polymorphisms were found; five within introns, one within exon 23, and one in the 3'-untranslated region (Table 3.2). Within exon 23, a single heterozygous mutation, p.Gln1236His, was found which is not considered to be pathogenic after a search of The Human DNA Polymerase Gamma Mutation Database (<http://tools.niehs.nih.gov/polg/>) and using Alamut™ software to assess pathogenicity. No other mutations were found. In the sibling of Patient 5, nine polymorphisms were found; five within introns, one within exon 7, one within exon 21, one within exon 23, and one in the 3'-untranslated region (Table 3.2).

It is assumed that Patient 5 carried the common *POLG* mutation p.Ala467Thr, the same as his sibling. The p.Glu1143Gly mutation is known to be a polymorphism and the p.Asp1219Glu mutation is a rare polymorphism with an unknown pathogenicity assessed by Alamut™ software. It is a conserved amino acid with PolyPhen-2 software predicting the mutation to be 'probably damaging' with a score of 0.999.

Exon	Patient 12	Sibling of Patient 5
7		c.1399 G>A, p.Ala467Thr
11+12	Intron 11, c.2071-22 T>C	Intron 11, c.2071-22 T>C
17	Intron 17, c. 2734+41, GTAG insert	Intron 17, c. 2734+41, GTAG insert
19+20	Intron 19, c.3105-36 A>G Intron 19, c.3105-11 T>C	Intron 19, c.3105-36 A>G Intron 19, c.3105-11 T>C
21		c.3428 A>G, p.Glu1143Gly
22	Intron 21, c.3483-19 T>G	Intron 21, c.3483-19 T>G
23	c.3708 G>T, p.Gln1236His	c.3657 T>G, p.Asp1219Glu
3'-UTR	c.3720+49	c.3720+49

Table 3.2. A list of *POLG* mutations sequenced in Patient 12 and in the sibling of Patient 5.

Table showing the mutations found in *POLG* in both Patient 12 and the sibling of Patient 5. Mutations causing amino acid changes are highlighted in the table. Patient 12 has a heterozygous point mutation in exon 23 causing an amino acid change. This mutation is not thought to be pathogenic. The sibling of Patient 5 has a heterozygous point mutation in exon 7 causing an amino acid change that is well-known to be pathogenic, a heterozygous point mutation in exon 21 that is thought to be a modifying mutation when it segregates with the p.Trp748Ser mutation, and a heterozygous point mutation in exon 23 (different to that of Patient 12), at a conserved amino acid that has unknown pathogenicity. Key: 3'-UTR=3'-untranslated region.

3.4.2 Patient Characteristics

I investigated a cohort of patients with symptoms of epilepsy and ataxia, and with a clinical diagnosis of Alpers' syndrome where available. As part of the disease progression, 11 of the 12 patients developed seizures, 8 patients developed a movement disorder such as ataxia or hemiplegia, 6 patients developed visual problems, and 5 patients developed liver failure. Patient 5 was a stillbirth at 34 weeks gestation but was considered for inclusion in the cohort as a *POLG* defect was identified in a sibling.

3.4.3 Morphological Assessment of Tissue

A haematoxylin and eosin (H&E) stain was used to assess and quantitate general cellular morphology; microvacuolation, atrophy, microinfarcts, and capillary proliferation in four brain regions. The patients are described within their groups based upon the availability of a genetic diagnosis: evidence of two recessive *POLG* mutations, no genetic diagnosis possible, no mutation in *POLG*, and a single stillbirth with the *POLG* mutations p.Ala467Thr, p.Glu1143Gly, and p.Asp1219Glu identified in a sibling.

3.4.3.1 Cerebellum

The pathology in the cerebellum is summarised in Table 3.3 for patients where this brain region was available.

Patients with evidence for *POLG* mutations (Figure 3.2; image B) show atrophy, microvacuolation, thinned cell layers, and eosinophilic neurons. Patient 1 shows a thinned granular cell layer, confirmed in the original neuropathologist's report. Patient 2 shows a thinned molecular layer and granular cell layer with dendrite proliferation throughout the molecular layer. Microvacuolation mainly in the white matter and the dentate nucleus is clearly seen in Patients 1 and 2.

A single microinfarct is seen in the cerebellum of Patient 6, involving an entire sulcus in the posterior-inferior region. The molecular layer, Purkinje cell layer, granular cell layer, and white matter are all involved. The area of the microinfarct was determined to be 15,935.2 μm^2 . An additional pre-motor cortex lesion was noted in the original neuropathologist's report. It was suggested in this report that the pre-motor cortex lesion may have initiated the epilepsy and be of a different origin to other lesions. One other patient, Patient 4, also showed signs of a microinfarct in the cerebellar cortex. Both of these patients were older patients in the cohort.

Patients with no genetic diagnosis available show atrophy, microvacuolation, capillary proliferation, and eosinophilic neurons. Patient 7 shows a thinned granular cell layer and flattened folia in addition to atrophy. All patients show microvacuolation in the white matter and the dentate nucleus. Patient 8 shows microvacuolation in focal areas of the granular cell layer. There is limited clinical and reported neuropathological data on this group of patients as they are historical cases from the University of Vienna.

The patient without a *POLG* mutation shows microvacuolation and eosinophilic neurons of the dentate nucleus only. Microvacuolation appears mainly in the white matter and the dentate nucleus and Patient 12 shows one the greatest degrees of microvacuolation of all the patients. A mild microvacuolation of the molecular layer was mentioned in the original neuropathologist's report.

The stillbirth, Patient 5 (Figure 3.2; image D) shows a severe capillary proliferation throughout the cerebellum, with no other abnormalities noted. The matched control tissue did not demonstrate a capillary proliferation.

The cerebellum shows pathology of both the grey and white matter, affecting both Purkinje cells and neurons of the dentate nucleus. The morphology of the cerebellum is more affected where a *POLG* mutation is confirmed or unknown, rather than in the patient without a *POLG* mutation where pathology is restricted to the white matter and the dentate nucleus. Patients with evidence for *POLG* mutations show a wider range of pathology, including microinfarcts.

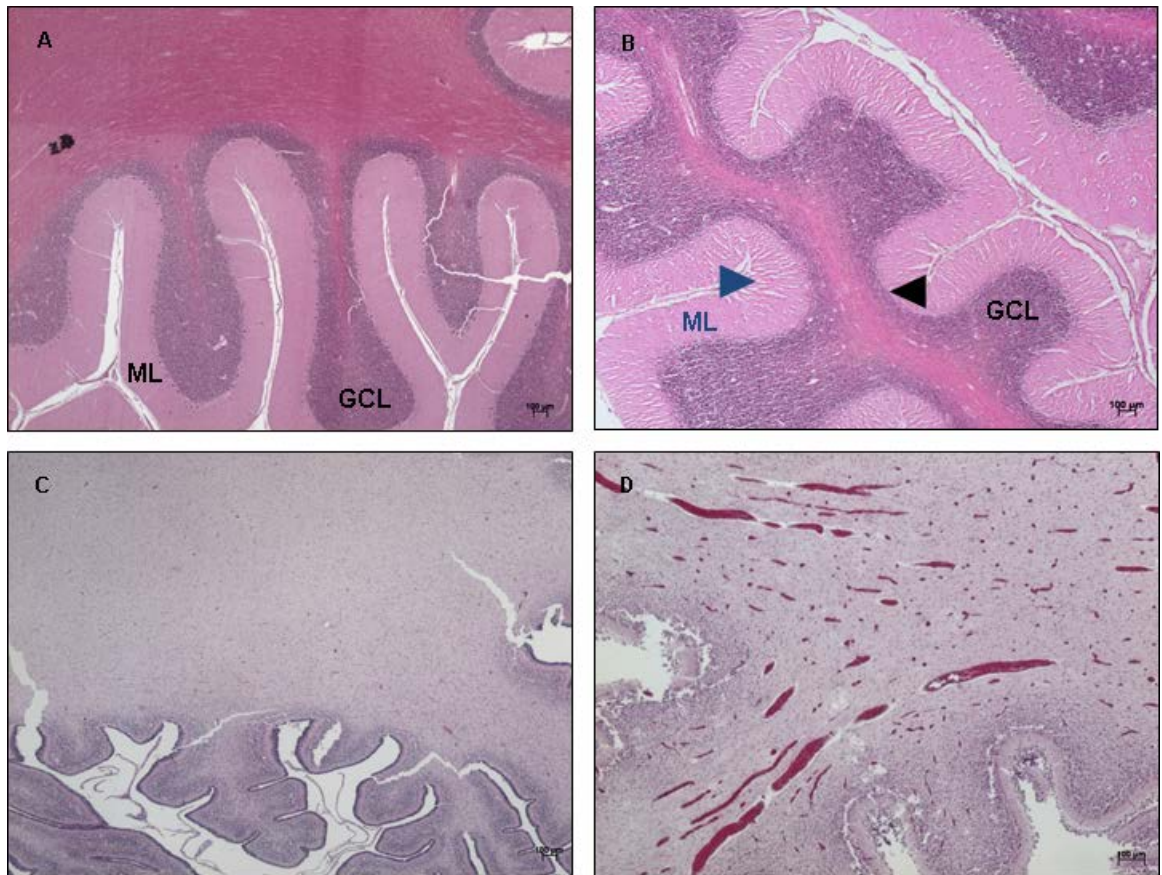


Figure 3.2. Neurodegenerative abnormalities in the cerebellum.

A=Control 6, B=Patient 6 *POLG* mutation-positive group, C=Control 5, D=Patient 5 stillbirth. Patient 6 (image B) shows a striated appearance of the molecular layer (ML) indicated by the blue arrow, and thinned granular cell layer (GCL) indicated by the black arrow. The control (image A) shows intact ML and GCL. Patient 5 shows capillary proliferation in the white matter (image D) whilst the control (image C) shows normal white matter. All sections stained with H&E. Scale bar = 100μm.

The brain area is unavailable for patients not listed in the table.

<i>POLG</i> mutation	Patient	Atrophy	MV	Capillary Proliferation	Microinfarct
+	1	+	+	-	-
	2	+	+	-	-
	6	-	-	-	+
+ s	5	-	-	+++	-
?	7	+	++	-	-
	8	+	+	+	-
	9	-	++	+	-
	10	-	+	+	-
	11	-	++	-	-
-	12	-	++	-	-

Table 3.3. Summary of neuropathology in the cerebellum.

Assessment is semi-quantitative using the scale -/+/++/+++, where - is the absence of a pathological feature and +++ is the presence of a severe pathological feature.

Key: MV=microvacuolation, s=stillbirth

3.4.3.2 Occipital Lobe

The pathology in the occipital lobe (BA19) is summarised in Table 3.4 for patients where this brain region was available.

Patients with evidence for *POLG* mutations (Figure 3.3; images C and D) show slight microvacuolation, capillary proliferation, and some neurons appearing eosinophilic and shrunken. Patient 2 shows slight microvacuolation in the upper cortical layers II and III, confirmed in the original neuropathologist's report.

Patients with no genetic diagnosis available (Figure 3.3; images B, E and F) show microvacuolation throughout the grey matter and considerable capillary proliferation.

The patient without a *POLG* mutation, Patient 12, shows microvacuolation in both grey and white matter, capillary proliferation, and eosinophilic neurons. There are small focal areas of necrosis in the grey matter throughout all layers, which are confirmed in the original neuropathologist's report.

The stillbirth, Patient 5, shows severe capillary proliferation throughout the occipital lobe and this is also noted in the cerebellum. The matched control tissue did not demonstrate a capillary proliferation.

The occipital lobe shows pathology primarily of the grey matter. The morphology of this brain area is more consistently affected where a *POLG* mutation is unknown yet it is surprising that more severe pathology is not seen, given its involvement in the clinical signs of Alpers' syndrome. Pathology is mainly seen in the grey matter; however the white matter is also notably affected in the patient without a *POLG* mutation.

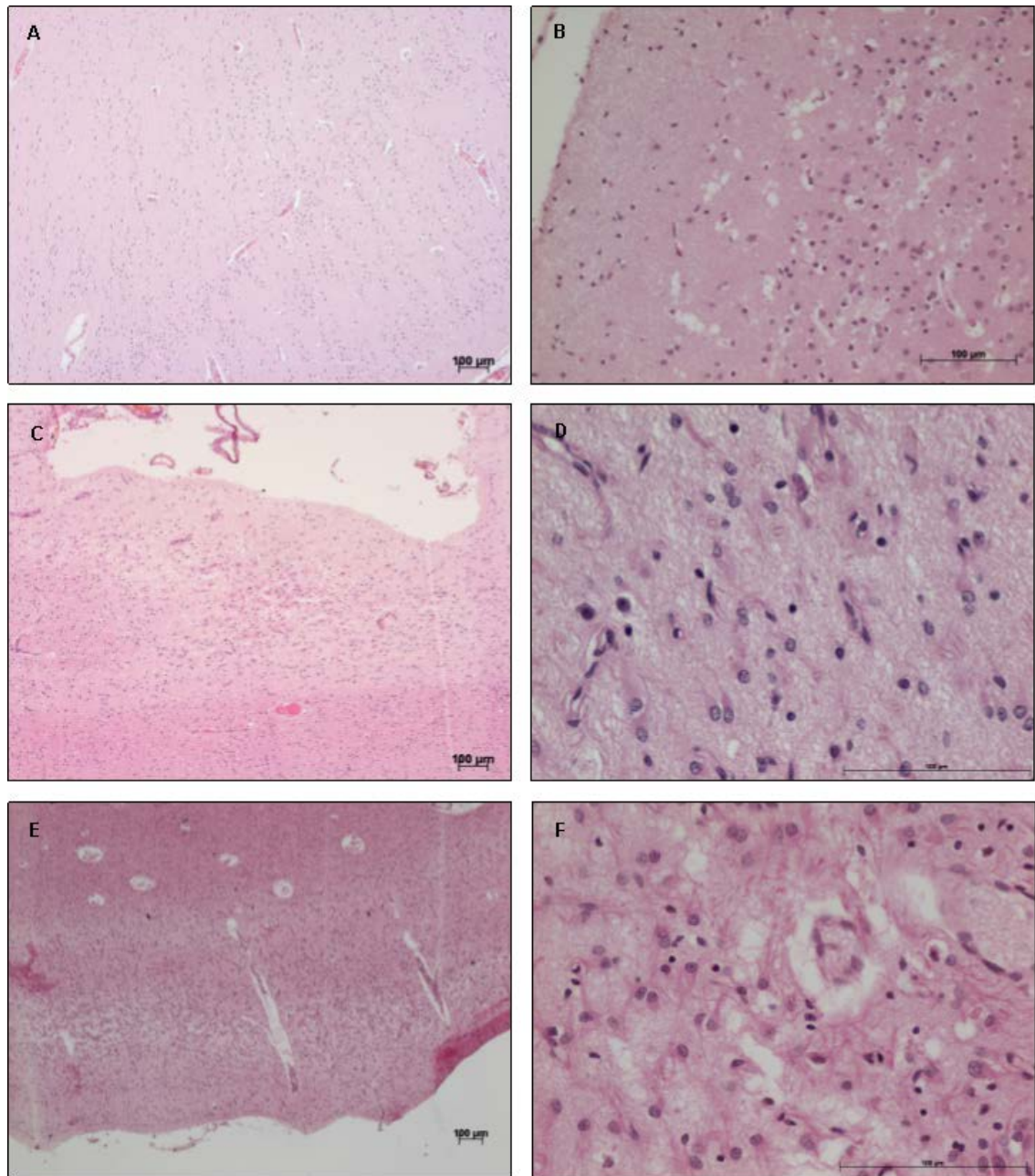


Figure 3.3. Microvacuolation in the occipital lobe.

A=Control 7, B=Patient 10 *POLG* mutation-undetermined group, C=Patient 2 *POLG* mutation-positive group, D= Patient 2 *POLG* mutation-positive group, E=Patient 11 *POLG* mutation-undetermined group, F= Patient 11 *POLG* mutation-undetermined group. All three patient images show microvacuolation in the grey matter. Image B is at a higher magnification to illustrate the pathology. Image D is a higher magnification of image C, and image F is a higher magnification of image E which show microvacuolation in the grey matter. All sections stained with H&E. Scale bar = 100µm.

The brain area is unavailable for patients not listed in the table.

<i>POLG</i> mutation	Patient	MV	Capillary Proliferation	Microinfarct
+	1	-	+	-
	2	+	-	-
+ s	5	-	+++	-
?	8	++	++	-
	10	++	++	-
	11	++	++	-
-	12	+	+	-

Table 3.4. Summary of neuropathology in the occipital lobe.

Assessment is semi-quantitative using the scale -/+/+/++/+++, where - is the absence of a pathological feature and +++ is the presence of a severe pathological feature.

Key: MV=microvacuolation, s=stillbirth

3.4.3.3 Parietal Lobe

The pathology in the parietal lobe (BA40) is summarised in Table 3.5 for patients where this brain region was available.

Patients with evidence for *POLG* mutations (Figure 3.4; images E and F) show microvacuolation in the deep grey matter layers, capillary proliferation and shrunken neurons. However, Patient 1 does not display any microvacuolation or capillary proliferation, and neurons appear small but possibly not shrunken, though mild spongiform changes are noted in the original neuropathologist's report.

Patients with no genetic diagnosis available show microvacuolation in the deep layers of the grey matter with large spaces around the neurons, and considerable capillary proliferation.

The patient without a *POLG* mutation (Figure 3.4; images B, C and D) shows microvacuolation in the deep layers of the grey matter, and particularly in the perivascular spaces. This was noted throughout the entire parietal tissue available, with the areas surrounding the vessels greatly enlarged by microvacuolation, not commented on in the original neuropathologist's report. This was not seen to this extent in any other patients.

The stillbirth, Patient 5, shows severe capillary proliferation and moderate microvacuolation throughout. A severe capillary proliferation is also seen in the cerebellum and occipital lobe. The matched control tissue did not demonstrate a capillary proliferation.

The parietal lobe shows pathology primarily of the deep grey matter layers. The morphology of this brain area is affected in all groups. Further comparisons between groups are difficult to draw due to single patients available in some groups. An exception is Patient 1, where no pathology is apparent.

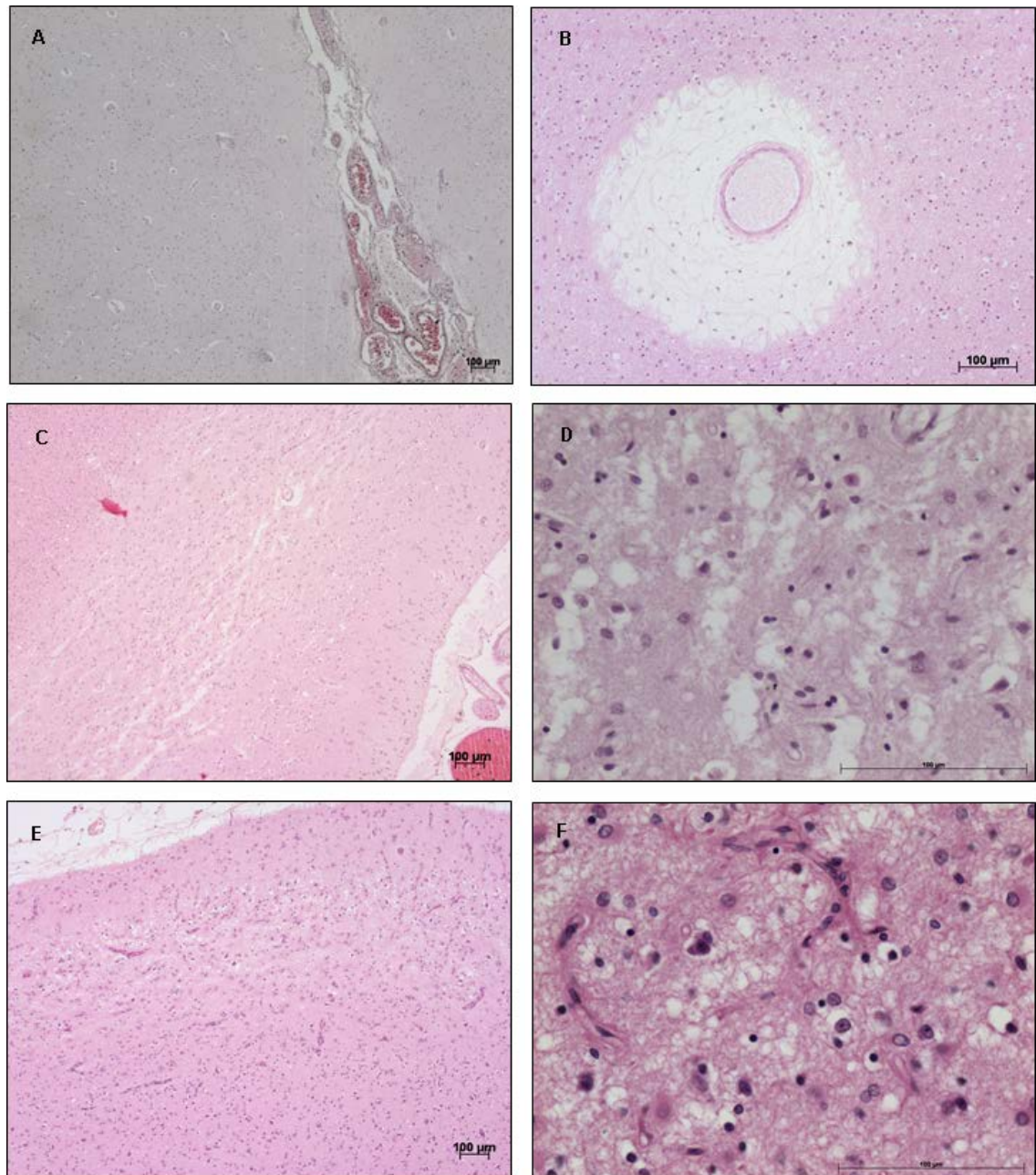


Figure 3.4. Microvacuolation in the parietal lobe.

A=Control 7, B=Patient 12 *POLG* mutation-absent group, C=Patient 12 *POLG* mutation-absent group, D=Patient 12 *POLG* mutation-absent group, E=Patient 2 *POLG* mutation-positive group, F=Patient 2 *POLG* mutation-positive group. All patient images show microvacuolation in the grey matter. Image B is at a higher magnification and shows microvacuolation in the perivascular space. Image D is a higher magnification of image C, and image F is a higher magnification of image E which show microvacuolation in the grey matter. All sections stained with H&E. Scale bar = 100µm.

The brain area is unavailable for patients not listed in the table.

<i>POLG</i> mutation	Patient	MV	Capillary Proliferation	Microinfarct
+	1	-	-	-
	2	+	+	-
	6	+	+	-
+ s	5	++	+++	-
?	8	++	+++	-
-	12	++	-	-

Table 3.5. Summary of neuropathology in the parietal lobe.

Assessment is semi-quantitative using the scale -/+/++/+++, where - is the absence of a pathological feature and +++ is the presence of a severe pathological feature.

Key: MV=microvacuolation, s=stillbirth

3.4.3.4 Basal Ganglia

The pathology in the basal ganglia is summarised in Table 3.6 for patients where this brain region was available. All nuclei of the basal ganglia were assessed where available.

Patients with evidence for *POLG* mutations (Figure 3.5; images C and D) show little pathology.

Patients with no genetic diagnosis available (Figure 3.5; image B) show microvacuolation and slight capillary proliferation.

The patient without a *POLG* mutation (Figure 3.5; images E and F) shows patchy microvacuolation confirmed in the original neuropathologist's report, and large spaces around the neurons of the caudate.

The stillbirth, Patient 5, shows severe capillary proliferation. A severe capillary proliferation is also seen in the cerebellum, occipital lobe, and parietal lobe. The matched control tissue did not demonstrate a capillary proliferation.

The basal ganglia show a lesser degree of pathology than other brain areas. The morphology of this brain area is slightly affected where a *POLG* mutation is unknown. A severe capillary proliferation is seen in Patient 5, a feature that has been noted in all brain areas studied for this patient. Capillary proliferation was not seen in the age-matched control, Control 5, and so is not considered a normal stage of development.

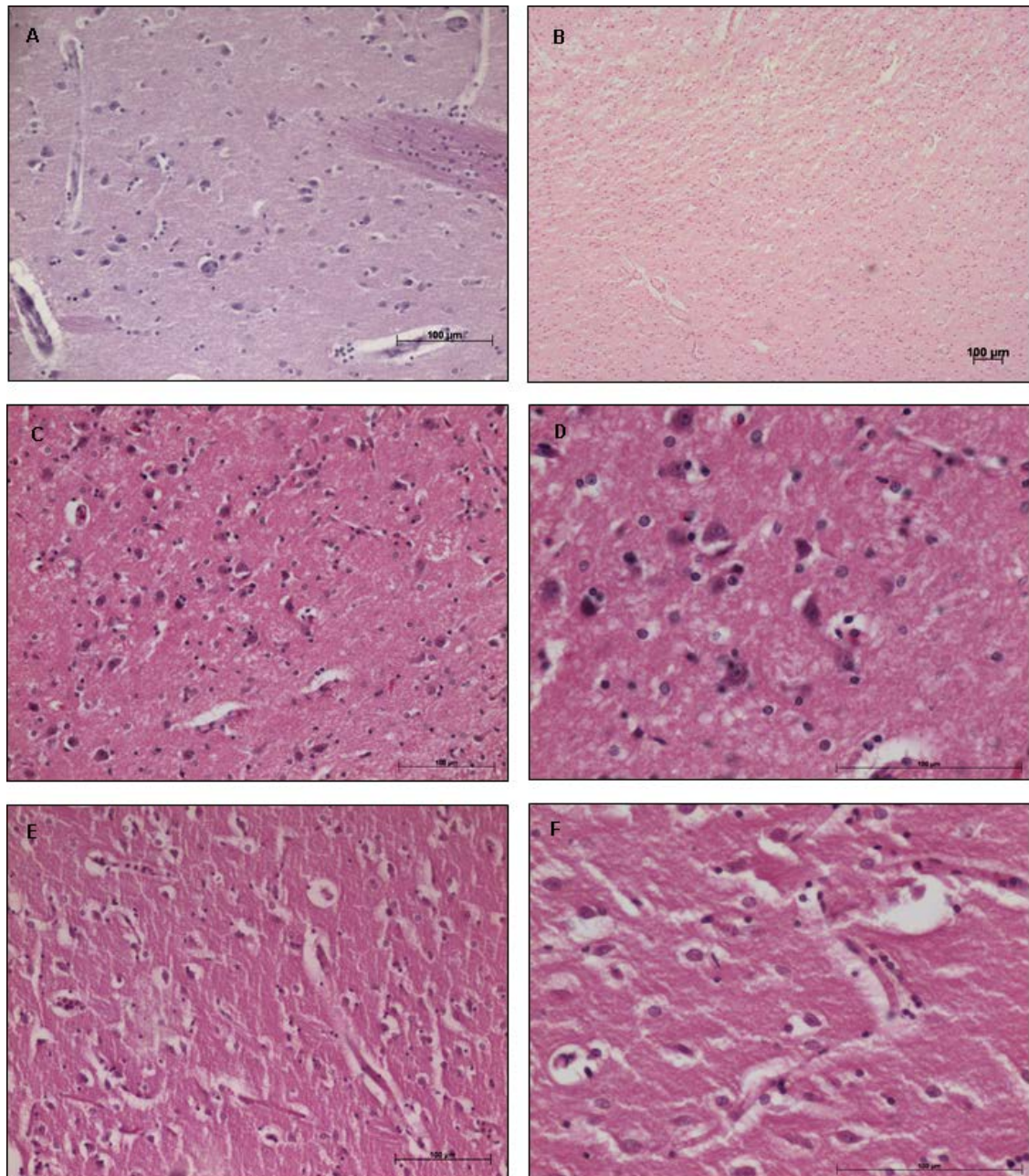


Figure 3.5. Microvacuolation in the caudate of the basal ganglia.

A=Control 6, B=Patient 9 *POLG* mutation-undetermined group, C=Patient 1 *POLG* mutation-positive group, D=Patient 1 *POLG* mutation-positive group, E=Patient 12 *POLG* mutation-absent group, F=Patient 12 *POLG* mutation-absent group. Image B is at a lower magnification and shows microvacuolation over a larger area. Image D is a higher magnification of image C which shows no microvacuolation. Image F is a higher magnification of image E which shows slight microvacuolation. All images are taken of caudate. All sections stained with H&E. Scale bar = 100µm.

The brain area is unavailable for patients not listed in the table.

<i>POLG</i> mutation	Patient	MV	Capillary Proliferation	Microinfarct
+	1	-	-	-
	2	-	-	-
+ s	5	-	+++	-
?	8	+	-	-
	9	+	+	-
	10	-	-	-
	11	+	+	-
-	12	+	-	-

Table 3.6. Summary of neuropathology in the basal ganglia.

Assessment is semi-quantitative using the scale -/+/+/++/+++, where - is the absence of a pathological feature and +++ is the presence of a severe pathological feature.

Key: MV=microvacuolation, s=stillbirth

3.4.4 Neuron Loss

A cresyl fast violet (CFV) stain was used to assess neuronal populations in patient and control tissue. Suitable control tissue was extremely difficult to obtain due to the age of the patients. However, a number of controls were obtained for each brain area.

In the cerebellum, both Purkinje cells and neurons of the dentate nucleus were assessed. Purkinje cells are one of the largest neuron types in the brain. They are the main efferent output of the cerebellum, ultimately controlling motor coordination, and have an inhibitory effect on the deep grey nuclei of the cerebellum. The dentate nucleus is the largest of the four deep grey nuclei within the white matter of the cerebellum. It has a role in motor coordination to plan and initiate voluntary movement, as well as a non-motor role in visuospatial functioning.

In the occipital and parietal lobes, neurons of cortical layers I-VI were assessed. In the basal ganglia, neurons of the caudate, putamen, and globus pallidus (both lateral and medial) were assessed.

Purkinje cells and cortical neurons were counted using reference spaces as described in *Chapter 2 Methods and Materials, 2.2.6 'Quantitative Methods'*. It was not possible to assess the neurons of the dentate nucleus or the basal ganglia fully quantitatively. Therefore, neurons of the dentate nucleus and the basal ganglia were assessed semi-quantitatively using the -/+ /++ /+++ scale as described in *Chapter 2 Methods and Materials, 2.2.7 'Semi-quantitative Methods'*. Where both percentage values and semi-quantitative data were available, they were displayed in the same table.

3.4.4.1 Cerebellum

Purkinje cells of the cerebellum were assessed in representative patients from two of the groups and in three controls, Control 1, a 13 month old female, Control 5 which is a female fetal control, and Control 6, a 19 year old female. Focal neuron loss was known to occur in the patients. This was examined by counting areas of the cerebellum known to exhibit focal neuron loss in one patient and then sampled in all patients and the controls.

Purkinje cells were qualitatively assessed (Figure 3.6) and quantitatively assessed using reference spaces and the length of the Purkinje cell layer taken to calculate for neuron density. A qualitative assessment only was made of neurons of the dentate nucleus. The results of these assessments are shown in Figure 3.7. Semi-quantitative assessment of both the Purkinje cells and the neurons of the dentate nucleus are summarised in Table 3.8. Where appropriate, both percentage values and a semi-quantitative assessment for a patient have been displayed together. These values correlate well.

The density of Purkinje cells reveal that these cells are greatly reduced in three of the five patients assessed when compared to controls. Patients and controls were matched based on age, with both non-fetal controls having a very similar average density (shown as 'Average Count per mm' in Table 3.7). The percentage of cell loss is similar in all three young patients; Patient 2, 64.6% loss; Patient 6, 44.4% loss; Patient 12, 48.2% loss. Patient 5, a stillbirth, showed a 5.8% loss of Purkinje cells which was not considered significant. These values are summarised in Table 3.7, grouping the patients with the matched control that was used to assess neuron loss.

Patients with evidence for *POLG* mutations (Figure 3.6; images B and D) show Purkinje cell loss and loss of neurons from the dentate nucleus. In patients showing Purkinje cell loss, this is concentrated in the biventer and tonsilla regions of the cerebellum which may indicate susceptible neurons in these regions. However, very little neuron loss is seen in Patient 1; there is no Purkinje cell loss but there is a mild loss of neurons from the dentate nucleus (+) (Table 3.8) which is confirmed in the original neuropathologist's report describing lesser pathology in the cerebellar hemispheres with greater pathology in the cerebellar vermis. It is currently unclear what factors have spared Purkinje cell loss in this patient. Patient 2, of a similar age to Patient 1, shows 64.6% loss of Purkinje cells and a mild loss of neurons from the dentate nucleus (+) (Table 3.8).

Patients with no genetic diagnosis available showed variable Purkinje cell and dentate nucleus neuron loss (not shown on Figure 3.7). Loss of Purkinje cells is not seen in two patients, is seen at a low level (+) in one patient, moderate level (++) in one patient, and severe level (+++) in one patient. Patients that show Purkinje cell loss do not always show a loss of neurons from the dentate nucleus (Table 3.8) suggesting that these groups of neurons may be affected differently in patients.

The patient without a *POLG* mutation (Figure 3.6; image C) shows a 48.2% Purkinje cell loss and a moderate loss of neurons from the dentate nucleus (++) (Table 3.8). Focal Purkinje cell loss is seen in some areas of the cerebellum of this patient.

No Purkinje cell loss is seen in Patient 5, the stillbirth, when compared to its control.

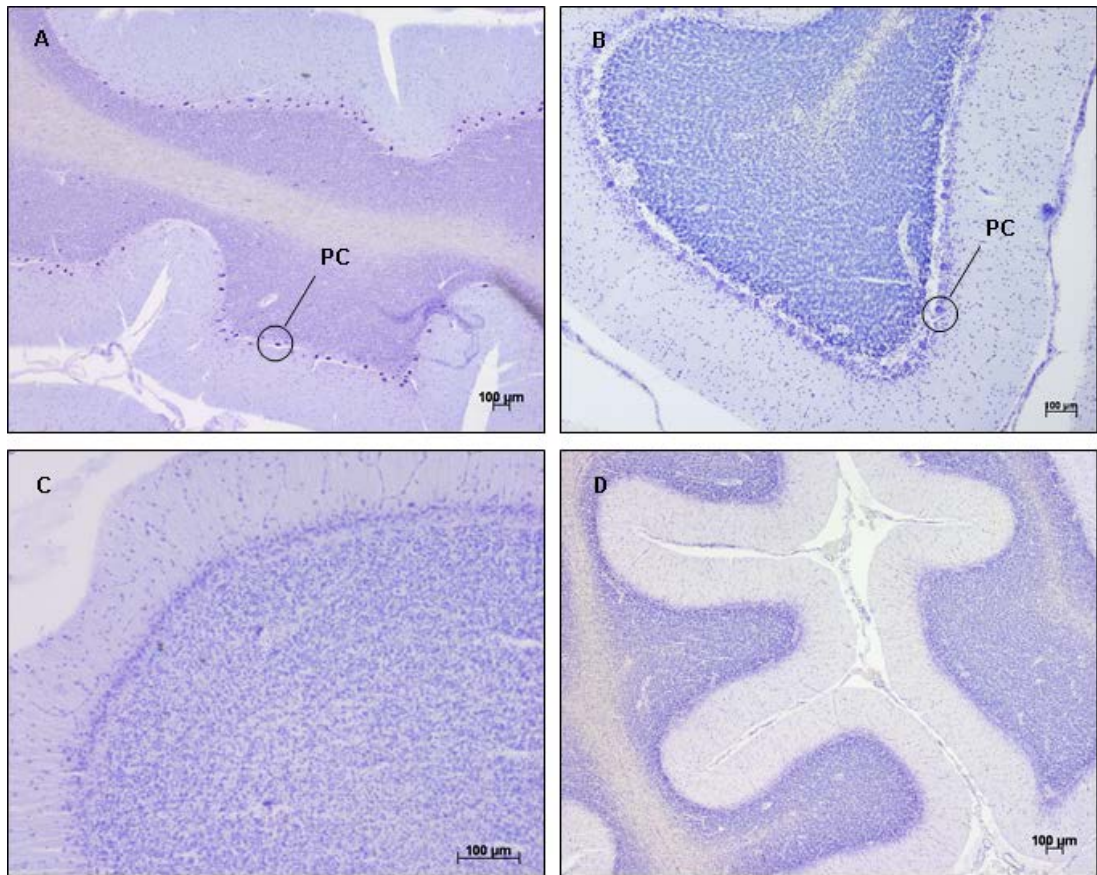


Figure 3.6. Neuron loss in the cerebellum.

A=Control 6, B=Patient 1 *POLG* mutation-positive group, C=Patient 12 *POLG* mutation-absent group, D=Patient 6 *POLG* mutation-positive group. Image B does not show any Purkinje cell loss. Image C is at a higher magnification showing focal Purkinje cell loss. Image D shows an area of complete Purkinje cell loss. All sections stained with CFV stain. Scale bar = 100µm.

Key: PC=Purkinje cell

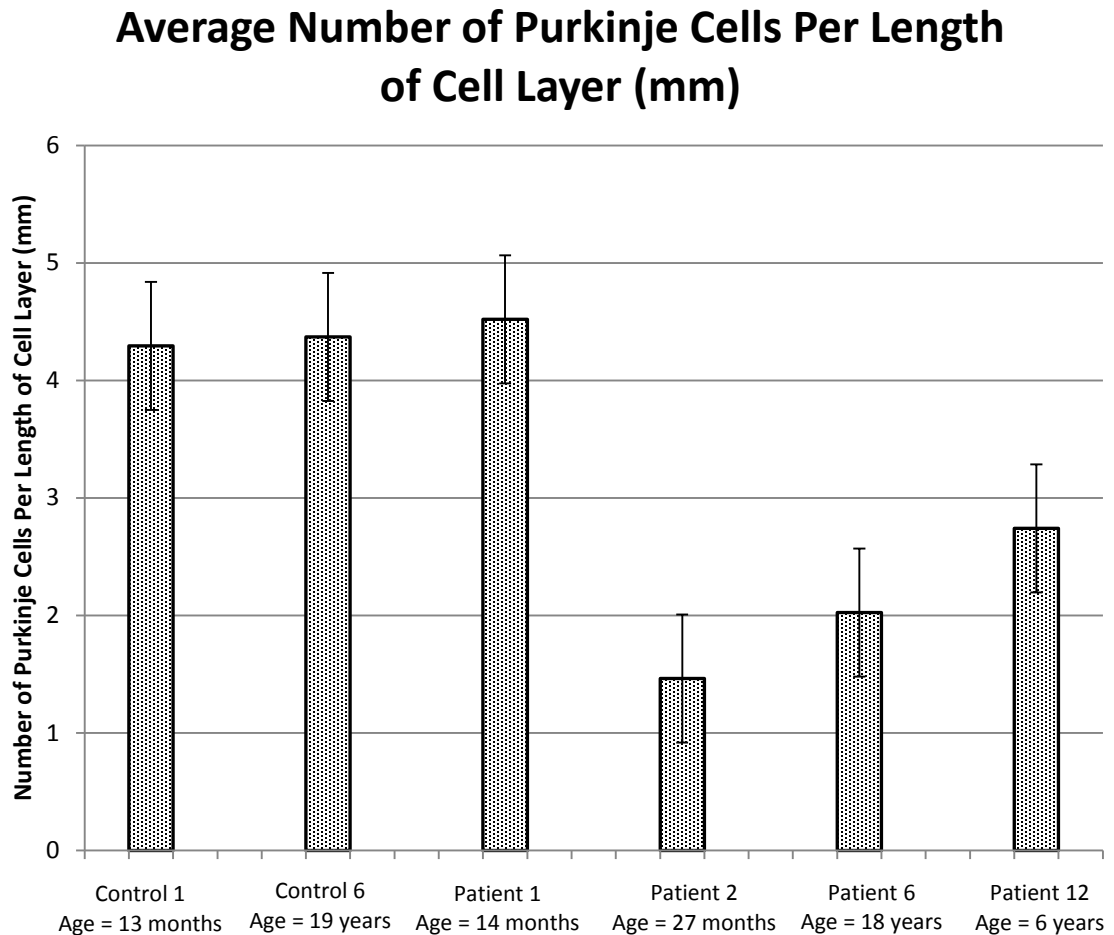


Figure 3.7. Average number of Purkinje cells per length of cell layer (mm) in the cerebellum of patients and controls.

Each column represents the average Purkinje cell count, over a total of 63 reference spaces over three separate microscope slides (21 reference spaces per slide). This value has been corrected for the length of the Purkinje cell layer assessed. Patient 12 was averaged over two available microscope slides (error bars represent \pm SEM over a total of 63 reference spaces).

The stillbirth, with a sibling that has an identified *POLG* mutation, does not show Purkinje cell loss when compared to a fetal control (Figure 3.8). There was also no loss of neurons from the dentate nucleus. There is a higher average number of Purkinje cells in both the fetal patient and fetal control. This may be due to undifferentiated Purkinje cells in the Purkinje cell layer. As they differentiate and connections throughout the brain become refined, fewer Purkinje cells will populate the layer.

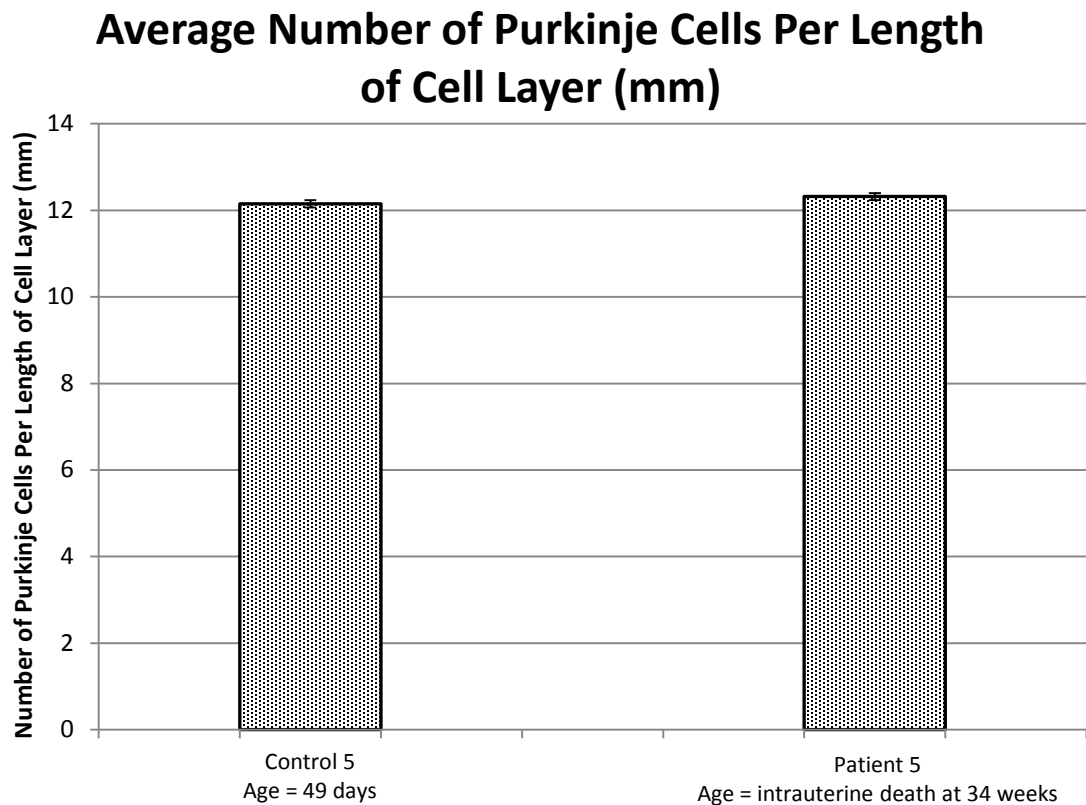


Figure 3.8. Average number of Purkinje cells per length of cell layer (mm) in the cerebellum of a stillbirth and a fetal control.

Each column represents the average Purkinje cell count, over a total of 63 reference spaces over three separate microscope slides (21 reference spaces per slide). This value has been corrected for the length of the Purkinje cell layer assessed (error bars represent \pm SEM over a total of 63 reference spaces).

Patient	Individual Slide Cell Count	Average Cell Count	CoV	Average Count per mm	Percent of the Control	Percent Purkinje Cell Loss
Control 1	151, 152, 160	154.33 (Range: 2-13)	0.032 (SD=4.933)	4.29		
Patient 1	146, 164, 158	156 (Range: 2-15)	0.059 (SD=9.165)	4.52	101.1%	0%
Patient 2	54, 56, 54	54.67 (Range: 0-10)	0.021 (SD=1.155)	1.46	35.43%	64.57%
Patient 12	86, 74	80 (Range: 0-7)	0.106 (SD=8.485)	2.74	51.85%	48.15%
Control 6	137, 131, 135	134.3 (Range: 3-12)	0.023 (SD=3.055)	4.37		
Patient 6	58, 78, 88	74.67 (Range: 0-11)	0.205 (SD=15.275)	2.02	55.6%	44.4%
Control 5	385, 386, 399	390 (Range: 7-38)	0.020 (SD=7.810)	12.15		
Patient 5	435, 325, 342	367.3 (Range: 0-35)	0.161 (SD=59.214)	12.31	94.18%	5.82%

Table 3.7. Calculation of Purkinje cell loss in the cerebellum.

The table shows the calculation of Purkinje cell loss from each patient. Patients are grouped showing the control used to calculate percentage neuron loss from. This control was chosen based its age and matched to the patient. The average cell count per microscope slide and the average cell count of all three slides are shown in the table, with the range of counted cells shown. The coefficient of variation and standard deviation are also shown. The average count when corrected for the length of the Purkinje cell layer (mm) is shown.

Key: CoV=coefficient of variation, SD=standard deviation

The brain area is unavailable for patients not listed in the table. The availability of the dentate nucleus was dependent upon the orientation of the sample taken by the original pathology team. In some patients, this led to the dentate nucleus being unavailable for analysis.

<i>POLG</i> Mutation	Patient	Purkinje Cell Loss	Dentate Nucleus Neuron Loss
+	1	0% (-)	+
	2	64.6% (+++)	+
	6	44.4% (++)	N/A
+ s	5	5.8% (-)	-
?	7	-	+
	8	+	-
	9	-	++
	10	-	-
	11	+++	+++
-	12	48.2% (++)	++

Table 3.8. Summary of neuron loss in the cerebellum.

Neuron loss of both Purkinje cells and neurons of the dentate nucleus is summarised in the above table. Both percentage loss values and semi-quantitative values are shown where appropriate.

Semi-quantitative assessment is using the scale -/+/++/+++, where – denotes no neuron loss, and +++ denotes severe neuron loss.

Key: N/A=data not available, s=stillbirth

3.4.4.2 Occipital Lobe

Neurons within all six cortical layers of the occipital lobe (BA19) were assessed in representative patients from two of the groups and one control; Control 7, an 18 year old female, since this was the only control available for this brain region.

Patients with evidence for *POLG* mutations (Figure 3.9; images B and C) show a moderate neuron loss. Patients 1 and 2 show over 40% neuron loss in the upper cortical layers I, II and III (Figure 3.10 and Table 3.9). There is less neuron loss in the lower cortical layers IV, V and VI. Spongiform changes and neuron loss in the superficial layers of Patients 1 and 2 is confirmed in the original neuropathologist's report.

Patients without a genetic diagnosis were assessed semi-quantitatively. The patients show variable neuron loss. Patient 8 and Patient 10 do not show neuron loss whilst Patient 11 shows a severe neuron loss (+++) in cortical layer V. There is limited clinical and reported neuropathological data on this group of patients as they are historical cases from the University of Vienna.

The patient without a *POLG* mutation (Figure 3.9; image D) shows mild neuron loss in layers I, III, IV and V. There is no neuron loss in layers II and VI (Figure 3.10 and Table 3.9).

The occipital lobe shows overall neuronal cell loss in layers I – III, with much less neuron loss identified in any of the patients in layers IV, V and VI. This is not attributed to microvacuolation in the upper cortical layers. The neuron loss in these upper layers may be attributable to the fact that these neurons were difficult to distinguish with confidence, with low numbers being counted for all patients and control. The *POLG* mutation-positive group shows more neuron loss in the upper cortical layers than the *POLG* mutation-absent patient. The lack of neuron loss is unusual considering the involvement the occipital lobe has in the neuropathology of Alpers' syndrome. As part of protocol, the NBTR centre processes region BA19 of the occipital lobe, the extrastriate cortical area. The primary visual cortex is Brodmann Area (BA) 17. This could explain why more pathology is not seen in these patients. Previous reports in the scientific literature do not regularly specify the area of occipital lobe examined.

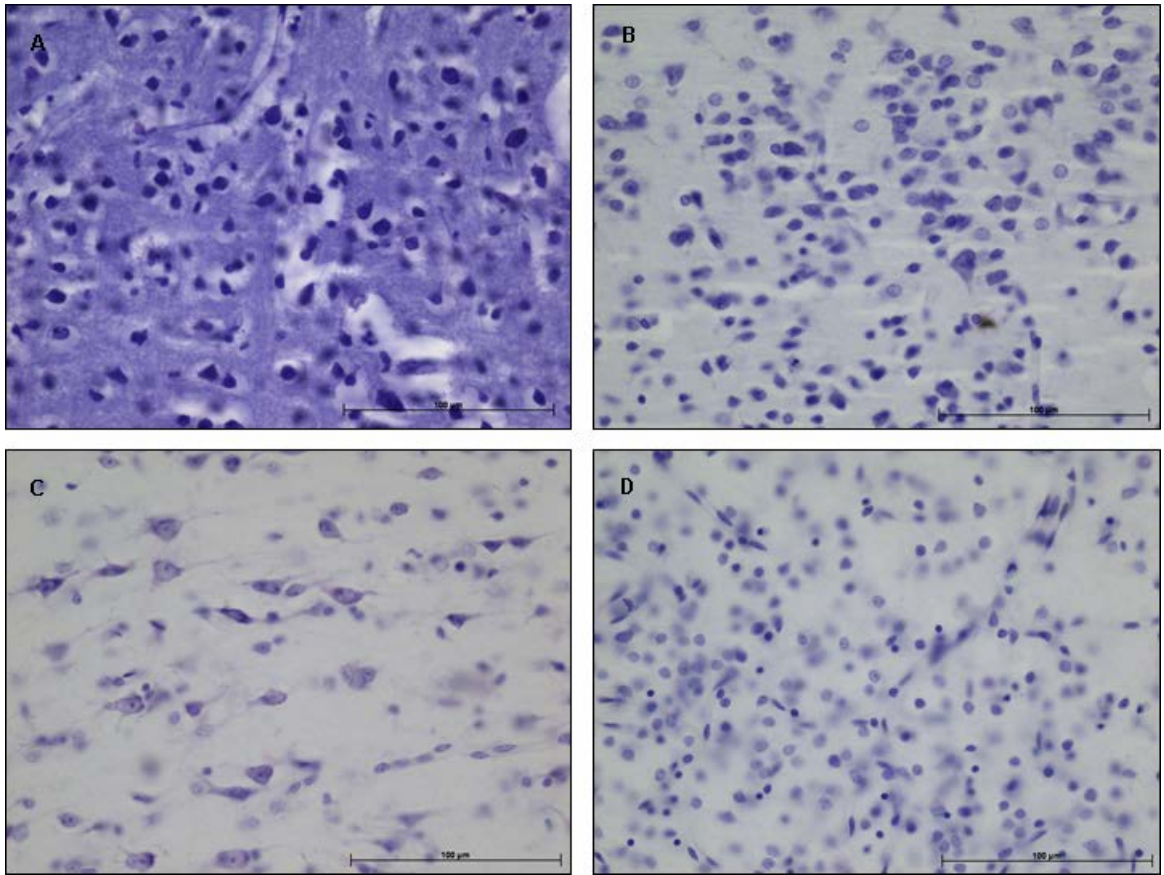


Figure 3.9. Neuron loss in the occipital lobe.

A=Control 7 cl19/20, B=Patient 1 *POLG* mutation-positive group cl29, C=Patient 2 *POLG* mutation-positive group cl28, D=Patient 12 *POLG* mutation-absent group cl30. Images B and C do not show any neuron loss in layer V. Image D shows focal neuron loss in layer V. All sections stained with CFV stain. Scale bar = 100µm.

Key: cl=coronal level

POLG Mutation	Patient	Percentage Neuron Loss					
		Layer I	Layer II	Layer III	Layer IV	Layer V	Layer IV
	Control 7 CoV	0.236	0.349	0.277	0.479	0.387	0.134
+	Patient 1	83.33%	55.82%	55.60%	31.41%	0%	34.74%
	CoV	0.471	0.091	0.144	0.426	0.401	0.425
	Patient 2	83.33%	68.12%	68.31%	33.61%	31.60%	5.26%
	CoV	0.471	0.044	0.420	0.187	0.303	0.294
?	Patient 8					-	
	Patient 10					-	
	Patient 11					+++	
-	Patient 12	27.80%	5.33%	44.01%	29.20%	20.09%	9.47%
	CoV	0.762	0.171	0.150	0.212	0.140	0.201

Table 3.9. Summary of neuron loss in the occipital lobe.

The table shows the neuron loss from each patient. Both percentage loss values and semi-quantitative values are shown where appropriate.

Semi-quantitative assessment is using the scale -/+/++/+++, where – denotes no neuron loss, and +++ denotes severe neuron loss.

Percentage loss is calculated the same way as for the cerebellum and patients are compared to Control 7 to calculate the percentage neuron loss. This control was the only control available for this brain region. The coefficient of variation is also shown.

Key: CoV=coefficient of variation

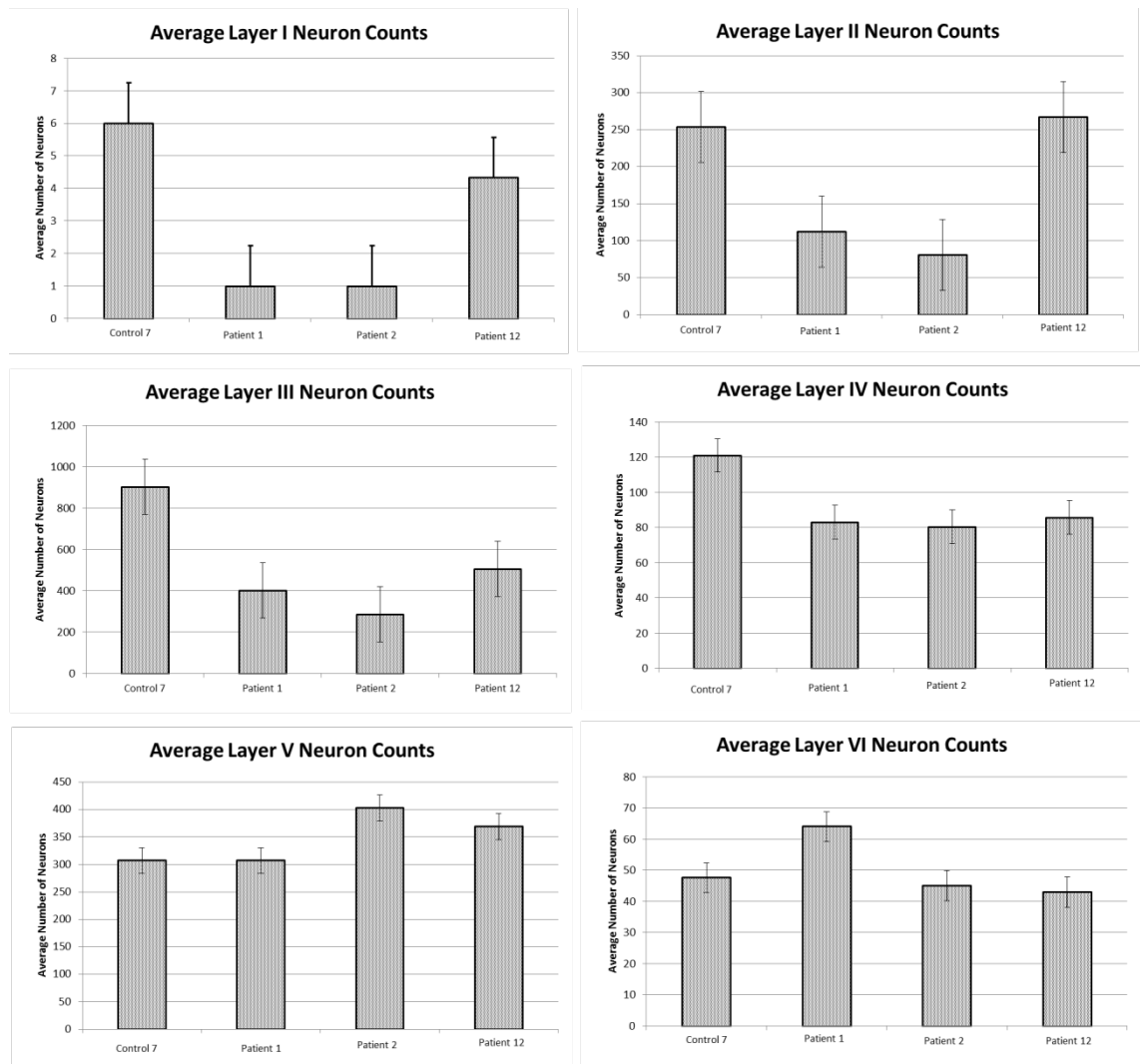


Figure 3.10. Neuron loss in the occipital lobe of patients and controls

Each column represents the average neuronal cell count, over a total of 15 reference spaces over three separate microscope slides (5 reference spaces per slide) (error bars represent \pm SEM over a total of 15 reference spaces).

3.4.4.3 Parietal Lobe

Neurons of all six cortical layers of the parietal lobe (BA40) were assessed in representative patients from two of the groups and in Control 1, a 13 month old female. Control 1 only was available for this brain region.

Patients with evidence for *POLG* mutations (Figure 3.11; images B and C) show severe neuron loss of over 50% in the upper cortical layers I, II, and III (Figure 3.12 and Table 3.10).

Patient 8 was the only patient available with no genetic diagnosis. This patient was assessed semi-quantitatively and shows no neuron loss.

The patient without a *POLG* mutation (Figure 3.11; image D) shows moderate neuron loss of over 40% in layers III and VI (Figure 3.12 and Table 3.10).

The parietal lobe shows overall neuronal cell loss in layers I – III, with less neuron loss identified in layers IV, V and VI. This is not attributed to microvacuolation in the upper cortical layers of Patient 1 and Patient 2, which showed very little microvacuolation. It may play a role in the neuron loss of Patient 12 however, which showed a moderate microvacuolation (++) and 34%-45% neuron loss in the cortical layers III - VI. The neurons in layer I were difficult to distinguish with confidence, with low numbers being counted for all patients and a slightly higher number being counted for the control. The *POLG* mutation-positive group shows a variable neuron loss, with Patient 1 showing loss through all layers concentrated in the upper cortical layers, while Patient 2 shows loss concentrated in the upper cortical layers I-III. The *POLG* mutation-absent group shows neuron loss in the lower cortical layers III and VI. This pattern between the *POLG* mutation-positive group and the *POLG* mutation-absent group is very similar to the occipital lobe.

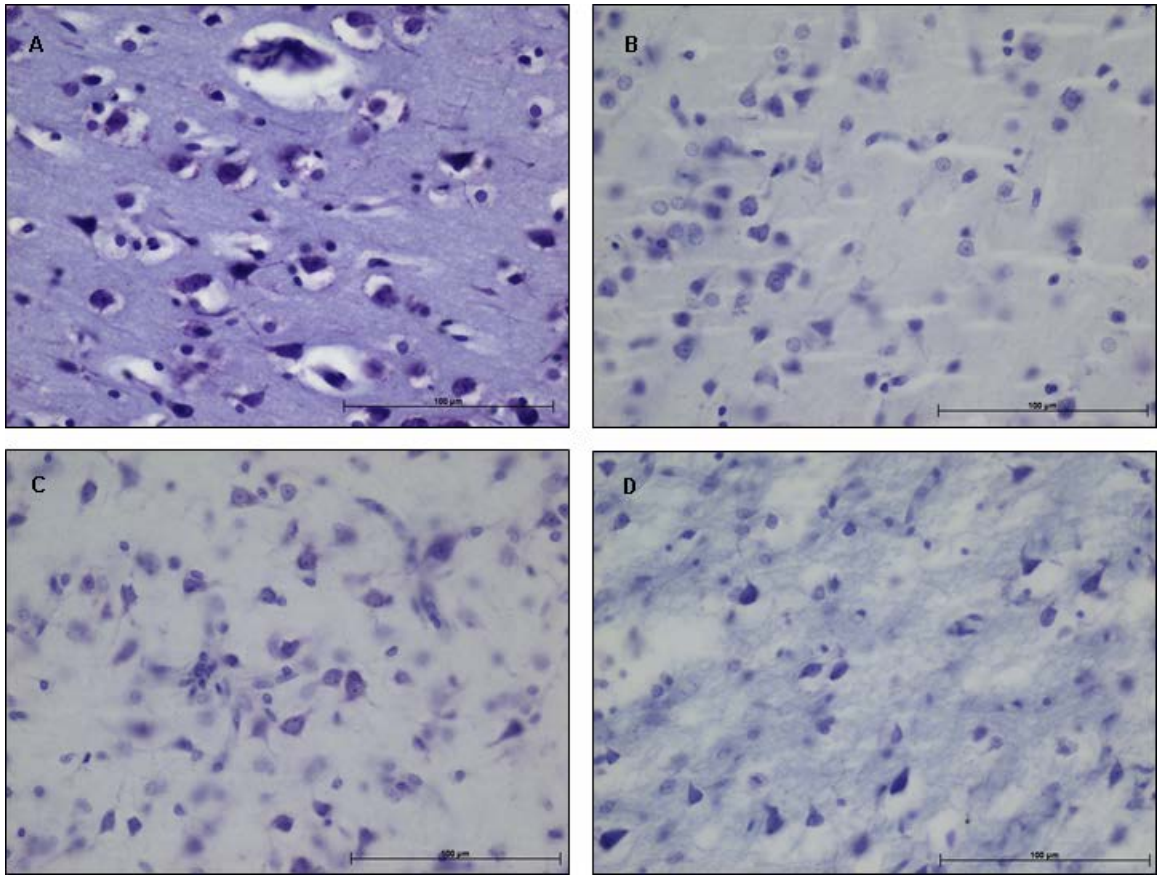


Figure 3.11. Neuron loss in the parietal lobe.

A=Control 1 cl22, B=Patient 1 *POLG* mutation-positive group cl28-30, C=Patient 2 *POLG* mutation-positive group cl25, D=Patient 12 *POLG* mutation-absent group cl24. Images B and C do not show any neuron loss in layer V. Image D shows neuron loss in layer V. All sections stained with CFV stain. Scale bar = 100µm.

Key: cl=coronal level

POLG Mutation	Patient	Percentage Neuron Loss					
		Layer I	Layer II	Layer III	Layer IV	Layer V	Layer IV
	Control 1 CoV	0.354	0.104	0.219	0.035	0.230	0.034
+	Patient 1	85%	55.49%	31.27%	26.99%	15.04%	8.05%
	CoV	ND	0.456	0.197	0.189	0.182	0.226
	Patient 2	100%	82.45%	80.22%	15.90%	31.74%	31.03%
	CoV	ND	0.137	0.216	0.199	0.264	0.156
?	Patient 8					-	
-	Patient 12	35%	3.51%	45.39%	34.20%	39.53%	41.38%
	CoV	0.118	0.175	0.383	0.483	0.299	0.488

Table 3.10. Summary of neuron loss in the parietal lobe.

The table shows the neuron loss from each patient. Both percentage loss values and semi-quantitative values are shown where appropriate.

Semi-quantitative assessment is using the scale -/+ /++ /+++ , where – denotes no neuron loss, and +++ denotes severe neuron loss.

Percentage loss is calculated the same way as for the cerebellum and patients are compared to Control 1 to calculate the percentage neuron loss. This control was the only control available for this brain region. The coefficient of variation is also shown.

Key: CoV=coefficient of variation, ND=not determined

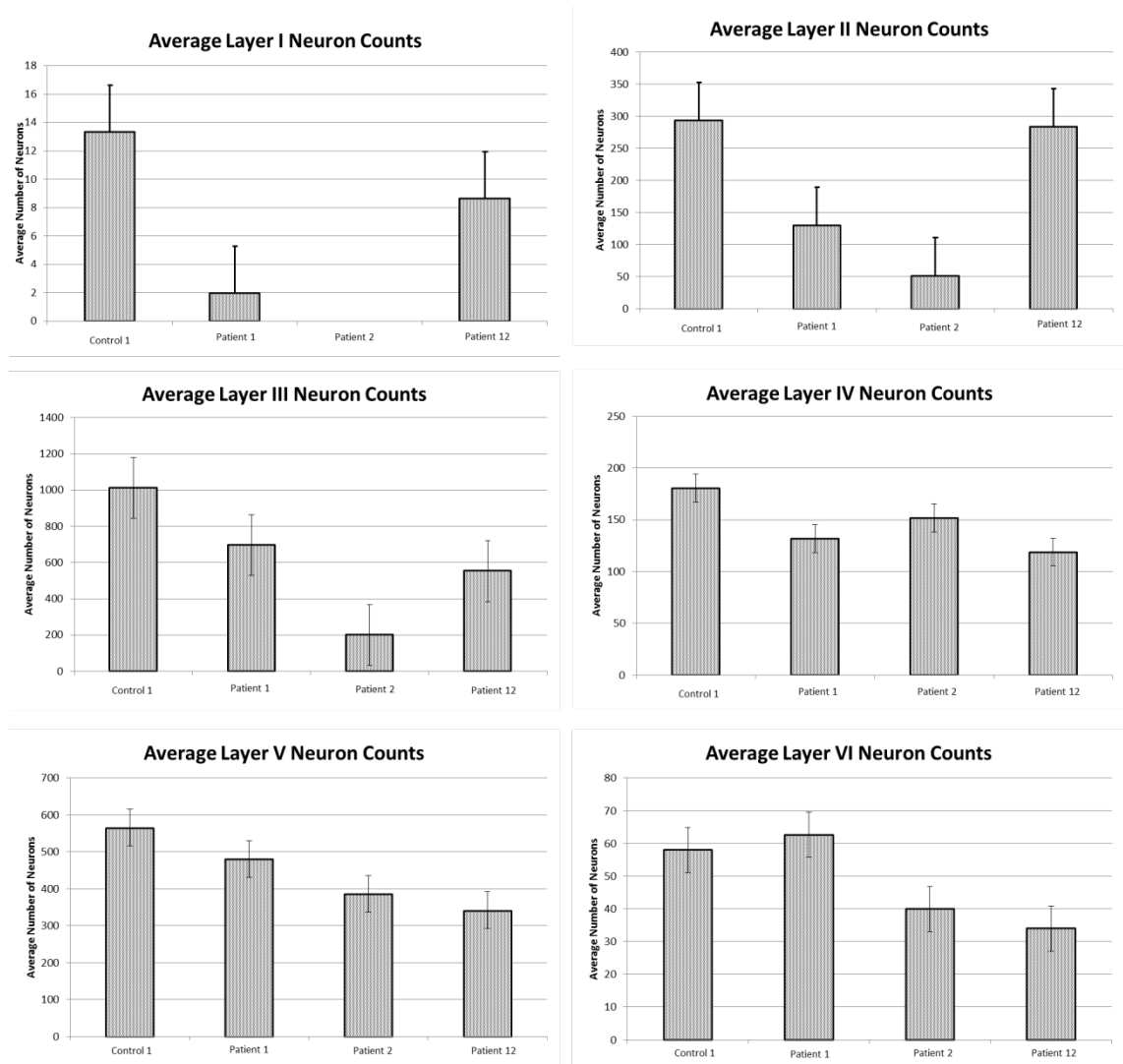


Figure 3.12. Neuron loss in the parietal lobe of patients and controls

Each column represents the average neuronal cell count, over a total of 15 reference spaces over three separate microscope slides (5 reference spaces per slide) (error bars represent \pm SEM over a total of 15 reference spaces).

3.4.4.4 Basal Ganglia

Semi-quantitative assessments of neuron loss in the basal ganglia were carried out in the same manner to the dentate nucleus of the cerebellum. There is good correlation between quantified percentage loss and semi-quantified assessment in previous brain areas assessed. The results are summarised in Table 3.11. Neurons of the caudate, putamen, and globus pallidus were assessed in all patients available and in Control 5, which is a fetal control, and Control 6, a 19 year old female.

There was no neuronal cell loss from patients with evidence for *POLG* mutations (Figure 3.13; images B and C), or from the patient without a *POLG* mutation (Figure 3.13; image D), or from stillbirth Patient 5.

There is a single patient with no genetic diagnosis available that shows neuron loss. Patient 9 shows mild neuron loss (+) in the caudate and moderate neuron loss (++) in the globus pallidus. No neuron loss is seen in any other patients of this group.

Neuron loss is seen in the basal ganglia of a single patient, with an unknown genetic diagnosis. No neuron loss is present in all other patients in all other groups or in the controls.

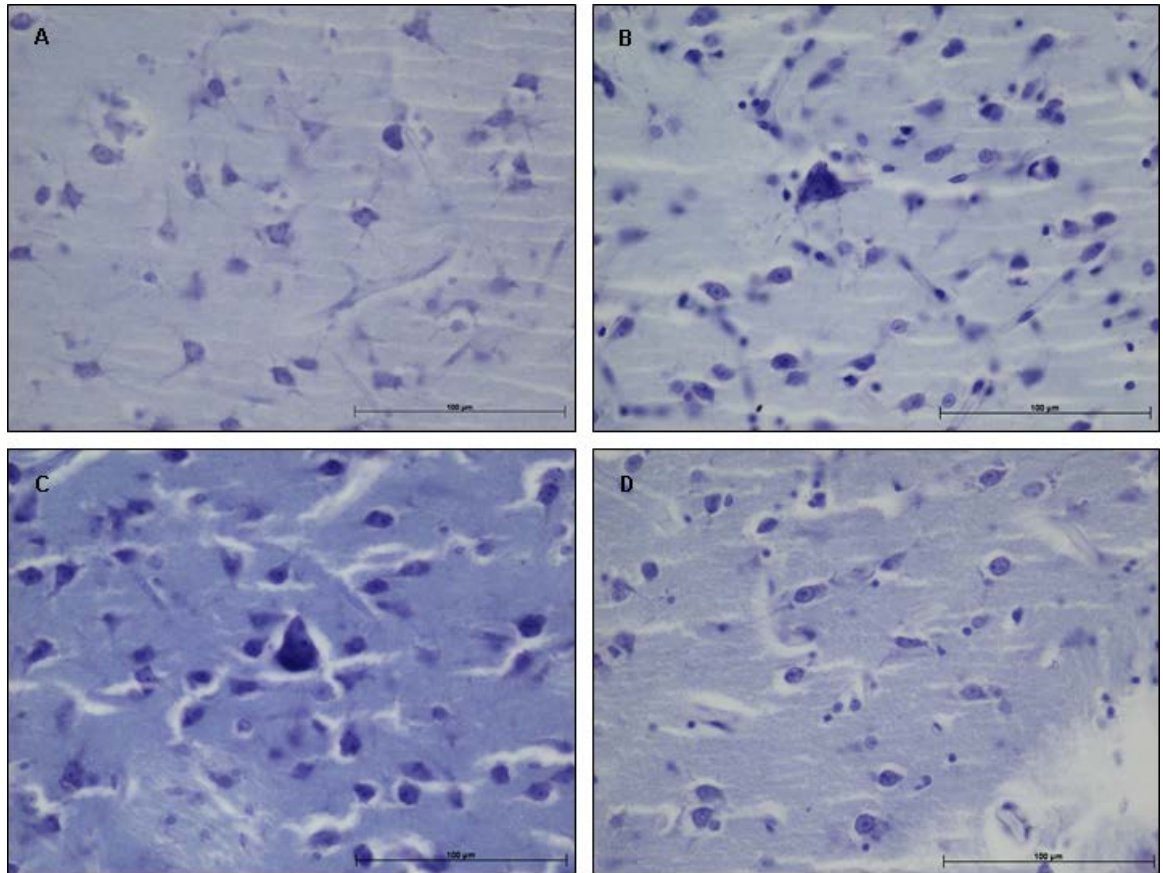


Figure 3.13. Neuron loss in the putamen of the basal ganglia.

A=Control 6, B=Patient 1 *POLG* mutation-positive group, C=Patient 2 *POLG* mutation-positive group, D=Patient 12 *POLG* mutation-absent group. Images B, C and D do not show any neuron loss in layer V. All images are taken of the putamen. All sections stained with CFV stain. Scale bar = 100μm.

<i>POLG</i> Mutation	Patient	Caudate	Putamen	Globus Pallidus
+	1	-	-	-
	2	-	-	-
+ s	5	-	-	-
?	8	N/A	-	-
	9	+	-	++
	10	N/A	-	-
	11	-	-	-
-	12	-	-	-

Table 3.11. Summary of neuron loss in the basal ganglia.

Neuron loss of the basal ganglia is summarised in the above table.

Assessment is semi-quantitative using the scale -/+/++/+++, where – denotes no neuron loss, and +++ denotes severe neuron loss.

Key: N/A=data not available, s=stillbirth

3.4.5 Astrogliosis

Astrocytes are ubiquitous cells of the CNS, providing a supporting role to cells of the blood-brain barrier, to neurons, and they also play a role in the repair of damaged tissue. This gives them a vital role in the functioning of the brain. They appear spider-like with numerous dendrite projections reaching out into the tissue, making contact with other cells. An antibody to the glial fibrillary acidic protein (GFAP) expressed by reactive astrocytes was used to assess astrocyte populations using the -/+/++/+++ scale as described in *Chapter 2 Methods and Materials, 2.2.7 'Semi-quantitative Methods'*.

3.4.5.1 Cerebellum

Astrocytes of the cerebellum are termed Bergmann glia and they are assessed in patients of the *POLG* groups below. Semi-quantitative assessment of a gliosis in the Bergmann glia of the cerebellum is summarised in Table 3.12.

Patients with evidence for *POLG* mutations (Figure 3.14; image B) show no astrogliosis in two patients and a moderate increase (++) in Patient 6. Patient 6 also has a microinfarct in the cerebellum, and much of the astrogliosis is present in the region of the infarct.

Patients with no genetic diagnosis available (Figure 3.14; images C and D) show a variable astrogliosis. Three patients show no astrogliosis, there is a mild increase (+) in one patient around the dentate nucleus only, and a moderate increase (++) in one patient.

The patient without a *POLG* mutation does not show astrogliosis.

The stillbirth, Patient 5, shows a mild astrogliosis (+) in both the grey matter and the white matter.

There is variable gliosis of Bergman glia in patients where a *POLG* mutation is confirmed or unknown. In the patient without a *POLG* mutation there is no gliosis. Astrogliosis does not appear to correlate well with neuronal cell loss.

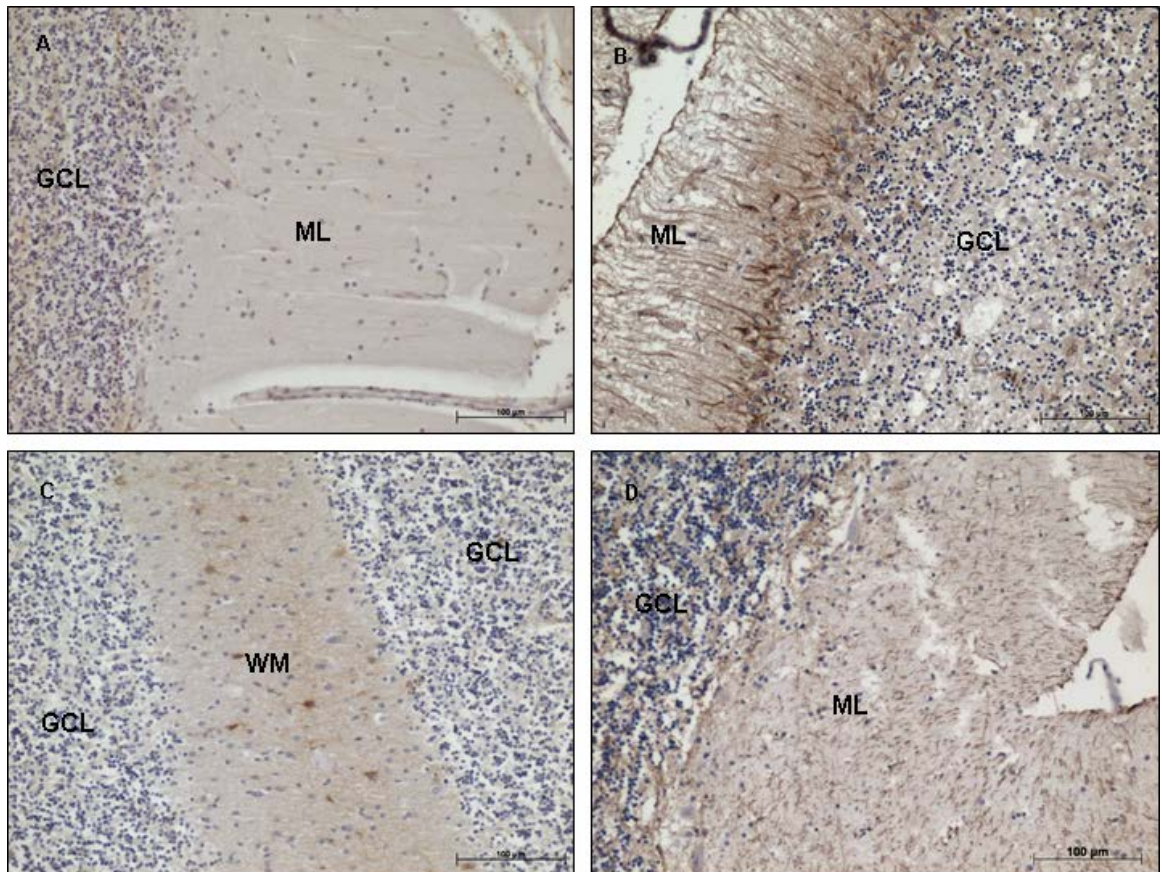


Figure 3.14. Bergmann glia of the cerebellum.

A=Control 6, B=Patient 6 *POLG* mutation-positive group, C=Patient 8 *POLG* mutation-undetermined group, D=Patient 11 *POLG* mutation-undetermined group. Image B shows widespread astroglia at the site of the microinfarct in the patient. The microinfarct is large and the entirety of it is not visible in the image. Image C does not show astroglia in the white matter. Image D shows moderate astroglia. All sections stained with GFAP antibody. Scale bar = 100µm.

Key: ML=molecular layer, GCL=granular cell layer, WM=white matter

The brain area is unavailable for patients not listed in the table.

POLG Mutation	Patient	Grey Matter	White Matter / Dentate Nucleus
+	1	-	-
	2	-	-
	6	++	++
+ s	5	+	+
?	7	-	-
	8	-	+
	9	-	-
	10	-	-
	11	++	++
-	12	-	-

Table 3.12. Summary of Bergmann glia of the cerebellum.

The increase in Bergmann glia in the cerebellum is summarised in the above table. Assessment is semi-quantitative using the scale -/+/++/+++, where – is defined as no change, + mild increase, ++ moderate increase, and +++ severe increase.

Key: s=stillbirth

3.4.5.2 Occipital Lobe

Suitable control tissue was extremely difficult to obtain due to the age of the patients and the availability of different brain regions. Control tissue was unavailable for this brain region.

Semi-quantitative assessment of astrogliosis the occipital lobe (BA19) is summarised in Table 3.13.

The patient with evidence for *POLG* mutations (Figure 3.15; images C and D), Patient 2, shows a severe increase (+++), exhibiting swollen astrocytes.

Patients with no genetic diagnosis available (Figure 3.15; images E and F) show a mild increase (+) for two patients, one showed an increase at the meninges in particular, and a severe increase (+++) for another patient in the grey matter in particular.

The patient without a *POLG* mutation (Figure 3.15; image B) shows severe astrogliosis (+++).

The stillbirth, Patient 5 (Figure 3.15; image A), shows a mild astrogliosis (+) in both the grey matter and the white matter.

There is a severe astrogliosis seen in patients of three of the groups. The stillbirth shows a much milder astrogliosis. Some patients where *POLG* mutation is confirmed or unknown have a milder gliosis. Astrogliosis appears to correlate well with neuronal cell loss, with more severe astrogliosis seen in patients showing greater neuron loss. Despite control tissue being unavailable, there is a clear gradation of astrogliosis and a difference between patients.

1

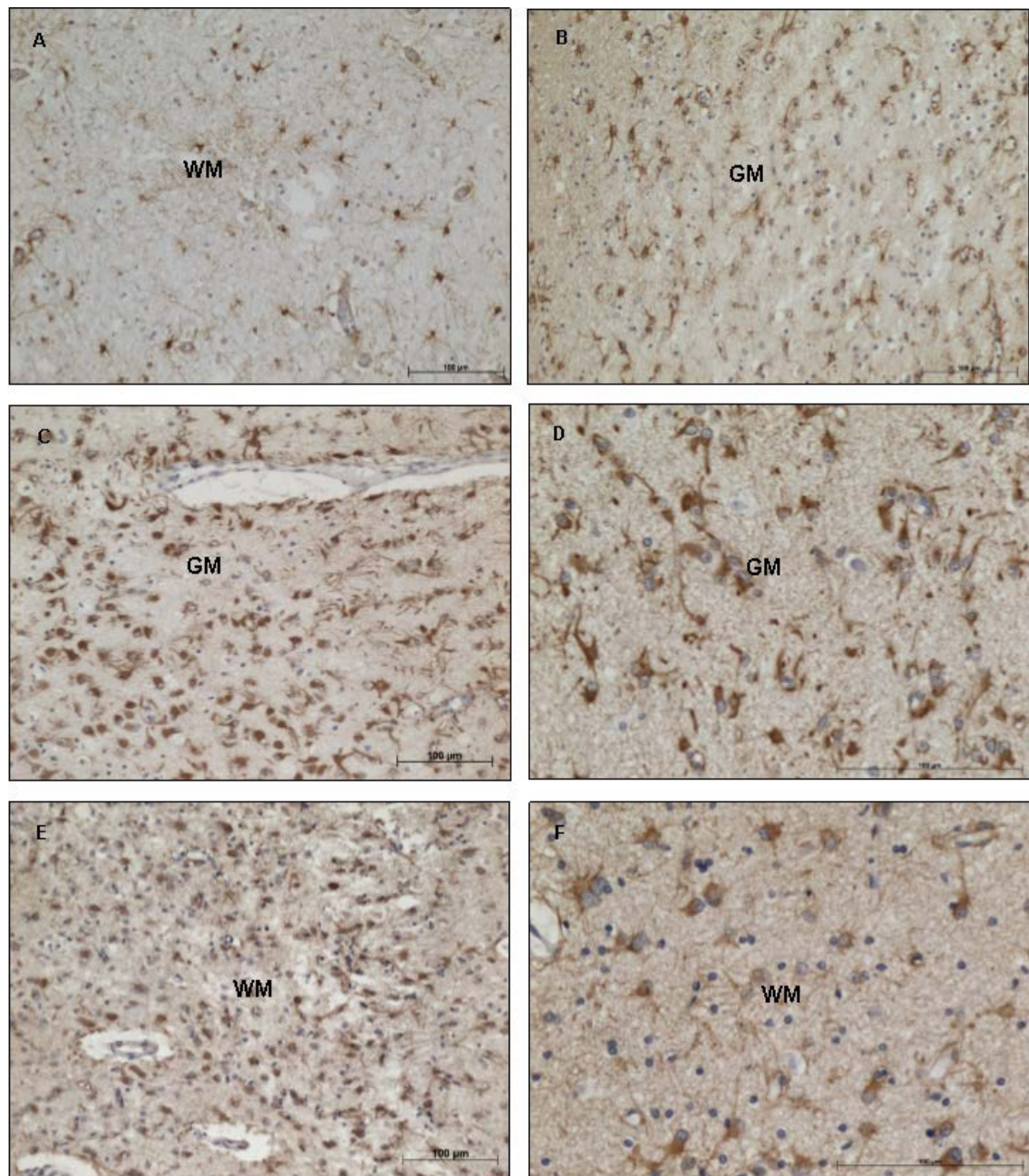


Figure 3.15. Astrogliosis in the occipital lobe.

A=Patient 5 stillbirth, B=Patient 12 *POLG* mutation-absent group, C=Patient 2 *POLG* mutation-positive group, D=Patient 2 *POLG* mutation-positive group, E=Patient 11 *POLG* mutation-undetermined group, F=Patient 11 *POLG* mutation-undetermined group. Image A shows mild astrogliosis. Images B-F show severe astrogliosis, with swollen astrocytes in images C-F. Image D is a higher magnification of image C, and image F is a higher magnification of image E which show severe astrogliosis in the grey and white matter. All sections stained with GFAP antibody. Scale bar = 100µm.

Key: GM=grey matter, WM=white matter

The brain area is unavailable for patients not listed in the table. The antibody stain for GFAP could not be performed for Patient 1 as the stain was very uneven after repeating.

<i>POLG</i> Mutation	Patient	Grey Matter	White Matter
+	2	+++	+++
+ s	5	+	+
?	8	+	+
	10	+	+
	11	+++	++
-	12	+++	++

Table 3.13. Summary of astrogliosis in the occipital lobe.

Astrogliosis in the occipital lobe is summarised in the above table.

Assessment is semi-quantitative using the scale -/+/+/++/+++, where – is defined as no change, + mild increase, ++ moderate increase, and +++ severe increase.

Key: s=stillbirth

3.4.5.3 Parietal Lobe

Suitable control tissue was extremely difficult to obtain due to the age of the patients and the availability of different brain regions. Control tissue was unavailable for this brain region.

Semi-quantitative assessment of astrogliosis the parietal lobe (BA40) is summarised in Table 3.14.

Patients with evidence for *POLG* mutations (Figure 3.16; images A and B) show a severe increase (+++) in the grey matter. In Patient 2 there is a severe increase in the grey matter with many of the astrocytes appearing large and swollen. There are fewer astrocytes present in the white matter which is not mentioned in the original neuropathologist's report. In Patient 6, the astrocytes also appear large and swollen and appear in particularly large numbers in the white matter, which is confirmed in the original neuropathologist's report.

There is a single patient with no genetic diagnosis available (Figure 3.16; images C and D) in this brain region. Patient 8 shows a mild increase (+). Astrocytes are particularly seen in the white matter and in the epithelial lining of the brain.

The patient without a *POLG* mutation (Figure 3.16; images E and F) shows a mild astrogliosis (+), particularly where there is also microvacuolation in the grey matter layers.

There is a severe astrogliosis in patients with a confirmed *POLG* mutation. Patients of the other two groups show a milder gliosis. However, astrogliosis does not appear to correlate well with neuronal cell loss. Despite control tissue being unavailable, there is a clear gradation of astrogliosis and a difference between patients.

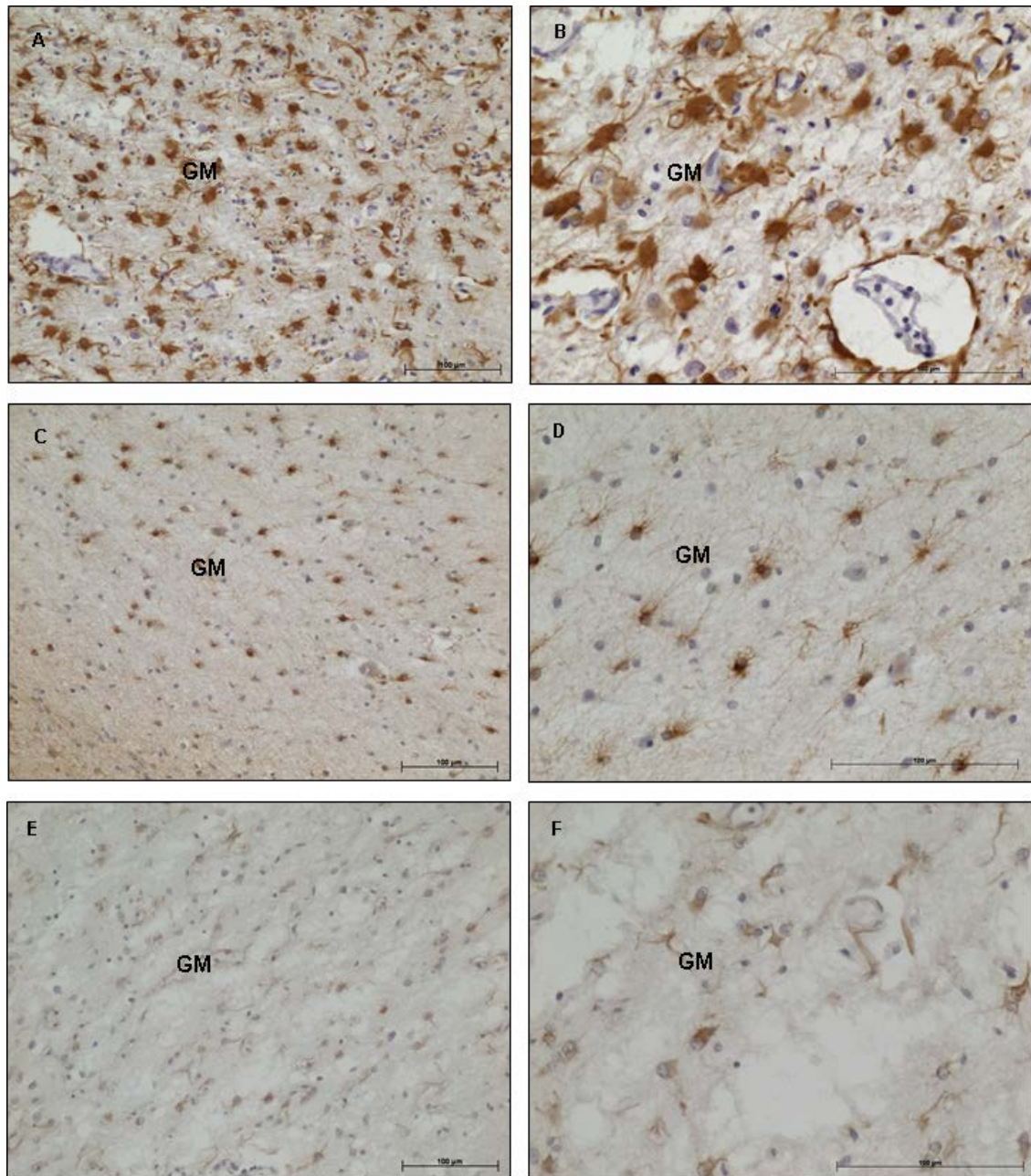


Figure 3.16. Astrogliosis in the parietal lobe.

A=Patient 6 *POLG* mutation-positive group, B=Patient 6 *POLG* mutation-positive group, C=Patient 8 *POLG* mutation-undetermined group, D=Patient 8 *POLG* mutation-undetermined group, E=Patient 12 *POLG* mutation-absent group, F=Patient 12 *POLG* mutation-absent group. Image A and image B, which is at a higher magnification, show extreme astrogliosis. Images C and image D, which is at a higher magnification, show mild astrogliosis with swollen astrocytes. Images E and image F, which is at a higher magnification, show mild astrogliosis. All sections stained with GFAP antibody. Scale bar = 100µm.

Key: GM=grey matter

The brain area is unavailable for patients not listed in the table. The antibody stain for GFAP could not be performed for Patient 1 as the stain was very uneven after repeating.

<i>POLG</i> Mutation	Patient	Grey Matter	White Matter
+	2	+++	-
	6	+++	+++
?	8	+	+
-	12	+	+

Table 3.14. Summary of astrogliosis in the parietal lobe.

Astrogliosis in the parietal lobe is summarised in the above table.

Assessment is semi-quantitative using the scale -/+ /++ /+++ , where – is defined as no change, + mild increase, ++ moderate increase, and +++ severe increase.

3.4.5.4 Basal Ganglia

The availability of each of the caudate, putamen, and globus pallidus for analysis was dependent upon the precise location of the sample that was taken by the original pathology team. In some patients, this led to two of the three areas being available for analysis.

Patients with evidence for *POLG* mutations show very mild levels of astrogliosis. Patient 2 does not exhibit astrogliosis. Patient 1 has a mild increase of astrocytes present in the globus pallidus only, where these astrocytes appear unusually large and swollen.

Patients with no genetic diagnosis available (Figure 3.17; images B, C and D) show no increase for one patient, a mild increase (+) in the caudate and globus pallidus for one patient, and a severe increase (+++) for two patients.

The patient without a *POLG* mutation does not show astrogliosis and nor does the stillbirth, Patient 5.

Patients with a confirmed *POLG* mutation show a very mild astrogliosis while no astrogliosis is present in the patient with no *POLG* mutation. There is severe to moderate astrogliosis in Patient 8 and Patient 11, with a milder astrogliosis in Patient 9. Astrogliosis does appear to correlate well with neuronal cell loss, except in Patient 8 and Patient 10, as no neuron loss was seen in any of the patients. Semi-quantitative assessment of astrogliosis the occipital lobe is summarised in Table 3.15.

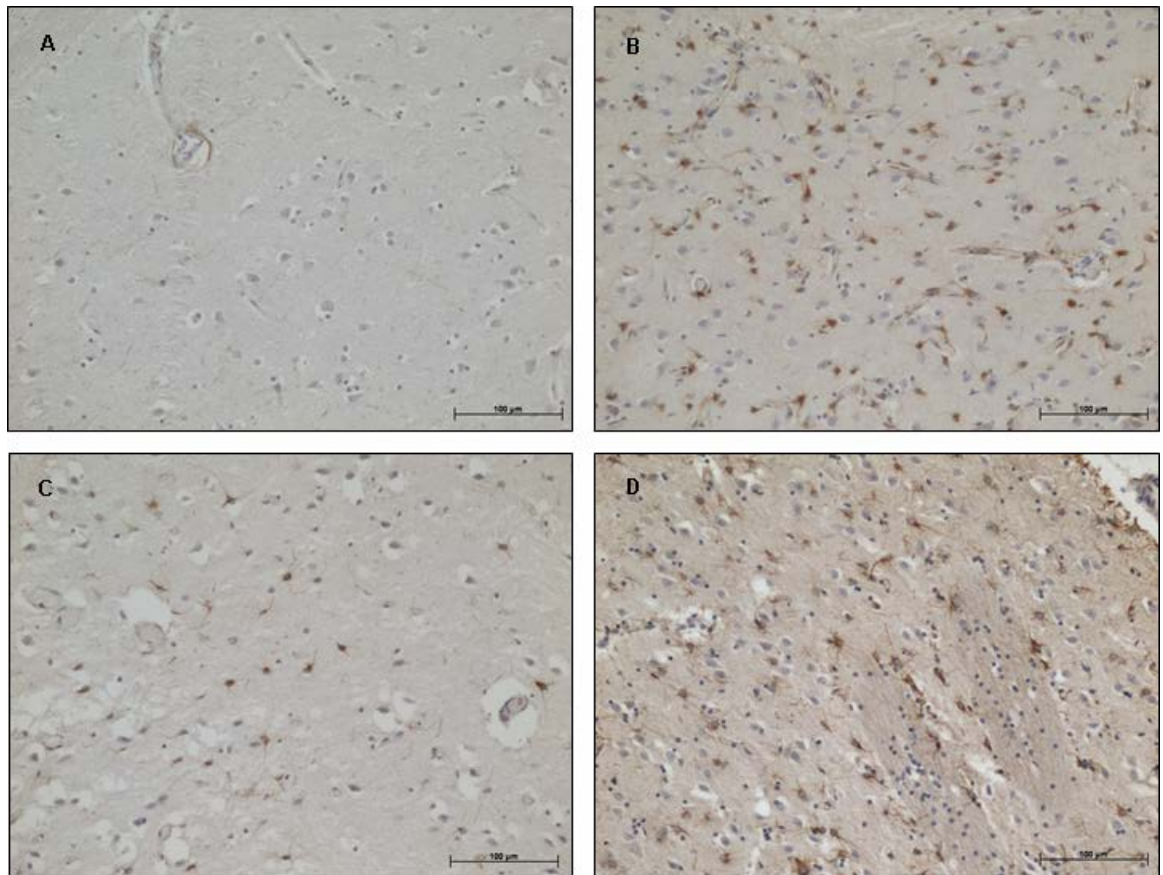


Figure 3.17. Astrogliosis in the basal ganglia.

A=Control 6 putamen, B=Patient 8 putamen *POLG* mutation-undetermined group, C=Patient 9 caudate *POLG* mutation-undetermined group, D=Patient 11 putamen *POLG* mutation-undetermined group. Images B, C and D show widespread astrogliosis. All sections stained with GFAP antibody. Scale bar = 100µm.

The brain area is unavailable for patients not listed in the table.

<i>POLG</i> Mutation	Patient	Caudate	Putamen	Globus Pallidus
+	1	-	-	+
	2	-	-	-
+ s	5	-	-	-
?	8	N/A	+++	++
	9	+	-	+
	10	N/A	-	-
	11	+++	+++	+++
-	12	-	-	-

Table 3.15. Summary of astrogliosis in basal ganglia.

Astrogliosis in the caudate, putamen, and globus pallidus of the basal ganglia is summarised in the above table.

Assessment is semi-quantitative using the scale -/+ /++ /+++ , where – is defined as no change, + mild increase, ++ moderate increase, and +++ severe increase.

Key: N/A=not available, s=stillbirth

3.4.6 Mitochondrial Localisation in Neurons

Mitochondria are found throughout the neuron and may move in a bidirectional manner along the axon towards the synaptic terminal or the cell body (soma), a process that occurs through mitochondrial axonal transport. A high mitochondrial density is required for oxidative phosphorylation that is able to respond to the physiological stresses of the cell. Mitochondrial density and localisation was visualised using an antibody to porin, a class of voltage-dependent anion channel (VDAC) on the outer membrane of mitochondria, involved in the passive diffusion of calcium and ions. Abnormal localisation was categorised as a darker ring of antibody around the periphery of the nucleus (perinuclear) or the periphery of the soma, or weak staining of porin at the periphery of the soma. The results are summarised in Table 3.16 and Table 3.17.

Patients with evidence for *POLG* mutations (Figure 3.18; images B, F and H) show variable mitochondrial density over all brain areas. In the cerebellum, patients show mainly a high density of mitochondria in both the Purkinje cells and neurons of the dentate nucleus. There is no abnormal localisation of mitochondria in the dentate nucleus but both Patient 1 and Patient 2 show perinuclear localisation in Purkinje cells, while Patient 2 and Patient 6 show areas of low mitochondrial density at one edge of the soma periphery. In the occipital lobe, Patient 1 shows some neurons with a low mitochondrial density, and Patient 2 shows a high mitochondrial density. There is no abnormal localisation of mitochondria. Patients 1, 2, and 6 all show a low mitochondrial density in the parietal lobe, but with no abnormal localisation of mitochondria. In the basal ganglia, the globus pallidus shows low mitochondrial density but with no abnormal localisation of mitochondria.

Patients without a genetic diagnosis (Figure 3.18; images C, D and J) show variable mitochondrial density over all brain areas. In the cerebellum, patients show a low density of mitochondria in neurons of the dentate nucleus, accompanied by perinuclear localisation. In Purkinje cells, Patient 7, Patient 9 and Patient 10 show a low mitochondrial density. In Patient 10, all of the Purkinje cells have low mitochondrial density. Patients 8-11 exhibit perinuclear localisation, with localisation around the periphery of the soma in Patient 8. In Patient 11, this abnormal perinuclear localisation was seen in only a single Purkinje cell. In the occipital lobe, there is a high density of mitochondria in all patients with no abnormal localisation of mitochondria. In the parietal lobe, only Patient 8 is available and shows a high density of mitochondria with no abnormal localisation. In the basal ganglia, Patient 9 and Patient 11 show evidence

of neurons with a low mitochondrial density. Patients 8, 10, and 11 show perinuclear localisation of mitochondria, predominantly in neurons of the globus pallidus.

The patient without a *POLG* mutation shows a high mitochondrial density in most brain areas. In the cerebellum, neurons of the dentate nucleus show a high density of mitochondria with no abnormal localisation of mitochondria. The Purkinje cells show a low density of mitochondria, accompanied by perinuclear localisation. In the occipital lobe, parietal lobe, and basal ganglia there is a high mitochondrial density in neurons with no abnormal localisation of mitochondria.

The stillbirth, Patient 5 shows a high density of mitochondria in neurons of the cerebellum and basal ganglia, with no abnormal localisation of mitochondria. The neurons of the occipital lobe and parietal lobe are too small and contain little cytoplasm to assess accurately.

Some of the control tissues also demonstrated a ring of high density staining with porin around the periphery of the nucleus in some neurons. The staining around the periphery of the nucleus was not as intense as that seen in neurons of the patients. This was most noticeable in larger neurons, such as Purkinje cells of the cerebellum. Depolarised mitochondria are returned from the synapse to the cell soma to be degraded and recycled. Clustering of mitochondria around the periphery of the nucleus can occur as part of the normal recycling of mitochondria. Clustering of mitochondria may happen in all neurons but it may be happening at a greater rate or in greater numbers in patient neurons. This is mentioned further in the discussion at the end of this chapter.

A low density of mitochondria in neurons may result in less efficient oxidative phosphorylation and deficiencies of electron transport chain complexes. Where this is accompanied by abnormal mitochondrial localisation, this may indicate physiological stress to the cell. Mitochondria are known to be transported from the synapse to the soma, retrograde transport, in order to be degraded and recycled. Depolarised mitochondria may cluster around the nucleus prior to degradation.

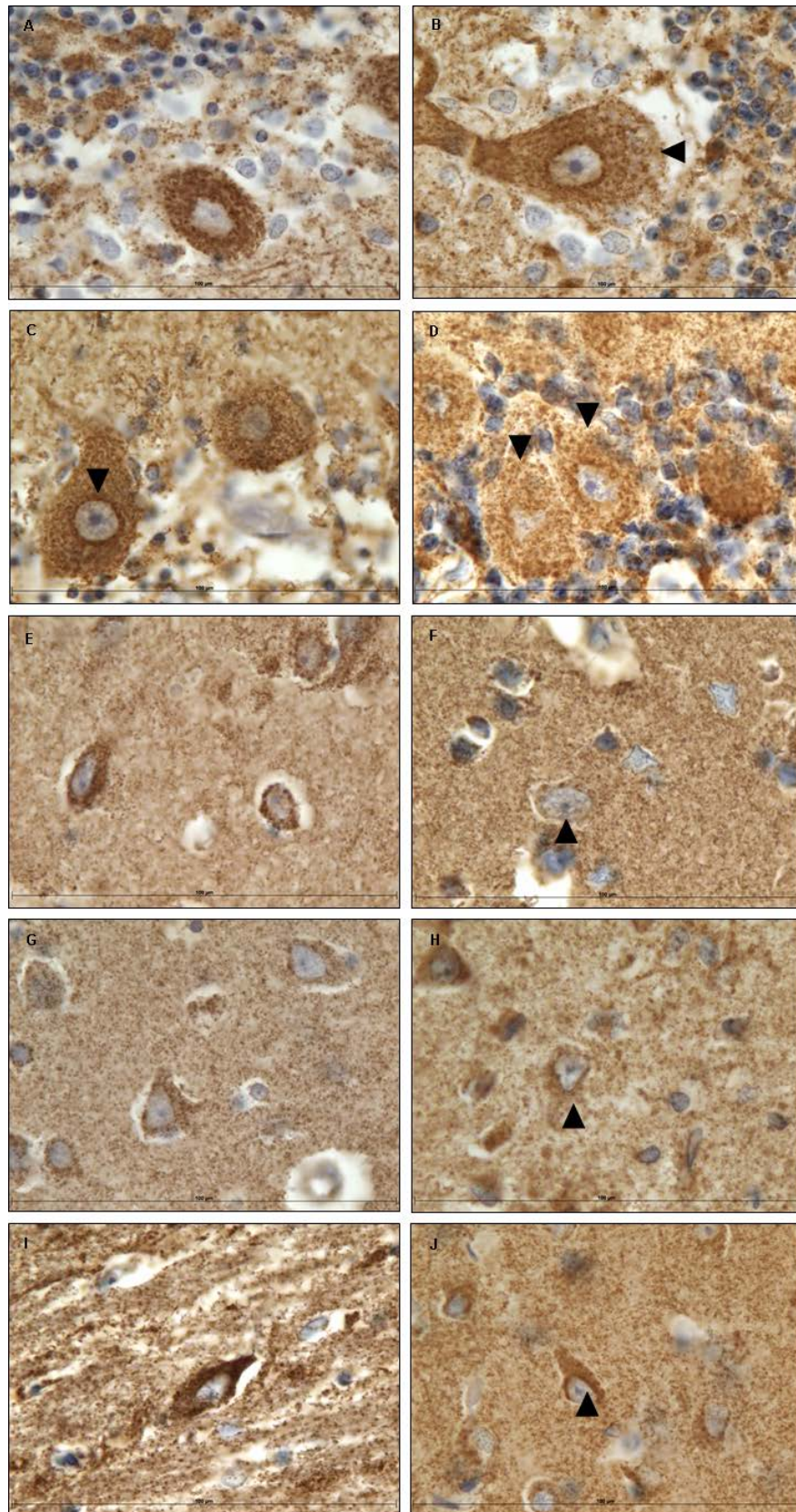


Figure 3.18. Mitochondrial localisation.

A=Control 1 cerebellum, B=Patient 2 *POLG* mutation-positive group cerebellum, C=Patient 9 *POLG* mutation-undetermined group cerebellum, D=Patient 10 *POLG* mutation-undetermined group cerebellum, E=Control 7 occipital lobe, F=Patient 1

POLG mutation-positive group occipital lobe, G=Control 7 parietal lobe, H=Patient 2 *POLG* mutation-positive group parietal lobe. I=Control 6 globus pallidus of the basal ganglia, J=Patient 10 *POLG* mutation-undetermined group globus pallidus of the basal ganglia. Image B shows low mitochondrial density at one edge of the soma periphery. Images C and J show perinuclear localisation of mitochondria. Images D, F, and H show low mitochondrial density. All sections stained with antibody to porin. Scale bar = 100µm.

		Cerebellum			
		Purkinje Cells		Dentate Nucleus	
<i>POLG</i> Mutation		Density	Abnormal Localisation	Density	Abnormal Localisation
	Control 1	High	Perinuclear circles	High	No
+	Patient 1	High	Perinuclear circles	High	No
	Patient 2	High	Perinuclear circles and localisation away from the soma periphery	High	No
	Patient 6	Some low	Localisation away from the soma periphery	N/A	N/A
+ s	Patient 5	High	No	High	No
?	Patient 7	Some low	No	Some low	Perinuclear circles
	Patient 8	High	Perinuclear circles and around soma periphery	Some low	Perinuclear circles
	Patient 9	Some low	Perinuclear circles	Some low	Perinuclear circles
	Patient 10	All low	Perinuclear circles	Some low	Perinuclear circles
	Patient 11	High	Perinuclear circles in a single neuron	Too few neurons to assess	
-	Patient 12	Some low	Perinuclear circles	High	No

Table 3.16. Summary of mitochondrial density and localisation in the cerebellum.

Mitochondrial density and localisation in Purkinje cells and neurons of the dentate nucleus in the cerebellum is summarised in the above table.

Key: N/A=data not available, s=stillbirth

<i>POLG</i> Mutation		Occipital Lobe (BA19)		Parietal Lobe (BA40)		Basal Ganglia	
		Density	Abnormal Localisation	Density	Abnormal Localisation	Density	Abnormal Localisation
	Control 6	N/A	N/A	N/A	N/A	High	Perinuclear circles
	Control 7	High	No	High	No	N/A	N/A
+	Patient 1	Some low	No	Some low	No	C-High P-High GP-Some low	No
	Patient 2	High	No	Some low	No	C-High P-High GP-Some low	No
	Patient 6	N/A	N/A	Some low	No	N/A	N/A
+ s	Patient 5	Neurons too small to assess accurately				C-High P-High GP-High	No
?	Patient 8	High	No	High	No	P-High GP-High	GP-Perinuclear circles
	Patient 9	N/A	N/A	N/A	N/A	C-High P-Some low GP-Some low	No
	Patient 10	High	No	N/A	N/A	P-High GP-High	Perinuclear circles
	Patient 11	High	No	N/A	N/A	C-Some low P-Some low GP-Some low	GP-Perinuclear circles
-	Patient 12	High	No	High	No	C-High P-High GP-High	No

Table 3.17. Summary of mitochondrial density and localisation in the occipital lobe, parietal lobe, and basal ganglia.

Mitochondrial density and localisation in neurons of the occipital lobe, parietal lobe, and basal ganglia is summarised in the above table.

Key: N/A=data not available, s=stillbirth, C=caudate, P=putamen, GP=globus pallidus

3.4.7 White Matter Abnormalities

A Loyez silver stain was used to assess myelin density in the white matter using the 0/1/2/3 scale as described in *Chapter 2 Methods and Materials, 2.2.7 'Semi-quantitative Methods'*.

Assessing myelin density also aided investigations into axonal abnormalities, when investigating whether there was primary or secondary myelin loss. A Bielschowsky silver stain was used to assess axonal abnormalities yet this stain was difficult to perform and analyse. Tissue was assessed in representative patients from two of the groups. Myelin loss is summarised in Table 3.18 and Table 3.19.

Patient 5 was excluded from assessment of white matter abnormalities, including loss of myelin, as myelin is not fully formed in patients as young as Patient 5 and its matched fetal control. The availability of each of the caudate, putamen, and globus pallidus for analysis was dependent upon the precise location of the sample that was taken by the original pathology team. In some patients, this led to two of the three areas being available for analysis.

Patients with evidence for *POLG* mutations show variable myelin loss in all brain areas. In the cerebellum (Figure 3.19; image B), Patient 1 shows moderate areas of myelin loss (++) and Patient 2 shows very mild (+) myelin loss. Patient 6 shows myelin loss only at the area of the microinfarct. In the occipital lobe (Figure 3.19; images C and D), there is mild (+) loss in Patient 1 and moderate (++) loss in Patient 2. In the parietal lobe (Figure 3.19; image E), there is no evidence of myelin loss. In the basal ganglia (Figure 3.19; image H), Patient 1 shows no evidence of myelin loss while Patient 2 shows severe loss (+++) of myelin in this area. A Bielschowsky stain shows some axonal loss, though myelin loss appears to be greater suggesting a primary loss of myelin in this group.

No data were available for patients without a genetic diagnosis.

The patient without a *POLG* mutation shows myelin loss in all brain areas. In the cerebellum, there is moderate (++) myelin loss that appears to be greater on one side of the dentate nucleus. In the occipital lobe, there is mild (+) myelin loss. In the parietal lobe (Figure 3.19; image F), there is pale staining of the myelin and a mild (+) loss of myelin. The Bielschowsky stain in the cerebellum, occipital lobe, and parietal lobe shows a loss of axons, indicating that the myelin loss is secondary to the axonal loss. In the basal ganglia, there is moderate (++) myelin loss throughout the caudate and

putamen and slight loss in the internal capsule. The Bielschowsky stain shows no loss of axons, indicating that in this region the myelin loss is primary. The length of tissue fixation for this patient is long-term (~14 years) for the cerebellum, parietal lobe, and basal ganglia, all areas which demonstrate myelin loss. However, the length of tissue fixation in the occipital lobe is short term (~1 month), in this area which demonstrates a marked myelin loss also. This suggests that the length of fixation does not have a great impact upon the efficacy of the Loyez silver stain.

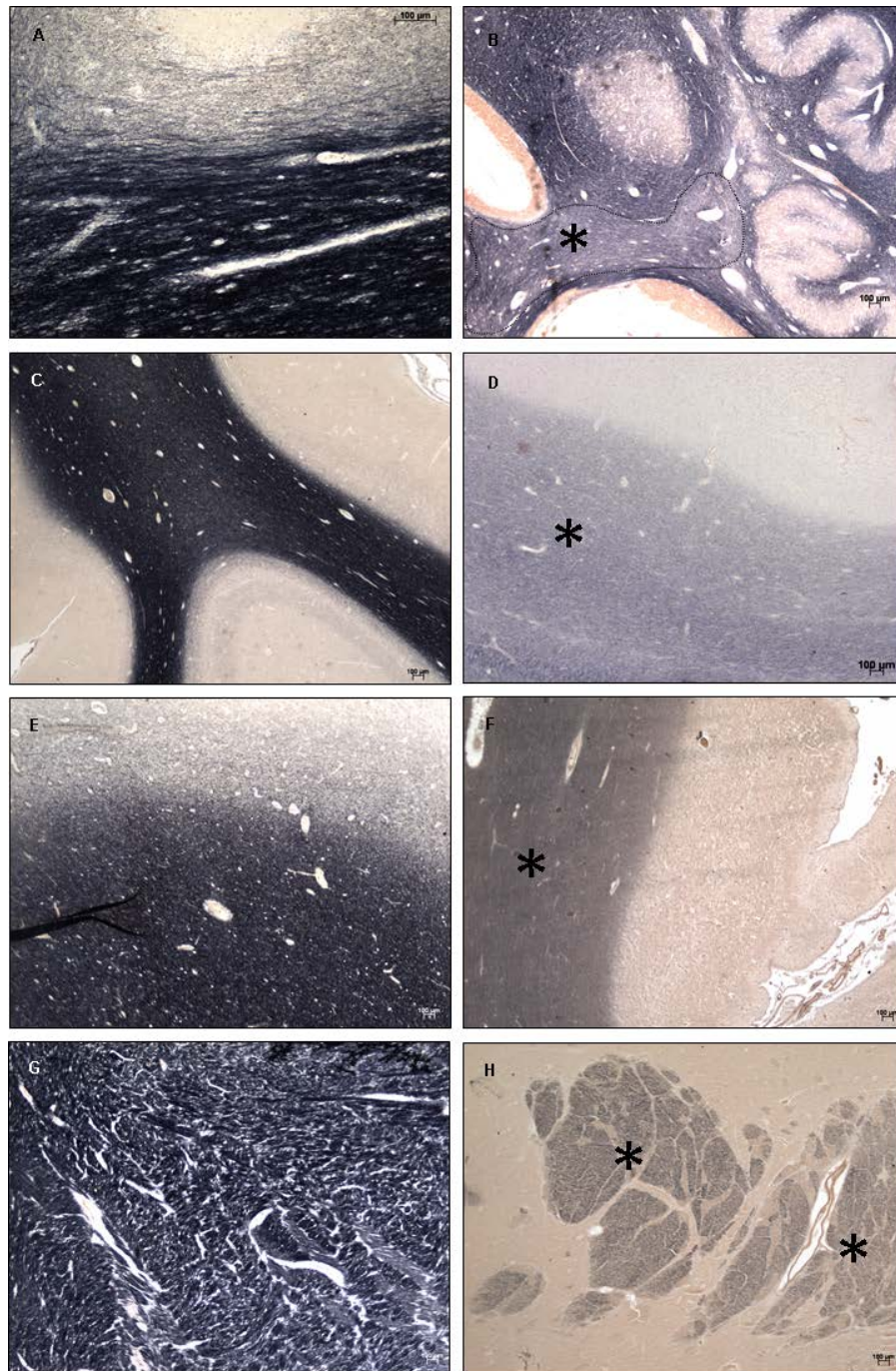


Figure 3.19. Myelin abnormalities.

An asterisk indicates regions of myelin loss. Image B shows a demarcated area of focal myelin loss.

A=Control 6 cerebellum, B=Patient 1 *POLG* mutation-positive group cerebellum, C=Patient 1 *POLG* mutation-positive group occipital lobe, D=Patient 2 *POLG* mutation-positive group occipital lobe, E=Patient 6 *POLG* mutation-positive group parietal lobe, F=Patient 12 *POLG* mutation-absent group parietal lobe, G=Control 6 internal capsule of the basal ganglia, H=Patient 2 *POLG* mutation-positive group internal capsule of the basal ganglia. Images A, C, E and G do not show any myelin loss. Images B, D, F and H show myelin loss in the white matter. All sections stained with Loyal silver stain. Scale bar = 100µm.

POLG Mutation		Staining Quantification						
		Tonsilla	Biventer	Posterior Inferior	Posterior Superior	Posterior Crescentic	Anterior Crescentic	Ala Centralis
	Control 6	N/A	N/A	3, 3, 3	3, 3, 3	3, 3, 3	N/A	N/A
+	Patient 1	1, 1, 3	2, 3, 3	2, 3, 3	3, 3, 3	2, 3, 3	3, 3, 3	3, 3, 2
	Patient 2	3, 3, 3	3, 3, 2	3, 3, 2	3, 3, 2	2, 3, 3	3, 2, 3	3, 3, 3
	Patient 6	3, 3, 3	3, 3, 3	3, 3, 3	3, 3, 3	3, 3, 3	N/A	N/A
-	Patient 12	1, 1, 2	1, 1, 2	1, 2, 2	1, 2, 2	2, 2, 2	1, 2, 2	2, 2, 3

Table 3.18. Myelin quantification in the cerebellum.

Loyez silver staining was performed on tissue from the cerebellum. Three images were taken for each cerebellar region at X10 magnification and assessed for myelin loss. Not all brain areas were available for assessment in each patient.

Myelin Assessment Key: 0=complete myelin loss, 1=marked loss of myelin staining, 2=slight pallor of myelin staining, 3=good myelin staining equivalent to controls.

Key: N/A=not available

POLG Mutation		Staining Quantification						
		Occipital Lobe (BA19)	Parietal Lobe (BA40)	Basal Ganglia				
				Caudate	Internal Capsule	Putamen	Medial Globus Pallidus	Lateral Globus Pallidus
	Control 6	N/A	N/A	3	3	3	3	3
+	Patient 1	2	3	1	3	3	3	2
	Patient 2	1	2	0	1	0	N/A	N/A
	Patient 6	N/A	3	N/A	N/A	N/A	N/A	N/A
-	Patient 12	1	2	0	2	1	N/A	N/A

Table 3.19. Myelin quantification in the occipital lobe, parietal lobe, and basal ganglia.

Loyez silver staining was performed on tissue from the occipital lobe, parietal lobe, and basal ganglia. Images were taken at X10 magnification and assessed for myelin loss.

Myelin Assessment Key: 0=complete myelin loss, 1=marked loss of myelin staining, 2=slight pallor of myelin staining, 3=good myelin staining equivalent to controls.

Key: N/A=not available

3.4.8 Microglial Activation

Microglia are glial cells of the immune system, found throughout the entire brain. Their function is to phagocytise foreign and unwanted material, removing it from the brain and preventing damage. They provide an interesting feature of neuropathology. An antibody to CD68, a highly glycosylated lysosomal membrane protein found on macrophages and activated microglia was used to assess CD68-positive cell populations in both grey and white matter. This was performed using the -/+/++/+++ scale as described in *Chapter 2 Methods and Materials, 2.2.7 'Semi-quantitative Methods'*. The results are summarised in Table 3.20.

The availability of each of the caudate, putamen, and globus pallidus for analysis was dependent upon the precise location of the sample that was taken by the original pathology team. In some patients, this led to two of the three areas being available for analysis. Some brain areas were unavailable for patients and therefore they were not listed in Table 3.20 or listed specifying 'not available' for the brain area.

Patients with evidence for *POLG* mutations show a widely varied pathology in all brain areas. In the cerebellum, Patient 6 shows a mild increase (+) around the region of the microinfarct. There is a moderate increase (++) for Patient 1 and Patient 2 (Figure 3.20; image B). In the occipital lobe (Figure 3.20; images C and D), there is a mild increase (+) in one patient, and a severe increase (++++) in one patient. In Patient 2 where there is a severe increase, the microglial cells appear swollen in the white matter, possibly due to having phagocytised any excess material. This correlates with a marked loss of myelin in the occipital lobe of Patient 2. In the parietal lobe (Figure 3.20; image F) there is a moderate increase (++) in Patients 1 and 2, and a severe increase (++++) in Patient 6. Where there is a severe increase, there is no evidence of any swollen microglia. In the basal ganglia, there is no increase in Patient 2, and a moderate increase (++) in Patient 1.

Patients with no genetic diagnosis available show a variable pathology. In the cerebellum, there is mild increase (+) in microglia in four patients, and a severe increase (++++) for one patient, especially in the white matter. In the occipital lobe, there is no increase in two patients, and a moderate increase (++) in one patient. In the parietal lobe, there is no increase in microglia. In the basal ganglia (Figure 3.20; image H), there is a mild increase throughout the basal ganglia in Patient 10. In Patient 8 there is a mild increase (+) in the putamen in any areas of microvacuolation or around any vessels, and a mild increase (+) throughout the globus pallidus. Patient 11 shows a

range of pathology in different areas; there is a mild increase (+) in the caudate, a moderate (++) increase in the putamen and globus pallidus, and a severe increase (+++) in the internal capsule (not shown in table). Patient 9 shows a moderate to severe increase (++/+++) throughout the basal ganglia.

The patient without a *POLG* mutation shows no increase in microglia in the cerebellum and basal ganglia. The parietal lobe (Figure 3.20; image E) shows a mild increase (+) throughout the grey and white matter, while the occipital lobe shows a severe increase (+++) in microglia. These are found almost entirely in the white matter, while the grey matter is almost free from microglia.

The stillbirth, Patient 5, shows no increase in microglia in any brain area.

Microglial activation correlates with myelin loss in the occipital lobe, with Patient 2 and Patient 12 showing a marked loss of myelin and a severe increase in microglia. However, this correlation does not hold for other brain areas as Patient 2 and Patient 12 show a marked loss of myelin throughout the basal ganglia, yet there is no increase in microglia.

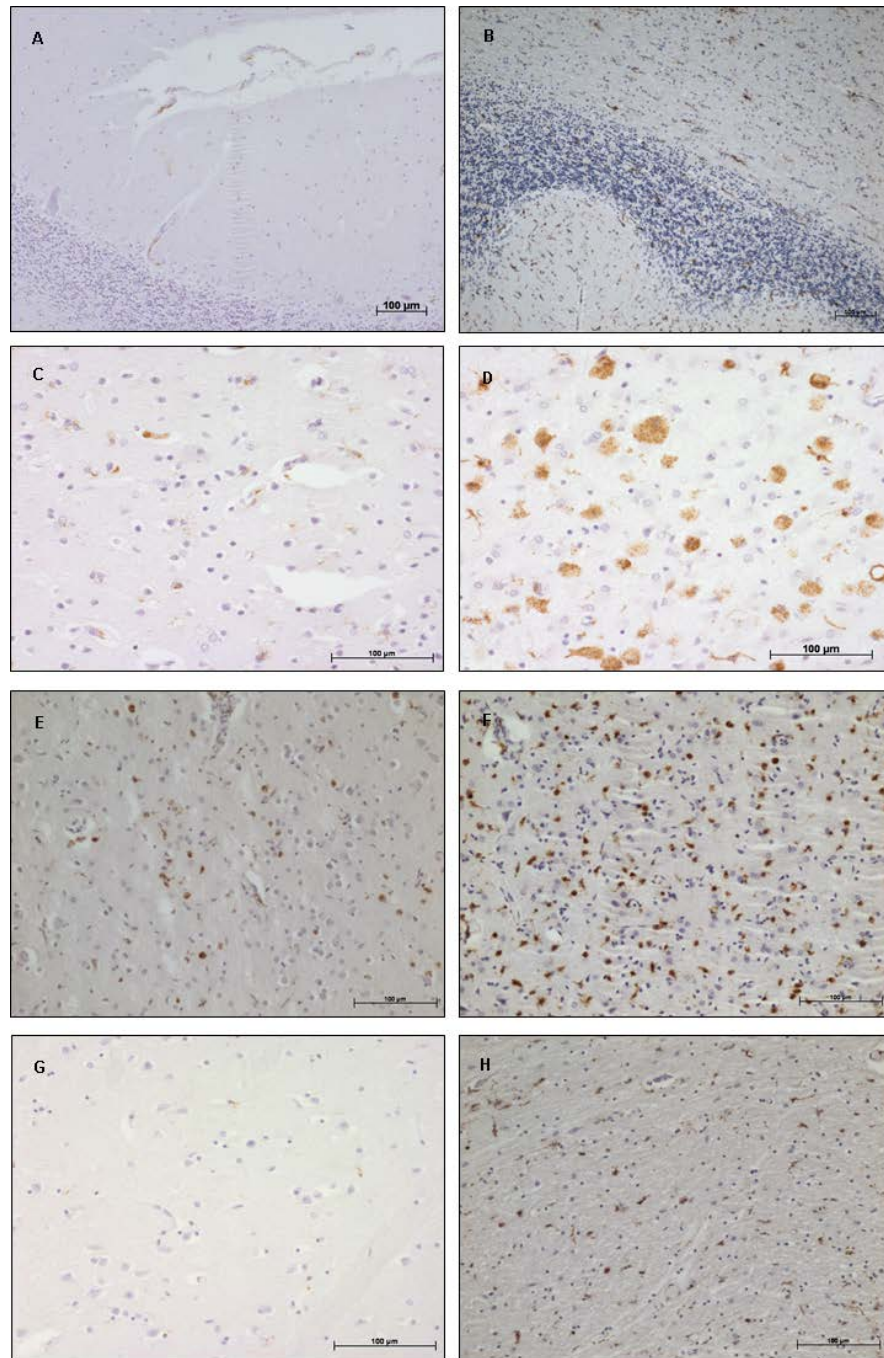


Figure 3.20. Microglial activation.

A=Control 6 cerebellum, B=Patient 2 *POLG* mutation-positive group cerebellum, C=Patient 1 *POLG* mutation-positive group occipital lobe, D=Patient 2 *POLG* mutation-positive group occipital lobe, E=Patient 12 *POLG* mutation-absent group parietal lobe, F=Patient 6 *POLG* mutation-positive group parietal lobe, G=Control 6 putamen of the basal ganglia, H=Patient 9 *POLG* mutation-undetermined group putamen of the basal ganglia. Images A, C, E and G do not show any activation. Images B, D, F and H show moderate to severe activation. Images A and B are taken at a lower magnification to illustrate microglial activation over a wide area. All sections stained with CD68 antibody. Scale bar = 100μm.

<i>POLG</i> Mutation	Patient	Cerebellum		Occipital Lobe (BA19)		Parietal Lobe (BA40)		Basal Ganglia		
		Grey Matter	White Matter	Grey Matter	White Matter	Grey Matter	White Matter	C	P	GP
+	1	++	++	+	+	++	++	++	++	++
	2	++	++	+++	+++	++	++	-	-	-
	6	+	+	N/A	N/A	+++	+++	N/A	N/A	N/A
+ s	5	-	-	-	-	-	-	-	-	-
?	7	+	+	N/A	N/A	N/A	N/A	N/A	N/A	N/A
	8	+	-	-	-	-	-	N/A	+	+
	9	+	-	N/A	N/A	N/A	N/A	+++	+++	+++
	10	+	-	-	-	N/A	N/A	N/A	+	+
	11	+++	++	++	++	N/A	N/A	+	++	++
-	12	-	-	+++	+	+	+	-	-	-

Table 3.20. Summary of microglial activation.

Microglial activation in the cerebellum, occipital lobe, parietal lobe, and basal ganglia is summarised in the above table.

Assessment is semi-quantitative using the scale -/+/+/++/+++, where - is defined as no change, + mild increase, ++ moderate increase, and +++ severe increase.

Key: N/A=data not available, s=stillbirth, C=caudate, P=putamen, GP=globus pallidus

3.5 Electron Microscopy

Transmission electron microscopy (TEM) was performed on patient and control fixed tissues. Disease Control 11, an 8 year old male with an undiagnosed familial neurodegenerative disorder that was suspected to be X-linked, and Control 12, a 51 year old male, were chosen to match the formalin-fixation time of the patient. A disease control was examined to account for the effects of generalised neurodegenerative disorders on the brain so that the cellular and mitochondrial degeneration in Alpers' syndrome specifically could be studied.

The occipital lobe was sampled and processed as this region is known to be one of the more severely affected brain areas in Alpers' syndrome. Systematically sampled random images were taken at low and high magnifications and structures were counted and analysed (Table 3.21).

No intact or identifiable cells are seen at low magnification. Structures identified as nuclei are visible in both patients and controls (Figure 3.21). Mitochondria are identified at higher magnification (Figure 3.22). These mitochondria have intact outer membranes and cristae are visible in many of the mitochondria for Disease Control 11 and Control 12. Patient 12 has a substantially sparser cytoplasm and fewer cellular organelles (Figure 3.21; image A) when compared to Disease Control 11 and Control 12 (Figure 3.21; images B and C respectively) and this is confirmed by diminished counts of visible and intact mitochondria and axonal structures.

Electron-dense inclusions were noted within mitochondria. These are visible in the patient and both controls (Figure 3.23). The number of electron-dense inclusions was counted and the majority of mitochondria contained either one or two inclusions. Both Disease Control 11 and Control 12 showed greater numbers of mitochondria with these inclusions present. However, it is important to note the highly degraded state of the tissue sample of Patient 12 and the low total counts of mitochondria recorded.

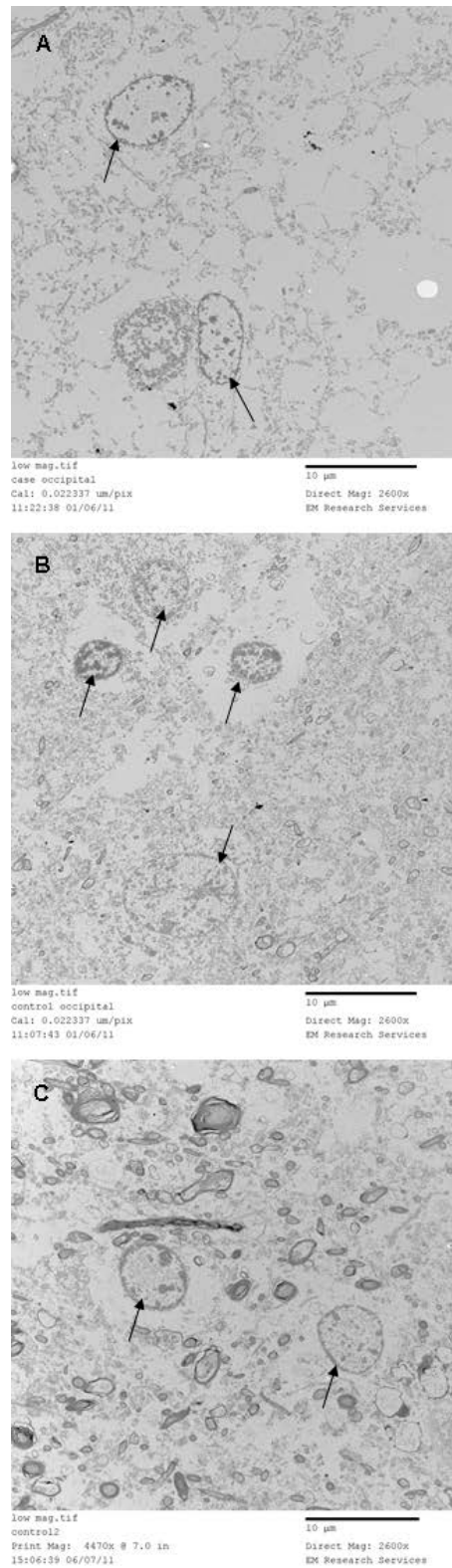


Figure 3.21. TEM images of formalin-fixed tissue taken at 2600X.

Tissue is from the occipital lobe. Image A=Patient 12 *POLG* mutation-absent group, B=Disease Control 11, C=Control 12. Image A shows a substantially sparser cytoplasm and fewer internal organelles than images B and C. Arrows indicate nuclei within the cytoplasm.

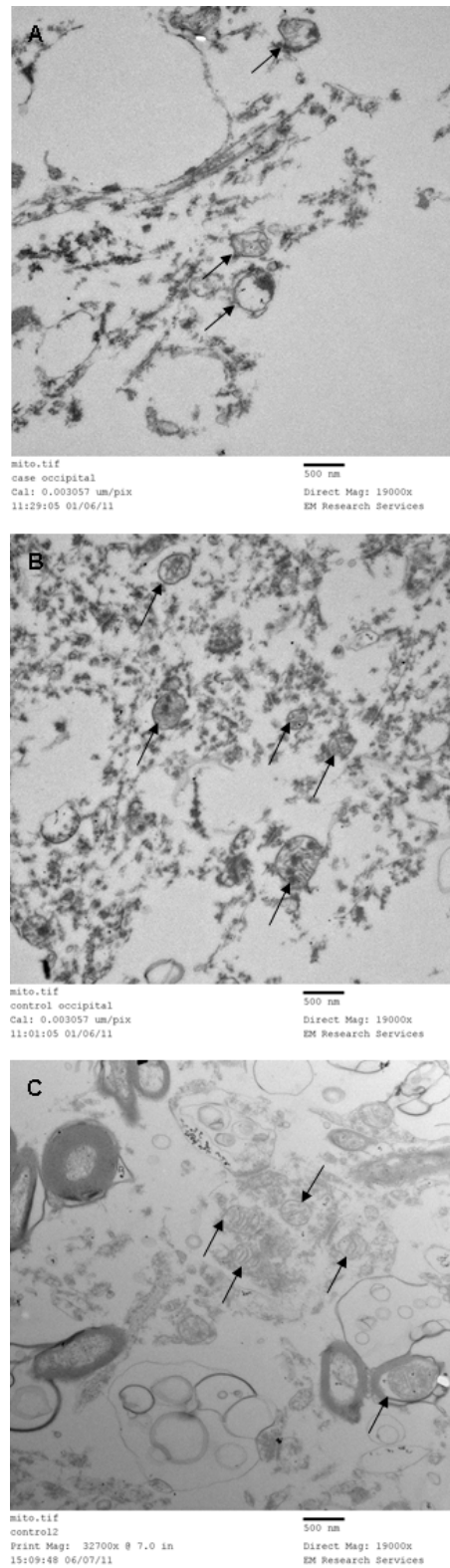


Figure 3.22. TEM images of formalin-fixed tissue taken at 19,000X.

Tissue is from the occipital lobe. A=Patient 12 *POLG* mutation-absent group, B=Disease Control 11, C=Control 12. Image A shows a substantially sparser cytoplasm and mitochondria with fewer internal cristae than images B and C. Arrows indicate mitochondria within the cytoplasm.

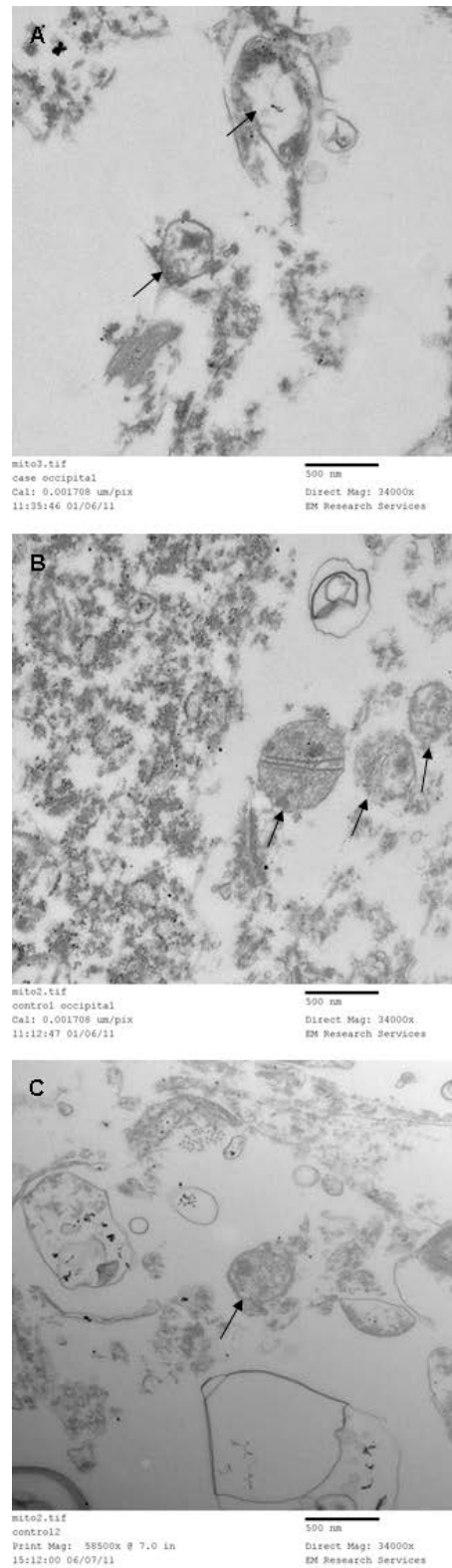


Figure 3.23. TEM images of formalin-fixed tissue taken at 34,000X.

Tissue is from the occipital lobe. A=Patient 12 *POLG* mutation-absent group, B=Disease Control 11, C=Control 12. Image A, B and C show electron-dense inclusions inside the mitochondria. Arrows indicate mitochondria containing electron-dense inclusions.

	Low Magnification (2600X)		High Magnification (19,000X)					
	Nuclei	Axons	Mitochondria	Mitochondria containing electron-dense inclusions	One electron-dense inclusion	Two electron-dense inclusions	Three electron-dense inclusions	Four electron-dense inclusions
Patient 12	38	146	56	23	16	6	1	0
Disease Control 11	25	1371	131	65	48	12	4	1
Control 12	22	3194	81	38	25	9	3	1

Table 3.21. Summary of EM structure counts in patient and controls.

Structures at low and high magnification were counted. Total values are given in the table for 20 images taken at each magnification for each patient and control. Cellular nuclei and axons were counted at a low magnification (2600X). The total number of mitochondria, the number of those mitochondria with electron-dense inclusions, and the number of mitochondria with one or more electron-dense inclusions were counted at a high magnification (19,000X). Cellular nuclei and mitochondria with a complete and intact membrane were counted. At least 50% of the structure must be within the image to be counted, in order to be certain of its identification.

3.6 Discussion

The clinical diagnosis of Alpers' syndrome is based upon the key triad of refractory seizures, psychomotor regression and cortical blindness, with posterior regions of the brain often reported to be affected (Uusimaa et al., 2008; Khan et al., 2012). This chapter has examined, in detail, the neuropathology present in a cohort of patients clinically diagnosed with Alpers' syndrome. The neuropathology is examined within each group and between each group to explore and contrast the prominent neuropathological features.

3.6.1 Patient Variability

I examined each patient individually from the *POLG* mutation-positive group and the *POLG* mutation-absent group because these groups are both clinically and genetically well-defined. I also investigated Patient 5, the stillbirth. Patients 3 and 4 are not included in this discussion as only frozen tissue was available and therefore the neuropathology and any respiratory chain abnormalities could not be fully investigated in the same manner as the rest of the cohort.

3.6.1.1 Patient 1

Patient 1, a 14 month old female compound heterozygous for the p.Ala467Thr and p.Gly48Ser mutations, clinically presented with ataxia, developmental regression, epilepsy, and liver failure. No visual problems were reported. Previous biochemical investigations showed complex I and COX deficiency in skeletal muscle. This patient did not show any Purkinje cell loss in the cerebellum which is confirmed in the original neuropathologist's report, where Purkinje cell loss was noted in the cerebellar vermis. Mild neuron loss was seen in the dentate nucleus and there was neuron loss in the upper cortical layers of the occipital lobe and parietal lobe. No neuron loss was seen in the caudate, putamen or globus pallidus of the basal ganglia. It is unusual that more neuron loss was not seen considering the aetiology of Alpers' syndrome and the clinical signs seen in the patient.

In addition, the cerebellum showed abnormal mitochondrial localisation in neurons, moderate microglial activation and some myelin loss. A Bielschowsky stain showed mild axonal loss though myelin loss is considered primary. This is surprising as there is no Purkinje cell loss in the cerebellum, suggesting all the axons should be intact. This suggests there may be some axonal damage not due to neuronal loss. However, the Bielschowsky silver stain is difficult to perform and analyse and therefore the results

are taken as a guide. The occipital lobe and parietal lobe showed little pathology with low mitochondrial density in neurons and neuron loss was concentrated in the upper cortical layers I-III. In the occipital lobe, there was mild myelin loss with some axonal loss, mild microglial activation, and mild capillary proliferation suggesting a milder pathology than expected. The basal ganglia showed little pathology with a moderate microglial activation and low mitochondrial density in neurons of the globus pallidus.

The investigations suggest that the neuropathological changes represent an early stage in the degenerative process, agreeing with the original neuropathologist's report. The neuropathology seen during these investigations suggest that other factors may have led to the neuronal dysfunction and the possibility of damage to other brain areas may have led to the clinical signs in this patient. Patient 2 is of a similar age and clinical course and exhibits substantially greater pathology than Patient 1, suggesting there is a patient-to-patient variability in the neuropathology that gives rise to the clinical symptoms.

3.6.1.2 Patient 2

Patient 2, a 27 month old male compound heterozygous for the p.Ala467Thr and p.Thr914Pro mutations, exhibited ataxia, visual problems that included hemianopia, epilepsy, and liver failure. Previous biochemical investigations showed COX deficiency in skeletal muscle. The patient showed severe Purkinje cell loss in the cerebellum with mild loss in the dentate nucleus. There was severe neuron loss in the upper cortical layers of the occipital lobe and parietal lobe. No neuron loss was seen in the caudate, putamen or globus pallidus of the basal ganglia.

In the cerebellum, pronounced dendrites ran through the molecular layer. There was abnormal mitochondrial localisation in neurons, moderate microglial activation and some myelin loss. A Bielschowsky stain was inconclusive to detect axonal loss. The occipital lobe showed severe astrogliosis and severe microglial activation, a strong immune reaction, with severe myelin loss. In the parietal lobe, there was low mitochondrial density in neurons, mild capillary proliferation, mild myelin loss and moderate microglial activation with a severe astrogliosis in the grey matter only. No astrogliosis was present in the white matter of the parietal lobe. The basal ganglia showed no pathology but an almost complete loss of myelin. The globus pallidus showed low mitochondrial density in neurons.

There is striking pathology in Patient 2; severe neuron loss with low mitochondrial density and abnormal mitochondrial localisation in surviving neurons. There is marked myelin loss and a severe astrogliosis. This is confirmed in the original neuropathologist's report, noting severe pathology of the cerebellum and occipital lobe. This correlates with the clinical symptoms of ataxia, visual abnormalities, and epilepsy.

3.6.1.3 Patient 6

Patient 6, an 18 year old female with a sibling compound heterozygous for the p.Trp748Ser and p.Arg1096Cys mutations, exhibited ataxia, visual problems, epilepsy, and liver failure. The patient showed moderate Purkinje cell loss in the cerebellum, the dentate nucleus was unavailable. The parietal lobe was not assessed for neuron loss as Patient 6 was not one of the representative patients were taken from the *POLG* mutation-positive group. The occipital lobe and basal ganglia were unavailable regions for this patient.

In the cerebellum, there was a microinfarct in the posterior-inferior region measuring 15,935.2 μm^2 . There was low mitochondrial density in neurons with abnormal mitochondrial localisation, a moderate astrogliosis, and mild microglial activation but no myelin loss. The original neuropathologist's report notes vacuolation in the cerebellar white matter, which was not seen in the slides. The parietal lobe showed low mitochondrial density in neurons, mild microvacuolation and mild capillary proliferation, with severe astrogliosis and severe microglial activation, a strong immune reaction. There was no myelin loss. This parietal lobe pathology is reflected in the original neuropathologist's report.

Patient 6 shows significant neuron loss in the cerebellum but no myelin loss in any brain area. There is a single microinfarct in the cerebellum, contributing to the astrogliosis and microglial activation seen in this area. This older teenage patient had severe refractory epilepsy throughout the two years of disease progression, reflected by the severity of the neuron loss and the microinfarct.

3.6.1.4 Stillbirth Patient 5

Patient 5, a stillborn male with a sibling heterozygous for the p.Ala467Thr and p.Glu1143Gly mutations, had decreased fetal movements and died intrauterine. After sequencing *POLG*, the sibling was also found to be heterozygous for the p.Asp1219Glu mutation, a mutation with an unknown pathogenicity. It is still possible that Patient 5 carries two recessive *POLG* mutations, which full sequencing of the

parental *POLG* genes may reveal. This patient was included in the cohort based upon the *POLG* disorder and genotype of the sibling, who was not diagnosed with Alpers' syndrome. The patient showed no Purkinje cell or dentate nucleus neuronal loss in the cerebellum with a high mitochondrial density. The neurons of the occipital lobe and parietal lobe were too small to be reliably quantified. No neuron loss was seen in the caudate, putamen or globus pallidus of the basal ganglia.

Due to the age of the patient, it was not possible to compare some aspects of neuropathology with other patients. The average number of Purkinje cells per mm was much higher in Patient 5 when compared to the other patients and controls. Also, the myelin sheath had not fully formed in the brain areas studied and could not be analysed. These were both noted in the fetal control and are not signs of pathology. Severe capillary proliferation was noted throughout the brain of the patient, which was not seen in the control. In addition, the cerebellum and occipital lobe both had a mild astrogliosis. The severe proliferation of capillaries could suggest a pathological reaction to stresses on the central nervous system as it was not demonstrated in the age-matched control.

3.6.1.5 Patient 12

Patient 12, a 6 year old male with no pathogenic mutation in *POLG*, exhibited ataxia, visual problems that included hemianopia and epilepsy. Previous biochemical investigations showed a normal respiratory chain although complex IV was slightly low in skeletal muscle. The patient showed moderate Purkinje cell loss with low mitochondrial density and abnormal mitochondrial localisation in the remaining neurons. There was neuronal loss from the dentate nucleus though remaining neurons showed a high mitochondrial density. There was moderate neuron loss in layer III of the occipital lobe and layers III and VI of the parietal lobe. No neuron loss was seen in the caudate, putamen or globus pallidus of the basal ganglia.

In the cerebellum, there was a moderate microvacuolation and moderate myelin loss. A Bielschowsky stain showed some axonal loss suggesting the myelin loss is secondary. However, the Bielschowsky silver stain is difficult to perform and analyse and therefore the results are taken as a guide. The occipital lobe showed a mild microvacuolation and capillary proliferation, with severe astrogliosis and severe microglial activation in the grey matter. Milder microglial activation was present in the white matter. In the parietal lobe, there was a moderate microvacuolation, mild microglial activation and

mild astrogliosis with a mild loss of myelin. The basal ganglia showed mild microvacuolation and an almost complete loss of myelin in the caudate and putamen.

As reported in the patients above, there is severe pathology in Patient 12. In addition to neuron loss, there is a more severe myelin loss shown over all four brain areas studied. The lack of a pathological mutation in *POLG* suggests a different course of disease progression to the patients in this cohort with a mutation in *POLG*.

3.6.2 *Within-group Variation*

Much variation has been demonstrated within the groups designated *POLG* mutation-positive group and *POLG* mutation-undetermined group. The *POLG* mutation-absent group consisted of a single patient. The stillbirth is not included in this discussion as it is a single patient with relatively little pathology to report.

The *POLG* mutation-positive group showed variation in age at symptom onset, clinical signs and neuropathological changes between patients of this group. All patients included in this group were compound heterozygous for one common mutation and one less common mutation, or had a sibling with pathogenic *POLG* mutations and were therefore assumed to have the same mutations. In this cohort, there was no correlation between the *POLG* mutation and the severity of the neuropathology. There was a correlation between the neuropathological changes and the age of the patient; microinfarcts appeared as the age of the patient increased. Both of the oldest patients in this group, Patient 4 and Patient 6, had microinfarcts present in the cerebellum. The progression of their illness lasted 4 years and 2 years, respectively. No other patients showed microinfarcts in any brain regions.

The *POLG* mutation-undetermined group showed great variation in the neuropathological changes between patients of this group. This can be explained by the unknown range of genotypes and the range of *POLG* and non-*POLG* mutations that may be present in this group. There is limited clinical data from this group, as they came from a different university to Patients 1-6, 12, the University of Vienna. The age at onset is similar between patients with clinical signs becoming apparent at a young age, before the age of 6 months. In all but Patient 11, there was a short clinical course that was less than 9 months. Patient 11 had a clinical course of 6.5 years, the longest of any patient in the cohort. There was a correlation between the neuropathology and the age of the patient; Patient 11, 7 years old, showed severe neuron loss in addition to moderate microvacuolation, astrogliosis and microglial activation in the cerebellum and

occipital lobe. The parietal lobe was not available and the basal ganglia showed no neuron loss.

The within-group variation is evident with a correlation of neuropathological findings with the age of the patient. The older patients of the *POLG* mutation-positive group with a clinical course lasting over one year showed the severe neuropathological feature of microinfarcts. The oldest patient of the *POLG* mutation-undetermined group showed the most severe neuropathological features of the group. There is no clear severity between the age and length of disease progression of the other patients. This suggests there is a natural variation in the clinical and neuropathological phenotypes when the course of disease is short and that the presence of microinfarcts is a clear factor for disease progression.

3.6.3 *Inter-group Variation*

There were clear differences between the *POLG* groups investigated. Each group showed signs of neuron loss, suggesting that neuron loss is a common and unmistakable feature of Alpers' syndrome. The stillbirth, Patient 5, did not show any significant level of neuron loss.

In the *POLG* mutation-positive group, the parietal lobe showed the most severe microglial activation and the occipital lobe showed the most severe astrogliosis compared to the other groups. Microglial activation and astrogliosis are reactions involved in immune response or to protect tissue and they often correlated with each other in a brain region. Low mitochondrial density was noted in the occipital lobe and parietal lobe, where density was high in other groups for these brain regions.

The stillbirth showed a severe capillary proliferation in all brain areas investigated. A mild astrogliosis was seen in the cerebellum and occipital lobe, with no microglial activation seen at all. There was moderate microvacuolation in the parietal lobe. This patient had relatively mild neuropathology, with capillary proliferation being the most severe response.

The *POLG* mutation-undetermined group showed a wide range of severities for each neuropathological feature. This reflects the unknown fixation lengths and unknown genotypes within this group and the possibility of a mixture of *POLG* and non-*POLG* mutations. The *POLG* mutation-undetermined group showed a more severe microvacuolation in 3 of the 4 brain areas. This group showed the most severe microglial activation and astrogliosis in the basal ganglia compared to other groups.

Mitochondrial density was low in both Purkinje cells and neurons of the dentate nucleus and frequently accompanied by abnormal mitochondrial localisation.

The *POLG* mutation-absent patient showed a severe phenotype, with much neuron loss and myelin loss in all brain areas. This may reflect mutations in a well-conserved gene, leading to an Alpers' syndrome phenotype. The *POLG* mutation-absent patient showed the most severe myelin loss in all brain areas and the occipital lobe showed the most severe microglial inflammation.

The inter-group variation is clear and does seem to correlate with genotype. Reports of the correlation of phenotype with genotype have suggested that non-*POLG* patients have a very early-onset, partly preserved Purkinje cells, and mainly preserved white matter (Sofou et al., 2012). This is in disagreement with what is seen in the cohort used in this study. In my cohort, the non-*POLG* genotype has a severe phenotype but a later symptom onset than most of the patients with a *POLG* mutation-positive phenotype. In the published study, patients with an undetermined phenotype have a mixed range of neuropathology and undefined phenotypes, which reflects the range of genotypes that could be present in this group. This disparity may arise from many of the non-*POLG* patients being discovered to have mtDNA mutations with other childhood neuropathological diseases not being fully ruled out.

3.6.4 *The Project's Findings in the Context of the Literature*

There are many case reports of patients with Alpers' syndrome in the scientific literature. Previous research into Alpers' syndrome has reported neuropathology in the CNS tissues of patients; atrophy, microvacuolation, capillary proliferation, neuron loss and astrogliosis being the most frequently reported features.

3.6.4.1 *Areas of Pathology*

This study has shown that pathology and neuron loss are most severe in the cerebellum, with much neuron loss in the upper layers of the occipital lobe. This is in agreement with studies that have shown severe pathology in the cerebellum (Harding 2008; Uusimaa et al., 2008) and occipital lobe (Harding et al., 1986; Khan et al., 2012). Fewer reports have been published on the involvement of the parietal lobe and basal ganglia, making these areas of interest to examine whether they show comparable levels of pathology to more well-studied brain areas.

In particular, the basal ganglia showed little pathology. Previously literature has reported atrophy, neuronal loss, and astrogliosis in the basal ganglia (Delarue et al., 2000; Kayihan et al., 2000; Wiltshire et al., 2008; Cardenas and Amato 2010) but this has not been noted for many patients in this cohort, suggesting that pathology is variable in patients and severe pathology of the basal ganglia is uncommon.

The research carried out in this project is comparable with the current scientific literature, raising further points. There is considerable pathology in the cerebellum, with less pathology in the occipital lobe, parietal lobe and basal ganglia. Pathology is present in all brain areas studied and quantitative evidence in support of this is demonstrated in this chapter.

3.6.4.2 Neuron Loss

Neuron loss is one of the most commonly reported neuropathological findings of Alpers' syndrome (Harding et al., 1995; Kayihan et al., 2000; Simonati et al., 2003a; Harding 2008; Wiltshire et al., 2008). Neuron loss was seen in almost all of the patients in this cohort; the cerebellum of Patient 1 being a notable exception.

Neuron loss was most severe in the cerebellum, with loss of Purkinje cells and dentate nucleus neurons occurring either concurrently or independently of each other. This suggests that Purkinje cells and neurons of the dentate nucleus are equally vulnerable in patients, though may not be affected to the same severity.

There was neuron loss from the occipital lobe, predominantly in the upper layers I-III. In those patients with a more severe neuron loss, this correlated with a more severe astrogliosis. Considering the widely reported pathology to the posterior of the brain in Alpers' syndrome patients, it is unusual that there was not a greater neuron loss in the occipital lobe in this cohort. It is possible that due to the sampling protocols of the Newcastle Brain Tissue Resource, the extrastriate cortical area is sampled and not the primary visual cortex. More profound change may be seen in the primary visual cortex.

There was neuron loss from the parietal lobe, predominantly in the upper layers I-III. In the occipital and parietal lobe, neuron loss is not attributed to microvacuolation in the upper cortical layers. However, it may have played a role in the parietal lobe neuron loss of Patient 12, which showed a moderate microvacuolation (++) and 34%-45% neuron loss in the cortical layers III - VI. Neuron loss in the upper grey matter layers may be partly attributable to the fact that these neurons were difficult to distinguish with confidence, with low numbers being counted for all patients and control.

Only one patient, Patient 9, showed neuron loss from the basal ganglia. This is an area infrequently reported to show pathology and neuron loss does not appear to be a main feature of neuropathology in the basal ganglia.

3.6.4.3 *Astrogliosis*

The research findings of this project agree with previous reports showing obvious astrogliosis in patients (Harding et al., 1995; Wiltshire et al., 2008). Severe astrogliosis can be correlated with severe neuron loss in the occipital lobe.

In this cohort, many of the patients exhibit swollen astrocytes, a feature which has not been previously reported in the literature for patients with Alpers' syndrome. The role of astrocytes in neurodegenerative conditions is not fully understood, these cells can play a role in the protection and preservation of neurons (Acarin et al., 2007) but may also play a role in the neurological aspects of other conditions, including HIV, where patients show astrogliosis (An and Scaravilli 1997).

3.6.4.4 *Mitochondrial Localisation*

Mitochondrial density was low in the neurons of the majority of patients and was frequently accompanied by an abnormal localisation of mitochondria around the periphery of the nucleus, the periphery of the soma, or localised away from an edge of the soma. This was most readily seen in large neurons, such as Purkinje cells of the cerebellum and the neurons of the globus pallidus of the basal ganglia.

Typically, mitochondria have a pan-cytoplasmic distribution throughout the cell body of the neuron. ATP is required throughout the neuron, nodes of Ranvier and synapse. Axonal transport distributes mitochondria towards the synapse in anterograde transport, where ATP is utilised for cellular processes. Depolarised mitochondria are then returned to the cell soma in retrograde transport, in order to be degraded and recycled. Clustering of mitochondria around the nucleus was noted in the control tissue in this study, and this may happen naturally in all neurons but it may be happening at a greater rate or in greater numbers in the neurons of patients with Alpers' syndrome. Depolarised mitochondria may cluster around the nucleus prior to degradation in other neurological disorders, and this has been documented in cell lines with mutations in *Parkin*, a gene implicated in Parkinson's disease (Okatsu et al., 2010). In HeLa cells, increased perinuclear clustering and movement of mitochondria away from the cell periphery is reported to occur after the disruption of the dynein complex (Varadi et al., 2004). The clear localisation of mitochondria around the periphery of the nucleus in the

neurons of many patients in this cohort, suggests that large numbers of mitochondria may be damaged and depolarised, compared to the controls.

3.6.4.5 White Matter Abnormalities

Involvement of the white matter in Alpers' syndrome is infrequently mentioned in the literature. There have been previous reports noting abnormalities of the white matter and myelin loss (Harding et al., 1995; Simonati et al., 2003b; Bao et al., 2008).

In this cohort, considerable white matter pathology was seen in the cerebellum, occipital lobe, and the basal ganglia in 3 of the 4 patients studied. Myelin loss was the most prominent pathology of the basal ganglia, as it had no neuron loss and less astrogliosis and microglial activation than other brain areas. This suggests that myelin loss may occur in the absence of other neuropathological features in patients. The white matter loss in Alpers' syndrome patients is most likely to be secondary to neuronal loss and the loss of neuronal axons. Primary loss of myelin cannot be ruled out completely, as Patient 12 displayed myelin loss but no axonal loss in the basal ganglia.

White matter abnormalities are a more important factor than is currently considered in the literature and warrants further investigation into the root cause of myelin loss, which could aid in the understanding of disease progression in Alpers' syndrome.

3.6.4.6 Microglial Activation

Microglia are ubiquitous immune cells, usually quiescent, that become activated in response to a variety of pathological stimuli. They are spatially restricted and this can indicate the area of any continuing disease processes (Banati et al., 2004).

Inflammation and microglial activation are not often reported as part of the neuropathology in patients with Alpers' syndrome. Reactive inflammatory changes have been previously described in the brain tissue of patients with Alpers' syndrome, though suggest that it was not involved in the disease progression (Nolte et al., 2013).

Activated microglia were seen in every patient in at least one brain area, except the stillbirth, Patient 5. A moderate to severe increase in these cells was often seen and correlated with the severity of astrogliosis, indicating areas of pathology despite there being no neuron loss. Interestingly, extremely swollen microglia were seen in the occipital lobe of Patient 2 which corresponded with microvacuolation and severe myelin

loss, possible indicators of the phagocytosis of degenerating cells and large amounts of materials.

3.6.4.7 Electron Microscopy

There are very few EM studies on tissue from patients with Alpers' syndrome. This project is one of the few to use the technique to examine the mitochondria in patient cells. This study noted a difference between the patient and disease control, with a greater difference between the patient and the control. Fewer cellular structures, including axons and mitochondria, were visible in the patient sample suggesting a greater extent of tissue degradation. Electron-dense inclusions were seen within the mitochondria of brain tissue examined from a patient diagnosed with Alpers' syndrome. Control tissue was tested at the same times as patient tissue and electron-dense inclusions were also found to be present in this tissue. The results of control tissue have not been previously reported in the literature, possibly due to case reports testing patient tissue only.

In agreement with the results in the patient tissue, a study noted electron-dense inclusions in liver and skeletal muscle mitochondria in a patient with Alpers' syndrome (Mangalat et al., 2012). A separate study examined two patients with a POLG-related encephalopathy and reported globoid inclusions in EM of muscle and brain mitochondria (Nolte et al., 2013).

A full analysis of the patient using EM techniques was difficult due to the degradation of the tissue sample. It is possible that the degradation was due, in part, to disease processes that damaged the tissue to a greater extent than was seen in either of the controls. The patient showed low numbers of mitochondria with few intact cristae when compared to the controls and this may suggest a particular vulnerability of these organelles. This approach is limited as cellular and mitochondrial morphology can be affected by post-mortem delay and fixation length. It can be difficult to obtain tissue of a suitable quality for EM studies and controls should be matched for age as well as fixation length.

3.6.5 Novel Findings

This project has a large cohort of patients over a large age range and diverse range of genetic diagnoses, which has not been published previously in the literature.

This study has shown that patients with Alpers' syndrome show a more diverse range of features than previously thought, including astrogliosis and white matter abnormalities. Pathology of the white matter occurred more often than was expected and in all brain regions. It had a greater pathology that was not reflected in the literature and the results of this study suggest that white matter pathology should be investigated as part of the neuropathology of Alpers' syndrome.

Structural abnormalities of mitochondria occur at the ultrastructural level, however great care should be taken in interpreting these findings. Through the use of EM techniques, this study has shown electron-dense inclusions in both the patient and fixation-matched control tissue. This may indicate an artefact of the fixation process highlighting the limitations of this approach.

Astrogliosis with swollen astrocytes of an abnormal morphology have not been previously reported in the literature. This is an interesting finding that may suggest a pathological role of astrocytes in the course of Alpers' syndrome. Astrocytes can play a role in the neurological aspects of other conditions; HIV patients show astrogliosis (An and Scaravilli 1997). However, astrocytes can show neuroprotective properties and their presence can lead to the preservation of neurons (Acarin et al., 2007). The full role of astrocytes in neurodegenerative conditions is not fully understood.

The knowledge that clinically diagnosed Alpers' syndrome may be due to both *POLG* and non-*POLG* mutations is leading to new area of research. So far, few studies have compared these possible groups (Sofou et al., 2012) which can add new data to an expanding array of possible genes involved in Alpers' syndrome.

3.7 Future Work

The work performed in this study has highlighted the need for a genetic diagnosis when studying patients clinically diagnosed with Alpers' syndrome. Genetic data can add much information and aid in the interpretation of clinical and neuropathological data. In the case of this cohort, current methods of DNA extraction were not successful and despite all efforts, a genetic diagnosis could not be made for some patients. Future attempts to elucidate the genetic status of the group with an undetermined *POLG* mutation may prove fruitful and allow fresh interpretations of the neuropathological data.

Work to uncover the aetiology of the clinical signs seen in the *POLG* mutation-absent patient is currently on-going. Whole exome sequencing has identified a potential candidate gene but further work is required to prove a link between the genetic defect and levels of cellular respiration. Data contributing to the knowledge of mutations in other genes leading to Alpers' syndrome, may vastly improve our understanding of the spectrum of mitochondrial disease and its impact upon the CNS.

Further assessment of the white matter of the group with an undetermined *POLG* mutation will be interesting and add to the investigations performed during the course of this project. The use of fully quantitative techniques to assess white matter abnormalities and porin localisation may be of use, particularly densitometric techniques.

This study has underlined the importance of full neuropathological, phenotypic and genotypic data when studying a patient cohort. The cohort in this project is the largest and most comprehensive that has been studied with Alpers' syndrome. Further investigations will add invaluable insights into what has already been determined in this project.

- Acarin, L., S. Villapol, M. Faiz, T. T. Rohn, B. Castellano and B. González (2007). "Caspase-3 activation in astrocytes following postnatal excitotoxic damage correlates with cytoskeletal remodeling but not with cell death or proliferation." GLIA **55**(9): 954-965.
- An, S. F. and F. Scaravilli (1997). "Early HIV-1 infection of the central nervous system." Archives d'Anatomie et de Cytologie Pathologiques **45**(2-3): 94-105.
- Banati, R. B., R. Egensperger, A. Maassen, G. Hager, G. W. Kreutzberg and M. B. Graeber (2004). "Mitochondria in activated microglia in vitro." Journal of Neurocytology **33**(5): 535-541.
- Bao, X., Y. Wu, L. J. C. Wong, Y. Zhang, H. Xiong, P. C. Chou, C. K. Truong, Y. Jiang, J. Qin, Y. Yuan, Q. Lin and X. Wu (2008). "Alpers syndrome with prominent white matter changes." Brain and Development **30**(4): 295-300.
- Cardenas, J. F. and R. S. Amato (2010). "Compound heterozygous polymerase gamma gene mutation in a patient with alpers disease." Seminars in Pediatric Neurology **17**(1): 62-64.
- Delarue, A., O. Paut, J. M. Guys, M. F. Montfort, V. Lethel, B. Roquelaure, J. F. Pellissier, J. Sarles and J. Camboulives (2000). "Inappropriate liver transplantation in a child with Alpers-Huttenlocher syndrome misdiagnosed as valproate-induced acute liver failure." Pediatric Transplantation **4**(1): 67-71.
- Elo, J. M., S. S. Yadavalli, L. Euro, P. Isohanni, A. Götz, C. J. Carroll, L. Valanne, F. S. Alkuraya, J. Uusimaa, A. Paetau, E. M. Caruso, H. Pihko, M. Ibba, H. Tyynismaa and A. Suomalainen (2012). "Mitochondrial phenylalanyl-trna synthetase mutations underlie fatal infantile alpers encephalopathy." Human Molecular Genetics **21**(20): 4521-4529.
- Harding, B. N., N. Alsanjari, S. J. M. Smith, C. M. Wiles, D. Thrush, D. H. Miller, F. Scaravilli and A. E. Harding (1995). "Progressive neuronal degeneration of childhood with liver disease (Alpers' disease) presenting in young adults." Journal of Neurology Neurosurgery and Psychiatry **58**(3): 320-325.
- Harding, B. N., J. Egger, B. Portmann and M. Erdohazi (1986). "Progressive neuronal degeneration of childhood with liver disease: A pathological study." Brain **109**(1): 181-206.
- Harding, B. N., Surtees, R.A.H (2008). Metabolic and neurodegenerative disease of childhood. Greenfield's neuropathology volume 1 Eighth

- Edition. S. Love, Louis, D.N., Ellison, D.W. London, UK, Hodder Arnold. **1**: 481 – 514.
- Hunter, M. F., H. Peters, R. Salemi, D. Thorburn and M. T. MacKay (2011). "Alpers syndrome with mutations in POLG: Clinical and investigative features." Pediatric Neurology **45**(5): 311-318.
- Kayihan, N., I. Nennesmo, B. G. Ericzon and A. NÅ©meth (2000). "Fatal deterioration of neurological disease after orthotopic liver transplantation for valproic acid-induced liver damage." Pediatric Transplantation **4**(3): 211-214.
- Khan, A., C. Trevenen, X. C. Wei, H. B. Sarnat, E. Payne and A. Kirton (2012). "Alpers syndrome: The natural history of a case highlighting neuroimaging, neuropathology, and fat metabolism." Journal of Child Neurology **27**(5): 636-640.
- Mangalat, N., N. Tatevian, M. Bhattacharjee and J. M. Rhoads (2012). "Alpers syndrome: An unusual etiology of failure to thrive." Ultrastructural Pathology **36**(4): 219-221.
- Nguyen, K. V., F. S. Sharief, S. S. L. Chan, W. C. Copeland and R. K. Naviaux (2006). "Molecular diagnosis of Alpers syndrome." Journal of Hepatology **45**(1): 108-116.
- Nolte, K. W., S. Trepels-Kottek, D. Honnef, J. Weis, C. G. Bien, A. van Baalen, K. Ritter, B. Czernin, S. Rudnik-Schöneborn, N. Wagner and M. Häusler (2013). "Early muscle and brain ultrastructural changes in polymerase gamma 1-related encephalomyopathy." Neuropathology **33**(1): 59-67.
- Okatsu, K., K. Saisho, M. Shimanuki, K. Nakada, H. Shitara, Y. Sou, M. Kimura, S. Sato, N. Hattori, M. Komatsu, K. Tanaka and N. Matsuda (2010). "P62/SQSTM1 cooperates with Parkin for perinuclear clustering of depolarized mitochondria." Genes to Cells **15**(8): 887-900.
- Simonati, A., M. Filosto, C. Savio, G. Tomelleri, P. Tonin, B. Dalla Bernardina and N. Rizzuto (2003a). "Features of cell death in brain and liver, the target tissues of progressive neuronal degeneration of childhood with liver disease (Alpers-Huttenlocher disease)." Acta Neuropathologica **106**(1): 57-65.
- Simonati, A., M. Filosto, G. Tomelleri, C. Savio, P. Tonin, A. Polo and N. Rizzuto (2003b). "Central-peripheral sensory axonopathy in a juvenile case of Alpers-Huttenlocher disease." Journal of Neurology **250**(6): 702-706.
- Sofou, K., A.-R. Moslemi, G. Kollberg, I. Bjarnadóttir, A. Oldfors, I. Nennesmo, E. Holme, M. Tulinius and N. Darin (2012). "Phenotypic and genotypic variability in Alpers syndrome." European Journal of Paediatric Neurology **16**(4): 379-389.

Uusimaa, J., R. Hinttala, H. Rantala, M. Päivärinta, R. Herva, M. Röyttä, H. Soini, J. S. Moilanen, A. M. Remes, I. E. Hassinen and K. Majamaa (2008). "Homozygous W748S mutation in the POLG1 gene in patients with juvenile-onset Alpers syndrome and status epilepticus." *Epilepsia* **49**(6): 1038-1045.

Varadi, A., L. I. Johnson-Cadwell, V. Cirulli, Y. Yoon, V. J. Allan and G. A. Rutter (2004). "Cytoplasmic dynein regulates the subcellular distribution of mitochondria by controlling the recruitment of the fission factor dynamin-related protein-1." *Journal of Cell Science* **117**(19): 4389-4400.

Visser, N. A., K. P. J. Braun, F. S. S. Leijten, O. van Nieuwenhuizen, J. H. J. Wokke and W. M. van den Bergh (2011). "Magnesium treatment for patients with refractory status epilepticus due to POLG1-mutations." *Journal of Neurology*: 1-5.

Wiltshire, E., G. Davidzon, S. Dimauro, H. O. Akman, L. Sadleir, L. Haas, J. Zuccollo, A. McEwen and D. R. Thorburn (2008). "Juvenile Alpers disease." *Archives of Neurology* **65**(1): 121-124.

Chapter 4 Respiratory Chain Deficiency in Patients with Alpers' Syndrome

4.1 Introduction

The mitochondrial polymerase gamma enzyme (POLG) is essential for mtDNA replication and is the only known polymerase in mammals to perform this action (Hance et al., 2005). Mutations in this gene may affect its function, leading to secondary mtDNA abnormalities. As mtDNA encodes 13 polypeptides making up the respiratory chain, the effect of mutated POLG on the mtDNA can have negative consequences for the respiratory chain in affected tissues.

There have been studies of respiratory chain deficiency in patients with a mitochondrial disease, due to mutations in *POLG* causing mtDNA defects. These studies have shown variable respiratory chain dysfunction, from normal respiratory chain activity (Milone et al., 2008; Isohanni et al., 2011) to a deficiency of complex I (Hakonen et al., 2008) and complex III (Blok et al., 2009). Normal respiratory chain functioning was seen in the skeletal muscle of five patients diagnosed with cPEO (Milone et al., 2008) and in the skeletal muscle of five patients with *POLG* mutations (Isohanni et al., 2011). Two patients diagnosed with MIRAS had complex I deficiency in neurons of the cerebellum and frontal cortex (Hakonen et al., 2008) while a patient with homozygous p.Ala467Thr mutations showed reduced complex III in the brain (Blok et al., 2009). Complex IV is less severely affected but has shown milder defects in neurons of patients with a *POLG*-related disorder, thought to be due to clonally expanded mtDNA deletions (Lax et al., 2012).

Mitochondrial respiratory chain impairment in the CNS and liver is a prominent feature of Alpers' syndrome. Studies of patients have examined respiratory chain defects in a variety of tissues, including liver and skeletal muscle. These have shown a loss of activity of multiple respiratory chain complexes (Delarue et al., 2000; Wiltshire et al., 2008; Schaller et al., 2011). However, as mentioned above concerning patients with *POLG* disorders, there have been reports of patients with Alpers' syndrome with normal respiratory chain activity in muscle, fibroblast and liver tissue samples (de Vries et al., 2008). Fewer studies have focussed on Alpers' syndrome than on other *POLG* disorders and there have been no published studies examining the respiratory chain in the brain tissue of diagnosed Alpers' syndrome patients. In addition, studies on Alpers' syndrome generally focus on case studies of a single patient or small number of

patients rather than a cohort of patients. These studies focus on specific parts of the respiratory chain, most often on complex I and complex IV due to the mtDNA defects resulting in a loss of function and assembly of these complexes.

Previous studies have mostly used homogenate tissue samples to quantify respiratory chain expression and activity (Hakonen et al., 2008; Blok et al., 2009), with some COX/SDH studies performed on single neurons (Lax et al., 2012). This study is unique in that it investigates the respiratory chain in single neurons in the brain of patients diagnosed with Alpers' syndrome. Examining tissue at the level of the single neuron greatly increases the sensitivity and accuracy of the results, and gives certainty of the extent and severity of deficiency in neurons. Studies of respiratory chain deficiency often examine complex I and complex IV, which are frequently affected by acquired mtDNA defects. The size and complexity of complex I, and the position of complex IV at the end of the chain transporting electrons, make them both agents for the failure of the respiratory chain. This study also examines complex III, which is seldom studied in single cells.

The previous chapter examined the neuropathology seen in a large cohort of patients with clinical Alpers' syndrome. This chapter will investigate the integrity of mitochondrial respiratory chain in neurons of the cerebellum, occipital lobe, parietal lobe, and basal ganglia in the same cohort.

4.2 Aims

Patients with Alpers' syndrome demonstrate clinical signs that correlate with areas of neuropathology. This chapter will investigate the pathology further by examining the respiratory chain in the four brain regions. The aims of this work are:

1. To semi-quantitatively assess protein expression of different subunits of the respiratory chain of mitochondria in neurons. This will be performed in CNS tissues of patients clinically diagnosed with Alpers' syndrome, and will compare the findings to those of controls.
2. To investigate the differences in the expression of the respiratory chain between the patient groups.

4.3 Methodological Approach

Antibodies were used to assess complexes of the respiratory chain in mitochondria in nine patients (Table 4.1), as described in *Chapter 2 Methods and Materials, 2.2.5.1 'Respiratory Chain Antibody Staining'*. A semi-quantitative assessment of the neurons was completed according to the scale – deficient/no staining, + weak staining, ++ weak to moderate staining, +++ intense staining. Deficiency of a respiratory chain complex was defined as greatly reduced expression or absence of a protein subunit. Patients 3 and 4 could not be assessed as no FFPE tissue was available. Patient 5 had tissue that had been fixed in formalin for 13 years. This made the tissue unreliable for quantifying respiratory chain antibodies. Therefore these patients are not included in the results. The patient without a mutation in *POLG*, Patient 12, had tissue that had been fixed in formalin for 14 years from the cerebellum, parietal lobe, and basal ganglia. This made the tissue unreliable for quantifying respiratory chain antibodies and only the occipital lobe was suitable for this study.

Patient	Age at Death	Sex	POLG Mutation
1	14 months	F	p.Ala467Thr; p.Gly848Ser
2	27 months	M	p.Ala467Thr; p.Thr914Pro
6	18 years	F	A sibling with p.Trp748Ser; p.Arg1096Cys
7	2.5 months	F	Unknown
8	5.5 months	M	Unknown
9	6.5 months	F	Unknown
10	13 months	M	Unknown
11	7 years	F	Unknown
12	6 years	M	None

Table 4.1. Details of the patients used in the study of respiratory chain deficiency.

4.4 Results

4.4.1 Staining Quantification

Visualisation of antibody staining was achieved through the use of DAB, which produces an insoluble brown polymer upon its oxidation. Semi-quantitative assessment of the patients and controls was done according to the scale below (Figure 4.1).

One hundred neurons were counted with each antibody in each patient. Neurons classed as weak to moderate (+) and intense (+++) were considered part of the natural variation of respiratory chain expression. Deficiency was defined as the combined numbers of neurons classed as deficient (-) and weak (+).

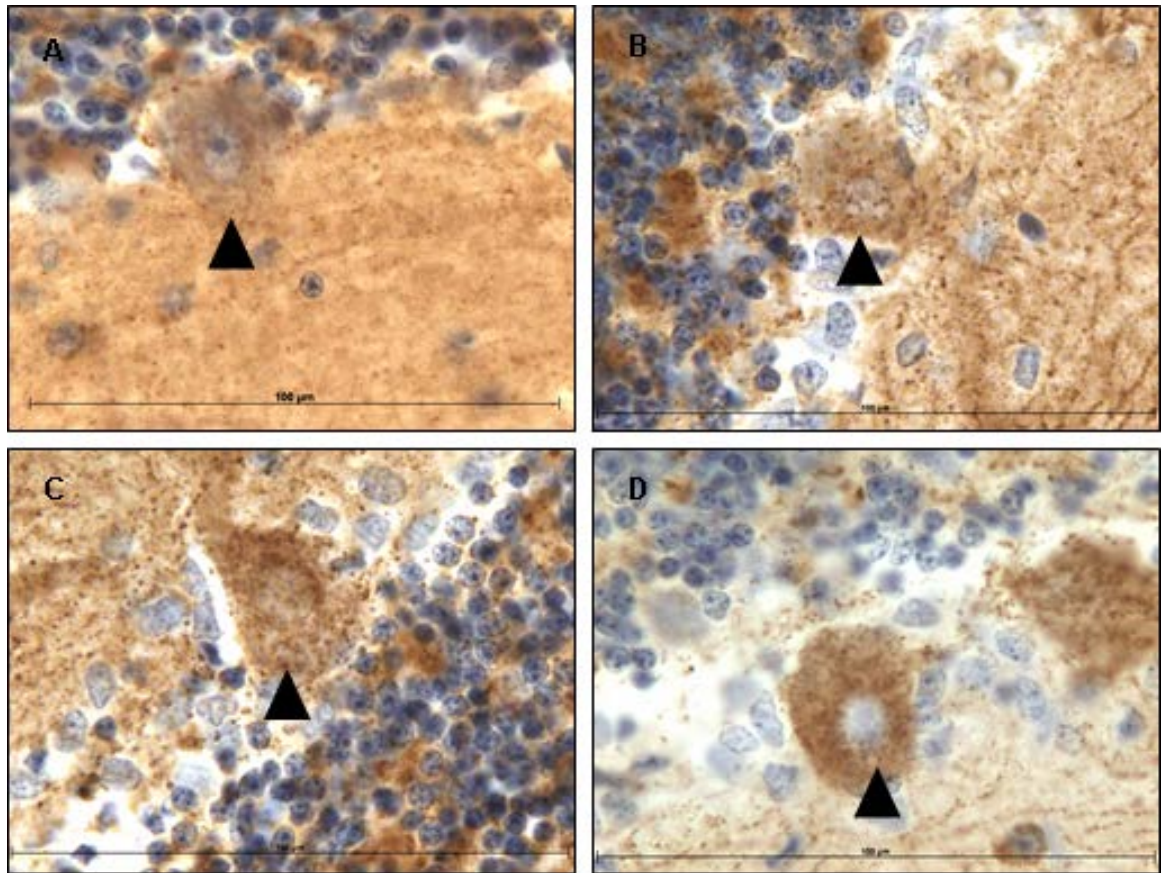


Figure 4.1. Semi-quantitative scale of antibody staining in neurons.

Key: Image A=deficient (-), image B=weak (+), image C=weak to moderate (++) , image D=intense (+++). The images shown are taken from the cerebellum. Arrowheads indicate Purkinje cells of the specified intensity.

4.4.2 Cerebellum

The Purkinje cells and the dentate nucleus were examined. The availability of the dentate nucleus was dependent upon the orientation of the sample taken by the original pathology team. In some patients, this led to the dentate nucleus being unavailable for analysis.

4.4.2.1 Purkinje Cells

Recognised by Czech physiologist Jan Evangelista Purkinje in 1837, Purkinje cells are large, GABA-ergic, inhibitory neurons of the cerebellum. They form a single cell-thick layer between the molecular layer and the granular cell layer, their dendrites branching out into the molecular layer, where stellate cells and basket cells may act upon the Purkinje cell. They are acted upon by mossy climbing fibres and parallel fibres, and Purkinje cells themselves act upon neurons of the deep grey nuclei, including the dentate nucleus. They are responsible for controlling motor coordination and voluntary movement.

4.4.2.1.1 Complex I – NADH: Ubiquinone Oxidoreductase

Complex I is a multi-subunit protein made up of at least 44 subunits; 37 subunits are nuclear-encoded, 7 are mitochondrially-encoded. Antibodies to four different subunits were tested to investigate all parts of the complex: CI-19 (*NDUFA13*) part of the hydrophilic domain, CI-20 (*NDUFB8*) and CI-39 (*NDUFA9*) part of the hydrophobic domain, and one of the core hydrophilic domain subunits CI-30 (*NDUFS3*). All subunits investigated were nuclear-encoded, as there are no suitable antibodies currently available to subunits encoded by the mitochondrial DNA.

In a subset of patients, CI-19 and CI-20 antibodies were tested only, as it became apparent there was little additional information being added to the investigation through the inclusion of CI-30 and CI-39 antibodies.

Patients with evidence for *POLG* mutations (Figure 4.2; image B) show moderate levels of deficiency in all four of the complex I subunits tested.

Patients with no genetic diagnosis available (Figure 4.2; images C and D) show moderate to high levels of deficiency in two of the complex I subunits tested.

All patients, except Patient 2 and Patient 7, show a complex I deficiency in the Purkinje cells. The *POLG* mutation-positive group shows the greatest levels of deficiency in complex I-20 and complex I-30. The *POLG* mutation-undetermined group shows the

highest levels of deficiency in complex I-19. The pattern of staining appears to be random with either of the complex subunit antibodies showing greater deficiency than the other three. The control shows no evidence of deficiency.

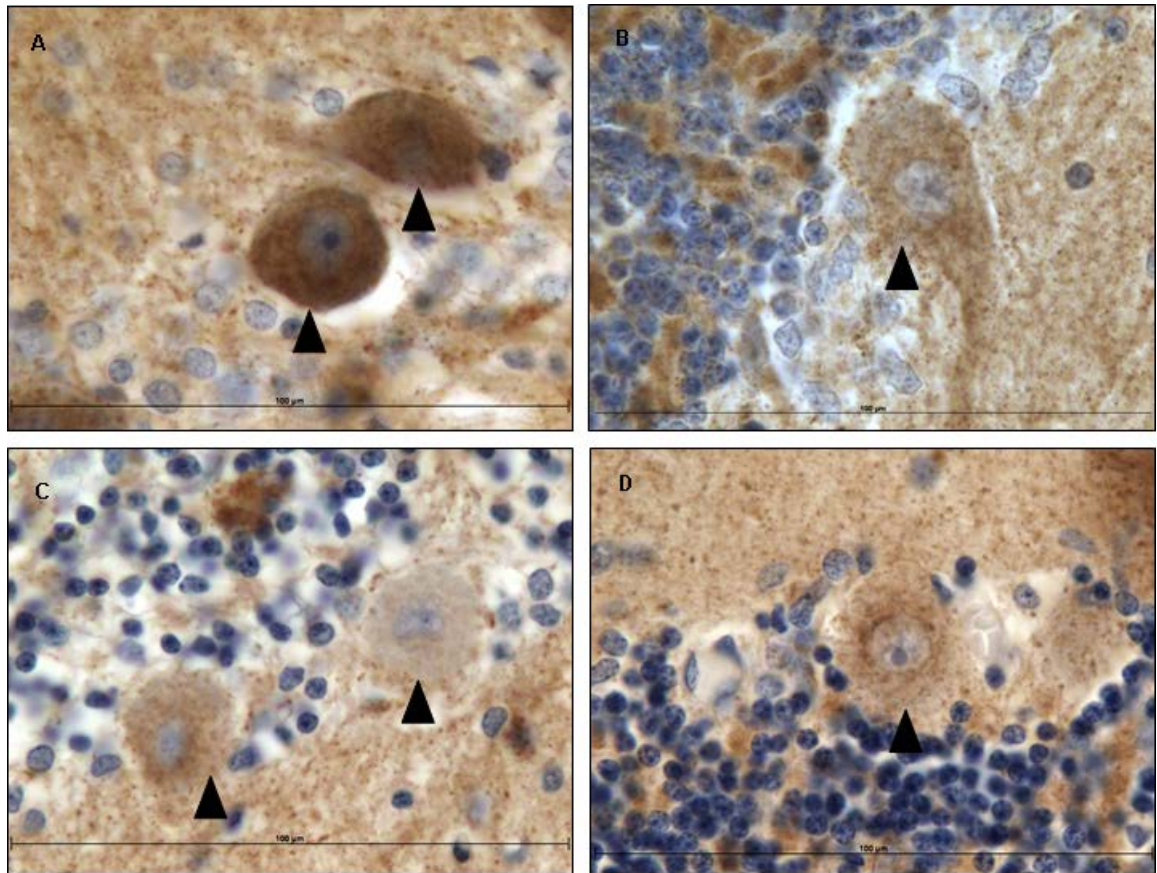


Figure 4.2. Staining with antibodies for complex I in the Purkinje cells of the cerebellum.

Arrowheads indicate neurons. All sections stained with complex I antibody. A=Control 6 CI-19, B=Patient 1 *POLG* mutation-positive group CI-19, C=Patient 11 *POLG* mutation-undetermined group CI-19, D=Patient 10 *POLG* mutation-undetermined group CI-19. Scale bar = 100µm.

Deficiency values for all subunits are shown in Table 4.2. The brain area is unavailable for patients not listed in the table. The antibody stain for CI-39 could not be performed for Patient 2 as the stain was very uneven after repeating.

<i>POLG</i> mutation	Patient	Complex I- 19	Complex I- 20	Complex I- 30	Complex I- 39
+	1	8%	22%	0%	8%
	2	1%	1%	0%	N/A
	6	11%	12%	25%	19%
?	7	3%	2%	N/A	N/A
	8	10%	3%	N/A	N/A
	9	61%	21%	N/A	N/A
	10	44%	13%	N/A	N/A
	11	63%	38%	N/A	N/A

Table 4.2. Table of complex I deficiency in Purkinje cells of the cerebellum.

Percentage of deficiency defined as deficient (-) and weak (+) neuron counts combined. One hundred neurons were counted with each antibody in each patient. Where FFPE tissue is unavailable or is known to have been fixed for longer than 6 months, no values are given.

Key: N/A=not available

4.4.2.1.2 Complex II – Succinate: Ubiquinone Oxidoreductase

Complex II is a multi-subunit protein made up of 4 subunits; subunits A, B, C, and D that are all nuclear-encoded. Electrons may enter the ETC at complex I or at complex II and continue to flow along the respiratory chain.

Patients with evidence for *POLG* mutations show little evidence of deficiency (<5%) (Figure 4.3; images B and C).

Almost all the patients with no genetic diagnosis available show no deficiency. One patient, Patient 10, shows moderate levels of complex II deficiency at 28% in the Purkinje cells of the cerebellum (Figure 4.3; image D) but 0% deficiency in all other areas studied, including in neurons of the dentate nucleus of the cerebellum.

In the majority of patients, there is no evidence for complex II deficiency. However, a single patient, Patient 10, showed moderate levels of deficiency which may have been due to issues that affected only the Purkinje cells. The fixation time of the tissue is unknown for Patient 10. The controls show no evidence of deficiency.

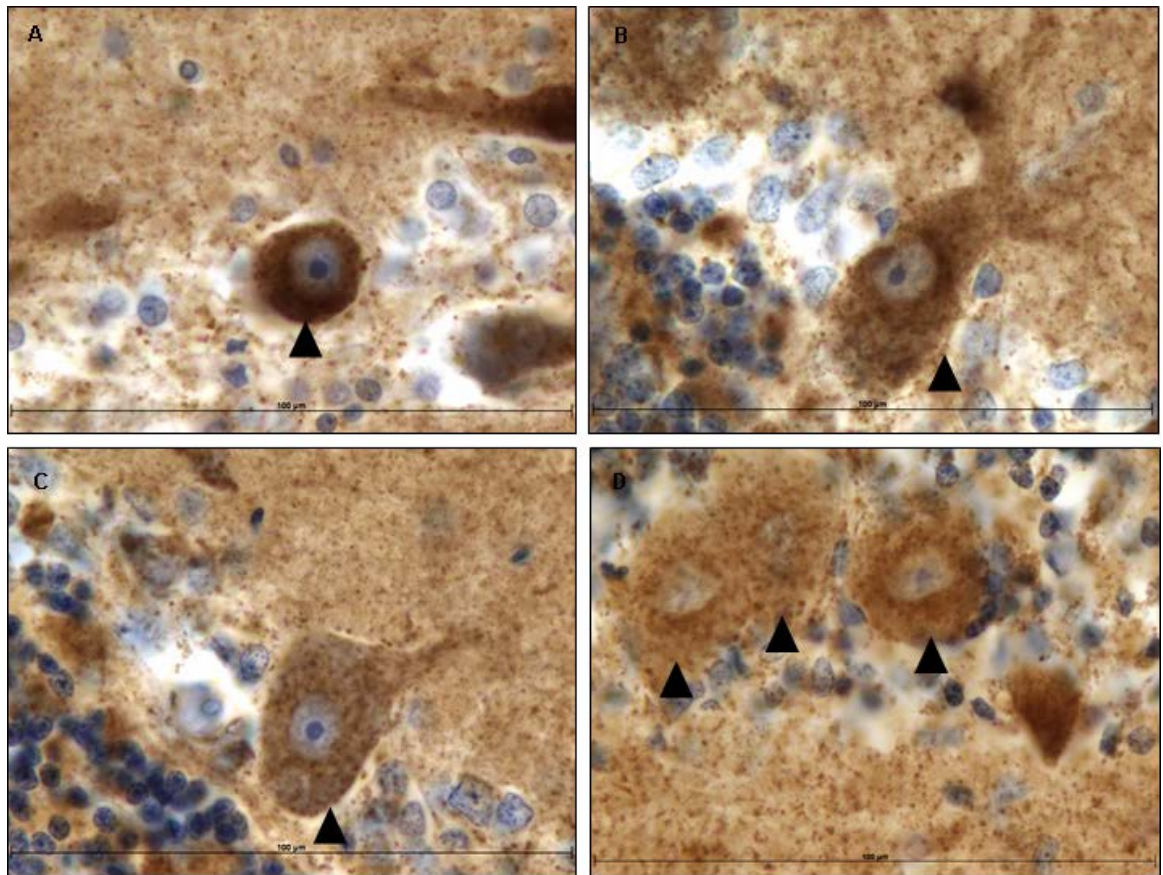


Figure 4.3. Staining with antibodies for complex II in the Purkinje cells of the cerebellum.

Arrowheads indicate neurons. All sections stained with complex II subunit 70 antibody. A=Control 6, B=Patient 1 *POLG* mutation-positive group, C=Patient 6 *POLG* mutation-positive group, D=Patient 10 *POLG* mutation-undetermined group. Scale bar = 100µm.

Deficiency values are shown in Table 4.3. The brain area is unavailable for patients not listed in the table.

<i>POLG</i> mutation	Patient	Complex II-70
+	1	0%
	2	1%
	6	5%
?	7	0%
	8	0%
	9	0%
	10	28%
	11	0%

Table 4.3. Table of complex II deficiency in Purkinje cells of the cerebellum.

Percentage of deficiency defined as deficient (-) and weak (+) neuron counts combined. One hundred neurons were counted in each patient. Where FFPE tissue is unavailable or is known to have been fixed for longer than 6 months, no values are given.

4.4.2.1.3 Complex III – Ubiquinol Cytochrome c Reductase

Complex III is a multi-subunit protein made up of 11 subunits; 10 subunits are nuclear-encoded, 1 is mitochondrially-encoded, cytochrome *b*. The antibody used for immunohistochemistry is raised against the Rieske subunit, an iron-sulphur protein that is nuclear-encoded with an important role in electron transfer.

Patients with evidence for *POLG* mutations (Figure 4.4; images B and C) show variable levels of complex III deficiency. One patient shows very little evidence of deficiency while two further patients show moderate levels of deficiency. Patient 2 shows moderate levels of complex III deficiency but is the only patient not to exhibit a complex I deficiency in this part of the brain.

Patients with no genetic diagnosis available (Figure 4.4; image D) show moderate to high levels of deficiency.

The control shows no evidence of deficiency.

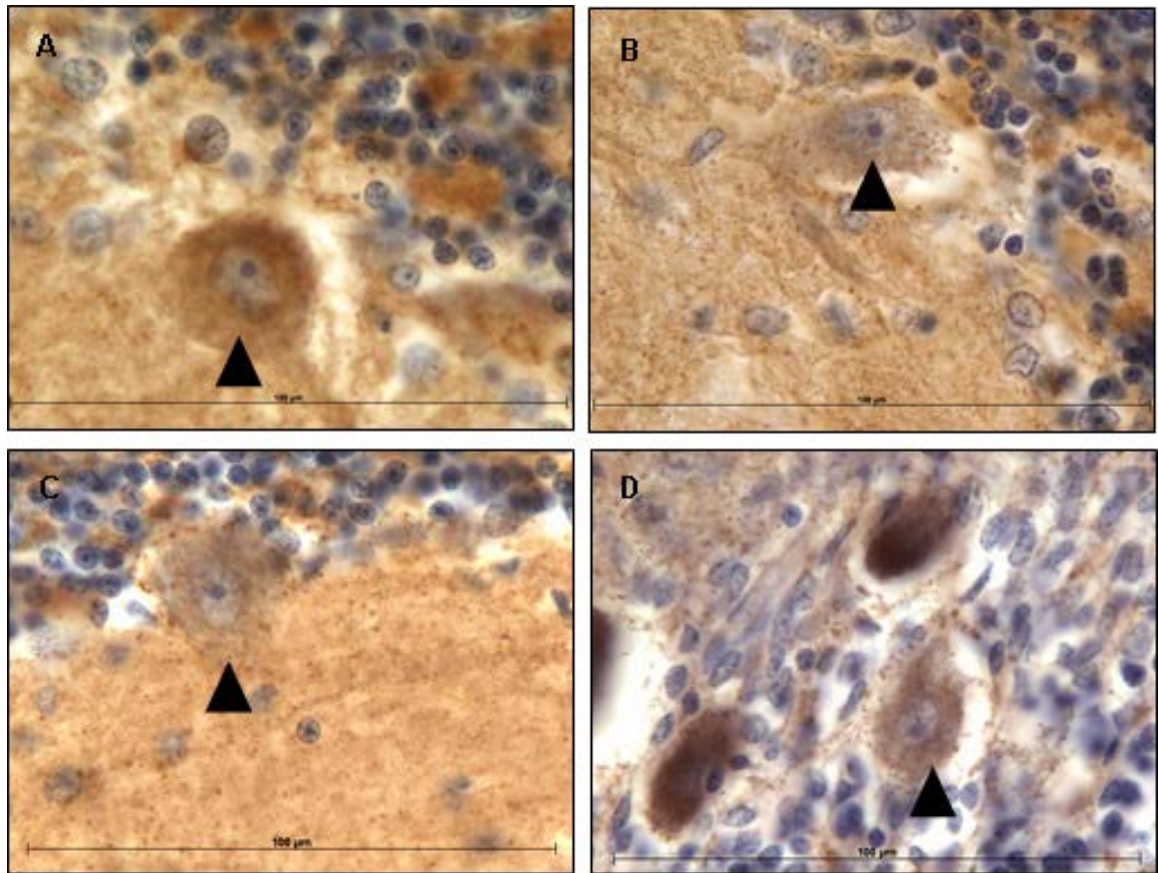


Figure 4.4. Staining with antibodies for complex III Rieske subunit in the Purkinje cells of the cerebellum.

Arrowheads indicate neurons. All sections stained with complex III Rieske subunit antibody. A=Control 10, B=Patient 6 *POLG* mutation-positive group, C=Patient 1 *POLG* mutation-positive group, D=Patient 8 *POLG* mutation-undetermined group. Scale bar = 100 μ m.

Deficiency values are shown in Table 4.4. The brain area is unavailable for patients not listed in the table. This antibody stain could not be performed for Patient 9 as the supply of tissue was depleted.

<i>POLG</i> mutation	Patient	Complex III-Rieske
+	1	1%
	2	39%
	6	27%
?	7	30%
	8	27%
	10	60%
	11	68%

Table 4.4. Table of complex III deficiency in Purkinje cells of the cerebellum.

Percentage of deficiency defined as deficient (-) and weak (+) neuron counts combined. One hundred neurons were counted in each patient. Where FFPE tissue is unavailable or is known to have been fixed for longer than 6 months, no values are given.

4.4.2.1.4 Complex IV – Cytochrome c Oxidase

Complex IV is a multi-subunit protein made up of 14 subunits; 11 subunits are nuclear-encoded, 3 are mitochondrially-encoded.

Patients with evidence for *POLG* mutations show little evidence of complex IV subunit I deficiency (Figure 4.5; image B). They show no complex IV subunit IV deficiency (Figure 4.6; images C and D).

Patients with no genetic diagnosis available show moderate levels of complex IV subunit I deficiency (Figure 4.5; images C and D). They show little evidence of complex IV subunit IV deficiency (Figure 4.6; image B).

The control shows no evidence of deficiency for both subunits.

It is unusual that Patient 11 shows a complex IV-IV deficiency of 14%, comparable to the complex IV-I deficiency of 18%. This is discussed in the Discussion section at the end of this chapter.

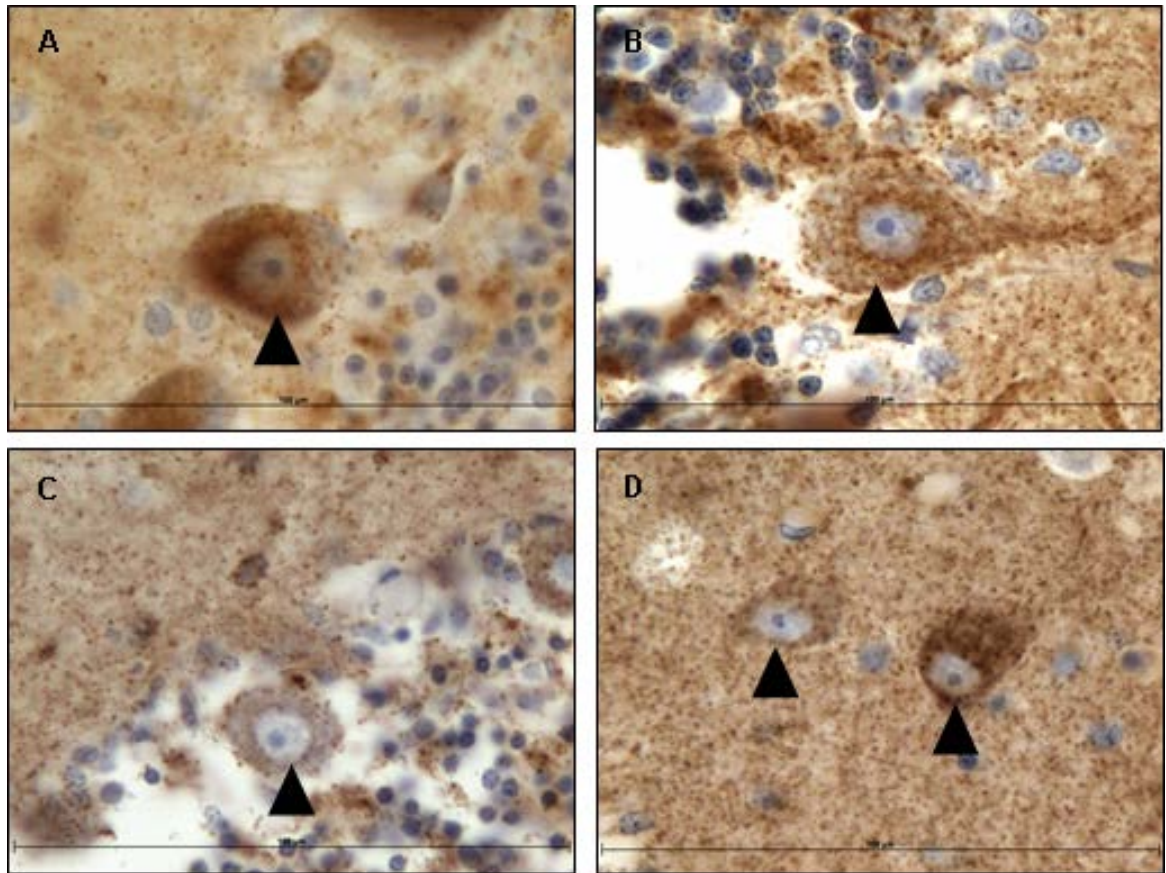


Figure 4.5. Staining with antibodies for complex IV subunit I in Purkinje cells of the cerebellum.

Arrowheads indicate neurons. All sections stained with complex IV subunit I antibody. A=Control 6, B=Patient 6 *POLG* mutation-positive group, C=Patient 9 *POLG* mutation-undetermined group, D=Patient 7 *POLG* mutation-undetermined group. Scale bar = 100 μ m.

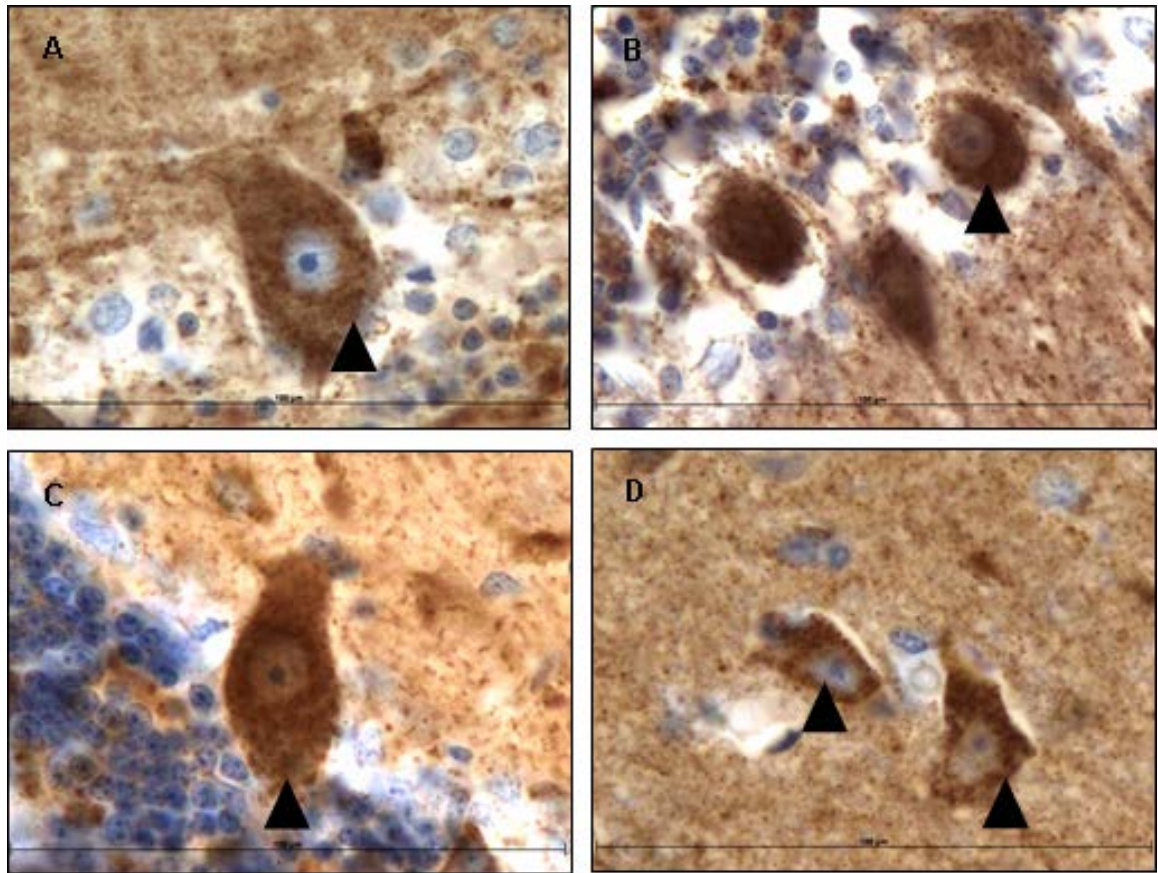


Figure 4.6. Staining with antibodies for complex IV subunit IV in Purkinje cells of the cerebellum.

Arrowheads indicate neurons. All sections stained with complex IV subunit IV antibody. A=Control 6, B=Patient 8 *POLG* mutation-undetermined group, C=Patient 1 *POLG* mutation-positive group, D=Patient 6 *POLG* mutation-positive group. Scale bar = 100 μ m.

Deficiency values for both subunits are shown in Table 4.5. The brain area is unavailable for patients not listed in the table.

<i>POLG</i> mutation	Patient	Complex IV-I	Complex IV-IV
+	1	1%	0%
	2	0%	0%
	6	15%	0%
?	7	0%	0%
	8	1%	0%
	9	33%	0%
	10	10%	8%
	11	18%	14%

Table 4.5. Table of complex IV deficiency in Purkinje cells of the cerebellum.

Percentage of deficiency defined as deficient (-) and weak (+) neuron counts combined. One hundred neurons were counted with each antibody in each patient. Where FFPE tissue is unavailable or is known to have been fixed for longer than 6 months, no values are given.

4.4.2.2 Dentate Nucleus

Neurons of the dentate nucleus are found in the deep white matter of the cerebellum. The dentate nucleus is the largest of four deep cerebellar nuclei, the others being the fastigial nucleus, the emboliform nucleus, and the globose nucleus. These neurons receive input from the premotor cortex and from Purkinje cells. The deep cerebellar nuclei are the main output of the cerebellum, projecting to regions of the cerebrum, including the frontal lobe and parietal lobe. The dentate nucleus controls the planning and initiation of voluntary movement, as well as playing a role in visuospatial awareness.

4.4.2.2.1 Complex I – NADH: Ubiquinone Oxidoreductase

Patients with evidence for *POLG* mutations (Figure 4.7; image B) show little evidence of complex I deficiency for the majority of subunits. There is a moderate to high level of deficiency of complex I-30. Patient 1 shows 53% deficiency of the core subunit complex I-30, affecting only neurons of the dentate nucleus. Normal levels of staining are seen in the Purkinje cells.

Patients with no genetic diagnosis available show a variable deficiency. Patient 7 and Patient 8 show no deficiency of complex I, but Patient 9 and Patient 10 show a moderate to high deficiency (Figure 4.7; images C and D).

The majority of patients, except Patient 7 and Patient 8, show a complex I deficiency in the dentate nucleus. Patient 1 shows a high level of deficiency of a single subunit, complex I-30, which occurs only in the neurons of the dentate nucleus. The *POLG* mutation-undetermined group shows the greatest levels of deficiency. Although Patient 8 does not show a deficiency in the dentate nucleus, this patient does show complex I deficiency in the Purkinje cells. As in the Purkinje cells, the affected subunits appear to be random with either of the complex subunit antibodies showing greater deficiency than the other three. The control shows no evidence of deficiency.

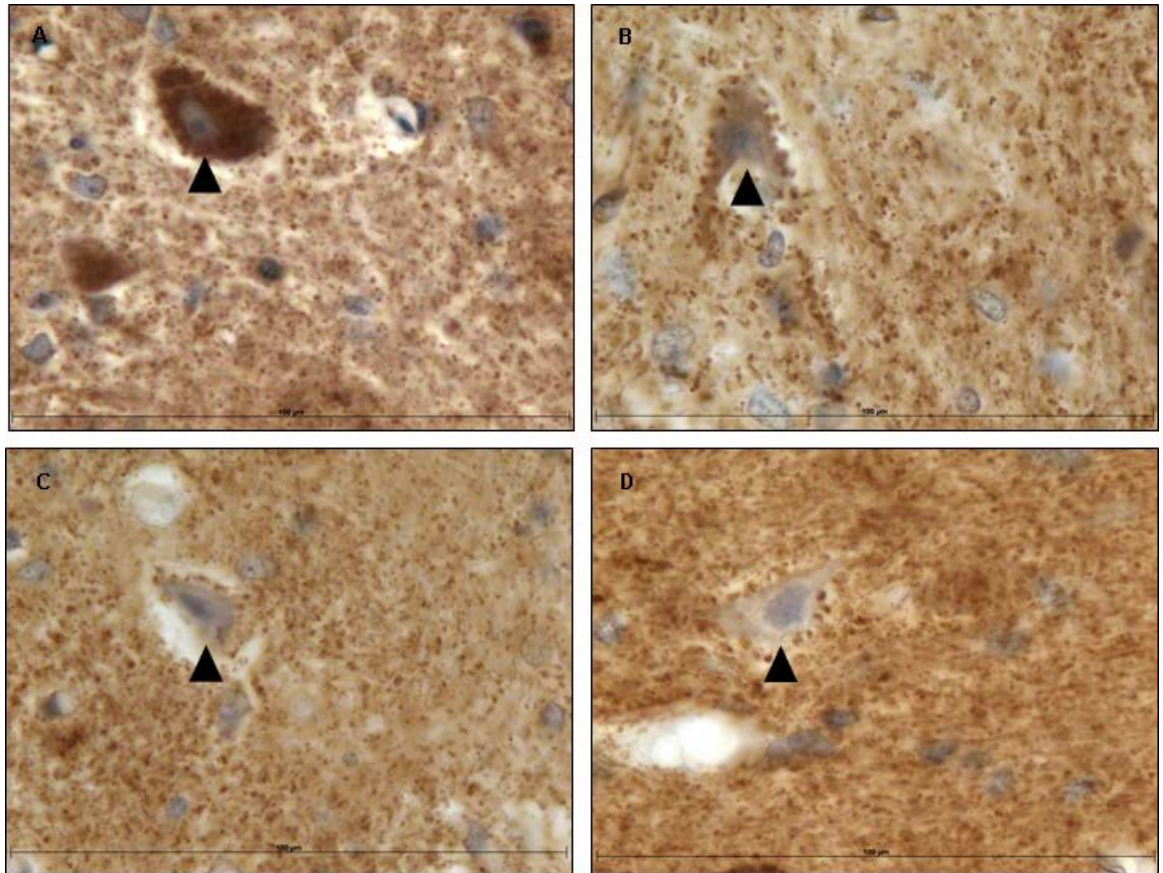


Figure 4.7. Staining with antibodies for complex I in neurons of the dentate nucleus in the cerebellum.

Arrowheads indicate neurons. All sections stained with complex I antibody. A=Control 1 CI-20, B=Patient 1 *POLG* mutation-positive group CI-20, C=Patient 9 *POLG* mutation-undetermined group CI-20, D=Patient 10 *POLG* mutation-undetermined group CI-20. Scale bar = 100µm.

Deficiency values for all subunits are shown in Table 4.6. The brain area is unavailable for patients not listed in the table. The availability of the dentate nucleus was dependent upon the orientation of the sample taken by the original pathology team. In some patients, this led to the dentate nucleus being unavailable for analysis, as for Patient 6.

<i>POLG</i> mutation	Patient	Complex I-19	Complex I-20	Complex I-30	Complex I-39
+	1	0%	10%	53%	11%
	2	0%	9%	14%	0%
?	7	2%	0%	N/A	N/A
	8	0%	0%	N/A	N/A
	9	68%	89%	N/A	N/A
	10	41%	24%	N/A	N/A

Table 4.6. Table of complex I deficiency in neurons of the dentate nucleus in the cerebellum.

Percentage of deficiency defined as deficient (-) and weak (+) neuron counts combined. One hundred neurons were counted with each antibody in each patient. Where FFPE tissue is unavailable or is known to have been fixed for longer than 6 months, no values are given.

Key: N/A=not available

4.4.2.2.2 *Complex II – Succinate: Ubiquinone Oxidoreductase*

Patients with evidence for *POLG* mutations or with no genetic diagnosis available show no deficiency (Figure 4.8). The controls show no evidence of deficiency.

There is no evidence for complex II deficiency in these patients. A single patient, Patient 10, showed moderate levels of deficiency in the Purkinje cells but not in the neurons of the dentate nucleus.

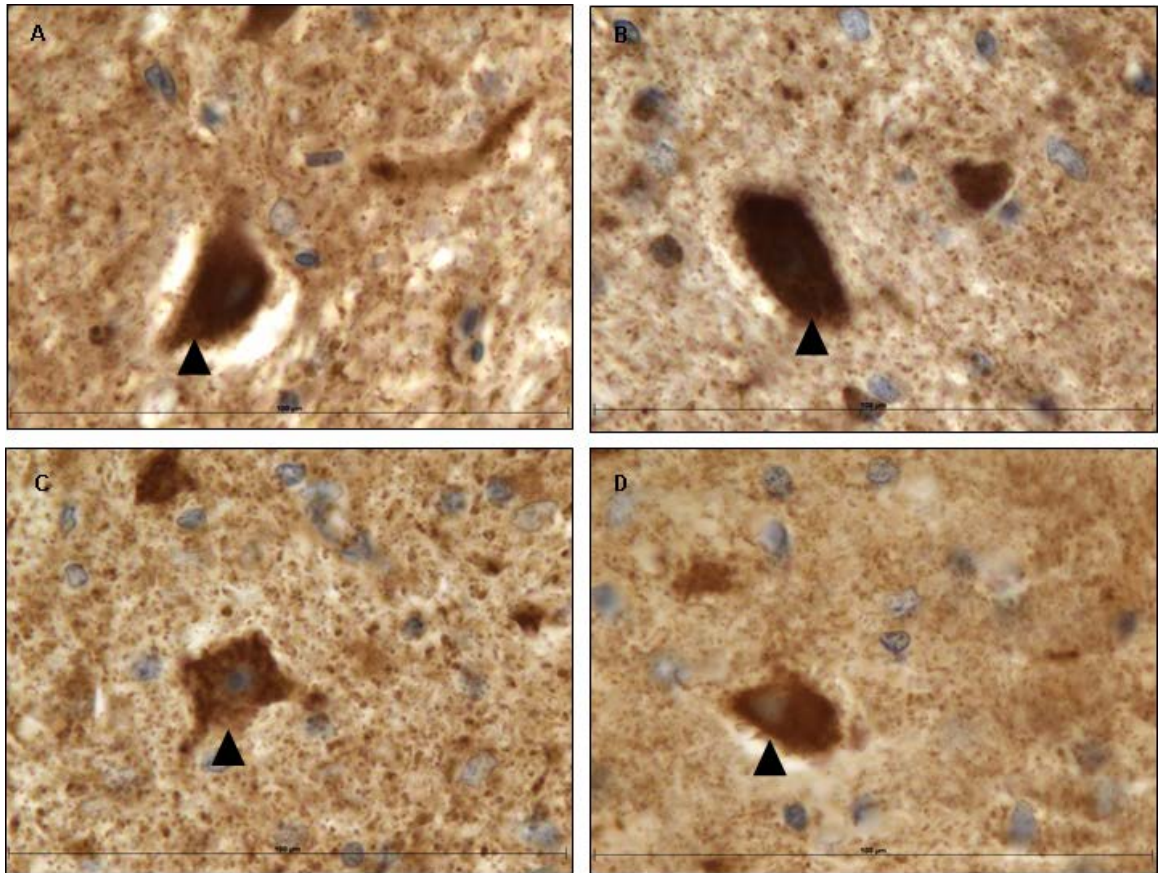


Figure 4.8. Staining with antibodies for complex II in neurons of the dentate nucleus in the cerebellum.

Arrowheads indicate neurons. All sections stained with complex II subunit 70 antibody. A=Control 6, B=Patient 1 *POLG* mutation-positive group, C=Patient 2 *POLG* mutation-positive group, D=Patient 10 *POLG* mutation-undetermined group. Scale bar = 100 μ m.

4.4.2.2.3 Complex III – Ubiquinol Cytochrome c Reductase

Patients with evidence for *POLG* mutations show a variable deficiency. Patient 1 shows no deficiency while Patient 2 shows a moderate deficiency (Figure 4.9; image B).

Patients with no genetic diagnosis available (Figure 4.9; images C and D) also show a variable deficiency. This ranges from no deficiency in Patient 10 to a moderate deficiency in Patient 7. Patient 2 shows moderate levels of complex III deficiency but is the only patient not to exhibit a complex I deficiency in this part of the brain.

There is a variable complex III deficiency in the dentate nucleus across both *POLG* groups. Patient 2 and Patient 7 show a moderate deficiency whilst Patient 1 and Patient 10 show no deficiency at all. The control shows no evidence of deficiency.

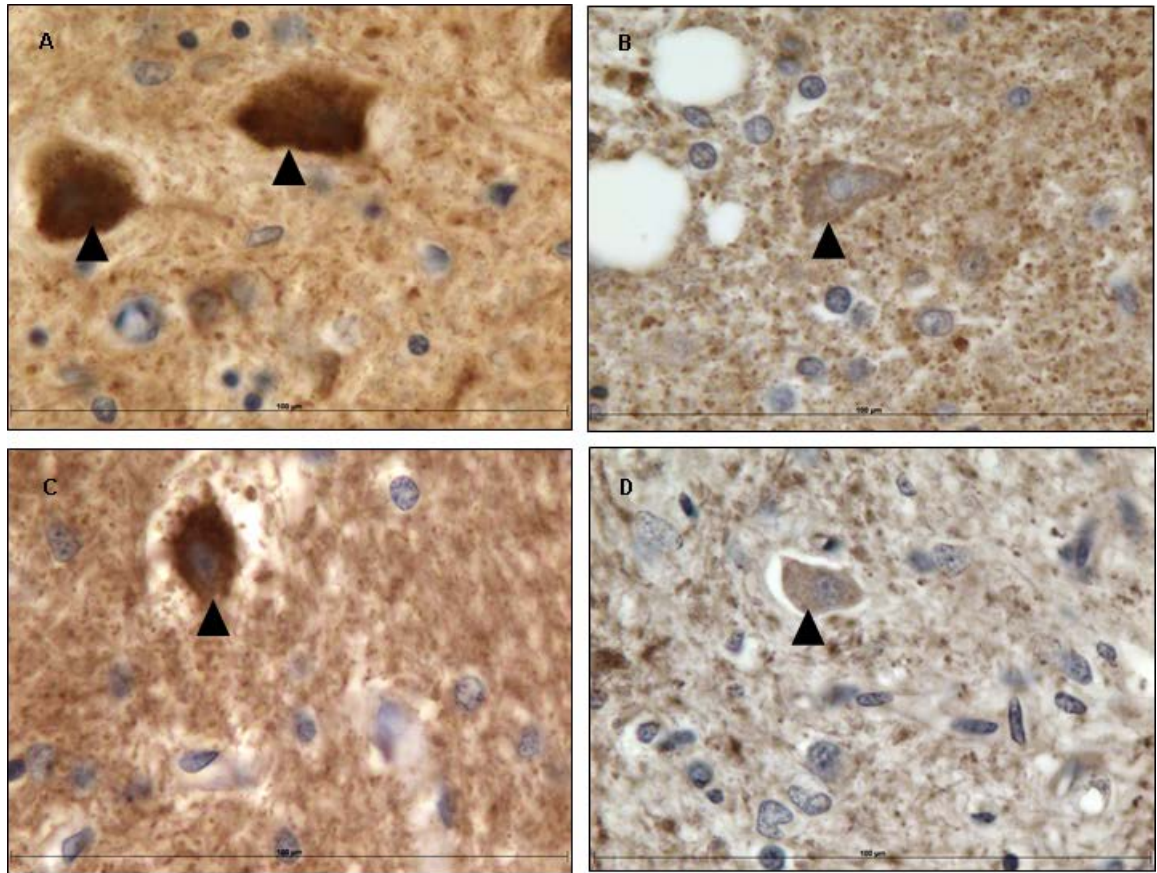


Figure 4.9. Staining with antibodies for complex III Rieske subunit in neurons of the dentate nucleus in the cerebellum.

Arrowheads indicate neurons. All sections stained with complex III Rieske subunit antibody. A=Control 10, B=Patient 2 *POLG* mutation-positive group, C=Patient 10 *POLG* mutation-undetermined group, D=Patient 11 *POLG* mutation-undetermined group. Scale bar = 100µm.

Deficiency values are shown in Table 4.7. The brain area is unavailable for patients not listed in the table. The availability of the dentate nucleus was dependent upon the orientation of the sample taken by the original pathology team. In some patients, this led to the dentate nucleus being unavailable for analysis, as for Patient 6 and Patient 11. This antibody stain could not be performed for Patient 9 as the supply of tissue was depleted.

<i>POLG</i> mutation	Patient	Complex III-Rieske
+	1	0%
	2	47%
?	7	49%
	8	10%
	10	0%

Table 4.7. Table of complex III deficiency in neurons of the dentate nucleus in the cerebellum.

Percentage of deficiency defined as deficient (-) and weak (+) neuron counts combined. One hundred neurons were counted in each patient. Where FFPE tissue is unavailable or is known to have been fixed for longer than 6 months, no values are given.

4.4.2.2.4 *Complex IV – Cytochrome c Oxidase*

Patients with evidence for *POLG* mutations show no complex IV subunit I deficiency (Figure 4.10; image B) and show no complex IV subunit IV deficiency (Figure 4.11; image B).

Patients with no genetic diagnosis available show a moderate complex IV subunit I deficiency in Patient 7 and Patient 9 only (Figure 4.10; images C and D). There is no complex IV subunit IV deficiency (Figure 4.11; images C and D).

The control shows no evidence of deficiency for both subunits.

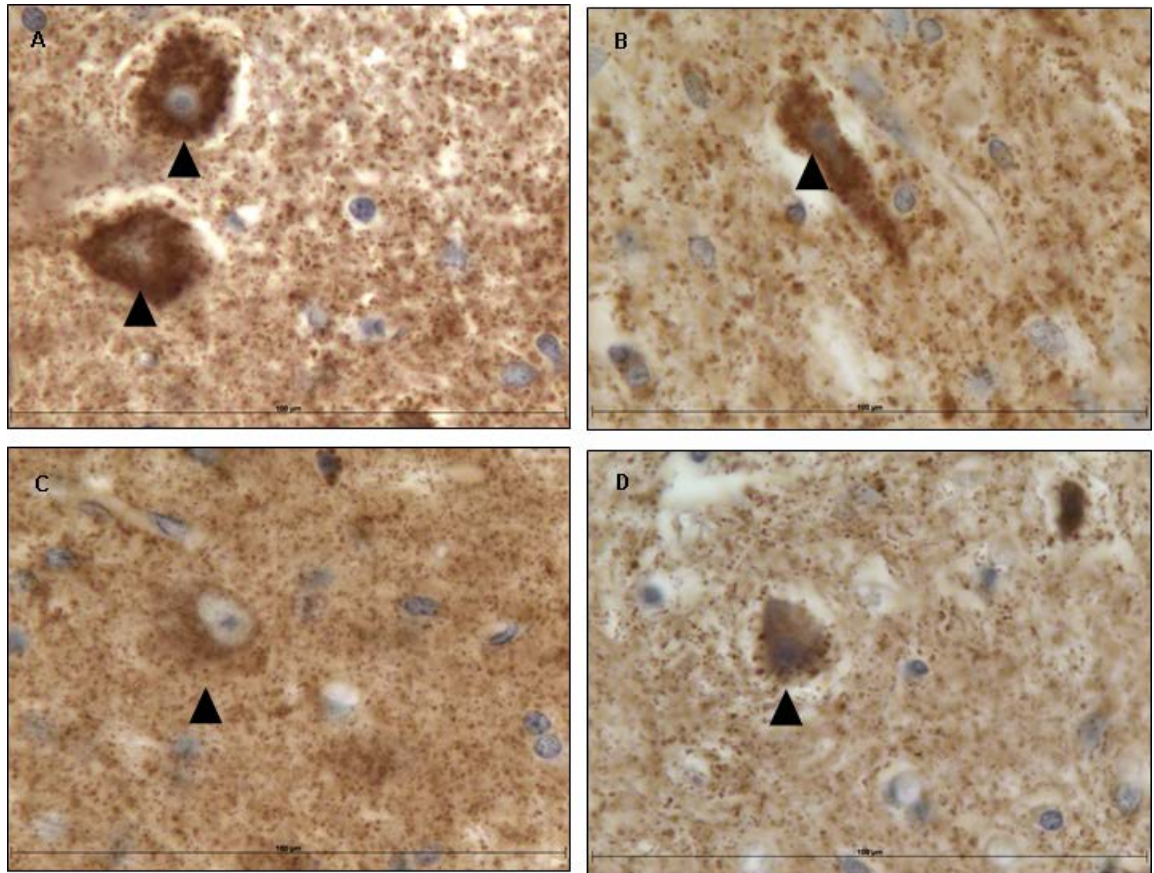


Figure 4.10. Staining with antibodies for complex IV subunit I in neurons of the dentate nucleus in the cerebellum.

Arrowheads indicate neurons. All sections stained with complex IV subunit I antibody. A=Control 1, B=Patient 2 *POLG* mutation-positive group, C=Patient 7 *POLG* mutation-undetermined group, D=Patient 9 *POLG* mutation-undetermined group. Scale bar = 100µm.

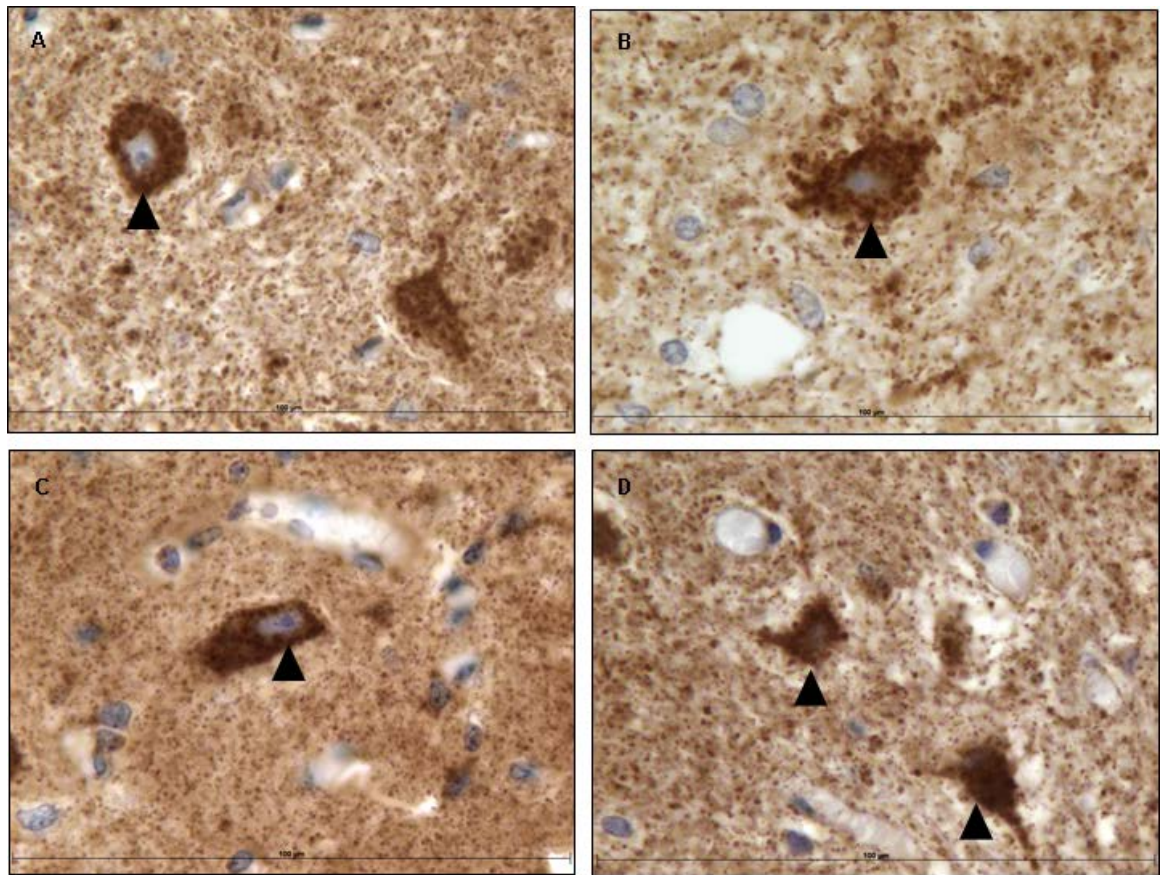


Figure 4.11. Staining with antibodies for complex IV subunit IV in neurons of the dentate nucleus in the cerebellum.

Arrowheads indicate neurons. All sections stained with complex IV subunit IV antibody. A=Control 1, B=Patient 2 *POLG* mutation-positive group, C=Patient 7 *POLG* mutation-undetermined group, D=Patient 9 *POLG* mutation-undetermined group. Scale bar = 100µm.

Deficiency values for both subunits are shown in Table 4.8. The brain area is unavailable for patients not listed in the table. The availability of the dentate nucleus was dependent upon the orientation of the sample taken by the original pathology team. In some patients, this led to the dentate nucleus being unavailable for analysis, as for Patient 6 and Patient 11.

<i>POLG</i> mutation	Patient	Complex IV-I	Complex IV-IV
+	1	2%	0%
	2	0%	0%
?	7	22%	0%
	8	0%	0%
	9	17%	1%
	10	0%	0%

Table 4.8. Table of complex IV deficiency in neurons of the dentate nucleus in the cerebellum.

Percentage of deficiency defined as deficient (-) and weak (+) neuron counts combined. One hundred neurons were counted with each antibody in each patient. Where FFPE tissue is unavailable or is known to have been fixed for longer than 6 months, no values are given.

A summary of respiratory chain deficiency values for the cerebellum is detailed in Table 4.9.

<i>POLG</i> mutation	Patient	Purkinje Cells								Dentate Nucleus							
		CI-19	CI-20	CI-30	CI-39	CII-70	CIII	CIV-I	CIV-IV	CI-19	CI-20	CI-30	CI-39	CII-70	CIII	CIV-I	CIV-IV
+	1	8%	22%	0%	8%	0%	1%	1%	0%	0%	10%	53%	11%	0%	0%	2%	0%
	2	1%	1%	0%	N/A	1%	39%	0%	0%	0%	9%	14%	0%	0%	47%	0%	0%
	6	11%	12%	25%	19%	5%	27%	15%	0%	N/A	N/A	N/A	N/A	N/A	N/A	N/A	N/A
?	7	3%	2%	N/A	N/A	0%	30%	0%	0%	2%	0%	N/A	N/A	0%	49%	22%	0%
	8	10%	3%	N/A	N/A	0%	27%	1%	0%	0%	0%	N/A	N/A	0%	10%	0%	0%
	9	61%	21%	N/A	N/A	0%	N/A	33%	0%	68%	89%	N/A	N/A	0%	N/A	17%	1%
	10	44%	13%	N/A	N/A	28%	60%	10%	8%	41%	24%	N/A	N/A	0%	0%	0%	0%
	11	63%	38%	N/A	N/A	0%	68%	18%	14%	N/A	N/A	N/A	N/A	N/A	N/A	N/A	N/A

Table 4.9. Summary of respiratory chain deficiency in the cerebellum.

Percentage of deficiency defined as deficient (-) and weak (+) neuron counts combined. One hundred neurons were counted with each antibody in each patient. Where FFPE tissue is unavailable or is known to have been fixed for longer than 6 months, no values are given.

Key: N/A=not available

4.4.3 Occipital Lobe

Brodmann Area 19 (BA19) of the occipital lobe was examined.

4.4.3.1 Pyramidal Neurons of Layer V

4.4.3.1.1 Complex I – NADH: Ubiquinone Oxidoreductase

In a subset of patients, CI-19 and CI-20 antibodies were tested only, as it became apparent there was little additional information being added to the investigation through the inclusion of CI-30 and CI-39 antibodies.

Patients with evidence for *POLG* mutations (Figure 4.12; images B) show little evidence of complex I deficiency in all four of the complex I subunits tested.

Patients with no genetic diagnosis available (Figure 4.12; image D) show moderate levels of complex I deficiency in two of the complex I subunits tested.

The patient without a *POLG* mutation (Figure 4.12; image C) shows a moderate level of deficiency with CI-39 and little evidence of deficiency with the other subunits. The occipital lobe in this patient had a fixation time of 1 month, so was therefore included for respiratory chain analysis. The cerebellum, parietal lobe, and basal ganglia had a fixation time of 14 years.

There is a complex I deficiency in the occipital lobe of the *POLG* mutation-undetermined group. The *POLG* mutation-positive group and *POLG* mutation-absent group show no deficiency or very few neurons with deficiency. The control shows no evidence of deficiency.

The lack of respiratory chain deficiency in this brain area is in contrast to the neuropathology. Possible reasons for this are discussed in the Discussion section at the end of this chapter.

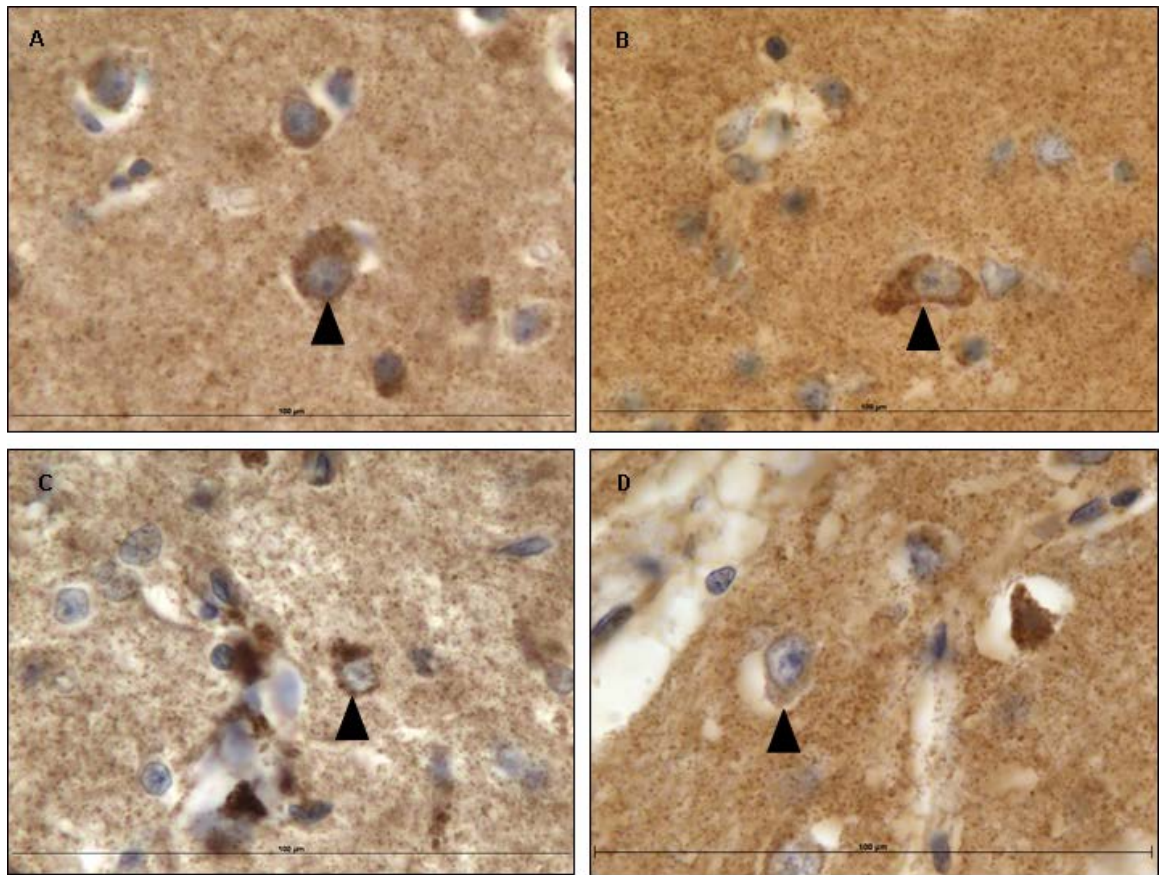


Figure 4.12. Staining with antibodies for complex I in the pyramidal neurons of the occipital lobe.

Arrowheads indicate neurons. All sections stained with complex I antibody. A=Control 7 CI-20, B=Patient 1 *POLG* mutation-positive group CI-20, C=Patient 12 *POLG* mutation-absent group CI-20, D=Patient 10 *POLG* mutation-undetermined group CI-20. Scale bar = 100µm.

Deficiency values for all subunits are shown in Table 4.10. The brain area is unavailable for patients not listed in the table.

<i>POLG</i> mutation	Patient	Complex I- 19	Complex I- 20	Complex I- 30	Complex I- 39
+	1	2%	2%	0%	3%
	2	2%	0%	0%	0%
?	8	14%	5%	N/A	N/A
	10	16%	8%	N/A	N/A
	11	2%	23%	N/A	N/A
-	12	0%	1%	0%	19%

Table 4.10. Table of complex I deficiency in the pyramidal neurons of the occipital lobe.

Values are given for neurons of layer V. Percentage of deficiency defined as deficient (-) and weak (+) neuron counts combined. One hundred neurons were counted with each antibody in each patient. Where FFPE tissue is unavailable or is known to have been fixed for longer than 6 months, no values are given.

Key: N/A=not available

4.4.3.1.2 Complex II – Succinate: Ubiquinone Oxidoreductase

Patients with evidence for *POLG* mutations, undetermined genetic diagnosis, or without a *POLG* mutation show no deficiency (Figure 4.13; images B, C and D).

There is no evidence for complex II deficiency in these patients. The controls show no evidence of deficiency.

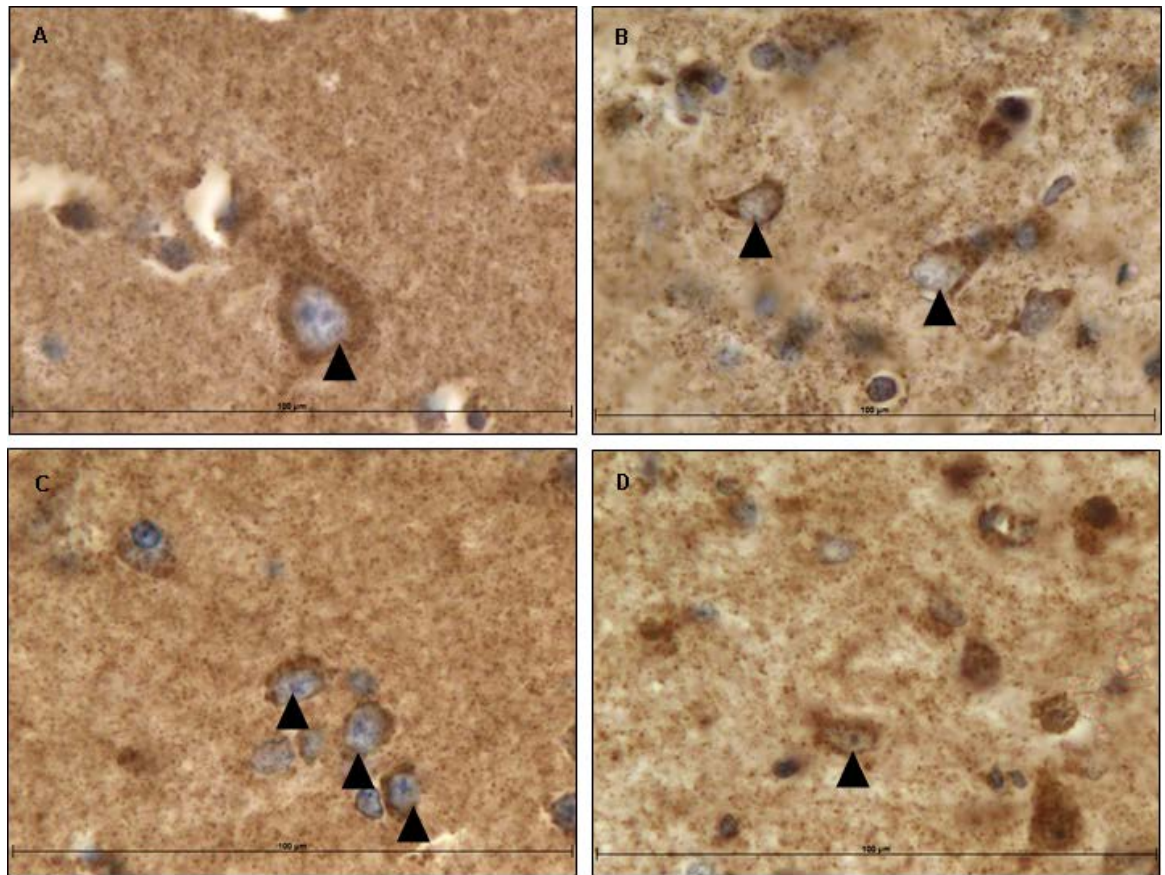


Figure 4.13. Staining with antibodies for complex II in the pyramidal neurons of the occipital lobe.

Arrowheads indicate neurons. All sections stained with complex II subunit 70 antibody. A=Control 7, B=Patient 12 *POLG* mutation-absent group, C=Patient 1 *POLG* mutation-positive group, D=Patient 2 *POLG* mutation-positive group. Scale bar = 100µm.

4.4.3.1.3 Complex III – Ubiquinol Cytochrome c Reductase

Patients with evidence for *POLG* mutations or without a *POLG* mutation (Figure 4.14; image C) show no complex III deficiency.

Patients with no genetic diagnosis available (Figure 4.14; images B and D) show moderate to high levels of complex III deficiency.

The control shows no evidence of deficiency.

Patient 10, no genetic diagnosis available, shows the highest complex III deficiency of 80% of all patients in all brain areas. The occipital lobe of this patient shows a moderate complex I deficiency of 16% CI-19 deficiency.

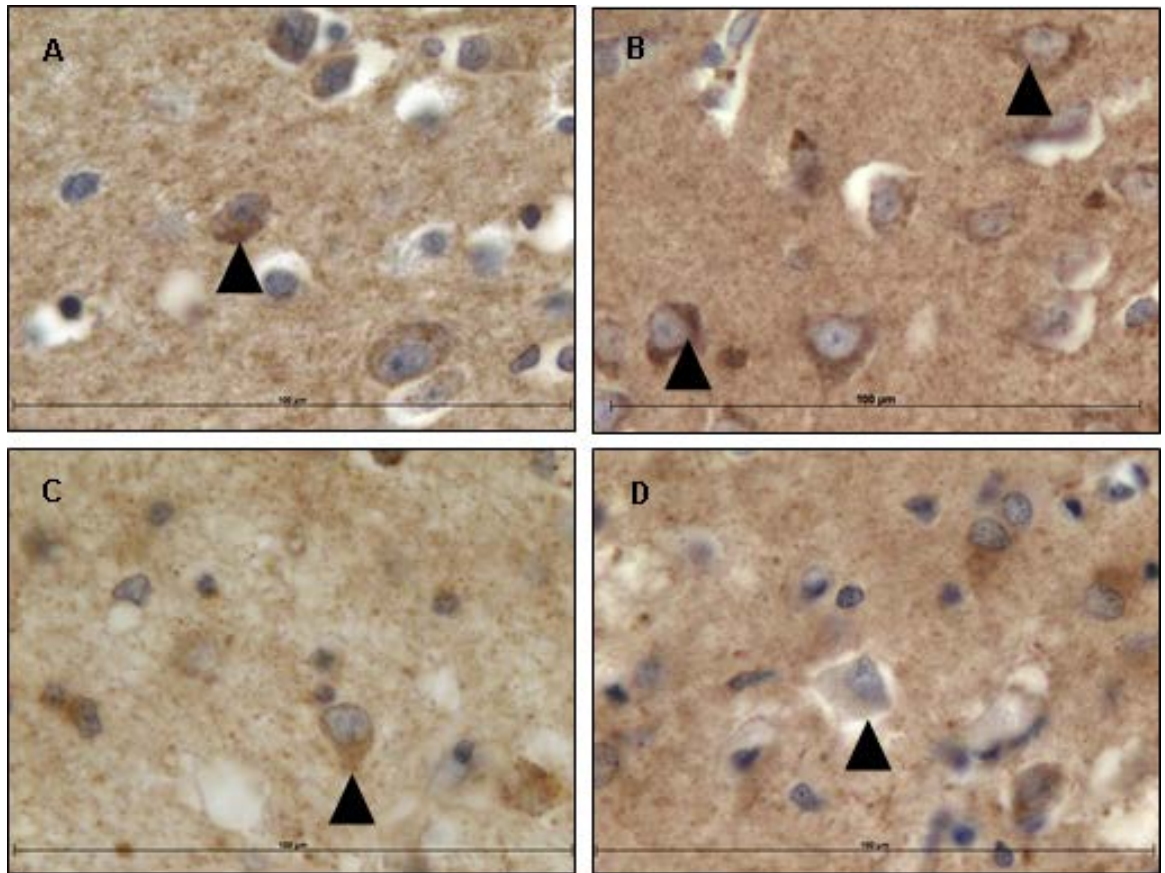


Figure 4.14. Staining with antibodies for complex III Rieske subunit in the pyramidal neurons of the occipital lobe.

Arrowheads indicate neurons. All sections stained with complex III Rieske subunit antibody. A=Control 7, B=Patient 8 *POLG* mutation-undetermined group, C=Patient 12 *POLG* mutation-absent group, D=Patient 11 *POLG* mutation-undetermined group. Scale bar = 100µm.

Deficiency values are shown in Table 4.11. The brain area is unavailable for patients not listed in the table. This antibody stain could not be performed for Patient 2 as the supply of tissue was depleted.

<i>POLG</i> mutation	Patient	Complex III-Rieske
+	1	0%
?	8	33%
	10	80%
	11	16%
-	12	0%

Table 4.11. Table of complex III deficiency in the pyramidal neurons of the occipital lobe.

Values are given for neurons of layer V. Percentage of deficiency defined as deficient (-) and weak (+) neuron counts combined. One hundred neurons were counted in each patient. Where FFPE tissue is unavailable or is known to have been fixed for longer than 6 months, no values are given.

4.4.3.1.4 Complex IV – Cytochrome c Oxidase

Patients with evidence for *POLG* mutations show no complex IV subunit I deficiency (Figure 4.15; images B and C) and no complex IV subunit IV deficiency (Figure 4.16; images C and D).

Patients with no genetic diagnosis available show little evidence of complex IV subunit I deficiency (Figure 4.15; image D). They show very little evidence of complex IV subunit IV deficiency.

The patient without a *POLG* mutation shows little evidence of complex IV subunit I deficiency and no complex IV subunit IV deficiency (Figure 4.16; image B). The occipital lobe in this patient had a fixation time of 1 month, so was therefore included for respiratory chain analysis. The cerebellum, parietal lobe, and basal ganglia had a fixation time of 14 years.

The control shows no evidence of deficiency for both subunits.

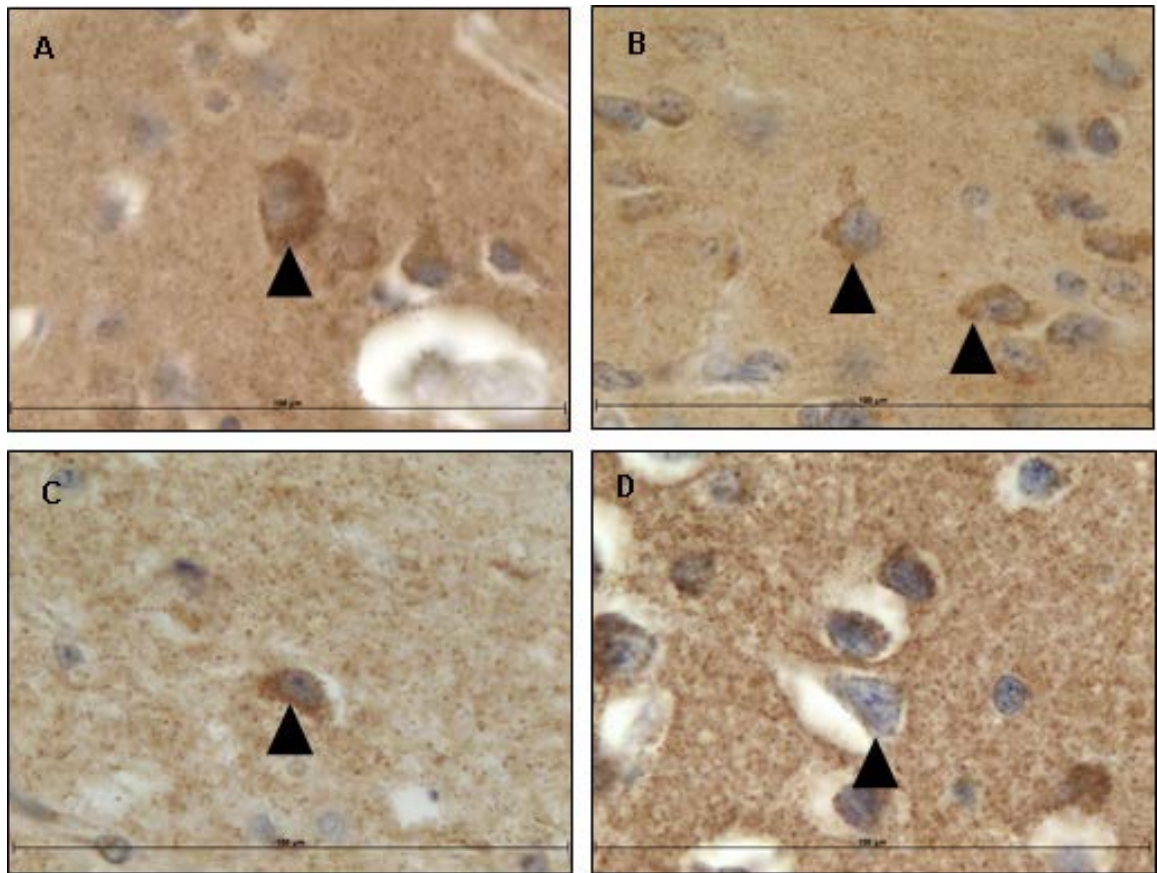


Figure 4.15. Staining with antibodies for complex IV subunit I in pyramidal neurons of the occipital lobe.

Arrowheads indicate neurons. All sections stained with complex IV subunit I antibody. A=Control 7, B=Patient 1 *POLG* mutation-positive group, C=Patient 2 *POLG* mutation-positive group, D=Patient 10 *POLG* mutation-undetermined group. Scale bar = 100µm.

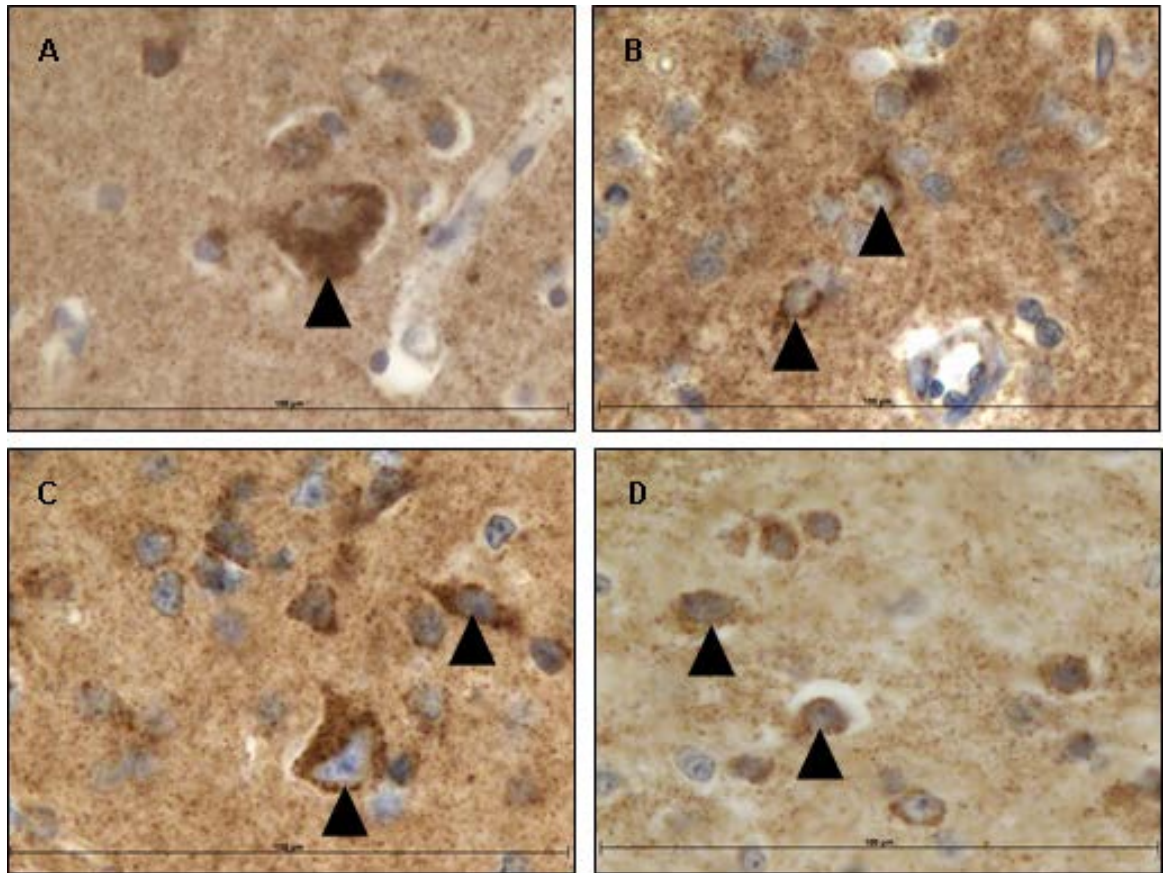


Figure 4.16. Staining with antibodies for complex IV subunit IV in pyramidal neurons of the occipital lobe.

Arrowheads indicate neurons. All sections stained with complex IV subunit IV antibody. A=Control 7, B=Patient 12 *POLG* mutation-absent group, C=Patient 1 *POLG* mutation-positive group, D=Patient 2 *POLG* mutation-positive group. Scale bar = 100 μ m.

Deficiency values for both subunits are shown in Table 4.12. The brain area is unavailable for patients not listed in the table.

<i>POLG</i> mutation	Patient	Complex IV-I	Complex IV-IV
+	1	0%	0%
	2	0%	0%
?	8	10%	1%
	10	18%	0%
	11	14%	1%
-	12	3%	0%

Table 4.12. Table of complex IV deficiency in the pyramidal neurons of the occipital lobe.

Values are given for neurons of layer V. Percentage of deficiency defined as deficient (-) and weak (+) neuron counts combined. One hundred neurons were counted with each antibody in each patient. Where FFPE tissue is unavailable or is known to have been fixed for longer than 6 months, no values are given.

A summary of respiratory chain deficiency values for the occipital lobe is detailed in Table 4.13.

		Occipital Lobe							
<i>POLG</i> mutation	Patient	CI-19	CI-20	CI-30	CI-39	CII-70	CIII	CIV-I	CIV-IV
+	1	2%	2%	3%	0%	0%	0%	0%	0%
	2	2%	0%	0%	0%	0%	N/A	0%	0%
?	8	14%	5%	N/A	N/A	0%	33%	10%	1%
	10	16%	8%	N/A	N/A	0%	80%	18%	0%
	11	2%	23%	N/A	N/A	0%	16%	14%	1%
-	12	0%	1%	0%	19%	0%	0%	3%	0%

Table 4.13. Summary of respiratory chain deficiency in the occipital lobe.

Values are given for neurons of layer V. Percentage of deficiency defined as deficient (-) and weak (+) neuron counts combined. One hundred neurons were counted with each antibody in each patient. Where FFPE tissue is unavailable or is known to have been fixed for longer than 6 months, no values are given.

Key: N/A=not available

4.4.4 Parietal Lobe

Brodmann Area 40 (BA40) of the parietal lobe was examined.

4.4.4.1 Pyramidal Neurons of Layer V

4.4.4.1.1 Complex I – NADH: Ubiquinone Oxidoreductase

In a subset of patients, CI-19 and CI-20 antibodies were tested only, as it became apparent there was little additional information being added to the investigation through the inclusion of CI-30 and CI-39 antibodies.

Patients with evidence for *POLG* mutations (Figure 4.17; images B, C and D) show either no deficiency or very few neurons with deficiency in complex I-30. The *POLG* mutation-undetermined group consisted of only one patient, Patient 8, which shows a particular deficiency in complex I-19.

The control shows no evidence of deficiency.

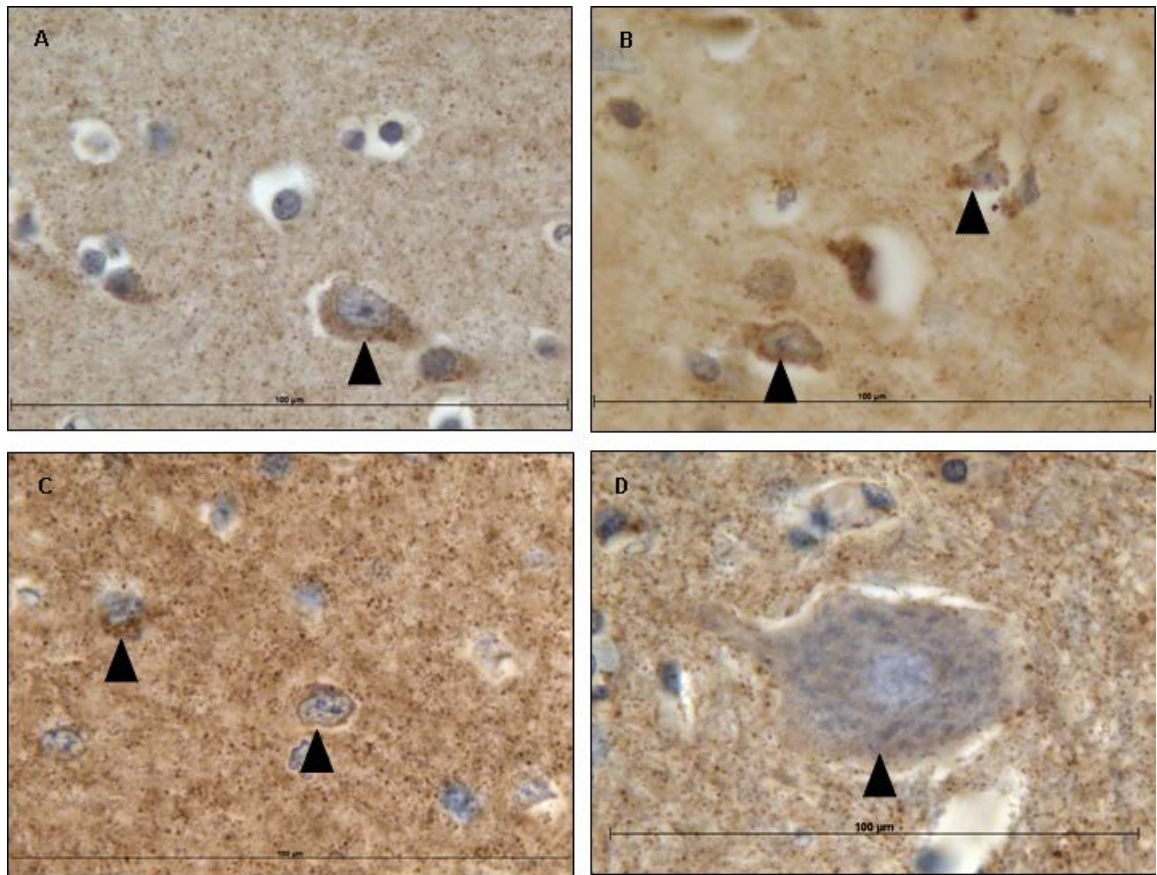


Figure 4.17. Staining with antibodies for complex I in the pyramidal neurons of the parietal lobe.

Arrowheads indicate neurons. All sections stained with complex I antibody. A=Control 7 CI-30, B=Patient 2 *POLG* mutation-positive group CI-30, C=Patient 1 *POLG* mutation-positive group CI-30, D=Patient 6 *POLG* mutation-positive group CI-30. Scale bar = 100µm.

Deficiency values for all subunits are shown in Table 4.14. The brain area is unavailable for patients not listed in the table.

<i>POLG</i> mutation	Patient	Complex I- 19	Complex I- 20	Complex I- 30	Complex I- 39
+	1	0%	0%	4%	2%
	2	5%	0%	9%	0%
	6	0%	1%	17%	0%
?	8	53%	19%	N/A	N/A

Table 4.14. Table of complex I deficiency in the pyramidal neurons of the parietal lobe.

Values are given for neurons of layer V. Percentage of deficiency defined as deficient (-) and weak (+) neuron counts combined. One hundred neurons were counted with each antibody in each patient. Where FFPE tissue is unavailable or is known to have been fixed for longer than 6 months, no values are given.

Key: N/A=not available

4.4.4.1.2 Complex II – Succinate: Ubiquinone Oxidoreductase

Patients with evidence for *POLG* mutations, undetermined genetic diagnosis, or without a *POLG* mutation show no deficiency (<2%) (Figure 4.18; images B, C and D).

There is no evidence for complex II deficiency in these patients. The controls show no evidence of deficiency.

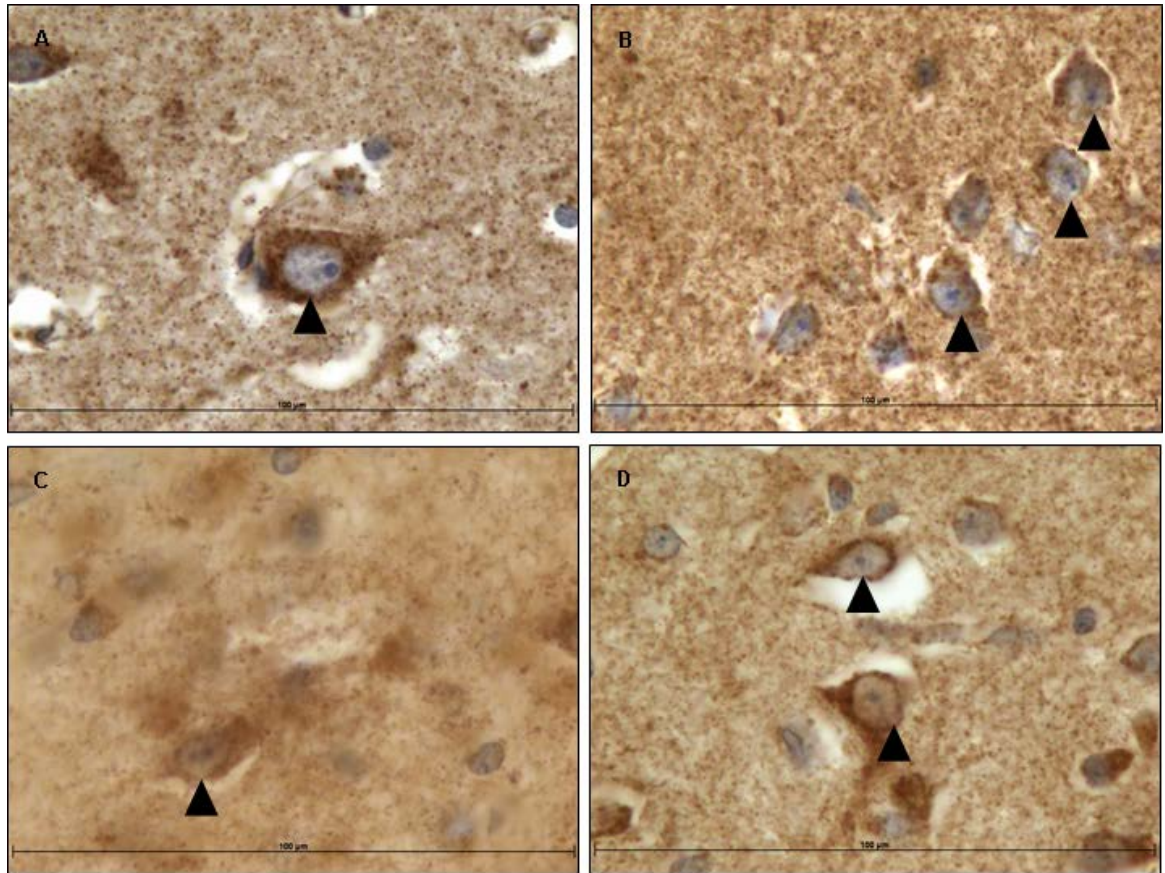


Figure 4.18. Staining with antibodies for complex II in the pyramidal neurons of the parietal lobe.

Arrowheads indicate neurons. All sections stained with complex II subunit 70 antibody. A=Control 7, B=Patient 1 *POLG* mutation-positive group, C=Patient 2 *POLG* mutation-positive group, D=Patient 8 *POLG* mutation-undetermined group. Scale bar = 100µm.

Deficiency values are shown in Table 4.15. The brain area is unavailable for patients not listed in the table.

<i>POLG</i> mutation	Patient	Complex II-70
+	1	2%
	2	0%
	6	0%
?	8	0%

Table 4.15. Table of complex II deficiency in the pyramidal neurons of the parietal lobe.

Percentage of deficiency defined as deficient (-) and weak (+) neuron counts combined. One hundred neurons were counted in each patient. Where FFPE tissue is unavailable or is known to have been fixed for longer than 6 months, no values are given.

4.4.4.1.3 Complex III – Ubiquinol Cytochrome c Reductase

Patients with evidence for *POLG* mutations (Figure 4.19; images B, C and D) show little evidence of complex III deficiency.

There was one patient, Patient 8, from the group with no genetic diagnosis available where the parietal lobe could be assessed. Patient 8 shows little evidence of complex III deficiency.

The control shows no evidence of deficiency.

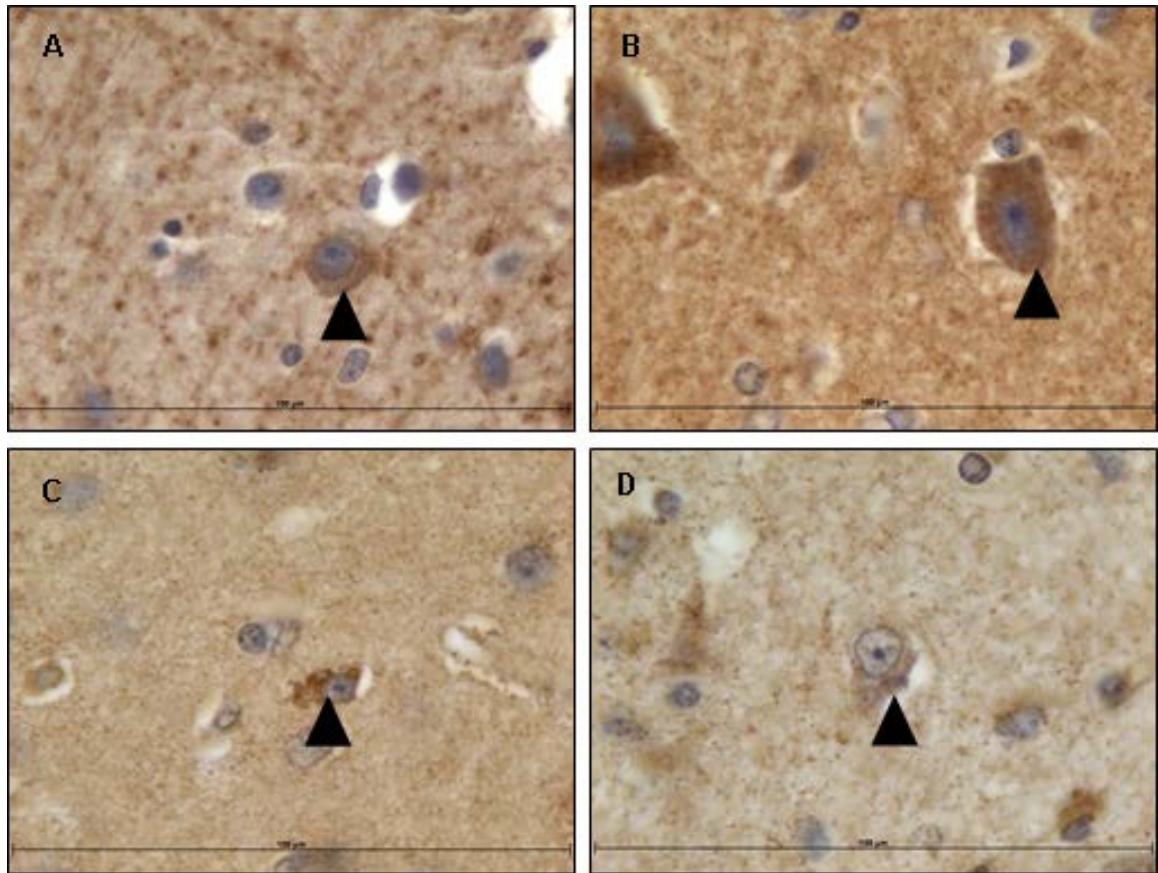


Figure 4.19. Staining with antibodies for complex III Rieske subunit in the pyramidal neurons of the parietal lobe.

Arrowheads indicate neurons. All sections stained with complex III Rieske subunit antibody. A=Control 7, B=Patient 6 *POLG* mutation-positive group, C=Patient 1 *POLG* mutation-positive group, D=Patient 2 *POLG* mutation-positive group. Scale bar = 100µm.

Deficiency values are shown in Table 4.16. The brain area is unavailable for patients not listed in the table.

<i>POLG</i> mutation	Patient	Complex III-Rieske
+	1	0%
	2	15%
	6	1%
?	8	13%

Table 4.16. Table of complex III deficiency in the pyramidal neurons of the parietal lobe.

Values are given for neurons of layer V. Percentage of deficiency defined as deficient (-) and weak (+) neuron counts combined. One hundred neurons were counted in each patient. Where FFPE tissue is unavailable or is known to have been fixed for longer than 6 months, no values are given.

4.4.4.1.4 *Complex IV – Cytochrome c Oxidase*

Patients with evidence for *POLG* mutations show little evidence of complex IV subunit I deficiency (Figure 4.20; images A, B and C) and no complex IV subunit IV deficiency (Figure 4.21; images A, B and C).

There was only one patient, Patient 8, from the group with no genetic diagnosis available where the parietal lobe could be assessed. Patient 8 shows little evidence of complex IV subunit I deficiency and little evidence of complex IV subunit IV deficiency.

The control shows no evidence of deficiency for both subunits.

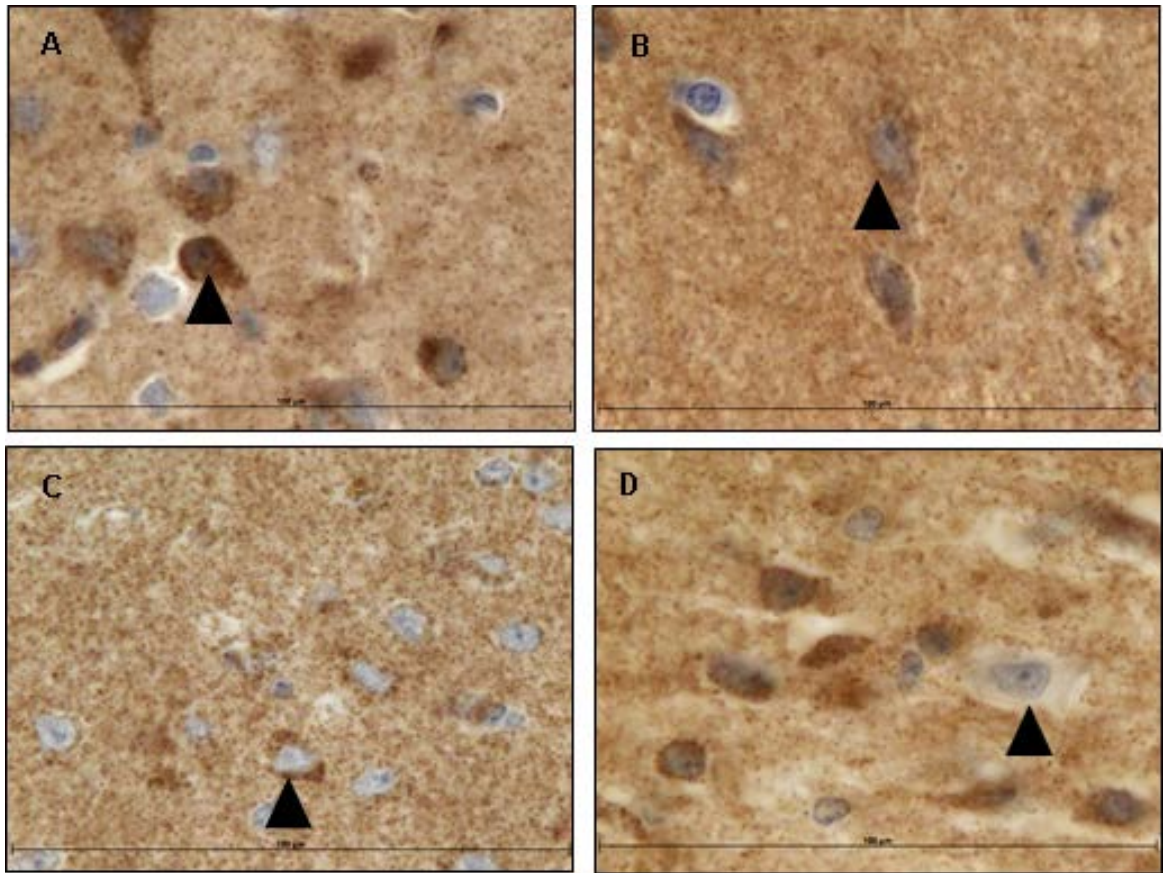


Figure 4.20. Staining with antibodies for complex IV subunit I in pyramidal neurons of the parietal lobe.

Arrowheads indicate neurons. All sections stained with complex IV subunit I antibody. A=Control 1, B=Patient 6 *POLG* mutation-positive group, C=Patient 1 *POLG* mutation-positive group, D=Patient 2 *POLG* mutation-positive group. Scale bar = 100µm.

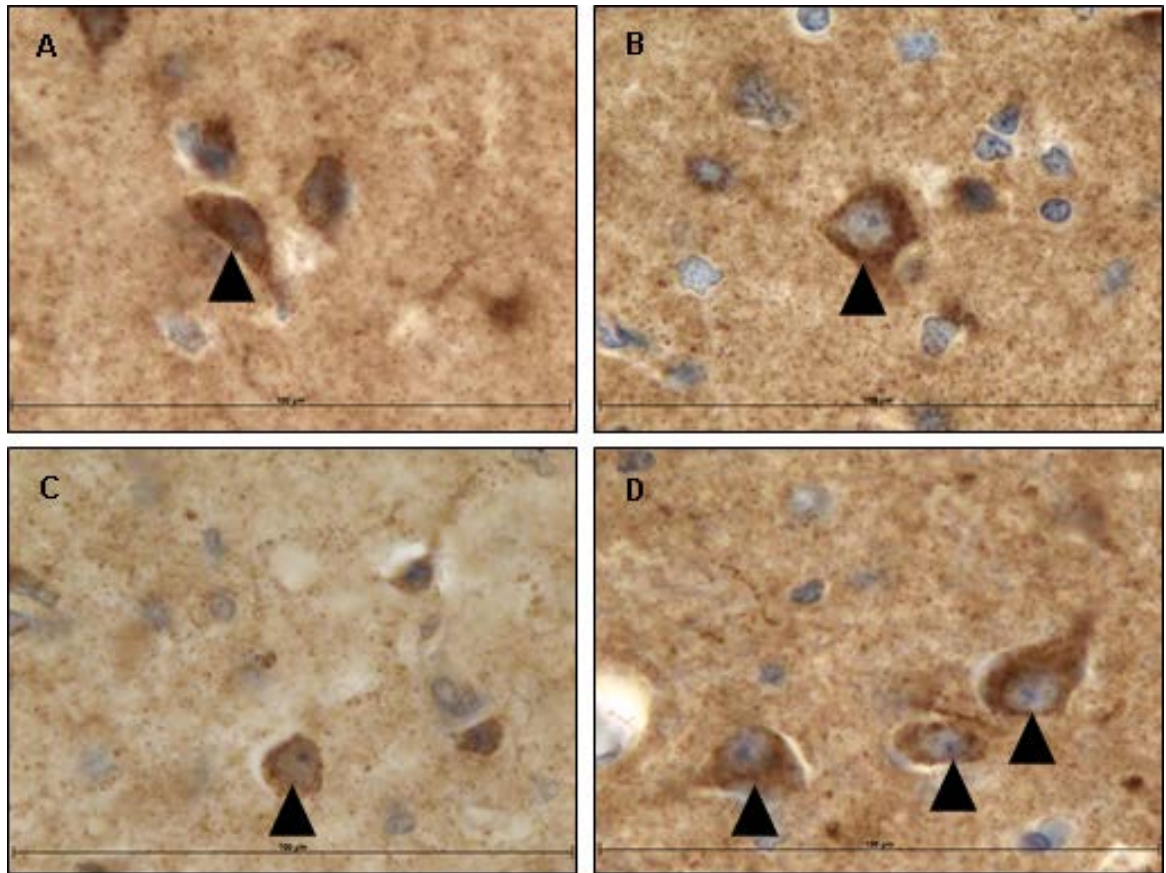


Figure 4.21. Staining with antibodies for complex IV subunit IV in pyramidal neurons of the parietal lobe.

Arrowheads indicate neurons. All sections stained with complex IV subunit IV antibody. A=Control 1, B=Patient 1 *POLG* mutation-positive group, C=Patient 2 *POLG* mutation-positive group, D=Patient 6 *POLG* mutation-positive group. Scale bar = 100µm.

Deficiency values for both subunits are shown in Table 4.17. The brain area is unavailable for patients not listed in the table.

<i>POLG</i> mutation	Patient	Complex IV-I	Complex IV-IV
+	1	5%	0%
	2	3%	0%
	6	0%	0%
?	8	4%	3%

Table 4.17. Table of complex IV deficiency in the pyramidal neurons of the parietal lobe.

Values are given for neurons of layer V. Percentage of deficiency defined as deficient (-) and weak (+) neuron counts combined. One hundred neurons were counted with each antibody in each patient. Where FFPE tissue is unavailable or is known to have been fixed for longer than 6 months, no values are given.

A summary of respiratory chain deficiency values for the parietal lobe is detailed in Table 4.18.

		Parietal Lobe							
<i>POLG</i> mutation	Patient	CI-19	CI-20	CI-30	CI-39	CII-70	CIII	CIV-I	CIV-IV
+	1	0%	0%	4%	2%	2%	0%	5%	0%
	2	5%	0%	9%	0%	0%	15%	3%	0%
	6	0%	1%	17%	0%	0%	1%	0%	0%
?	8	53%	19%	N/A	N/A	0%	13%	4%	3%

Table 4.18. Summary of respiratory chain deficiency in the parietal lobe.

Values are given for neurons of layer V. Percentage of deficiency defined as deficient (-) and weak (+) neuron counts combined. One hundred neurons were counted with each antibody in each patient. Where FFPE tissue is unavailable or is known to have been fixed for longer than 6 months, no values are given.

Key: N/A=not available

4.4.5 Basal Ganglia

4.4.5.1 Caudate, Putamen, and Globus Pallidus

The basal ganglia is a structure of grey matter located deep in the white matter of the cerebrum. It functions in control of voluntary movement and cognitive functions. It consists of well-defined areas; the caudate, the putamen, the medial globus pallidus, and the lateral globus pallidus. The caudate and putamen are together named the striate nucleus because they contain the same inhibitory classes of neurons; medium spiny neurons, and both GABA-ergic and cholinergic interneurons. These two structures are separated by a tract of axons named the internal capsule. The striate nucleus receives input mainly from the frontal lobe and also from the cerebral cortex, and the output from the striate nucleus acts upon the substantia nigra and globus pallidus to regulate voluntary motor function. The caudate and putamen may have different functions: the caudate affecting eye movements and cognitive functions, and the putamen affecting motor control. The putamen and the globus pallidus together are named lentiform nucleus. The lentiform nucleus receives input from the striate nucleus and acts upon the subthalamic nucleus to modulate motor function.

The availability of each of the caudate, putamen, and globus pallidus for analysis was dependent upon the precise location of the sample that was taken by the original pathology team. In some patients, this led to two of the three areas being available for analysis.

4.4.5.1.1 Complex I – NADH: Ubiquinone Oxidoreductase

In a subset of patients, CI-19 and CI-20 antibodies were tested only, as it became apparent there was little additional information being added to the investigation through the inclusion of CI-30 and CI-39 antibodies.

Patients with evidence for *POLG* mutations (Figure 4.22; images C) show low to moderate levels of complex I deficiency in all four of the complex I subunits tested.

Patients with no genetic diagnosis available (Figure 4.22; images B and D) show low to moderate levels of complex I deficiency in two of the complex I subunits tested.

The *POLG* mutation-undetermined group shows a complex I deficiency in the basal ganglia in complex I-19 and complex I-20. The *POLG* mutation-positive group shows deficiency in complex I-20 and complex I-39. The control shows no evidence of deficiency.

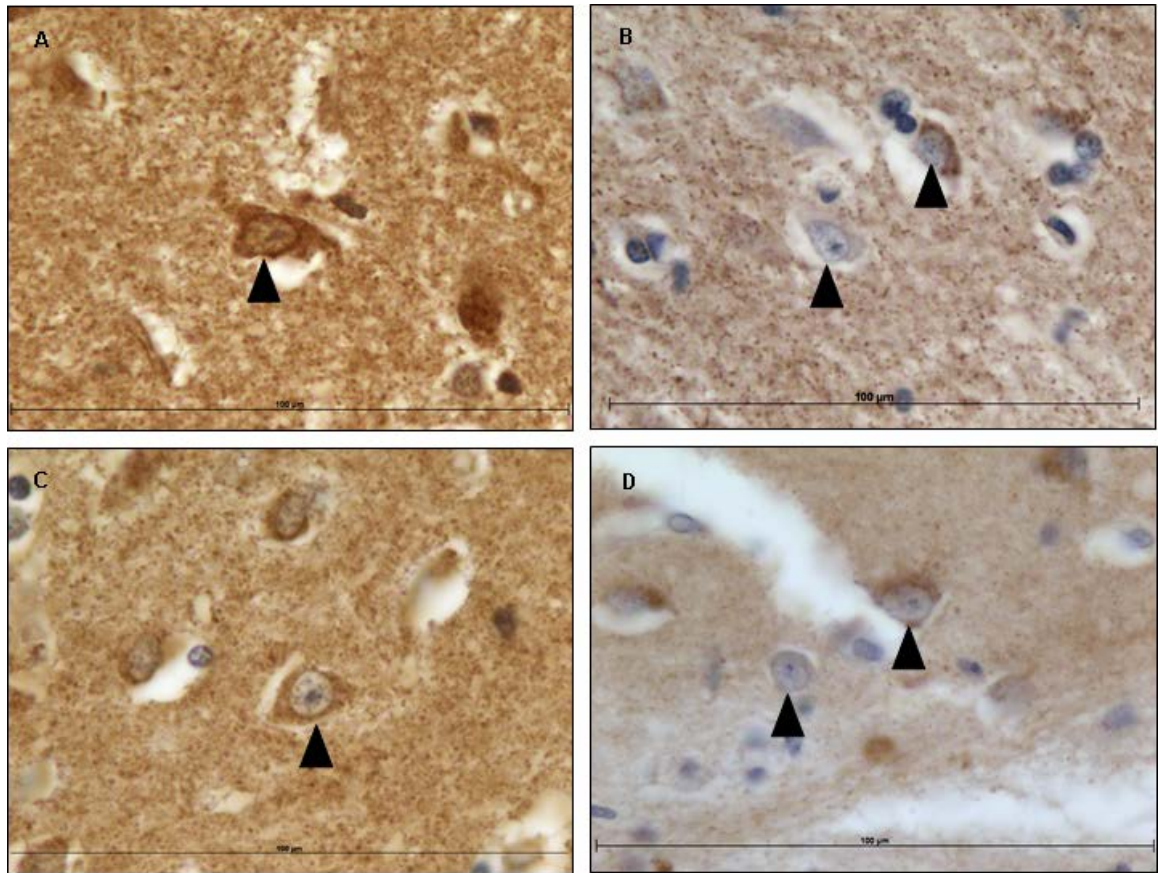


Figure 4.22. Staining with antibodies for complex I in neurons of the basal ganglia.

Arrowheads indicate neurons. All sections stained with complex I antibody. A=Control 6 CI-19, B=Patient 11 *POLG* mutation-undetermined group CI-19, C=Patient 1 *POLG* mutation-positive group CI-19, D=Patient 10 *POLG* mutation-undetermined group CI-19. All images are taken of the putamen. Scale bar = 100µm.

Deficiency values for all subunits are shown in Table 4.19. The brain area is unavailable for patients not listed in the table. Complex I-30 and complex I-39 results are not included as they were only available for Patient 1 and did not show extreme deficiency.

POLG mutation	Patient	Complex I-19	Complex I-20
+	1	C – 0%	C – 18%
		P – 2%	P – 1%
		GP – 0%	GP – 3%
?	8	C – N/A	C – N/A
		P – 10%	P – 2%
		GP – 4%	GP – 0%
	9	C – 13%	C – 14%
		P – 41%	P – 7%
		GP – 26%	GP – 0%
	10	C – N/A	C – N/A
		P – 0%	P – 0%
		GP – 0%	GP – 0%
	11	C – 15%	C – 12%
		P – 19%	P – 19%
		GP – 18%	GP – N/A

Table 4.19. Table of complex I deficiency in the basal ganglia.

Values are given for neurons from the caudate, putamen, and globus pallidus. Percentage of deficiency defined as deficient (-) and weak (+) neuron counts combined. One hundred neurons were counted with each antibody in each patient. Where FFPE tissue is unavailable or is known to have been fixed for longer than 6 months, no values are given.

Key: N/A=not available, C=caudate, P=putamen, GP=globus pallidus

4.4.5.1.2 Complex II – Succinate: Ubiquinone Oxidoreductase

Patients with evidence for *POLG* mutations, undetermined genetic diagnosis, or without a *POLG* mutation show no deficiency (<6%) (Figure 4.23; images B, C and D).

There is no evidence for complex II deficiency in these patients. The controls show no evidence of deficiency.

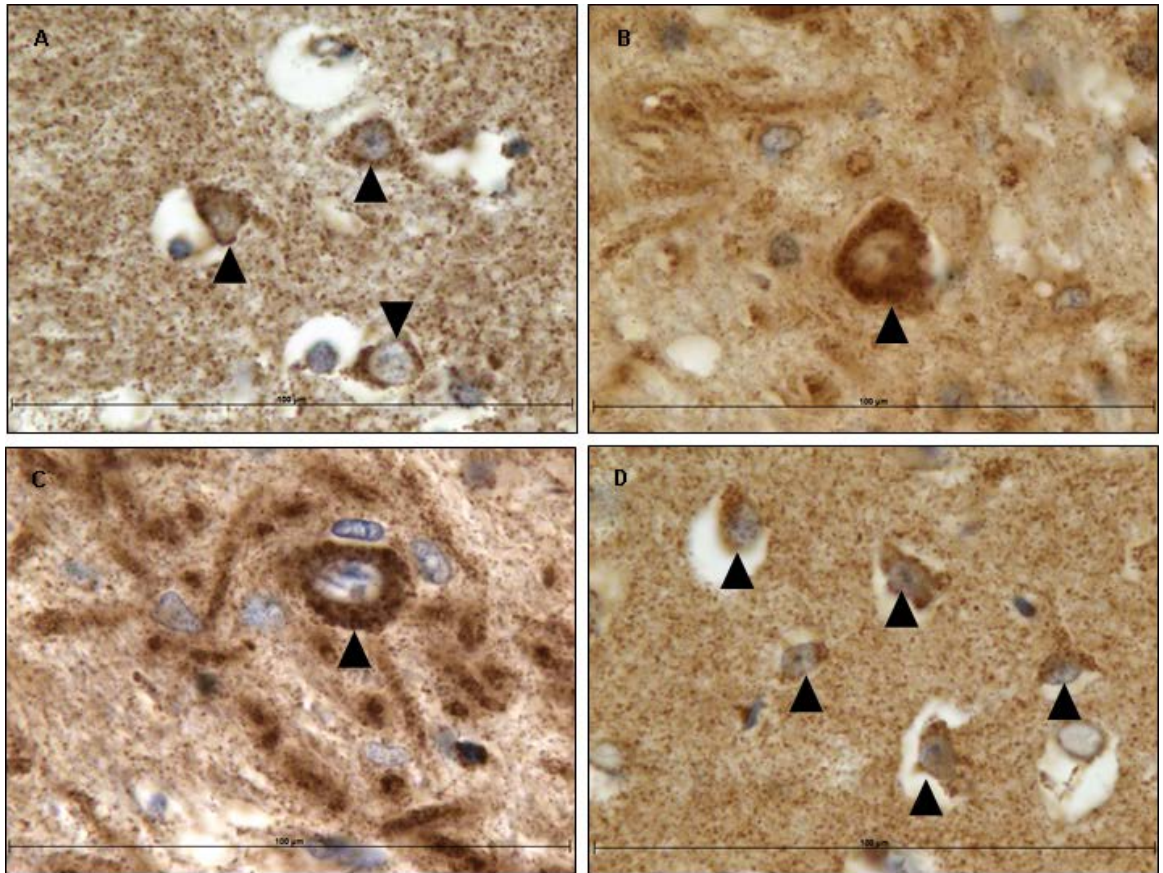


Figure 4.23. Staining with antibodies for complex II in neurons of the basal ganglia.

Arrowheads indicate neurons. All sections stained with complex II subunit 70 antibody. A=Control 6 putamen, B=Patient 11 *POLG* mutation-undetermined group globus pallidus, C=Patient 1 *POLG* mutation-positive group globus pallidus, D=Patient 9 *POLG* mutation-undetermined group putamen. Scale bar = 100µm.

Deficiency values are shown in Table 4.20. The brain area is unavailable for patients not listed in the table.

<i>POLG</i> mutation	Patient	Complex II-70
+	1	C – 0%
		P – 1%
		GP – 0%
?	8	C – N/A
		P – 0%
		GP – 0%
	9	C – 0%
		P – 1%
		GP – 6%
	10	C – N/A
		P – 0%
		GP – 0%
	11	C – 0%
		P – 0%
		GP – 0%

Table 4.20. Table of complex II deficiency in the basal ganglia.

Percentage of deficiency defined as deficient (-) and weak (+) neuron counts combined. One hundred neurons were counted in each patient. Where FFPE tissue is unavailable or is known to have been fixed for longer than 6 months, no values are given.

Key: N/A=not available, C=caudate, P=putamen, GP=globus pallidus

4.4.5.1.3 Complex III – Ubiquinol Cytochrome c Reductase

The availability of each of the caudate, putamen, and globus pallidus for analysis was dependent upon the precise location of the sample that was taken by the original pathology team. In some patients, this led to two of the three areas being available for analysis.

Patients with evidence for *POLG* mutations (Figure 4.24; image D) show moderate levels of complex III deficiency.

Patients with no genetic diagnosis available (Figure 4.24; images B and C) show low to moderate levels of complex III deficiency.

The control shows no evidence of deficiency.

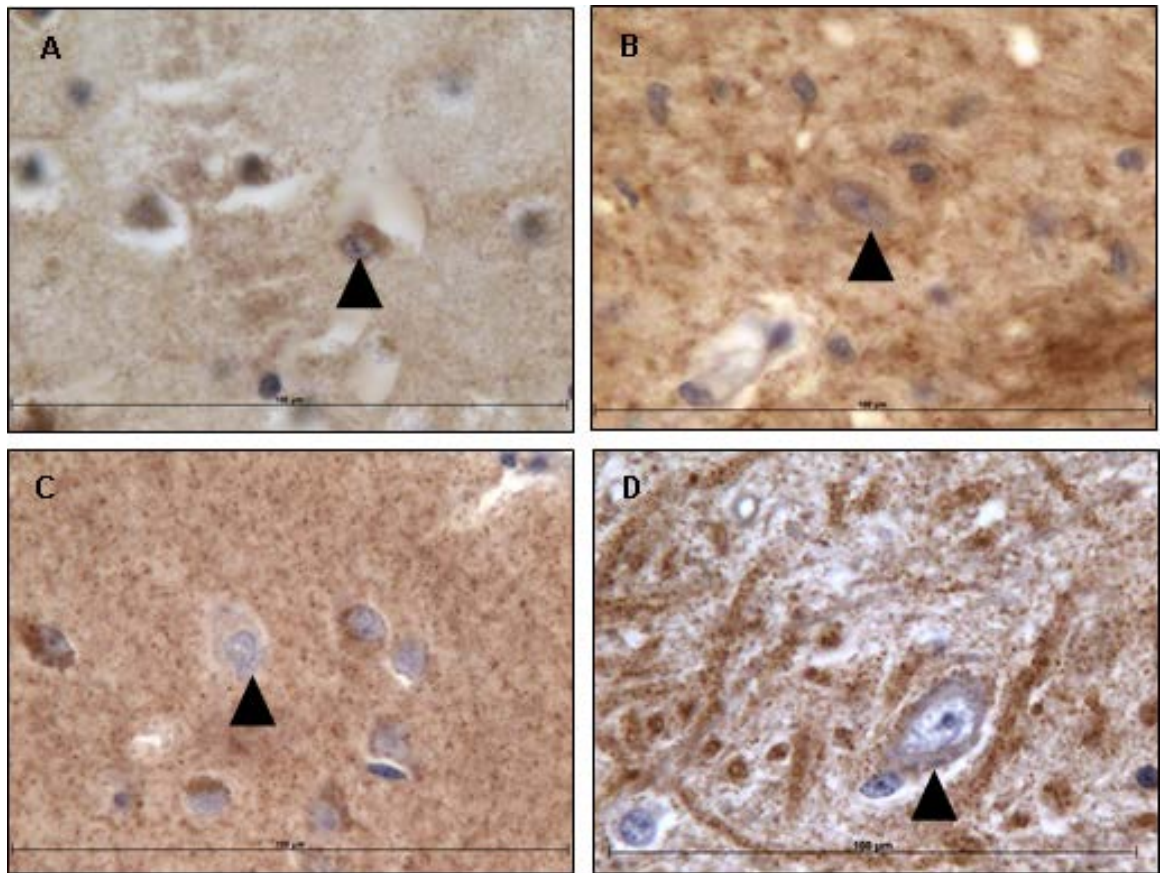


Figure 4.24. Staining with antibodies for complex III Rieske subunit in neurons of the basal ganglia.

Arrowheads indicate neurons. All sections stained with complex III Rieske subunit antibody. A=Control 5 putamen, B=Patient 8 *POLG* mutation-undetermined group globus pallidus, C=Patient 10 *POLG* mutation-undetermined group putamen, D=Patient 1 *POLG* mutation-positive group globus pallidus. Scale bar = 100µm.

Deficiency values are shown in Table 4.21. The brain area is unavailable for patients not listed in the table. This antibody stain could not be performed for Patient 11 as the supply of tissue was depleted.

<i>POLG</i> mutation	Patient	Complex III-Rieske
+	1	C – 14%
		P – 0%
		GP – 32%
?	8	C – N/A
		P – 7%
		GP – 33%
	9	C – 13%
		P – 40%
		GP – 17%
	10	C – N/A
		P – 2%
		GP – 1%

Table 4.21. Table of complex III deficiency in the basal ganglia.

Values are given for neurons from the caudate, putamen, and globus pallidus. Percentage of deficiency defined as deficient (-) and weak (+) neuron counts combined. One hundred neurons were counted in each patient. Where FFPE tissue is unavailable or is known to have been fixed for longer than 6 months, no values are given.

Key: N/A=not available, C=caudate, P=putamen, GP=globus pallidus

4.4.5.1.4 Complex IV – Cytochrome c Oxidase

The availability of each of the caudate, putamen, and globus pallidus for analysis was dependent upon the precise location of the sample that was taken by the original pathology team. In some patients, this led to two of the three areas being available for analysis.

Patients with evidence for *POLG* mutations show little evidence of complex IV subunit I deficiency (Figure 4.25; image B) and no complex IV subunit IV deficiency (Figure 4.26; image B).

Patients with no genetic diagnosis available show low to moderate levels of complex IV subunit I deficiency (Figure 4.25; images C and D). They show little evidence of complex IV subunit IV deficiency (Figure 4.26; images C and D).

The control shows no evidence of deficiency for both subunits.

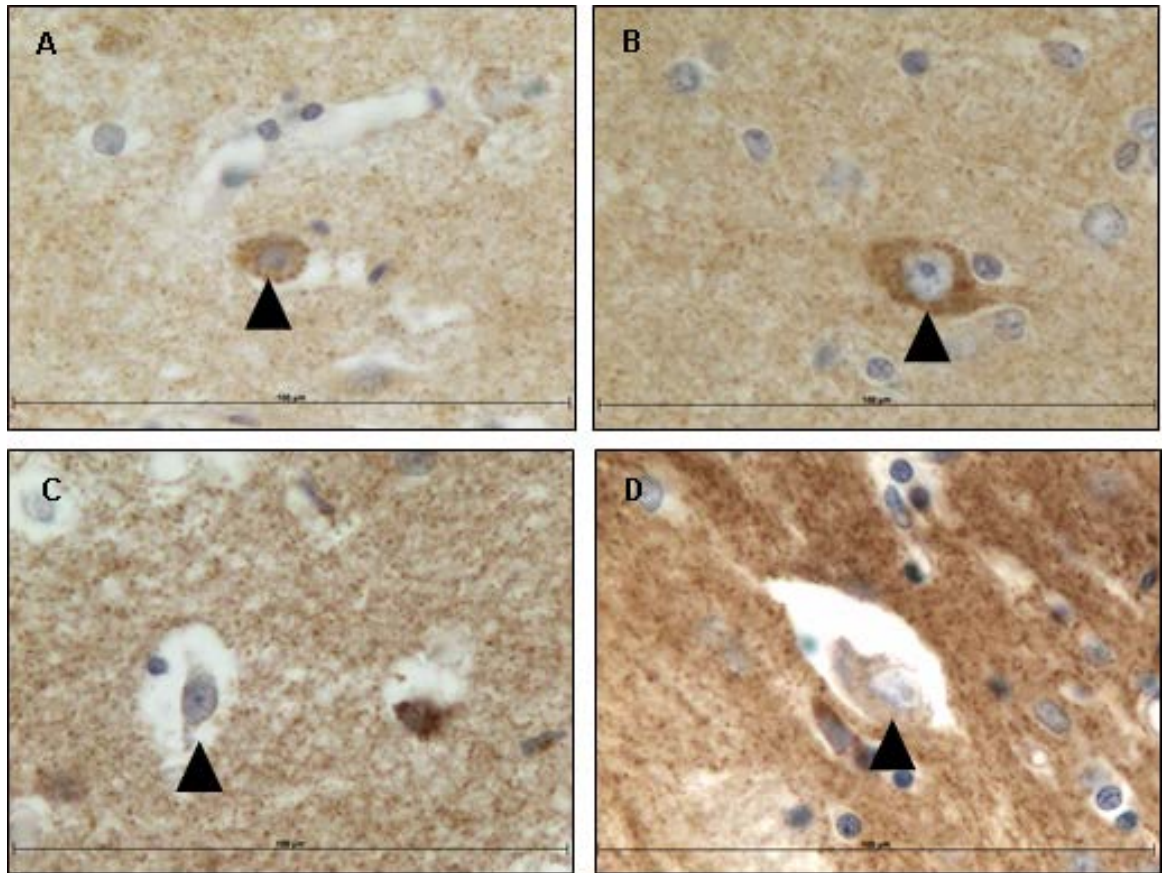


Figure 4.25. Staining with antibodies for complex IV subunit I in neurons of the basal ganglia.

Arrowheads indicate neurons. All sections stained with complex IV subunit I antibody. A=Control 6 putamen, B=Patient 1 *POLG* mutation-positive group caudate, C=Patient 9 *POLG* mutation-undetermined group caudate, D=Patient 11 *POLG* mutation-undetermined group caudate. Scale bar = 100µm.

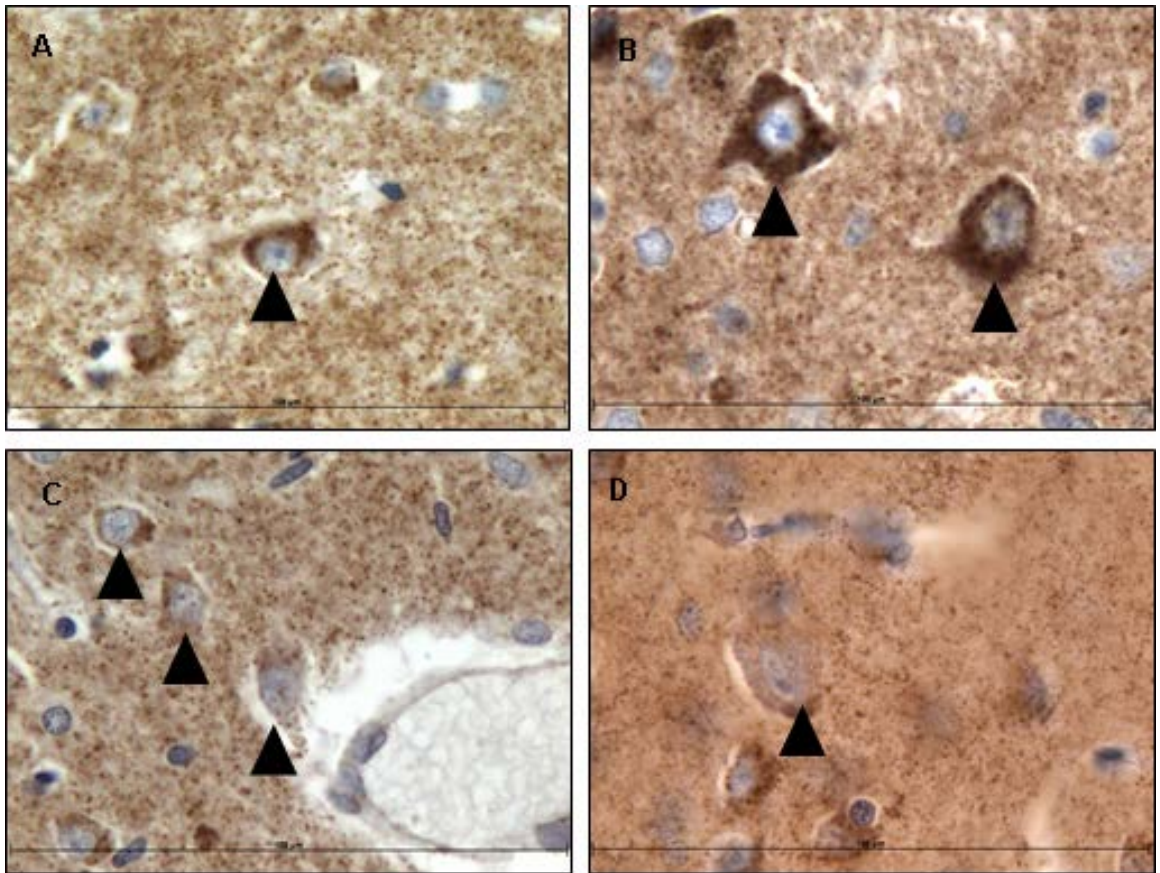


Figure 4.26. Staining with antibodies for complex IV subunit IV in neurons of the basal ganglia.

Arrowheads indicate neurons. All sections stained with complex IV subunit IV antibody. A=Control 6 putamen, B=Patient 1 *POLG* mutation-positive group caudate, C=Patient 11 *POLG* mutation-undetermined group putamen, D=Patient 10 *POLG* mutation-undetermined group putamen. Scale bar = 100 μ m.

Deficiency values for both subunits are shown in Table 4.22. The brain area is unavailable for patients not listed in the table.

<i>POLG</i> mutation	Patient	Complex IV-I	Complex IV-IV
+	1	C – 5%	C – 0%
		P – 1%	P – 0%
		GP – 0%	GP – 0%
?	8	C – N/A	C – N/A
		P – 2%	P – 0%
		GP – 2%	GP – 0%
	9	C – 3%	C – 0%
		P – 11%	P – 4%
		GP – 2%	GP – 0%
	10	C – N/A	C – N/A
		P – 2%	P – 1%
		GP – 0%	GP – 0%
	11	C – 4%	C – 0%
		P – 15%	P – 10%
		GP – 0%	GP – 0%

Table 4.22. Table of complex IV deficiency in the basal ganglia.

Values are given for neurons from the caudate, putamen, and globus pallidus. Percentage of deficiency defined as deficient (-) and weak (+) neuron counts combined. One hundred neurons were counted with each antibody in each patient. Where FFPE tissue is unavailable or is known to have been fixed for longer than 6 months, no values are given.

Key: N/A=not available, C=caudate, P=putamen, GP=globus pallidus

A summary of respiratory chain deficiency values for the basal ganglia is detailed in Table 4.23.

		Basal Ganglia					
<i>POLG</i> mutation	Patient	CI-19	CI-20	CII-70	CIII	CIV-I	CIV-IV
+	1	C – 0%	C – 18%	C – 0%	C – 14%	C – 5%	C – 0%
		P – 2%	P – 1%	P – 1%	P – 0%	P – 1%	P – 0%
		GP – 0%	GP – 3%	GP – 0%	GP – 32%	GP – 0%	GP – 0%
?	8	C – N/A	C – N/A	C – N/A	C – N/A	C – N/A	C – N/A
		P – 10%	P – 2%	P – 0%	P – 7%	P – 2%	P – 0%
		GP – 4%	GP – 0%	GP – 0%	GP – 33%	GP – 2%	GP – 0%
	9	C – 13%	C – 14%	C – 0%	C – 13%	C – 3%	C – 0%
		P – 41%	P – 7%	P – 1%	P – 40%	P – 11%	P – 4%
		GP – 26%	GP – 0%	GP – 6%	GP – 1%	GP – 2%	GP – 0%
	10	C – N/A	C – N/A	C – N/A	C – N/A	C – N/A	C – N/A
		P – 0%	P – 0%	P – 0%	P – 2%	P – 2%	P – 1%
		GP – 0%	GP – 0%	GP – 0%	GP – 1%	GP – 0%	GP – 0%
	11	C – 15%	C – 12%	C – 0%	C – N/A	C – 4%	C – 0%
		P – 19%	P – 19%	P – 0%	P – N/A	P – 15%	P – 10%
		GP – 18%	GP – N/A	GP – 0%	GP – N/A	GP – 0%	GP – 0%

Table 4.23. Summary of respiratory chain deficiency in the basal ganglia.

Values are given for neurons of layer V. Percentage of deficiency defined as deficient (-) and weak (+) neuron counts combined. One hundred neurons were counted with each antibody in each patient. Where FFPE tissue is unavailable or is known to have been fixed for longer than 6 months, no values are given.

Key: N/A=not available, C=caudate, P=putamen, GP=globus pallidus

A summary of the respiratory chain deficiency in all brain areas of all patients is detailed in Table 4.24.

POLG Mutation	Patient	Cerebellum								Occipital Lobe							
		I-19	I-20	I-30	I-39	II	III	IV-I	IV-IV	I-19	I-20	I-30	I-39	II	III	IV-I	IV-IV
+	1	PC-8% DN-0%	PC-22% DN-10%	PC-0% DN-53%	PC-8% DN-11%	PC-0% DN-0%	PC-1% DN-0%	PC-1% DN-2%	PC-0% DN-0%	2%	2%	3%	0%	0%	0%	0%	0%
	2	PC-1% DN-0%	PC-1% DN-9%	PC-0% DN-14%	PC-N/A DN-0%	PC-1% DN-0%	PC-39% DN-47%	PC-0% DN-0%	PC-0% DN-0%	2%	0%	0%	0%	0%	N/A	0%	0%
	6	PC-11%	PC-12%	PC-25%	PC-19%	PC-5%	PC-27%	PC-15%	PC-0%	N/A	N/A	N/A	N/A	N/A	N/A	N/A	N/A
?	7	PC-3% DN-2%	PC-2% DN-0%	N/A	N/A	PC-0% DN-0%	PC-30% DN-49%	PC-0% DN-22%	PC-0% DN-0%	N/A	N/A	N/A	N/A	N/A	N/A	N/A	N/A
	8	PC-10% DN-0%	PC-3% DN-0%	N/A	N/A	PC-0% DN-0%	PC-27% DN-10%	PC-1% DN-0%	PC-0% DN-0%	14%	5%	N/A	N/A	0%	33%	10%	1%
	9	PC-61% DN-68%	PC-21% DN-89%	N/A	N/A	PC-0% DN-0%	N/A	PC-33% DN-17%	PC-0% DN-1%	N/A	N/A	N/A	N/A	N/A	N/A	N/A	N/A
	10	PC-44% DN-41%	PC-13% DN-24%	N/A	N/A	PC-28% DN-0%	PC-60% DN-0%	PC-10% DN-0%	PC-8% DN-0%	16%	8%	N/A	N/A	0%	80%	18%	0%
	11	PC-63%	PC-38%	N/A	N/A	PC-0%	PC-68%	PC-18%	PC-14%	2%	23%	N/A	N/A	0%	16%	14%	1%
-	12	N/A								0%	1%	0%	19%	0%	0%	3%	0%

POLG Mutation	Patient	Parietal Lobe								Basal Ganglia							
		I-19	I-20	I-30	I-39	II	III	IV-I	IV-IV	I-19	I-20	I-30	I-39	II	III	IV-I	IV-IV
+	1	0%	0%	4%	2%	2%	0%	5%	0%	C-0% P-2% GP-0%	C-18% P-1% GP-3%	C-4% P-1% GP-3%	C-23% P-2% GP-5%	C-0% P-1% GP-0%	C-14% P-0% GP-32%	C-5% P-1% GP-0%	C-0% P-0% GP-0%
	2	5%	0%	9%	0%	0%	15%	3%	0%	N/A	N/A	N/A	N/A	N/A	N/A	N/A	N/A
	6	0%	1%	17%	0%	0%	1%	0%	0%	N/A	N/A	N/A	N/A	N/A	N/A	N/A	N/A
?	7	N/A	N/A	N/A	N/A	N/A	N/A	N/A	N/A	N/A	N/A	N/A	N/A	N/A	N/A	N/A	N/A
	8	53%	19%	N/A	N/A	0%	13%	4%	3%	P-10% GP-4%	P-2% GP-0%	N/A	N/A	P-0% GP-0%	P-7% GP-33%	P-2% GP-2%	P-0% GP-0%
	9	N/A	N/A	N/A	N/A	N/A	N/A	N/A	N/A	C-13% P-41% GP-26%	C-14% P-7% GP-0%	N/A	N/A	C-0% P-1% GP-6%	C-13% P-40% GP-17%	C-3% P-11% GP-2%	C-0% P-4% GP-0%
	10	N/A	N/A	N/A	N/A	N/A	N/A	N/A	N/A	P-0% GP-0%	P-0% GP-0%	N/A	N/A	P-0% GP-0%	P-2% GP-1%	P-2% GP-0%	P-1% GP-0%
	11	N/A	N/A	N/A	N/A	N/A	N/A	N/A	N/A	C-15% P-19% GP-18%	C-12% P-19% GP-N/A	N/A	N/A	C-0% P-0% GP-0%	N/A	C-4% P-15% GP-0%	C-0% P-10% GP-0%
-	12	N/A								N/A							

Table 4.24. Summary of respiratory chain deficiency in all brain areas.

Values are given for neurons of layer V. Percentage of deficiency defined as deficient (-) and weak (+) neuron counts combined. One hundred neurons were counted with each antibody in each patient. Where FFPE tissue is unavailable or is known to have been fixed for longer than 6 months, no values are given.

Key: N/A=not available, PC=Purkinje cell, DN=dentate nucleus, C=caudate, P=putamen, GP=globus pallidus

4.4.6 Respiratory Chain Deficiency in Glial Cells

Glial cells are ubiquitous cells of the CNS that perform many different functions. They support the functioning of neurons by providing simple sugars as an energy source for the neurons, insulate the axons of neurons, surround the neurons and physically support them, and provide an immune response.

Respiratory chain deficiency is seen in the glial cells of two patients, described in the next paragraphs. A severe astrogliosis was noted in the pathological changes of these patients and so a stain for astrocytes has been included. Changes to the glial cells of the parietal lobe are described below.

4.4.6.1 Patient 2

Patient 2 shows evidence for *POLG* mutations, harbouring the p.Ala467Thr and p.Thr914Pro mutations.

A stain for astrocytes, a common glial cell was used to assess the increase in cell population. Patient 2 shows normal staining with GFAP, showing the astrocyte population (Figure 4.27; image A). The parietal lobe shows a severe astrogliosis in the grey matter with many fewer astrocytes being present in the white matter. The astrocytes appear large and swollen. Porin staining of the glial cells (image B) shows only a slight deficiency, suggesting that many mitochondria are present in the glia. However, complex I (image C) and complex III (image D) staining of the glial cells shows a moderate deficiency.

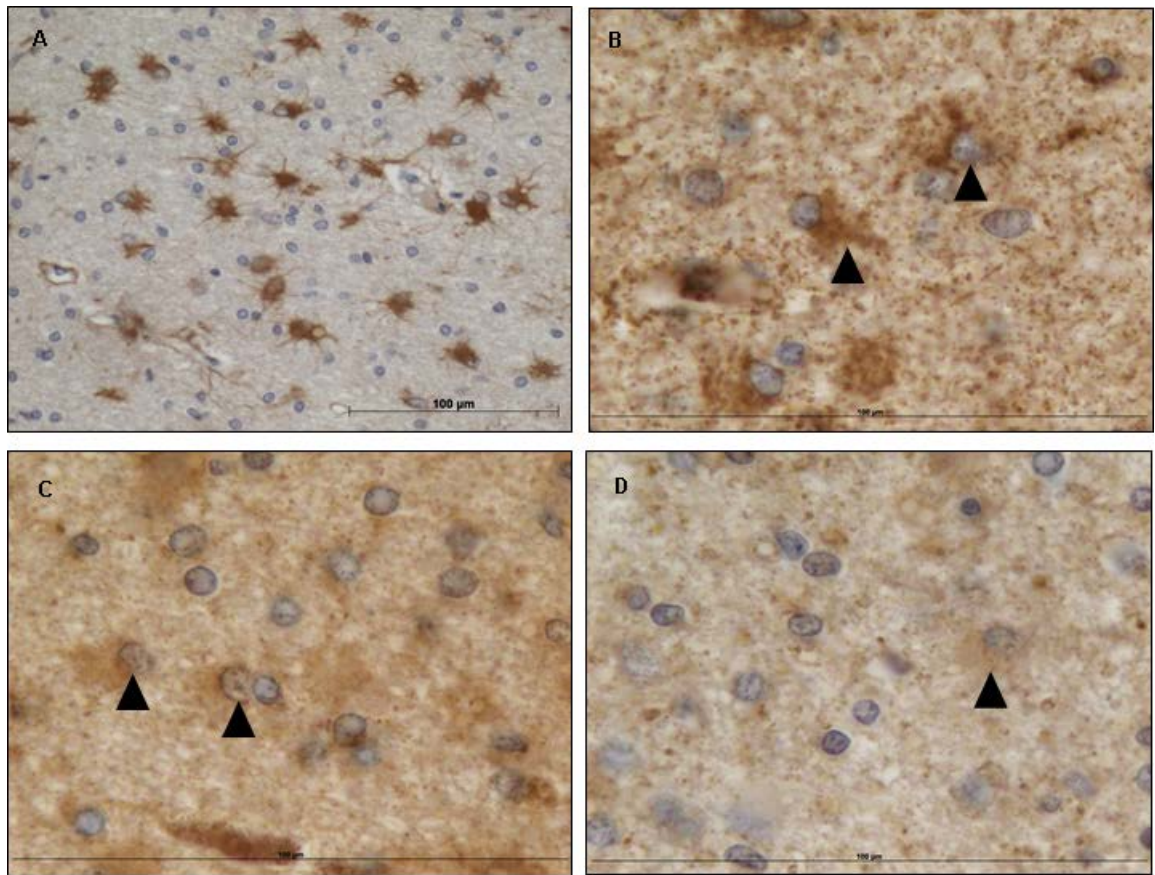


Figure 4.27. Respiratory chain deficiency within glial cells in the parietal lobe of Patient 2.

A=GFAP, B=porin, C=CI-19, D=CIII Rieske subunit. Image A shows a severe astrogliosis. Image B shows a slight deficiency in porin. Images C and D show a moderate deficiency in complex I and complex III. All images taken of Patient 2 *POLG* mutation-positive group. Scale bar = 100µm.

4.4.6.2 Patient 6

Patient 6 shows evidence for *POLG* mutations, whose sibling harbours the p.Trp748Ser and p.Arg1096Cys mutations.

A stain for astrocytes, a common glial cell was used to assess the increase in cell population. Patient 6 shows normal staining with GFAP, showing the astrocyte population (Figure 4.28; image A). The parietal lobe shows a severe astrogliosis in the grey and white matter. The astrocytes appear large and swollen. Porin staining (image B) shows a severe deficiency, suggesting extremely few mitochondria are present in the glial cells. Complex I (image D) staining and complex II (image C) staining of the glial cells both show a severe deficiency.

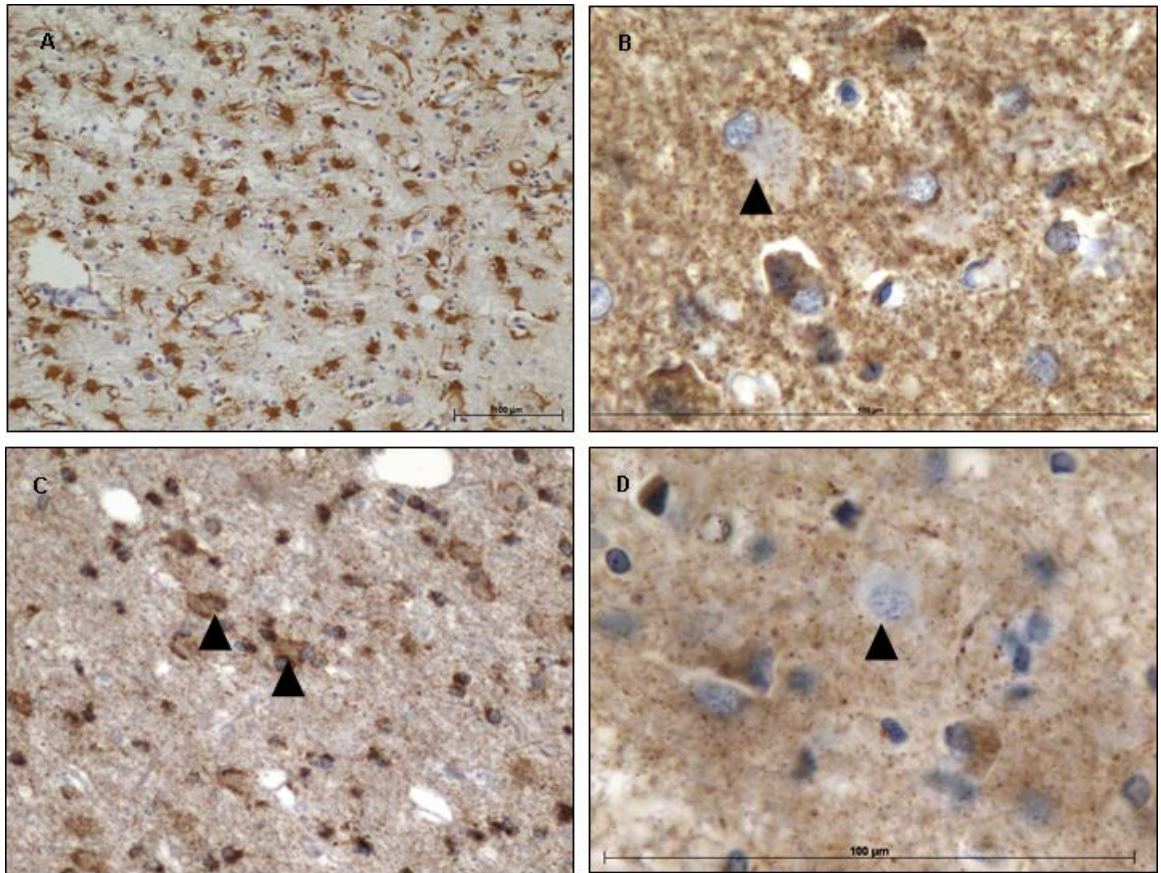


Figure 4.28. Respiratory chain deficiency within glial cells in the parietal lobe of Patient 6.

A=GFAP, B=porin, C=CII-70, D=CI-30. Image A shows a severe astrogliosis. Image B shows a severe deficiency in porin. Image C shows a severe deficiency in complex II. Image D shows a severe deficiency in complex I. All images taken of Patient 6 *POLG* mutation-positive group. Scale bar = 100µm.

4.5 Discussion

4.5.1 Respiratory Chain Deficiency In Relation to Neuropathology

This chapter has examined the respiratory chain deficiency in neurons. In the previous chapter, I examined my cohort for features of neuropathology and now these are examined in relation to one another. The cerebellum shows the greatest changes in respiratory chain function and extensive neuropathology. The occipital lobe shows slight changes of the respiratory chain but moderate neuropathology. The parietal and basal ganglia show some changes of the respiratory chain and mild neuropathology.

The occipital lobe shows an unexpected lack of correlation between the neuropathology and respiratory chain deficiency, even in patients where there was moderate neuropathology and a confirmed POLG mutation. There was neuron loss, predominantly seen in the upper grey matter layers, with moderate neuropathology throughout, yet extremely little respiratory chain deficiency is noted. This is very surprising in an area of the brain where there has been much reported involvement in patients with Alpers' syndrome. The occipital lobe is an area of high metabolic activity and the neurons in this area may be more vulnerable to dysfunction of the respiratory chain. It is possible there may have been more pyramidal neurons than were assessed during this project and that these neurons may have had a respiratory chain dysfunction. If these neurons had died they could therefore not be examined and counted in this study. The remaining neurons may have been those that did not show a respiratory chain dysfunction and those were the neurons that were counted. An additional possibility considers that there are other neuronal subtypes present in the occipital cortex and some of these subtypes may have been too small to accurately examine and count at the highest magnification available, X100 magnification. These neurons may have shown respiratory chain dysfunction but were not counted. This may suggest that there are neurons that are differentially vulnerable to respiratory chain dysfunction and that this situation may be unique to the occipital lobe, as the lack of respiratory chain dysfunction was not seen in other brain areas. A third consideration may be given to the vascular regions of the occipital lobe, where a high metabolic demand requires a suitable vascular supply. There is evidence in other mitochondrial disorders with seizure involvement, e.g. MELAS, that infarcts, lesions and neurodegeneration may arise from vascular abnormalities after seizure activity (Iizuka et al., 2003). The neurons of the occipital lobe in patients with Alpers' syndrome may be vulnerable to these vascular changes after seizure activity and this may result in an

imbalance between an increased energy demand and the ATP availability in the neuron.

4.5.2 *Respiratory Chain Deficiency in Neurons*

This is the first time that the respiratory chain has been studied at this level of detail in neurons in patients with Alpers' syndrome. There was an overall trend that complex I and complex III showed the greatest deficiency in all brain areas of the patients. Complex IV subunit I shows a moderate deficiency which was always greater than the few neurons with complex IV subunit IV deficiency. Complex II deficiency was seen in a single patient. Respiratory chain deficiency will be discussed in more detail in the following sections.

4.5.2.1 *Complex I*

Complex I is the largest of the respiratory chain proteins, encoded by both nuclear and mitochondrial genes. Its assembly into a multi-subunit protein requires assembly factors and may progress through intermediate stages (Antonicka et al., 2003). There was a clear deficiency of complex I in seven of the patients investigated and in all brain areas. Four antibodies to complex I subunits were used: CI-19 (*NDUFA13*), CI-20 (*NDUFB8*), CI-39 (*NDUFA9*), and one of the core subunits, CI-30 (*NDUFS3*). All of these subunits are nuclear-encoded and directly unaffected by mtDNA abnormalities. The most severe deficiencies were observed in the cerebellum, with both the Purkinje cells and neurons of the dentate nucleus exhibiting up to 89% complex I deficiency. Less severe deficiencies were noted in the occipital lobe, parietal lobe, and basal ganglia yet in some patients these were substantial; Patient 8 showed a 53% deficiency of CI-19 in the parietal lobe, and Patient 9 showed a 41% deficiency of CI-19 in the putamen of the basal ganglia. Severe loss of a single complex I subunit was seen in Patient 1; 53% deficiency of the core subunit complex I-30 was seen in neurons of the dentate nucleus. Normal levels of staining are seen in the Purkinje cells of this patient. Greater levels of CI-30 deficiency are also seen in the parietal lobe of Patient 6 (17%) where there is no deficiency in other subunits. However, it is also clear that greater loss of any individual subunit of complex I can occur in neurons. This suggests that neurons may be more vulnerable to loss of the core subunits of complex I but that loss of an individual subunit can occur and may be tolerated if other subunits are intact.

The most severe complex I deficiency of the Purkinje cells or dentate nucleus correlated with a greater degree of loss of that neuronal type. In Patient 9, Purkinje

cells showed a 61% and 21% deficiency with CI-19 and CI-20 subunits respectively, with no discernable neuron loss, while the dentate nucleus showed 68% and 89% deficiency with CI-19 and CI-20 subunits respectively, with moderate neuron loss. This suggests that surviving neurons show deficiency in areas where a greater number of neurons have already been lost and we may be seeing a snapshot of this process as further respiratory chain deficiency leads to increased neuronal cell death.

Complex I deficiency, is the most common defect in mitochondrial patients (Darin et al., 2001), yet it is an underdiagnosed condition and can occur in many heterogeneous disorders. A previous study in this lab has shown that patients with *POLG* mutations show a predominant complex I and complex IV deficiency of both Purkinje cells and neurons of the dentate nucleus in the cerebellum (Lax 2011). The study did not investigate for signs of complex III deficiency.

Complex I deficiency may result in increased reactive oxygen species (ROS) production and it has been shown in fibroblast cell lines that those with a higher ROS production occurs in cells with the most severe complex I deficiency (Verkaart et al., 2007). This increased ROS production may be contributing to neuron death and degeneration.

Assembly of complex I, occurring through intermediate stages and facilitated by assembly factors, is dependent on the structure and integrity of both nuclear- and mitochondrially-encoded subunits in order to form the large complex (Lazarou et al., 2007). Deficiency of subunits may reduce the efficacy of assembly, leading to a complex I deficiency. This may have a subsequent effect on other complexes within the supercomplex structure and compromise the respiratory chain's capacity for ATP production.

4.5.2.2 Complex II

Complex II is a nuclear-encoded complex, involved in both the electron transport chain and the citric acid cycle. There was an obvious deficiency of complex II in one patient, Patient 10. This was apparent in the Purkinje cells of the cerebellum showing a deficiency of 28%, but not in neurons of the dentate nucleus which showed no deficiency. All other patients showed little or no complex II deficiency with <6% of the neurons revealing evidence of complex II dysfunction over all brain areas. This was expected as all four subunits of complex II are nuclear-encoded and therefore not directly affected by mtDNA deletions, mutations or mtDNA copy number. The complex II deficiency observed in Patient 10 is unusual and there may be other factors

influencing this observation in Purkinje cells. This patient also exhibited a very low mitochondrial density which was detected when staining with an antibody for porin (see *Chapter 3 Neuropathological Features of Patients With Alpers' Syndrome, 3.4.6 'Mitochondrial Localisation in Neurons'*).

4.5.2.3 Complex III

There was an obvious and severe deficiency of complex III in most of the patients and in most brain areas. An antibody to the iron-sulphur protein (Rieske subunit), which has a direct role in electron transfer, was used in this study. Defects in complex III can lead to early-onset disorders associated with respiratory chain deficiency, including clinical signs of seizures, developmental delay and increased serum lactate levels (Fernandez-Vizarra et al., 2007) and GRACILE syndrome (Visapää et al., 2002).

Complex I and complex III are considered the main producers of ROS (Chen et al., 2003) and disruption of these complexes within the supercomplex may increase ROS production (Maranzana et al., 2013). In addition, the core subunits, including the Rieske subunit, facilitate assembly of the complex. Defects of complex III assembly due to mutations in an assembly factor have been shown to lead to diminished incorporation of the Rieske subunit, leading to a loss of complex activity (Fernandez-Vizarra et al., 2007).

4.5.2.4 Complex IV

This study examined two subunits of complex IV; the mitochondrially-encoded subunit I and the nuclear-encoded subunit IV. Complex IV subunit I (COX I) was the only mitochondrially-encoded subunit that was used to study respiratory chain deficiency. A low to moderate deficiency of COX I was seen in all brain areas and this subunit showed a greater deficiency in patients than subunit IV (COX IV). This suggests that damage to mtDNA has decreased COX I availability, a process that has not affected nuclear DNA and COX IV. However, the mitochondrially-encoded COX I subunit showed a milder deficiency than with nuclear-encoded complex I and complex III subunits. This was unexpected and it may be that other mitochondrially-encoded subunits of complex I and complex III were lost and that this destabilised the entire complex.

COX IV shows little evidence of deficiency in some patients, yet this is always in concordance with a greater deficiency in COX I. This is associated with the loss of COX I and potentially a loss of structured assembly of the entire complex. In the

cerebellum, Patient 11 displayed a combined COX I and COX IV deficiency which has been seen previously in the cerebellum of patients with *POLG* mutations (Lax et al., 2012), though a combined deficiency was not seen in the cerebellum of Patient 6 and Patient 9 which primarily showed a COX I deficiency.

4.5.2.5 Patient Variability

The patients in this cohort showed a wide variation in the level of respiratory chain deficiency. There was a clear decreased expression of complex I and complex III respiratory chain subunits in patients and many brain areas showed neurons that were weak or deficient in these complexes.

Patient 1 was an interesting exception to the findings in the rest of the cohort. This patient showed the clinical signs of seizures, ataxia and liver failure. There was no neuron loss documented in any brain areas where the respiratory chain was investigated. There was a complex I deficiency but little complex III deficiency in the cerebellum. In the occipital and parietal lobes, there was no complex I or complex III deficiency. However, there was both a complex I and complex III deficiency in the basal ganglia. This suggests that the survival of neurons is linked to the integrity of the respiratory chain.

Patient 2 showed moderate levels of complex III deficiency in the cerebellum (39% and 47%) but there is little evidence of complex I deficiency (between 0% and 14%) in this part of the brain. In the parietal lobe, there is a slightly greater deficiency of complex III (15%) than complex I (between 0% and 9%). The comparison of complex I and complex III could not be made in the occipital lobe or basal ganglia due to a lack of suitable tissue. This finding is intriguing because deficiencies of complex I and complex IV are considered the most significant to mitochondrial disorders. This suggests that a complex III deficiency may be tolerated by the surviving neurons and could be an important indicator of mitochondrial disease.

Patient 10, no genetic diagnosis available, showed the highest complex III deficiency in the occipital lobe, at 80%, of all patients in all brain areas. The occipital lobe of this patient showed a moderate complex I deficiency of 16% complex I-19 deficiency and a moderate complex IV-I deficiency of 18%. There was no complex IV-IV deficiency. In the cerebellum, there was a moderate complex II deficiency, at 28%, in Purkinje cells. Selective complex III deficiency in the occipital lobe is unusual. This suggests, as with Patient 2 above, that a complex III deficiency may be tolerated in neurons and it should not be overlooked when analysing respiratory chain deficiencies in patients with

mitochondrial disease. A selective complex II deficiency in Purkinje cells is also unusual. There may be other factors influencing this observation of complex II deficiency in Purkinje cells, such as very low mitochondrial density as mentioned above (see section 4.5.2.2 'Complex II').

Patient 11, no genetic diagnosis available, showed a complex IV-IV deficiency of 14%, comparable to the complex IV-I deficiency of 18% in the Purkinje cells of the cerebellum. The cerebellum showed a high complex I deficiency of 63% complex I-19 deficiency and a high complex III deficiency of 68%. There was no complex II deficiency.

4.5.2.6 *Within-group Variation*

The *POLG* mutation-positive group showed deficiency in complex I and complex III in the cerebellum and parietal lobe. There were variable levels of complex III deficiency; Patient 1 shows little evidence of deficiency in the cerebellum and occipital lobe, while Patient 2 and Patient 6 show moderate levels of deficiency. Complex II did not show deficiency. Complex IV subunit I showed slightly weaker staining than subunit IV in the cerebellum and parietal lobe, but no deficiency of either subunit in the occipital lobe.

The *POLG* mutation-undetermined group showed the most severe complex I deficiency in the cerebellum. The parietal lobe also showed a complex I deficiency with the single highest percentage of complex I deficiency being found in Patient 8; this was a 53% deficiency of complex I-19. There was no complex II deficiency. Complex III showed moderate to high levels of deficiency in the cerebellum and occipital lobe, with less evidence of deficiency in the parietal lobe and basal ganglia. Complex IV subunit I showed slightly weaker staining than complex IV subunit IV in the cerebellum and occipital lobe.

The *POLG* mutation-absent patient could be studied for respiratory chain deficiency in the occipital lobe only, due to a fixation length of more than 6 months in all other brain areas. Complex I showed little evidence of deficiency in all subunit except CI-39 (19%). Complex II did not show deficiency. Complex III was not deficient in the occipital lobe (0%). Complex IV subunit I showed very slightly more deficiency (3%) than subunit IV (0%).

4.5.2.7 *Inter-group Variation*

The *POLG* mutation-positive group showed a moderate complex I and complex III deficiency. Patient 1 showed only a complex I deficiency in the cerebellum while

Patient 2 showed both a complex I and complex III deficiency. The occipital lobe showed little evidence of deficiency. This suggests a mixed pattern of respiratory chain deficiency that is variable between patients, though commonly showing a complex I deficiency. The *POLG* mutation-undetermined group showed the most severe complex I and complex III deficiencies in all four brain areas. The *POLG* mutation-absent patient could be studied for respiratory chain deficiency only in the occipital lobe. This patient showed little or no deficiency in all respiratory chain subunits (<3%), apart from complex I-39, in which there was a deficiency of 19%.

In all groups, complex I deficiency was seen, often in association with a complex III deficiency which can be of the same severity. The *POLG* mutation-undetermined group showed the most severe deficiencies, which may reflect the unknown mutations present in this group.

4.5.3 Respiratory Chain Deficiency in Glial Cells

Glial cells are found throughout the brain, performing many vital functions and supporting the neurons within the brain tissue. The parietal lobe was examined in two patients and is considered in this discussion. Further brain areas and patients could not be examined in the time frame of this project.

Patient 2 shows complex I and complex III deficiencies, though mitochondria appear to be present in the glial cells. This indicates a respiratory chain deficiency in the glial cells, despite little evidence of complex I deficiency (5% CI-19 and 9% CI-30) and moderate complex III deficiency (15%) in the neurons of the parietal lobe of Patient 2. Complex II shows no deficiency, which was expected as this is a nuclear-encoded subunit and unaffected by mtDNA mutations.

Patient 6 shows mitochondrial deficiency and respiratory chain deficiencies of complex I and complex II. Staining with an antibody to porin shows low mitochondrial density in the glial cells while complex I and complex II-70 show moderate to high levels of deficiency. This highlights the loss of the respiratory chain and a low mitochondrial density which both reduces the capability of OXPHOS in the cell and increases the demand for energy from remaining mitochondria, increasing oxidative stress and damaging levels of ROS. This appears to only affect glial cells as complex II is intact in the neurons of Patient 6.

Patient 2 was a child patient of 27 months old at death and had a relatively short course of disease progression of 10 months. By contrast, Patient 6 was a young adult

patient of 18 years old at death and had a longer course of disease progression of 2 years. Both of these disease progressions are compatible with Alpers' syndrome, and the severity of the glial cells respiratory chain deficiency may reflect the length of disease progression. A longer disease progression may result in a greater respiratory chain deficiency leading to a loss of mitochondria over time.

Due to the large numbers of visible glial cells with or without respiratory chain deficiency, it is possible that the glial cells are a rapidly proliferating cell type, such as astrocytes or microglia (Janeczko 1991), that require increased energy to allow for the changes in the physiological state of the cell. Respiratory chain deficiency has been noted in the astrocytes of patients with mitochondrial disease (Lax et al., 2012) and cells positively identified as astrocytes through GFAP staining appeared swollen, an observation in rat models with chronic sodium valproate administration (Sobaniec-Lotowska 2001). The activation of microglia requires increased energy and this may have an impact upon mitochondria within these cells, resulting in an increased respiration rate (Reichner et al., 1995). Electron microscopy investigation has shown changes to mitochondrial morphology in activated microglia, resulting in elongated, crescentiform, or ring-shaped mitochondria (Banati et al., 2004).

Further analysis of this would be required, showing dual GFAP-positive staining or CD68-positive staining with additional respiratory chain antibody deficiency in the same cells.

4.5.4 The Project's Findings in the Context of the Literature

The literature reports biochemical and histochemical studies of patient tissues which show a range of respiratory chain deficiencies. Liver, muscle, and fibroblasts are the most usual cell types to be studied in patients with *POLG* disorders, due to their relevance to the features of the disease or their ease of sampling. When tested, liver is often reported to show biochemical respiratory chain abnormalities whilst muscle and fibroblast samples may appear normal. It may be that defects in the *POLG* enzyme lead to secondary mtDNA mutations which may accumulate in post-mitotic tissues. As fibroblasts are mitotic cells, they may not develop the level of secondary mtDNA mutations seen in post-mitotic tissues. However, defective mtDNA replication may cause a more severely decreased oxidative phosphorylation in mitotic tissues as these cells require increased mtDNA replication during cell division. The mechanisms underlying tissue specificity in *POLG* disorders are currently unclear.

The previous literature on patients with *POLG* mutations contains mixed reports of respiratory chain abnormalities. This ranges from no reported respiratory chain deficiency in patients with a single *POLG* mutation (Hakonen et al., 2008) and no reported respiratory chain deficiency in patients with two recessive *POLG* mutations (Milone et al., 2008), to a severe deficiency involving multiple complexes in patients with two recessive *POLG* mutations (Isohanni et al., 2011). The cohort examined in this project is in agreement with the previous investigations that found a respiratory chain deficiency, primarily of complex I, in neurons of the brain.

The previous literature on patients with Alpers' syndrome describes respiratory chain deficiency of multiple complexes in a range of tissues, including liver, muscle, and fibroblasts (Table 4.25). Respiratory chain investigations in neurons from the brain have not previously been described in the literature. A 3 year old male patient with Alpers-Huttenlocher syndrome was reported with respiratory chain deficiencies in muscle tissue of complex I at 19%, complex II at 59%, complex III at 36%, and complex IV at 40% of control muscle values (Delarue et al., 2000). A 17 year old female patient with Alpers' syndrome, harbouring the p.Thr851Ala and p.Arg1047Trp *POLG* mutations, showed normal levels of complexes I, II, II+III, III and IV in muscle homogenate (Wiltshire et al., 2008). In a liver biopsy from this patient, enzymes studies showed complex I at 8%, complex III at 33%, and complex IV at 19% of control values, with normal complex II and elevated citrate synthase.

A range of tissues were affected by respiratory chain dysfunction. Interestingly, muscle was affected in two of these cases and unaffected in another despite other tissue types showing dysfunction. This highlights that muscle cannot be relied upon to be a diagnostic tissue when investigating Alpers' syndrome (Gauthier-Villars et al., 2001; Nguyen et al., 2005; Delonlay et al., 2013).

Variability in the complex deficiency between different brain areas, and different tissue types reported in the literature, suggests the possibility of epigenetic effects upon the mitochondria in these neurons. This is a recent area of investigation that will provide many new and interesting aspects of mitochondrial disease and may shed more light on the understanding of tissue specificity in mitochondrial disease (Byun and Baccarelli 2014).

Respiratory Chain Abnormality (% of control value)	Tissue Studied	Type of Investigation	POLG Mutation	Publication
Complex I 8% Complex III 33% Complex IV 19%	Liver	Biochemical	p.Thr851Ala; p.Arg1047Trp	(Wiltshire et al., 2008)
Reduced complex I and IV	Liver	Biochemical	p.Ala467Thr; c.3643+2T>C	(Roels et al., 2009)
COX-deficiency	Liver	Histochemical test for enzyme activity		
Reduced complex I, III, and IV	Liver	Biochemical	p.Ala467Thr; c.1251-2A>T	(Schaller et al., 2011)
Reduced complex I, III, IV	Liver	Biochemical	p.Ala467Thr; p.Trp748Ser; p.Gly848Ser; p.Arg852Cys; p.Ser305Arg; p.Leu966Arg; p.Arg232His; p.His277Leu	(Hunter et al., 2011)
Complex I 25% Complex III 31% Complex IV 52%	Liver	Biochemical	p.Gly848Ser; p.Trp748Ser	(Davidzon et al., 2005)
COX-deficiency	Liver	Histochemical test for enzyme activity	p.Ala467Thr; p.Ala467Thr	(Boes et al., 2009)
COX-deficiency	Liver	Histochemical test for enzyme activity	p.Ala467Thr; p.Leu605Arg	(Stewart et al., 2009)
Reduced complex I	Liver	Biochemical	Unknown	(Gauthier-Villars et al., 2001)
Reduced complexes	Liver	Biochemical	p.Trp748Ser; p.I948fsX968 p.Ala467Thr; p.T326fsX387 p.Leu428Pro; p.Ala467Thr	(Sarzi et al., 2007)

Respiratory Chain Abnormality (% of control value)	Tissue Studied	Type of Investigation	POLG Mutation	Publication
Reduced complex IV	Liver	Histochemical test for enzyme activity	p.Ala467Thr; p.Ala467Thr	(Nguyen et al., 2005)
Normal	Liver		p.Trp748Ser; p.Gly848Ser	
Complex I 19% Complex II 59% Complex III 36% Complex IV 40%	Muscle	Biochemical	Not confirmed	(Delarue et al., 2000)
Partial COX-deficiency	Muscle	Histochemical test for enzyme activity	p.Ala467Thr; p.Thr914Pro	(Morris et al., 1996)
COX-deficiency	Muscle	Histochemical test for enzyme activity	p.Ala467Thr; p.Leu605Arg	(Stewart et al., 2009)
COX-deficiency			p.Ala467Thr; p.Gly848Ser	
5% COX-deficient fibres			p.Ala467Thr; p.Gly848Ser	
Normal			p.Gly11Asp; p.Ala467Thr; p.Arg852Cys	
Reduced complex IV	Muscle	Biochemical	p.Ala467Thr; c.1251-2A>T	(Schaller et al., 2011)
Reduced complex I, III, IV	Muscle	Histochemical test for enzyme activity	p.Arg227Trp; p.Ala467Thr;	(de Vries et al., 2007)
Reduced complex I, II, III			p.Gly848Ser; p.Ala467Thr	
Reduced complex I, III			p.Ala957Pro; p.Ala467Thr	
Normal Reduced complex I Reduced complex I-III Reduced complex I-IV COX-deficiency	Muscle	Biochemical and histochemical test for enzyme activity	p.Ala467Thr; p.Arg574Trp; p.Gly848Ser; p.Trp748Ser; p.Gly303Arg; p.Ag232His; p.Met1163Arg	(Sofou et al., 2012)

Respiratory Chain Abnormality (% of control value)	Tissue Studied	Type of Investigation	POLG Mutation	Publication
Normal	Muscle	Biochemical	Unknown	(Gauthier-Villars et al., 2001)
Normal	Muscle	Biochemical	p.Trp748Ser	(Naess et al., 2012)
Normal	Muscle	Histochemical test for enzyme activity	p.Ala467Thr;	(Nguyen et al., 2005)
Normal	Muscle		p.Trp748Ser; p.Gly848Ser	
Normal	Muscle	Biochemical	p.Trp748Ser; p.Y1210fs1216X	(Ferrari et al., 2005)
Normal	Muscle	Histochemical test for enzyme activity	Not confirmed	(Schwabe et al., 1997)
Normal	Muscle	Biochemical	p.Thr851Ala; p.Arg1047Trp	(Wiltshire et al., 2008)
Normal	Muscle	Biochemical	p.Ala467Thr; c.3643+2T>C	(Roels et al., 2009)
Normal	Muscle	Biochemical	p.Trp748Ser; p.I948fsX968 p.Ala467Thr; p.T326fsX387 p.Ala467Thr; IVS20nt+2T>C	(Sarzi et al., 2007)
Reduced complex I	Fibroblasts	Biochemical	p.Ala467Thr; c.3643+2T>C	(Roels et al., 2009)
Normal	Fibroblasts	Biochemical	p.Ala467Thr; c.1251-2A>T	(Schaller et al., 2011)
Normal	Fibroblasts	Histochemical test for enzyme activity	p.Arg227Trp; p.Ala467Thr; p.Gly848Ser; p.Ala957Pro	(de Vries et al., 2007)
Normal	Fibroblasts	Biochemical	p.Trp748Ser; p.Y1210fs1216X	(Ferrari et al., 2005)

Table 4.25. Published studies of respiratory chain investigations in patients with Alpers' syndrome.

This table is a comprehensive list of publications. The list is extensive at the time of writing. Science publication databases Pubmed and Web of Knowledge were used with the search terms 'Alpers syndrome' and 'Alpers syndrome respiratory chain deficiency'.

Key: COX=cytochrome c oxidase

4.5.5 *Novel Findings*

This is the first study to examine the severity of respiratory chain deficiency in single neurons in the brains of patients diagnosed with Alpers' syndrome. This project has tested a battery of respiratory chain antibodies in single neurons in a large cohort of patients, which has not been published previously in the literature.

In addition to neurons exhibiting a complex I deficiency, there was a complex III deficiency in all four brain areas. Complex III is rarely investigated in mitochondrial diseases and has revealed a new facet in the pathology of Alpers' syndrome. Complex IV showed a slight deficiency in subunit I while subunit IV showed no change. The occipital lobe demonstrated little respiratory chain deficiency, though moderate neuropathology was shown in this area in patients with a POLG defect. This is surprising and may be due to the fact that neurons with a respiratory deficiency had already disappeared while neurons without any deficiency remained and were counted. The neurons in these young patients were small and it is also possible that some neuronal subtypes may have been too small to assess at the highest magnification of X100. If these neuronal subtypes showed respiratory chain deficiency, it would not have been possible to assess them during this project.

The use of sodium valproate is not recommended in patients with a mitochondrial disease. Unfortunately, it may be administered prior to a full diagnosis. The chronic administration of sodium valproate to healthy rat models resulted in swollen astrocytes in the cerebellum (Sobaniec-Lotowska 2001). Although the mechanism by which sodium valproate becomes harmful in patients with a metabolic disorder is not fully understood, pathological features in healthy rat models suggests that similar pathology may occur in patients with mitochondrial disease. In patients of the cohort, the degree of swelling in the glial cells was different between the two patients examined, suggesting a progression of this pathological feature. In addition, the glial cells were found to have a respiratory chain deficiency which has not been reported in Alpers' syndrome previously. In future projects, further brain areas could be examined for signs of glial cell pathology.

4.6 Future Work

The work performed in this study has highlighted the need for large cohorts when examining respiratory chain deficiencies in Alpers' syndrome. Bringing together many patients allows for deficiencies to be compared between groups of similar patients.

Further assessment of complex I deficiencies in patients would be interesting, allowing research into the assembly of complex I and whether complex I deficiency in patients with Alpers' syndrome is due, in part, to an assembly problem.

Further investigations are needed into respiratory chain deficiencies in glial cell populations in different brain regions and in greater numbers of patients. Discovering the function of the respiratory chain deficient glial cells and correlating the severity of the respiratory chain deficiency, in neurons and glial cells, with the length of disease progression may give insight into the progression of Alpers' syndrome and into *POLG* disorders. Astrocytes were seen that were greatly swollen while others had a milder swollen morphology. Research into whether the degree of swelling correlates with the severity of the disease features would aid understanding into the morphological change in these astrocytes. Whether multiple glial cell populations exhibit respiratory chain deficiencies may increase our knowledge of the pathology and progression of Alpers' syndrome and give hope for possible therapies.

This study has underlined the importance of quantifying the respiratory chain deficiency seen in the neurons of patients, and of examining all cells that play a role in supporting these neurons.

- Antonicka, H., I. Ogilvie, T. Taivassalo, R. P. Anitori, R. G. Haller, J. Vissing, N. G. Kennaway and E. A. Shoubridge (2003). "Identification and Characterization of a Common Set of Complex I Assembly Intermediates in Mitochondria from Patients with Complex I Deficiency." Journal of Biological Chemistry **278**(44): 43081-43088.
- Banati, R. B., R. Egensperger, A. Maassen, G. Hager, G. W. Kreutzberg and M. B. Graeber (2004). "Mitochondria in activated microglia in vitro." Journal of Neurocytology **33**(5): 535-541.
- Blok, M. J., B. J. Van Den Bosch, E. Jongen, A. Hendrickx, C. E. De Die-Smulders, J. E. Hoogendijk, E. Brusse, M. De Visser, B. T. Poll-The, J. Bierau, I. F. De Coo and H. J. Smeets (2009). "The unfolding clinical spectrum of POLG mutations." Journal of Medical Genetics **46**(11): 776-785.
- Boes, M., J. Bauer, H. Urbach, C. E. Elger, S. Frank, M. Baron, G. Zsurka, W. S. Kunz and C. Kornblum (2009). "Proof of progression over time: Finally fulminant brain, muscle, and liver affection in Alpers syndrome associated with the A467T POLG1 mutation." Seizure **18**(3): 232-234.
- Byun, H. M. and A. A. Baccarelli (2014). "Environmental exposure and mitochondrial epigenetics: Study design and analytical challenges." Human Genetics **133**(3): 247-257.
- Chen, Q., E. J. Vazquez, S. Moghaddas, C. L. Hoppel and E. J. Lesnefsky (2003). "Production of reactive oxygen species by mitochondria: Central role of complex III." Journal of Biological Chemistry **278**(38): 36027-36031.
- Darin, N., A. Oldfors, A. R. Moslemi, E. Holme and M. Tulinius (2001). "The incidence of mitochondrial encephalomyopathies in childhood: Clinical features and morphological, biochemical, and DNA abnormalities." Annals of Neurology **49**(3): 377-383.
- Davidzon, G., M. Mancuso, S. Ferraris, C. Quinzii, M. Hirano, H. L. Peters, D. Kirby, D. R. Thorburn and S. DiMauro (2005). "POLG mutations and Alpers syndrome." Annals of Neurology **57**(6): 921-923.
- de Vries, M., R. Rodenburg, E. Morava, E. M. van Kaauwen, H. ter Laak, R. Mullaart, I. Snoeck, P. van Hasselt, P. Harding, L. W. van den Heuvel and J. M. Smeitink (2007). "Multiple oxidative phosphorylation deficiencies in severe childhood multi-system disorders due to polymerase gamma (POLG1) mutations." European Journal of Pediatrics **166**(3): 229-234.

- de Vries, M. C., R. J. Rodenburg, E. Morava, M. Lammens, L. P. W. van den Heuvel, G. C. Korenke and J. A. M. Smeitink (2008). "Normal biochemical analysis of the oxidative phosphorylation (OXPHOS) system in a child with POLG mutations: A cautionary note." Journal of Inherited Metabolic Disease: 1-4.
- Delarue, A., O. Paut, J. M. Guys, M. F. Montfort, V. Lethel, B. Roquelaure, J. F. Pellissier, J. Sarles and J. Camboulives (2000). "Inappropriate liver transplantation in a child with Alpers-Huttenlocher syndrome misdiagnosed as valproate-induced acute liver failure." Pediatric Transplantation **4**(1): 67-71.
- Delonlay, P., A. Rötig and H. B. Sarnat (2013). Respiratory chain deficiencies. **113**: 1651-1666.
- Fernandez-Vizarra, E., M. Bugiani, P. Goffrini, F. Carrara, L. Farina, E. Procopio, A. Donati, G. Uziel, I. Ferrero and M. Zeviani (2007). "Impaired complex III assembly associated with BCS1L gene mutations in isolated mitochondrial encephalopathy." Human Molecular Genetics **16**(10): 1241-1252.
- Ferrari, G., E. Lamantea, A. Donati, M. Filosto, E. Briem, F. Carrara, R. Parini, A. Simonati, R. Sanier and M. Zeviani (2005). "Infantile hepatocerebral syndromes associated with mutations in the mitochondrial DNA polymerase- γ A." Brain **128**(4): 723-731.
- Gauthier-Villars, M., P. Landrieu, V. Cormier-Daire, E. Jacquemin, D. Chrétien, A. Rötig, P. Rustin, A. Munnich and P. De Lonlay (2001). "Respiratory chain deficiency in alpers syndrome." Neuropediatrics **32**(3): 150-152.
- Hakonen, A. H., S. Goffart, S. Marjavaara, A. Paetau, H. Cooper, K. Mattila, M. Lampinen, A. Sajantila, T. Lönnqvist, J. N. Spelbrink and A. Suomalainen (2008). "Infantile-onset spinocerebellar ataxia and mitochondrial recessive ataxia syndrome are associated with neuronal complex I defect and mtDNA depletion." Human Molecular Genetics **17**(23): 3822-3835.
- Hance, N., M. I. Ekstrand and A. Trifunovic (2005). "Mitochondrial DNA polymerase gamma is essential for mammalian embryogenesis." Human Molecular Genetics **14**(13): 1775-1783.
- Hunter, M. F., H. Peters, R. Salemi, D. Thorburn and M. T. MacKay (2011). "Alpers syndrome with mutations in POLG: Clinical and investigative features." Pediatric Neurology **45**(5): 311-318.
- Iizuka, T., F. Sakai, S. Kan and N. Suzuki (2003). "Slowly progressive spread of the stroke-like lesions in MELAS." Neurology **61**(9): 1238-1244.
- Isohanni, P., A. H. Hakonen, L. Euro, I. Paetau, T. Linnankivi, E. Liukkonen, T. Wallden, L. Luostarinen, L. Valanne, A. Paetau, J. Uusimaa, T. Lönnqvist, A. Suomalainen and H. Pihko (2011). "POLG1 manifestations in childhood." Neurology **76**(9): 811-815.

- Janeczko, K. (1991). "The proliferative response of S-100 protein-positive glial cells to injury in the neonatal rat brain." Brain Research **564**(1): 86-90.
- Lax, N. Z. (2011). Understanding the mechanisms of neurodegeneration in mitochondrial disease. Unpublished Ph.D. Thesis., University of Newcastle: U.K.
- Lax, N. Z., P. D. Hepplewhite, A. K. Reeve, V. Nesbitt, R. McFarland, E. Jaros, R. W. Taylor and D. M. Turnbull (2012). "Cerebellar ataxia in patients with mitochondrial DNA disease: A molecular clinicopathological study." Journal of Neuropathology and Experimental Neurology **71**(2): 148-161.
- Lazarou, M., M. McKenzie, A. Ohtake, D. R. Thorburn and M. T. Ryan (2007). "Analysis of the assembly profiles for mitochondrial- and nuclear-DNA-encoded subunits into complex I." Molecular and Cellular Biology **27**(12): 4228-4237.
- Maranzana, E., G. Barbero, A. I. Falasca, G. Lenaz and M. L. Genova (2013). "Mitochondrial respiratory supercomplex association limits production of reactive oxygen species from Complex I." Antioxidants and Redox Signaling.
- Milone, M., N. Brunetti-Pierri, L. Y. Tang, N. Kumar, M. M. Mezei, K. Josephs, S. Powell, E. Simpson and L. J. C. Wong (2008). "Sensory ataxic neuropathy with ophthalmoparesis caused by POLG mutations." Neuromuscular Disorders **18**(8): 626-632.
- Morris, A. A. M., R. Singh-Kler, R. H. Perry, P. D. Griffiths, A. D. Burt, W. Chee Pian, D. Gardner-Medwin and D. M. Turnbull (1996). "Respiratory chain dysfunction in progressive neuronal degeneration of childhood with liver disease." Journal of Child Neurology **11**(5): 417-419.
- Naess, K., M. Barbaro, H. Bruhn, R. Wibom, I. Nennesmo, U. von Döbeln, N. G. Larsson, A. Nemeth and N. Lesko (2012). "Complete deletion of a *POLG1* allele in a patient with Alpers syndrome." JIMD Reports **4**: 67-73.
- Nguyen, K. V., E. Østergaard, S. Holst Ravn, T. Balslev, E. Rubæk Danielsen, A. Vardag, P. J. McKiernan, G. Gray and R. K. Naviaux (2005). "POLG mutations in Alpers syndrome." Neurology **65**(9): 1493-1495.
- Reichner, J. S., J. A. Mulligan and H. C. Bodenheimer Jr (1995). "Electron transport chain activity in normal and activated rat macrophages." Journal of Surgical Research **59**(6): 636-643.
- Roels, F., P. Verloo, F. Eyskens, B. François, S. Seneca, B. De Paepe, J.-J. Martin, V. Meersschaut, M. Praet, E. Scalais, M. Espeel, J. Smet, G. Van Goethem and R. Van Coster (2009). "Mitochondrial mosaics in the liver of 3 infants with mtDNA defects." BMC Clinical Pathology **9**(1): 1-12.

- Sarzi, E., A. Bourdon, D. Chrétien, M. Zarhrate, J. Corcos, A. Slama, V. Cormier-Daire, P. de Lonlay, A. Munnich and A. Rötig (2007). "Mitochondrial DNA Depletion is a Prevalent Cause of Multiple Respiratory Chain Deficiency in Childhood." The Journal of Pediatrics **150**(5): 531-534.e536.
- Schaller, A., D. Hahn, C. B. Jackson, I. Kern, C. Chardot, D. C. Belli, S. Gallati and J. Nuoffer (2011). "Molecular and biochemical characterisation of a novel mutation in POLG associated with Alpers syndrome." BMC Neurology **11**.
- Schwabe, M. J., W. B. Dobyns, B. Burke and D. L. Armstrong (1997). "Valproate-induced liver failure in one of two siblings with alpers disease." Pediatric Neurology **16**(4): 337-343.
- Sobaniec-Lotowska, M. E. (2001). "Ultrastructure of Purkinje cell perikarya and their dendritic processes in the rat cerebellar cortex in experimental encephalopathy induced by chronic application of valproate." International Journal of Experimental Pathology **82**(6): 337-348.
- Sofou, K., A.-R. Moslemi, G. Kollberg, I. Bjarnadóttir, A. Oldfors, I. Nennesmo, E. Holme, M. Tulinius and N. Darin (2012). "Phenotypic and genotypic variability in Alpers syndrome." European Journal of Paediatric Neurology **16**(4): 379-389.
- Stewart, J. D., S. Tennant, H. Powell, A. Pyle, E. L. Blakely, L. He, G. Hudson, M. Roberts, D. du Plessis, D. Gow, L. D. Mewasingh, M. G. Hanna, S. Omer, A. A. Morris, R. Roxburgh, J. H. Livingston, R. McFarland, D. M. Turnbull, P. F. Chinnery and R. W. Taylor (2009). "Novel POLG1 mutations associated with neuromuscular and liver phenotypes in adults and children." Journal of Medical Genetics **46**(3): 209-214.
- Verkaart, S., W. J. H. Koopman, S. E. van Emst-de Vries, L. G. J. Nijtmans, L. W. P. J. van den Heuvel, J. A. M. Smeitink and P. H. G. M. Willems (2007). "Superoxide production is inversely related to complex I activity in inherited complex I deficiency." Biochimica et Biophysica Acta - Molecular Basis of Disease **1772**(3): 373-381.
- Visapää, I., V. Fellman, J. Vesa, A. Dasvarma, J. L. Hutton, V. Kumar, G. S. Payne, M. Makarow, R. Van Coster, R. W. Taylor, D. M. Turnbull, A. Suomalainen and L. Peltonen (2002). "GRACILE syndrome, a lethal metabolic disorder with iron overload, is caused by a point mutation in BCS1L." American Journal of Human Genetics **71**(4): 863-876.
- Wiltshire, E., G. Davidzon, S. Dimauro, H. O. Akman, L. Sadleir, L. Haas, J. Zuccollo, A. McEwen and D. R. Thorburn (2008). "Juvenile Alpers disease." Archives of Neurology **65**(1): 121-124.

Chapter 5 Mitochondrial DNA Deletion and Depletion in Alpers' Syndrome

5.1 Introduction

The integrity of mitochondrial DNA (mtDNA) is central to the functioning of the respiratory chain and the production of ATP. POLG is the sole DNA polymerase to replicate mtDNA in mammalian cells and is essential for life (Hance et al., 2005). POLG is encoded by a nuclear gene, mutations of which may result in dysfunction of the polymerase and inaccurate replication of mtDNA. This inaccurate replication has been reported to lead to deletions in the mtDNA (Van Goethem et al., 2001; Kollberg et al., 2006) and to a depletion of mtDNA content (Naviaux et al., 1999; Uusimaa et al., 2008). MtDNA deletion and depletion may result in a reduced expression of respiratory chain complexes, leading to respiratory chain deficiency and reducing the capacity for oxidative phosphorylation and ATP production, leading to cellular dysfunction. The CNS is very susceptible to changes in ATP levels, and both mtDNA deletion and depletion may act to decrease the amount of ATP produced and ultimately have a negative effect on the functioning of the CNS and brain.

Previous studies have examined mtDNA deletion and depletion in patients with Alpers' syndrome in a variety of tissues, including muscle, liver, brain, and fibroblasts, describing either mtDNA deletion, depletion, or a combination of both (Naviaux et al., 1999; Ferrari et al., 2005; Kollberg et al., 2006). It is unclear whether one form of mtDNA damage is more prominent than the other, or whether they may occur together in a single cell. Unfortunately, many studies have been unable to answer this question. The method of tissue analysis is of great importance regarding what can be interpreted from the results of a study. The type of tissue is central to accurately assessing the health of mtDNA in neurons. The studies mentioned previously do not specify the type of tissue used to achieve the results, whether homogenate tissue or a single cell analysis. The analysis of single neurons allows for the increased sensitivity of a test and the accurate assessment of any mtDNA deletion and depletion.

The previous chapters examined the neuropathology and respiratory chain deficiency in different brain areas of the cohort. This chapter will investigate mtDNA deletions and depletion and quantify this in single neurons from a subset of patients from the cohort.

5.2 Aims

Patients with Alpers' syndrome have shown clear respiratory chain dysfunction in neurons. The aims of this work are:

1. To assess the mtDNA damage (mtDNA deletions and mtDNA depletion) in single neurons taken from frozen brain tissue.
2. To investigate mtDNA damage in a wide age range of patients. MtDNA damage will be investigated in a young patient and in older teenage-adult patients, each with age-matched control tissue.

5.3 Methodological Approach

5.3.1 Patients and Controls

Three patients and three age-matched controls were analysed to assess mtDNA damage (Table 5.1). These patients from the cohort were chosen based upon frozen tissue availability.

Patient	Age at Death (years)	Sex	POLG Mutation	Available Brain Areas
Patient 3	17	M	p.Ala467Thr; p.Ala467Thr	Frontal lobe
Control 3	19	M	N/A	Parietal lobe, frontal lobe, temporal lobe
Patient 4	24	F	p.Ala467Thr; p.Trp748Ser	Parietal lobe, occipital lobe, cerebellum, basal ganglia, frontal lobe, temporal lobe
Control 4	27	M	N/A	Parietal lobe, frontal lobe, temporal lobe
Patient 12	6	M	None	Parietal lobe, occipital lobe, basal ganglia
Control 9	6	F	N/A	Parietal lobe, occipital lobe, cerebellum, basal ganglia

Table 5.1. Details of the patients and controls used in the study of mtDNA abnormalities.

Frozen tissue was used for patients and controls.

Key: N/A=not applicable

5.3.2 SDH Histochemistry

Frozen brain tissue sections from three patients and three controls (Table 5.1) were assessed by SDH histochemistry in order to visualise neurons. Sequential COX/SDH histochemistry was used to provide further information, highlighting neurons with a mtDNA defect which was shown by neurons that were COX-deficient and SDH-positive. This was performed for one patient but could not be performed for all patients as the SDH reactivity proved to be low in most of the tissue samples, possibly due to the length of time in storage.

20µm sections of frozen tissue were mounted on PEN slides (Leica Microsystems) and SDH histochemistry performed. After air drying, laser capture micro-dissection of single neurons was performed using the Zeiss Laser Microdissection System. Cells lysed overnight at 56°C using Tris-HCl buffer, Tween 1% and proteinase K. The next day, the proteinase K was deactivated at 95°C for 10 minutes before further applications.

5.3.3 Real-time PCR

The lysate from each neuron was tested in triplicate using quantitative real-time PCR with precise fluorogenic TaqMan probes (Applied Biosystems) to assess the amplification of the mitochondrial genes *MT-ND1* and *MT-ND4*. The percentage of deletions in mtDNA was calculated using the relative proportions of amplified *MT-ND4* to *MT-ND1*, using the Δ Ct method. The depletion of mtDNA (copy number) in single neurons was calculated using a standard curve derived from control samples of known copy number. The values were corrected to account for lysate volume and neuron area (µm²). A Ct value of less than 30 was considered to indicate DNA in the sample.

A well-known limitation of real-time PCR is that it is inaccurate when detecting low levels of heteroplasmy, below 30%, as the sensitivity of the method does not allow for detection of these low levels. The technique may detect up to 30% heteroplasmy even if no mtDNA deletions are present. Suitable methods for detecting low levels of heteroplasmy are only available for specific mutations using PCR-based methods, for example SYBR Green.

5.3.4 Statistical Testing

Both parametric and non-parametric statistical tests were used in this study. The normality of the data and the variance of the data were assessed using the Anderson-Darling normality test and the F-test of Variances. If the data were statistically normal with normal variance, the unpaired two-tailed t-test was used. For data that were not statistically normal, the non-parametric Mann-Whitney U test was used.

5.4 Results

5.4.1 Mitochondrial DNA Deletion

MtDNA deletion was assessed in single neurons subjected to SDH histochemistry and analysed with real-time PCR. Sequential COX/SDH histochemistry was not performed as the SDH reactivity proved to be low in most of the tissue, possibly due to the length of time in storage.

Neurons were assessed from control tissues and showed values that were compatible with no mtDNA deletions being present.

5.4.1.1 Young Adult Patients – Single Histochemistry

Patient 3, a 17 year old male, was a *POLG* mutation-positive patient that was sex-/age-matched to Controls 3 and 4. The frontal lobe only was available and neurons were tested from this region. The tissue was subjected to SDH histochemistry only.

Patient 3 shows high levels of mtDNA deletions in a subset of neurons (Figure 5.1). The majority of neurons from Patient 3 had values within the experimental error of the assay (see above). This indicates that a subset of neurons from the patient may contain mtDNA deletions. The values in neurons from controls were compatible with no mtDNA deletions being present.

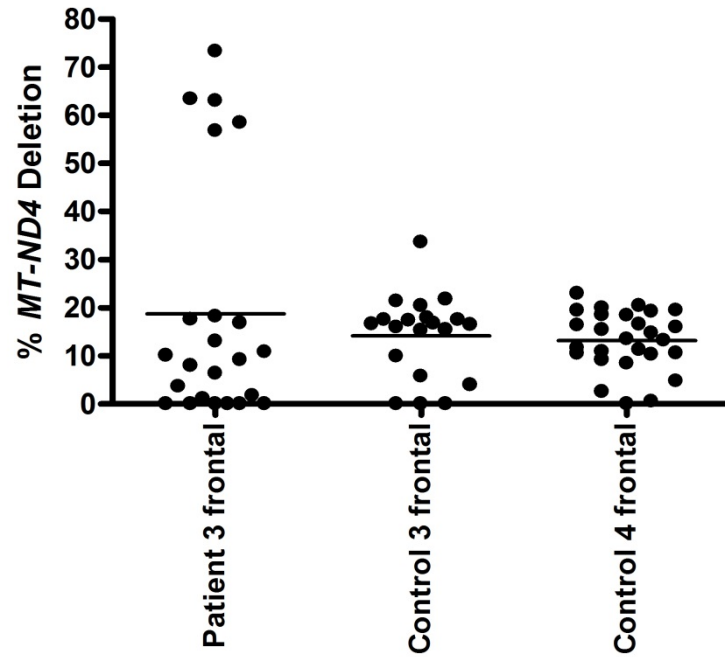


Figure 5.1. *MT-ND4* deletions in frontal lobe of Patient 3 and Controls 3 and 4.

The majority of neurons of the frontal lobe of Patient 3 have percentage values within the experimental error of the assay. A subset of neurons has high percentage values of *MT-ND4* deletions.

Patient 4, a 24 year old female, was a *POLG* mutation-positive patient that was age-matched to Controls 3 and 4. Neurons were tested from the parietal lobe, frontal lobe and temporal lobe. These three brain regions were chosen in order to have matching control brain regions to compare the patient results to, as other brain regions were not available for the controls. The tissue was subjected to SDH histochemistry only.

Patient 4 shows evidence of mtDNA deletions in a small subset of neurons from the parietal lobe (Figure 5.2). The majority of neurons from Patient 4 had values within the experimental error of the assay. No mtDNA deletions were observed in the frontal lobe and temporal lobe. The values in neurons from controls were compatible with no mtDNA deletions being present.

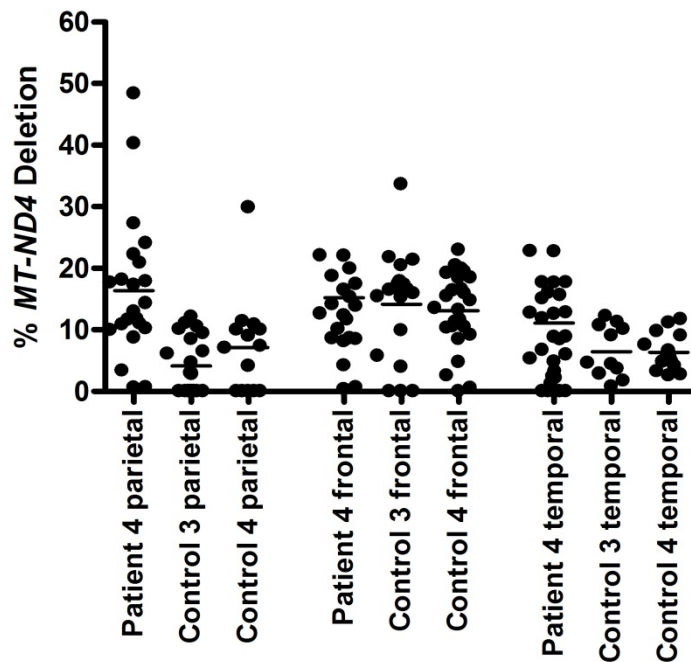


Figure 5.2. *MT-ND4* deletions in Patient 4 and Controls 3 and 4.

The majority of neurons of the parietal lobe of Patient 4 have percentage values within the experimental error of the assay. A subset of neurons in the parietal lobe has high percentage values of *MT-ND4* deletions. The neurons of the frontal lobe and temporal lobe have percentage values within the experimental error of the assay.

5.4.1.2 *Young Adult Patients – Sequential Histochemistry*

Sequential COX/SDH histochemistry was assessed for Patient 4 only. Patient 3 was not considered for this assessment as single SDH histochemistry was weak on the glass slides, so sequential COX/SDH histochemistry was not considered useful or informative.

Only mtDNA deletions could be assessed when using sequential COX/SDH histochemistry as 3' 3-diaminobenzidine (DAB), used in the visualisation of COX histochemistry, has been shown to interfere with the PCR method used in calculating DNA copy number (Murphy et al., 2012).

Six different brain areas were available for Patient 4 and neurons were tested from the occipital lobe, parietal lobe, basal ganglia, cerebellum, frontal lobe and temporal lobe. The tissues were subjected to sequential COX/SDH histochemistry.

The results show that both COX-positive and COX-deficient neurons contain mtDNA deletions. Whilst in many brain regions there was a slight increase in the number of cells with high levels of mtDNA deletion in COX-deficient neurons, a clear difference was only observed in the Purkinje cells of the cerebellum (Figure 5.3). In the basal ganglia, it was the lateral area of the globus pallidus that showed a clear difference (Figure 5.4).

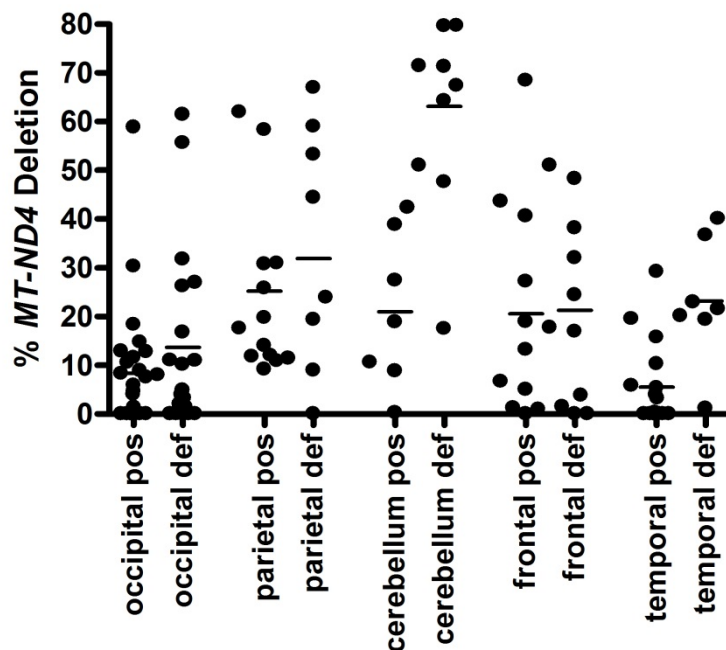


Figure 5.3. *MT-ND4* deletions in Patient 4 taken from slides with sequential COX/SDH histochemistry.

The percentage of *MT-ND4* deletions in COX-positive neurons are compared to COX-deficient neurons in Patient 4. Purkinje cells were investigated from the cerebellum. Pyramidal neurons were investigated from the cerebral brain areas. A clear increase in the percentage of *MT-ND4* deletions in COX-deficient neurons compared to COX-positive neurons is seen in the cerebellum.

Key: pos=COX-positive, def=COX-deficient

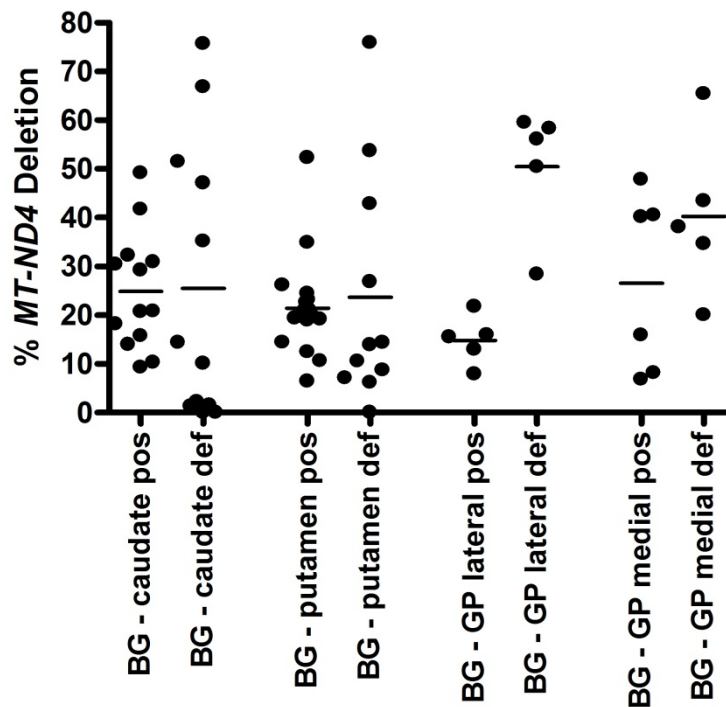


Figure 5.4. *MT-ND4* deletions in Patient 4 taken from slides with sequential COX/SDH histochemistry from the basal ganglia.

The percentage of *MT-ND4* deletions in COX-positive neurons are compared to COX-deficient neurons in Patient 4. This figure shows the percentage of *MT-ND4* deletions in different areas of the basal ganglia. A clear increase in the percentage of *MT-ND4* deletions in COX-deficient neurons compared to COX-positive neurons is seen in the lateral globus pallidus.

Key: pos=COX-positive, def=COX-deficient

5.4.1.3 Young Child Patient

Patient 12, a 6 year old male without a *POLG* mutation, was age-matched to Control 9. Three different brain areas were available: the occipital lobe, the parietal lobe and the basal ganglia. The tissues were subjected to SDH histochemistry only.

The neurons from Patient 12 and from Control 9 had mtDNA deletion values within the experimental error of the assay (Figure 5.5). These values were compatible with no mtDNA deletions being present.

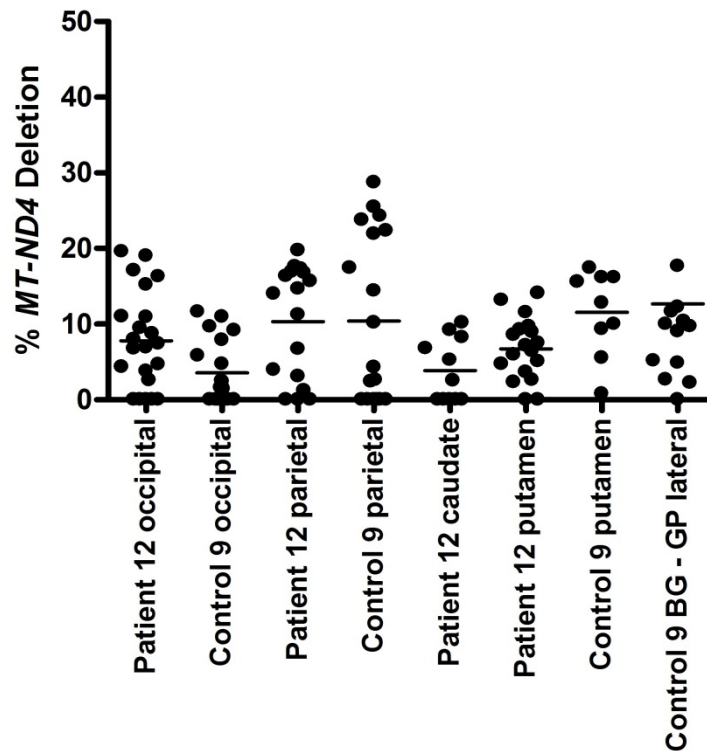


Figure 5.5. *MT-ND4* deletions in Patient 12 and Control 9.

The neurons of the occipital lobe, parietal lobe, and basal ganglia of Patient 12 have percentage values within the experimental error of the assay.

Key: BG=basal ganglia, GP=globus pallidus

5.4.2 *Mitochondrial DNA Depletion*

MtDNA depletion (copy number) was assessed in single neurons subjected to SDH histochemistry and assessed with real-time PCR. Sequential COX/SDH histochemistry was not performed as 3' 3-diaminobenzidine (DAB), used in the visualisation of COX histochemistry, has been shown to interfere with the PCR method used in calculating DNA copy number.

Neurons were assessed from control tissues. Some control neurons gave values that suggested they contained a low mtDNA copy number. This may be due to a variation produced by the real-time PCR method and due to this a large number of neurons were assessed for both controls and patients. The mean value of mtDNA copy number in the group of assessed neurons for a particular brain area was taken for controls and compared to the mean value of mtDNA copy number in the group of assessed neurons for the patient.

5.4.2.1 *Young Adult Patients*

Patient 3, a 17 year old male, was a *POLG* mutation-positive patient that was sex-/age-matched to Controls 3 and 4. The frontal lobe only was available and neurons were tested from this region. The tissue was subjected to SDH histochemistry only.

Patient 3 shows low mtDNA copy number (Figure 5.6) that is significantly different from the control values in the frontal lobe.

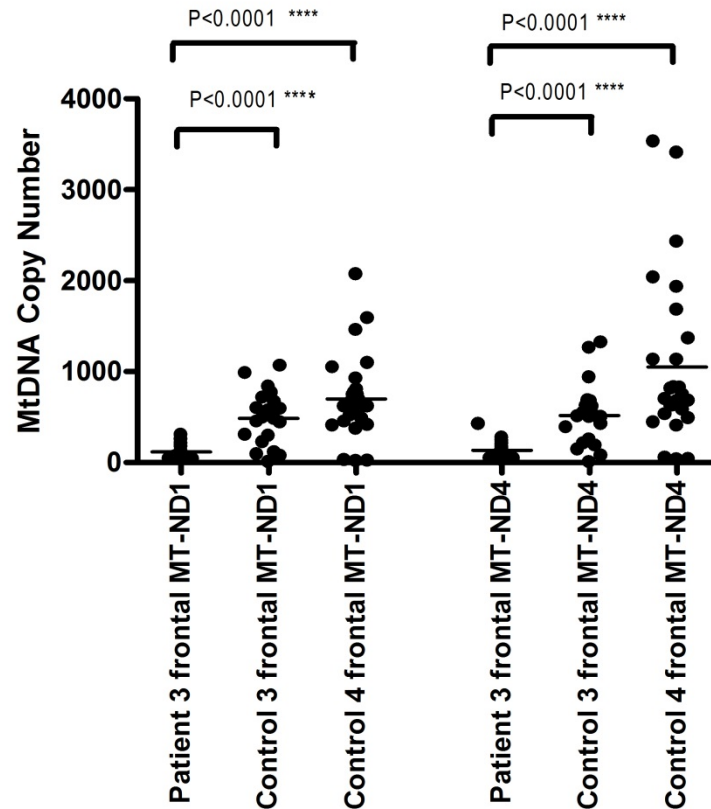


Figure 5.6. MtDNA copy number in frontal lobe of Patient 3 and Controls 3 and 4.

The neurons of the frontal lobe of Patient 3 have a low mtDNA copy number that is significantly different to control values. The Mann-Whitney U test was used. * $P < 0.05$, ** $P < 0.01$, *** $P < 0.001$, **** $P < 0.0001$. MtDNA copy number is expressed as the number of mtDNA molecules per neuronal cell body area (μm^2).

Patient 4, a 24 year old female, was a *POLG* mutation-positive patient that was age-matched to Controls 3 and 4. Neurons were tested from the parietal lobe, frontal lobe and temporal lobe. These three brain regions were chosen in order to have matching control brain regions to compare the patient results to, as other brain regions were not available for the controls. The tissues were subjected to SDH histochemistry only.

Patient 4 shows low mtDNA copy number. This is significantly different from the control for both *MT-ND1* and *MT-ND4* in the parietal lobe (Figure 5.7) and the frontal lobe (Figure 5.8). MtDNA copy number is not significantly different between Patient 4 and both controls in the temporal lobe (Figure 5.9).

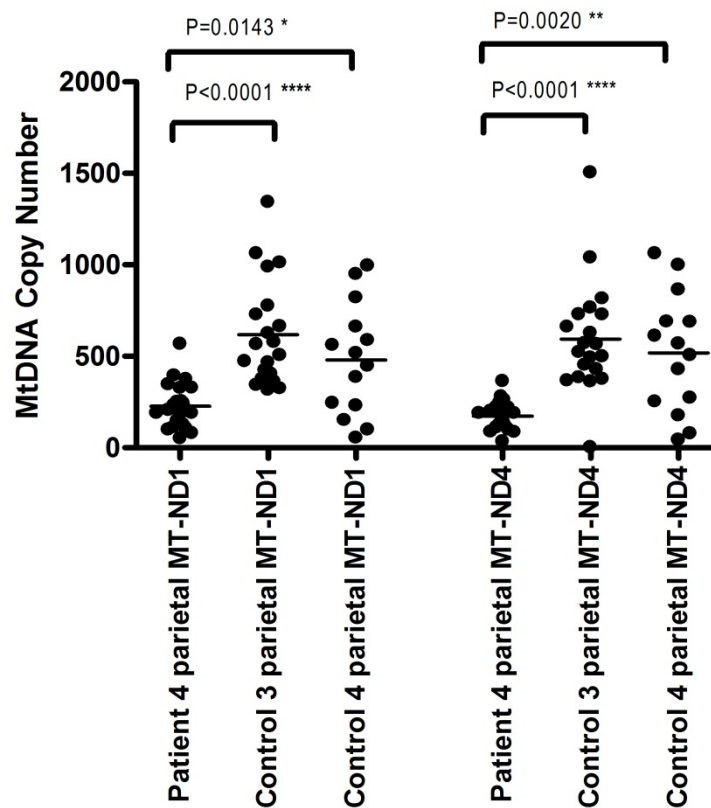


Figure 5.7. MtDNA copy number in parietal lobe of Patient 4 and Controls 3 and 4.

The neurons of the parietal lobe of Patient 4 have a low mtDNA copy number that is significantly different to control values. The Mann-Whitney U test was used. * $P < 0.05$, ** $P < 0.01$, *** $P < 0.001$, **** $P < 0.0001$. MtDNA copy number is expressed as the number of mtDNA molecules per neuronal cell body area (μm^2).

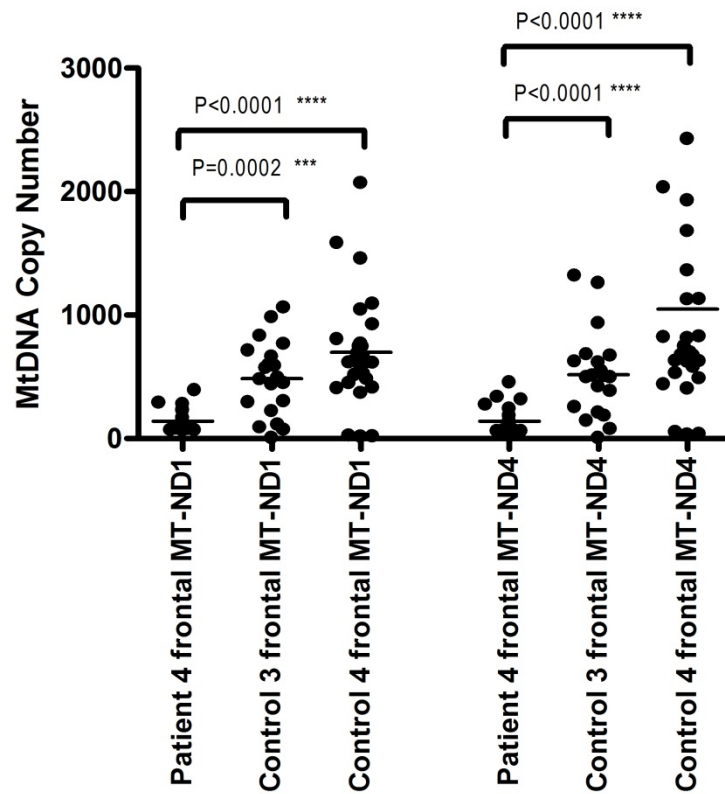


Figure 5.8. MtDNA copy number in frontal lobe of Patient 4 and Controls 3 and 4.

The neurons of the frontal lobe of Patient 4 have a low mtDNA copy number that is significantly different to control values. The Mann-Whitney U test was used. * $P < 0.05$, ** $P < 0.01$, *** $P < 0.001$, **** $P < 0.0001$. MtDNA copy number is expressed as the number of mtDNA molecules per neuronal cell body area (μm^2).

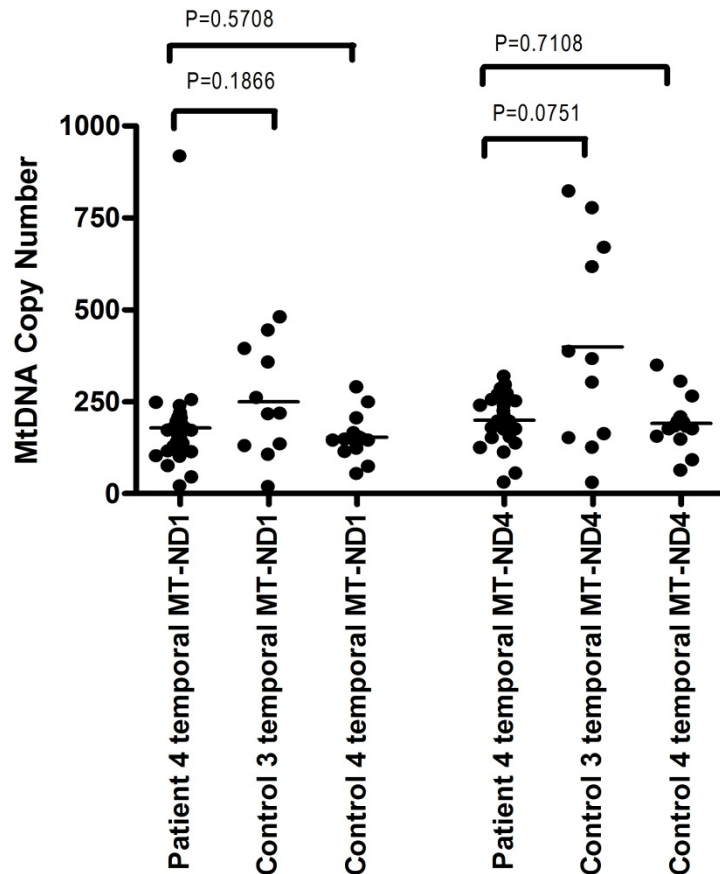


Figure 5.9. MtdNA copy number in temporal lobe of Patient 4 and Controls 3 and 4.

The neurons of the temporal lobe of Patient 4 have a mtDNA copy number that is not significantly different to control values. An unpaired two-tailed t-test was used. The Mann-Whitney U test was used to determine the values for Patient 4 *MT-ND4* vs Control 3 *MT-ND4*, and Patient 4 *MT-ND1* vs Control 4 *MT-ND1* as the variances differed significantly. * $P < 0.05$, ** $P < 0.01$, *** $P < 0.001$, **** $P < 0.0001$. MtdNA copy number is expressed as the number of mtDNA molecules per neuronal cell body area (μm^2).

5.4.2.2 Young Child Patient

Patient 12, a 6 year old male without a *POLG* mutation, was age-matched to Control 9. Three different brain areas were available and neurons were tested from the occipital lobe, parietal lobe and basal ganglia. The tissues were subjected to SDH histochemistry only.

Patient 12 shows low mtDNA copy number. This is significantly different between the range of neuronal values of the patient and the range of neuronal values of the control in the occipital lobe (Figure 5.10), the parietal lobe (Figure 5.11) and the putamen (Figure 5.12).

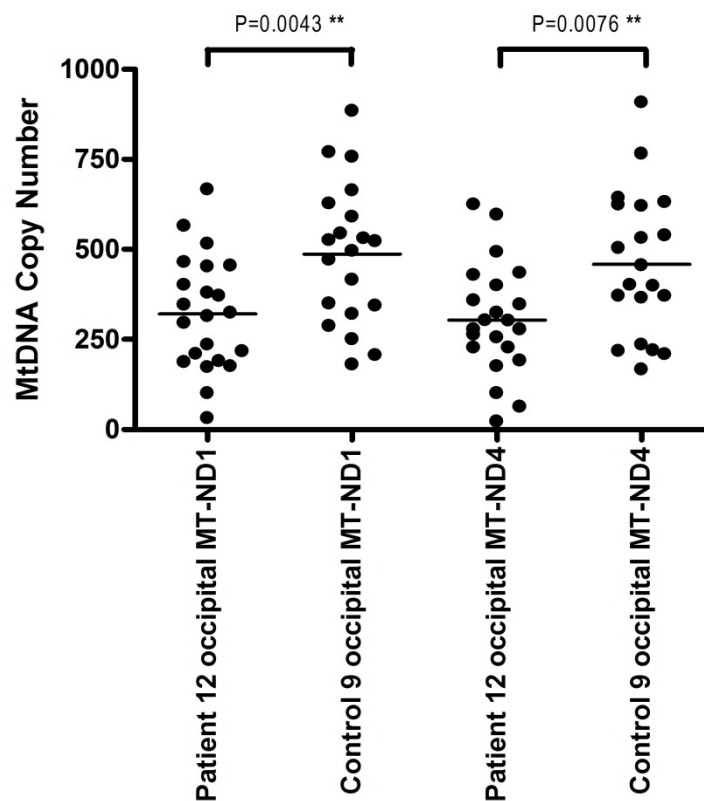


Figure 5.10. MtDNA copy number in occipital lobe Patient 12 and Control 9.

The neurons of the occipital lobe of Patient 12 have a low mtDNA copy number that is significantly different to control values. An unpaired two-tailed t-test was used. * $P < 0.05$, ** $P < 0.01$, *** $P < 0.001$, **** $P < 0.0001$. MtDNA copy number is expressed as the number of mtDNA molecules per neuronal cell body area (μm^2).

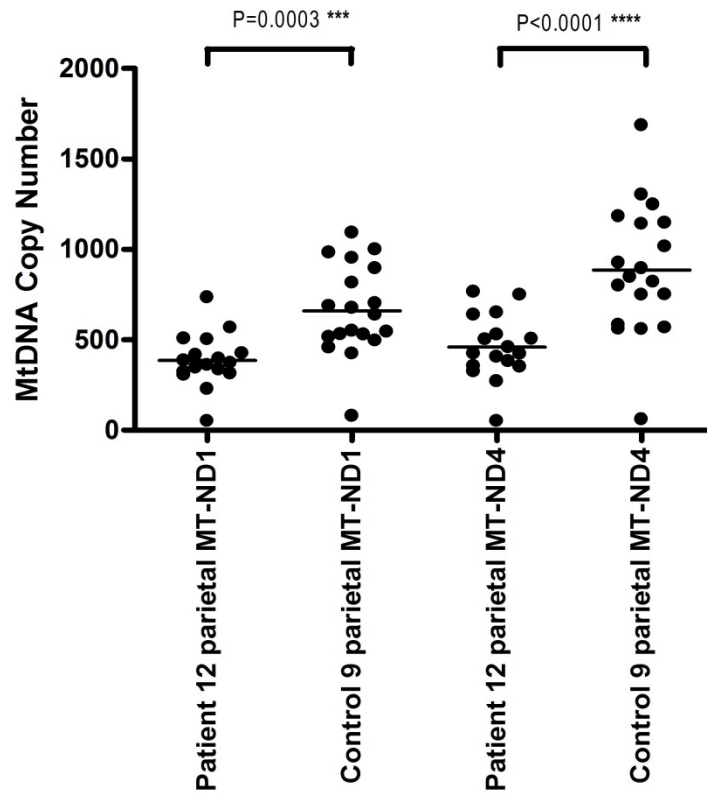


Figure 5.11. MtDNA copy number in parietal lobe Patient 12 and Control 9.

The neurons of the parietal lobe of Patient 12 have a low mtDNA copy number that is significantly different to control values. An unpaired two-tailed t-test was used. * $P < 0.05$, ** $P < 0.01$, *** $P < 0.001$, **** $P < 0.0001$. MtDNA copy number is expressed as the number of mtDNA molecules per neuronal cell body area (μm^2).

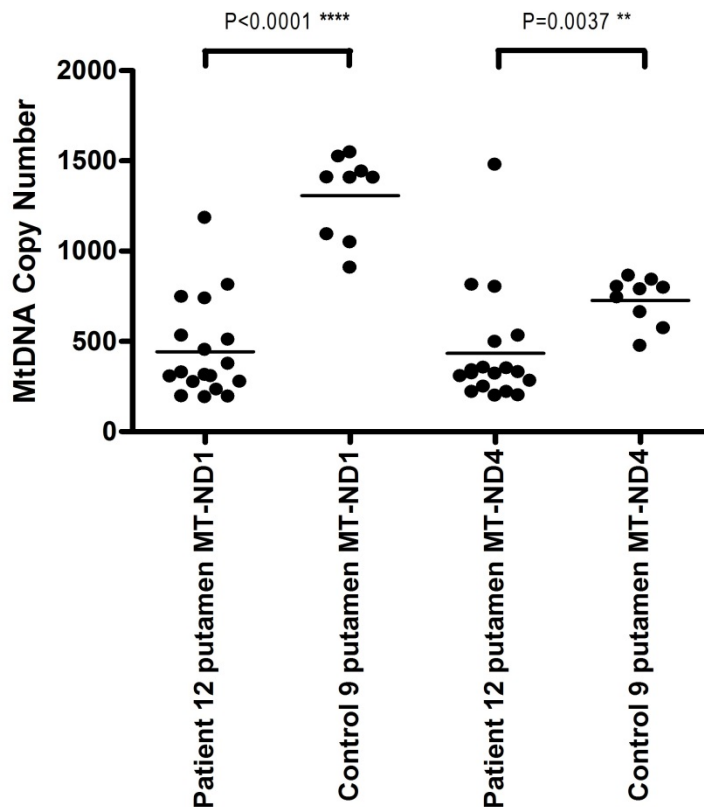


Figure 5.12. MtDNA copy number in the putamen of the basal ganglia from Patient 12 and Control 9.

The neurons of the putamen of the basal ganglia of Patient 12 have a low mtDNA copy number that is significantly different to control values. An unpaired two-tailed t-test was used to determine the values for *MT-ND1*. The Mann-Whitney U test was used to determine the values for *MT-ND4* as the variances differed significantly. * $P < 0.05$, ** $P < 0.01$, *** $P < 0.001$, **** $P < 0.0001$. MtDNA copy number is expressed as the number of mtDNA molecules per neuronal cell body area (μm^2).

5.5 Discussion

This chapter has examined for the presence of mtDNA abnormalities in neurons of patients with confirmed *POLG* mutations and a patient with no mutations in *POLG*.

5.5.1 Inter-group Variation

Patient 12, a 6 year old male, is a young child patient with no mutation in *POLG* (Table 5.1). In the occipital lobe, parietal lobe, and caudate and putamen of the basal ganglia, the patient shows levels of mtDNA deletion within the experimental error of this assay (<30%).

Patients 3 and 4 are young adult patients with common mutations in *POLG*; Patient 3, a 17 year old male, is homozygous for the p.Ala467Thr mutation and Patient 4, a 24 year old female, is compound heterozygous for the p.Ala467Thr and p.Trp748Ser mutations (Table 5.1).

Patient 3 shows both low levels (<30%) and high levels (>70%) of mtDNA deletion in subsets of neurons. There are two clear groupings of neurons with either low or high levels of mtDNA deletions. This may indicate a changing level of mtDNA loss in some neurons and a change towards an increased number of neurons with high levels of mtDNA deletions over time. The two populations have very distinct mtDNA deletion levels which may also indicate different neuronal subtypes that were sampled. It is not possible to morphologically distinguish different neuronal subtypes in a frozen tissue sample and neuronal subtypes that are more vulnerable to mtDNA damage may be present in the sample. Patient 3 shows moderate levels of mtDNA depletion in the frontal lobe.

Patient 4 shows levels of mtDNA deletion within the experimental error of this assay (<30%) in the parietal lobe, frontal lobe, and temporal lobe. The parietal lobe shows some neurons with moderate levels of deletion (>30% and <70%). The patient shows moderate levels of mtDNA depletion in the parietal lobe and frontal lobe. The temporal lobe is relatively spared and does not show any mtDNA depletion, which agrees with the general clinical description of Alpers' syndrome of there being no features of the disease directly correlating with temporal lobe damage. It is possible that neurons in this area of the brain are not as susceptible to damage as neurons in the occipital lobe and frontal lobe.

Depletion of mtDNA appears to play a greater role in Alpers' syndrome and results in reduced expression of respiratory chain complexes and impaired OXPHOS capabilities. Both the young patient and adult patients have more significant levels of mtDNA depletion than mtDNA deletion. MtDNA deletions do not appear to be consistently at high levels in any of the patients. However, the adult patients show a subset of their neurons with high levels of mtDNA deletion, suggesting that these deletions increase in some neurons over time.

5.5.2 COX-Positive and COX-Deficient Neurons

MtDNA deletions were assessed in COX-positive and COX-deficient neurons from Patient 4, in order to investigate whether there is a difference between mtDNA deletion levels in neurons showing mitochondrial abnormalities. MtDNA depletion was not assessed as 3' 3-diaminobenzidine (DAB), used in the visualisation of COX histochemistry, has been shown to interfere with the PCR method used in calculating DNA copy number (Murphy et al., 2012).

All the brain regions studied showed a trend of a higher percentage of deletions in the COX-deficient neurons when compared to the COX-positive neurons. Unsurprisingly, this suggests that COX-deficient neurons harbour more mtDNA deletions than COX-positive neurons and that these mtDNA deletions could have affected the mitochondria's capability to perform oxidative phosphorylation. Neurons that are COX-deficient and show levels of mtDNA deletion within the experimental error of this assay (<30%) may have a true deletion level that is higher because low levels are not accurately detected by the real-time PCR method. Alternative methods to quantify low levels of mtDNA deletions and depletion currently include other PCR-based techniques, such as nested real-time PCR.

5.5.3 The Project's Findings in the Context of the Literature

The previous literature on patients with Alpers' syndrome contains many reports of mtDNA depletion (Naviaux et al., 1999; Naviaux and Nguyen 2004; Ferrari et al., 2005; Scalais et al., 2012). The findings in this study are in agreement with previous investigations that found mtDNA depletion in patient tissues. Additionally, mtDNA deletions have been reported in muscle tissue of patients with Alpers' syndrome (Kollberg et al., 2006), however mtDNA deletions are not as commonly reported as mtDNA depletion. This study found mtDNA depletion seemed to be more prevalent than mtDNA deletions in terms of the mtDNA defect detected.

A study assessing patient groups both with *POLG* mutations and without *POLG* mutations suggested differences in mtDNA abnormalities. Patients with *POLG* mutations showed more mtDNA deletions and/or mtDNA depletion but patients without *POLG* mutations showed no mtDNA deletions or depletion (Sofou et al., 2012). My study does not agree with this as both patient groups with either *POLG* mutations or without *POLG* mutations showed mtDNA damage. However, greater numbers of patients and controls are needed to confirm this. The lack of mtDNA damage in the patients without a *POLG* mutation in the published study is odd and may be attributable to the use of skeletal muscle and blood tissue samples to analyse the mtDNA, extracting mtDNA from homogenate tissue as opposed to single cells. The data compiled in this thesis chapter have been derived from single cell analysis of neurons from different regions of the brain, allowing for a much more sensitive test for the presence of mtDNA deletions and depletion in patients. The inclusion of neurons from a greater number of controls per patient group would further increase the accuracy of the test.

Studies investigating both mtDNA deletion and depletion have primarily looked at muscle and liver tissues, with fewer studies including brain tissue for examination. Investigations into a patient with Alpers' syndrome showed reduced mtDNA content of 15% and 33% in liver and muscle respectively with a normal mtDNA content in brain, relative to controls (Uusimaa et al., 2008). It is unusual that brain tissue appeared to have no mtDNA deletions or depletion. However, if a homogenate tissue sample was used for the analysis then a mixture of neurons and other less susceptible cell types would have been included in the sample and this may explain the result of no mtDNA depletion.

Other studies have examined non-CNS tissues including skeletal muscle, liver, and fibroblast cells and these have shown variable and tissue-specific mtDNA damage. A reported case exhibited a reduced mtDNA content of 8% in skeletal muscle and 8% in liver, and in another patient reduced mtDNA content of 23% in liver compared to the control (Taanman et al., 2009). In a separate study, a patient showed severely reduced mtDNA content of 78% and 15% in skeletal muscle and liver respectively with a normal mtDNA content of fibroblasts, relative to controls (Schaller et al., 2011). A patient showed reduced mtDNA content of 21%, 27%, and 98% in skeletal muscle, liver and blood respectively, compared to controls (Scalais et al., 2012). These studies show severely reduced mtDNA content in liver, variably reduced mtDNA content in skeletal muscle, and near normal mtDNA content in fibroblast and blood samples.

Fibroblasts rarely show mtDNA depletion or acquire the mtDNA defects to the same levels seen in post-mitotic cells. The liver shows moderate to high levels of mtDNA depletion which coincides with the severe pathology seen during the course of the disease. Skeletal muscle shows moderate levels of mtDNA depletion which suggests a level of pathology that does not manifest itself during the early stages of the disease. Symptoms in skeletal muscle are rarely described in the literature and may indicate a sub-pathological role for mtDNA abnormalities in muscle.

5.5.4 Novel Findings

This study performed real-time PCR analysis on single neurons from a young patient and two teenage-adult patients with *POLG* disorders. The analysis of individual neurons, as opposed to a homogenate tissue sample, has increased the sensitivity of the test and allowed the assessment of questions about neuronal vulnerability. MtDNA depletion appeared to be a more significant defect in the patients than mtDNA deletion levels, signifying that depletion plays a greater role in the disease progression of Alpers' syndrome. Greater levels of mtDNA depletion occur in both the young patient and in adult patients suggesting mtDNA depletion is a prominent feature at all ages. MtDNA deletions are seen in a subset of neurons from the adult patients but not in the young patient, suggesting that mtDNA deletions can accumulate to higher levels over time. MtDNA depletion affects neurons in the parietal and frontal lobes in adult patients, and the parietal and occipital lobes, as well as the putamen of the basal ganglia in a young patient. MtDNA depletion is not detected in the temporal lobe when assessed in adult patients. This is a rarely studied brain area in patients as the general clinical description of Alpers' syndrome does not necessarily correlate with temporal lobe damage and there is no neuropathological evidence in the pathologist's report to suggest that there is temporal lobe damage in these patients; a finding reiterated in this study.

5.6 Future Work

The work performed in this study has highlighted the need for further cellular studies of mtDNA abnormalities in patients with *POLG* mutations and Alpers' syndrome. The effect of mtDNA abnormalities on the respiratory chain and on oxidative phosphorylation is not fully understood. Further studies into the mechanism of this will add to our understanding of how the disease pathology progresses, particularly in patients with clinically diagnosed Alpers' syndrome where no *POLG* mutations are present. Also, a greater number of controls are required to compare with patient results. Suitable control tissue is extremely difficult to obtain due to the sensitivity of the age of the control, and this should be taken into account for timescale considerations of a study.

MtDNA depletion appears to play a greater role in disease progression, though mtDNA deletions are present in older patients. The types of deletion present in the mtDNA of affected neurons will be highly informative of what is happening in the cells and may lead to studies of cell therapy that could benefit patients in the early stages of disease.

- Ferrari, G., E. Lamantea, A. Donati, M. Filosto, E. Briem, F. Carrara, R. Parini, A. Simonati, R. Sanier and M. Zeviani (2005). "Infantile hepatocerebral syndromes associated with mutations in the mitochondrial DNA polymerase- γ A." Brain **128**(4): 723-731.
- Hance, N., M. I. Ekstrand and A. Trifunovic (2005). "Mitochondrial DNA polymerase gamma is essential for mammalian embryogenesis." Human Molecular Genetics **14**(13): 1775-1783.
- Kollberg, G., A. R. Moslemi, N. Darin, I. Nennesmo, I. Bjarnadottir, P. Uvebrant, E. Holme, A. Melberg, M. Tulinius and A. Oldfors (2006). "POLG1 mutations associated with progressive encephalopathy in childhood." Journal of Neuropathology and Experimental Neurology **65**(8): 758-768.
- Murphy, J. L., T. E. Ratnaike, E. Shang, G. Falkous, E. L. Blakely, C. L. Alston, T. Taivassalo, R. G. Haller, R. W. Taylor and D. M. Turnbull (2012). "Cytochrome c oxidase-intermediate fibres: Importance in understanding the pathogenesis and treatment of mitochondrial myopathy." Neuromuscular Disorders **22**(8): 690-698.
- Naviaux, R. K. and K. V. Nguyen (2004). "POLG Mutations Associated with Alpers' Syndrome and Mitochondrial DNA Depletion." Annals of Neurology **55**(5): 706-712.
- Naviaux, R. K., W. L. Nyhan, B. A. Barshop, J. Poulton, D. Markusic, N. C. Karpinski and R. H. Haas (1999). "Mitochondrial DNA polymerase γ deficiency and mtDNA depletion in a child with Alpers' syndrome." Annals of Neurology **45**(1): 54-58.
- Scalais, E., B. Francois, P. Schlessler, R. Stevens, C. Nuttin, J. J. Martin, R. Van Coster, S. Seneca, F. Roels, G. Van Goethem, A. Löfgren and L. De Meirleir (2012). "Polymerase gamma deficiency (POLG): Clinical course in a child with a two stage evolution from infantile myocerebrohepatopathy spectrum to an Alpers syndrome and neuropathological findings of Leigh's encephalopathy." European Journal of Paediatric Neurology **16**(5): 542-548.
- Schaller, A., D. Hahn, C. B. Jackson, I. Kern, C. Chardot, D. C. Belli, S. Gallati and J. Nuoffer (2011). "Molecular and biochemical characterisation of a novel mutation in POLG associated with Alpers syndrome." BMC Neurology **11**.
- Sofou, K., A.-R. Moslemi, G. Kollberg, I. Bjarnadóttir, A. Oldfors, I. Nennesmo, E. Holme, M. Tulinius and N. Darin (2012). "Phenotypic and genotypic

variability in Alpers syndrome." European Journal of Paediatric Neurology **16**(4): 379-389.

Taanman, J. W., S. Rahman, A. T. Pagnamenta, A. A. M. Morris, M. Bitner-Glindzicz, N. I. Wolf, J. V. Leonard, P. T. Clayton and A. H. V. Schapira (2009). "Analysis of mutant DNA polymerase γ in patients with mitochondrial DNA depletion." Human Mutation **30**(2): 248-254.

Uusimaa, J., R. Hinttala, H. Rantala, M. Päivärinta, R. Herva, M. Rötttä, H. Soini, J. S. Moilanen, A. M. Remes, I. E. Hassinen and K. Majamaa (2008). "Homozygous W748S mutation in the POLG1 gene in patients with juvenile-onset Alpers syndrome and status epilepticus." Epilepsia **49**(6): 1038-1045.

Van Goethem, G., B. Dermaut, A. Löfgren, J. J. Martin and C. Van Broeckhoven (2001). "Mutation of POLG is associated with progressive external ophthalmoplegia characterized by mtDNA deletions." Nature Genetics **28**(3): 211-212.

Chapter 6 Final Discussion

6.1 Introduction

Mitochondrial disorders represent a significant burden of disease on the population. It is estimated that at least one in every two hundred members of a healthy population may carry a pathogenic mitochondrial mutation (Elliott et al., 2008) and the risk of developing a mitochondrial DNA disease is determined to be on average 16.5 in 100,000 individuals (Schaefer et al., 2008). The first mitochondrial disease was described in 1962 describing a patient with a hypermetabolism disorder (Luft et al., 1962). Hundreds of mitochondrial disorders have since been described and our understanding of the aetiology and mechanisms leading to these disorders has grown.

Alpers' syndrome is an early-onset, autosomal recessive disorder primarily affecting the CNS and liver. The first report describing the syndrome was made in 1931 (Alpers 1931) with additional clinical signs of liver involvement described in 1976 (Huttenlocher et al., 1976). The discovery that this disorder was primarily due to mutations in *POLG* polymerase (Naviaux et al., 1999) was quickly followed by the report of damage to the mtDNA in patients (Naviaux and Nguyen 2004). Previous studies have reported neuropathological features that include neuron loss, astrogliosis, and capillary proliferation affecting the cerebellum and occipital lobe (Harding 2008; Uusimaa et al., 2008). White matter abnormalities are investigated much less frequently yet reports of myelin loss are intriguing and require much closer scrutiny in future studies (Bao et al., 2008). Respiratory chain deficiency has been described in a variety of tissue types, including skeletal muscle, liver, and fibroblasts (Wiltshire et al., 2008; Schaller et al., 2011). However, the characterisation of respiratory chain deficiency in single neurons has not been previously described in the literature. MtDNA damage has been described in patients in the form of mtDNA deletions, mtDNA depletion, or a combination of both (Ferrari et al., 2005; Kollberg et al., 2006). However, much of these data are based upon the findings in homogenate tissue samples, comprising all cell types, which is not considered to be accurate in determining mtDNA damage in neuronal cells.

The aims of this study were to characterise the neuropathological features in four brain regions, explore the nature of respiratory chain deficiencies in neurons, and determine the predominant type of mtDNA damage in the single neurons of twelve patients with Alpers' syndrome and *POLG* disorders.

6.2 Major Findings

6.2.1 Neuropathological Features

A number of histological stains and immunological antibodies were employed to investigate a variety of neuropathological features in both patients and controls. These were used to explore morphological features, neuron loss, astrogliosis, white matter abnormalities, microglial activation, and mitochondrial mass and abnormal mitochondrial localisation.

The cerebellum was the most severely affected area of the brain, with the occipital lobe exhibiting moderate pathology. The parietal lobe showed mild pathology and the basal ganglia showed almost no pathology but strikingly, this region did show severe white matter loss. The most severe neuropathological feature was dependent upon the *POLG* group investigated. The *POLG* mutation-positive group displayed a more severe astrogliosis and severe microglial activation, with low mitochondrial density, while the *POLG* mutation-absent group displayed a more severe myelin loss in all areas. The neuropathological differences between groups with or without *POLG* mutations demonstrate differences in the underlying mechanisms of disease formation due to the possible different gene mutations.

Neuron loss was seen in all patients, except stillbirth Patient 5. Neuron loss was found to be most severe in the cerebellum and in the upper cortical layers of the occipital lobe and parietal lobe. Neuron loss was correlated with astrogliosis in the occipital lobe only. Astrogliosis was severe across all groups and there were swollen astrocytes noted in some patients. A number of patients showed a reduced mitochondrial mass in neurons, most notably Patient 10, where all Purkinje cells showed low mitochondrial density. Abnormal mitochondrial localisation was also seen, which was categorised as either a perinuclear distribution, distribution around the periphery of the soma, or a weak staining of porin at the periphery of the soma. Abnormal localisation was most noticeable in the larger Purkinje cells and neurons of the globus pallidus of the basal ganglia due to their size and the volume of cell cytoplasm visible. Myelin loss in the white matter was a prominent feature and was seen in the cerebellum, occipital lobe, and the basal ganglia in 3 of the 4 patients studied. The myelin loss appeared to be primary, although in some instances in Patient 12, with no detected *POLG* mutation, there was possible secondary loss of myelin due to axonal loss. The Bielschowsky silver stain is difficult to perform and analyse and the results of this method have been taken as a guide. Microglial activation was present in most patients and the severity

correlated with the severity of astrogliosis. Extremely swollen microglia were seen in the occipital lobe of Patient 2, which corresponded with microvacuolation and severe myelin loss, possible indicators of the phagocytosis of degenerating cells and large amounts of material. Severe neuropathology can be seen in all patients, whether the *POLG* mutation is known or unknown. The posterior areas of the brain, the cerebellum and the occipital lobe, are the more severely affected areas. The parietal lobe and basal ganglia show less pathology. The neuropathology seen in this cohort suggests that the extent and pattern of pathology is variable in patients and that severe pathology of the basal ganglia is uncommon.

Studies using electron microscopy (EM) techniques investigated an Alpers' syndrome patient and controls matched for the length of formalin fixation time. The patient had sparser cytoplasm and fewer visible cellular organelles than both controls, suggesting a more rapid cellular breakdown due to pre-fixation factors. Electron-dense inclusions were seen within the mitochondria of brain tissue examined from a patient diagnosed with Alpers' syndrome and in control tissue, which was tested at the same time. Investigations of control tissue have not been previously reported in the literature, possibly due to the testing of patient tissue only.

It is important to investigate and record the neuropathology present in patients with Alpers' syndrome. It provides clear guidelines of the pathology found in the CNS of patients, allowing neuropathologists to confirm a patient diagnosis and to expand the diagnostic criteria for future use.

6.2.2 *Respiratory Chain Deficiency*

A battery of antibodies was used to all four complexes in the electron chain in order to investigate respiratory chain deficiency in single neurons of patients. A semi-quantitative assessment of Purkinje cells and pyramidal neurons of cortical layer V was performed. These are large neurons with a relatively large area of visible cytoplasm by which to visually evaluate respiratory chain dysfunction.

A predominant loss of complex I and complex III in the cerebellum, parietal lobe and basal ganglia was seen. The occipital lobe showed almost no respiratory chain loss in neurons. This was very surprising and it is possible that there has been a loss of deficient neurons, while neurons with a relatively intact respiratory chain remain. It is also possible that the respiratory chain deficiency may be present in smaller neurons of a different subtype which are too small to accurately examine in the setting of this project. The most severe respiratory chain deficiency was seen in patients of the *POLG*

mutation-undetermined group, reflecting the effect of unknown mutations that are present in this group.

Complex I and complex III showed a more severe deficiency over all brain areas. This may be due to the large size and relative instability of complex I. Complex I is reported to interact with complex III in the formation of the supercomplex (Acín-Pérez et al., 2004) and that disruption of these complexes can lead to increased ROS production (Maranzana et al., 2013). This may lead to damaged mitochondria and mtDNA, leading to further respiratory chain deficiency. In some patients, complex III deficiency was severe with a much milder complex I deficiency. In Patient 2 and Patient 10 this severe complex III deficiency with a milder complex I deficiency is clear. This suggests that a complex III deficiency may be tolerated by the surviving neurons and could serve as an indicator of respiratory chain dysfunction in surviving neurons. It is possible that the variability in antibody staining may be partly due to other factors, including antibody staining technique and the analysis of different brain regions.

Complex II showed a moderate deficiency in the Purkinje cells of Patient 10. This was the only patient to exhibit a complex II deficiency. In Patient 10, this deficiency is linked to low mitochondrial density which is present in all Purkinje cells. In a number of patients, complex IV-I (COX I) showed a slight deficiency, and always a greater deficiency than complex IV-IV (COX IV). This may be due to mtDNA damage that has decreased COX I availability, a mitochondrially-encoded subunit. This damage would not have directly affected COX IV, a nuclear-encoded subunit. However, the mitochondrially-encoded COX I subunit showed a milder deficiency than with nuclear-encoded complex I and complex III subunits. This was unexpected and it may be that other mitochondrially-encoded subunits of complex I and complex III that had not been examined had been lost and that this destabilised the entire complex.

Respiratory chain deficiency represents an important pathological phenotype of mitochondrial disease. Multiple deficiencies of complex I, III, and IV have been found in neurons of this cohort of patients, with a wide variability in antibody staining exhibited across all patients. This variability and deficiency over different brain areas suggests the possibility of an epigenetic effect upon the mitochondria in these neurons.

6.2.4 MtDNA Deletion and Depletion

Both SDH staining and real-time PCR was used to assess mtDNA damage in single neurons obtained through laser-capture microdissection. From the current literature, it is unclear whether mtDNA damage is predominantly mtDNA deletion, mtDNA depletion, or a combination of both mtDNA deletion and depletion. Homogenate tissue samples are often used to assess this damage.

In the neurons of both young and adult patients, mtDNA depletion is more severe than mtDNA deletion. This occurs in patients irrespective of the *POLG* mutation status. MtDNA deletions were seen at low levels; however these were unlikely to be accurately detected by the method of real-time PCR. In a subset of neurons in the adult patients, mtDNA deletion levels were detected at high levels of above 70% mtDNA deletion. This may indicate a dynamic level of mtDNA loss and a move towards increased numbers of neurons with increasing levels of mtDNA deletions.

MtDNA deletions were assessed in COX-positive and COX-deficient neurons from a single adult patient. The COX-deficient neurons were found to harbour greater levels of mtDNA deletions than COX-positive neurons. Neurons that displayed both COX-deficiency and showed levels of mtDNA deletion within the experimental error of this assay (<30%), may have a true deletion level that is higher. This is because low levels of mtDNA deletions cannot be accurately detected by the real-time PCR method.

MtDNA damage is linked to respiratory chain deficiency, which has been shown by this study to predominantly consist of mtDNA depletion, demonstrating the first report of mtDNA abnormalities in single neurons of patients with Alpers' syndrome.

6.3 Strengths and Limitations

This study was carried out with ethical approval from the Newcastle and North Tyneside Local Research Ethics Committees, ethical approval number 2002/205. CNS tissue donated to the NBTR, University of Vienna, and University of Bonn was used. A major strength of this study lies in the large cohort used for the investigations, inclusive of a wide age range of patients which reflects the increasing number of reports in the literature that describe clinically diagnosed cases of Alpers' syndrome in older teenage patients. Patients both with *POLG* mutations and without *POLG* mutations have been included to reflect the growing number of cases of Alpers' syndrome that are clinically diagnosed and yet do not harbour a mutation in *POLG*. Genes currently reported to lead to an Alpers' syndrome-like phenotype include the *FARS2* gene (Elo et al., 2012)

and *C10orf2* gene that codes for the helicase Twinkle (Hunter et al., 2011). There may be other genes that lead to an Alpers' syndrome-like phenotype to be reported in the future and next-generation sequencing techniques may be beneficial in these cases, to determine the underlying molecular basis of the disorder.

This study describes the investigation of respiratory chain deficiency in single neurons. This is the first time that this has been investigated in single neurons from the brains of patients with Alpers' syndrome and allows for examination of respiratory chain deficiencies in the neurons only, as opposed to a mixture of cell types, possibly each with a different level of deficiency. This method allows for the assessment of the surviving neuronal population exclusively.

A limitation of this study is the rarity of the disease and the sensitive nature of the tissue required, which resulted in considerable difficulty in acquiring suitable tissue from young patients and control subjects in all brain areas being investigated. Tissue was acquired from a number of facilities and applications were made to many more facilities. The suitability of the tissue for each particular branch of investigations was an important factor to consider. The tissue that was used for genetic investigations was found to be not suitable due to the length of fixation in formalin and embedding in paraffin wax. Frozen tissue or a previously extracted DNA sample would have been more suitable if available. The tissue for EM studies was of limited suitability due to a long fixation time in formalin. Tissue from patients with a short formalin fixation time or free from fixation in formalin would have been more suitable if available. There were limitations of some of the technique used. Semi-quantitative assessments were performed as more fully quantitative methods were not optimised for the retrieval of data, as with assessment of the white matter. The employment of quantitative densitometric methods would be useful to future studies of myelin loss and respiratory chain deficiency.

6.5 Future Work

This research has examined the neuropathological features in a large cohort of patients with a range of ages and underlying genetic mutations. In some cases the genetic mutation could not be fully assessed, and this highlights the importance of the facilities that look after and provide these resources to researchers.

Efforts to explore the underlying genetic mutations in all patients diagnosed with Alpers' syndrome will allow for a better understanding of the spectrum of *POLG* disease. Patients with clinical signs of Alpers' syndrome and no mutation in *POLG* expand the genetic classification of Alpers' syndrome and stress the importance of a genetic diagnosis. The use of next-generation sequencing techniques and whole exome sequencing may be advantageous in determining the genetic mutations in these patients. The finding and categorisation of novel mutations in *POLG* can further aid our understanding of the effect of mutations upon the function of the *POLG* polymerase.

Abnormalities of the white matter are infrequently reported in cases of Alpers' syndrome. This study has reported considerable myelin loss in patients, including severe loss in the basal ganglia, an area not often associated with evidence of neuropathology. This highlights the importance of examining myelin loss, and other white matter abnormalities, in brain areas that may show no other neuropathological features, such as the basal ganglia. In addition, the use of fully quantitative techniques, including densitometric measurements, may remove the investigator bias and allow for a more rigorous comparison between patients and controls and between different patients.

A predominant complex I and complex III deficiency of the respiratory chain was observed in neurons. The use of cell studies, such as induced pluripotent stem cells (iPSCs), may prove beneficial in future investigations to explore any further mechanisms behind respiratory chain deficiency, for example whether impaired complex assembly is involved. The respiratory chain deficiency seen in glial cells warrants further investigation and poses many interesting questions regarding the cell type or cell types with a respiratory chain deficiency and the role played by these cells in the disease progression of Alpers' syndrome. iPSC culture systems may be applied to both these avenues of further research, having the potential to further explore the mechanisms involved in respiratory chain deficiency and possible abnormalities of the supercomplex, and allowing these to be studied in different cell types.

MtDNA depletion was the more severe consequence of mtDNA damage seen in all patients studied. MtDNA deletions were present at high levels in a small subset of neurons tested. The types of mtDNA deletions present in neurons, whether mostly large-scale deletions or smaller rearrangements, will be of interest and may shed light on the function and survival of neurons susceptible to the effect of *POLG* mutations.

6.6 Conclusions

The investigation of patients, from the neuropathology occurring in the brain and the presence of respiratory chain dysfunction, to the integrity of mtDNA in a single neuron has revealed a variable complex I and complex III deficiency in neurons and glial cells. Predominant mtDNA depletion in single neurons with mtDNA deletions occurring in a smaller subset of neurons leads us closer to understanding the mechanism of *POLG*-induced mtDNA damage, though further investigations are needed to understand the mechanism of respiratory chain deficiency and its tissue-specific manifestation. The progress towards understanding the mechanism of *POLG* mutations in the aetiology of Alpers' syndrome is leading us forward, to possible new therapies where there is hope for many children and their families.

- Acín-Pérez, R., M. P. Bayona-Bafaluy, P. Fernández-Silva, R. Moreno-Loshuertos, A. Pérez-Martos, C. Bruno, C. T. Moraes and J. A. Enríquez (2004). "Respiratory complex III is required to maintain complex I in mammalian mitochondria." Molecular Cell **13**(6): 805-815.
- Alpers, B. J. (1931). "Diffuse progressive degeneration of the gray matter of the cerebrum." Arch Neurol Psychiatry **25**: 469-505.
- Bao, X., Y. Wu, L. J. C. Wong, Y. Zhang, H. Xiong, P. C. Chou, C. K. Truong, Y. Jiang, J. Qin, Y. Yuan, Q. Lin and X. Wu (2008). "Alpers syndrome with prominent white matter changes." Brain and Development **30**(4): 295-300.
- Elliott, H. R., D. C. Samuels, J. A. Eden, C. L. Relton and P. F. Chinnery (2008). "Pathogenic Mitochondrial DNA Mutations Are Common in the General Population." American Journal of Human Genetics **83**(2): 254-260.
- Elo, J. M., S. S. Yadavalli, L. Euro, P. Isohanni, A. Götz, C. J. Carroll, L. Valanne, F. S. Alkuraya, J. Uusimaa, A. Paetau, E. M. Caruso, H. Pihko, M. Ibba, H. Tynismaa and A. Suomalainen (2012). "Mitochondrial phenylalanyl-trna synthetase mutations underlie fatal infantile alpers encephalopathy." Human Molecular Genetics **21**(20): 4521-4529.
- Ferrari, G., E. Lamantea, A. Donati, M. Filosto, E. Briem, F. Carrara, R. Parini, A. Simonati, R. Sanier and M. Zeviani (2005). "Infantile hepatocerebral syndromes associated with mutations in the mitochondrial DNA polymerase- γ A." Brain **128**(4): 723-731.
- Harding, B. N., Surtees, R.A.H (2008). Metabolic and neurodegenerative disease of childhood. Greenfield's neuropathology volume 1 Eighth Edition. S. Love, Louis, D.N., Ellison, D.W. London, UK, Hodder Arnold. **1**: 481 – 514.
- Hunter, M. F., H. Peters, R. Salemi, D. Thorburn and M. T. MacKay (2011). "Alpers syndrome with mutations in POLG: Clinical and investigative features." Pediatric Neurology **45**(5): 311-318.
- Huttenlocher, P. R., G. B. Solitare and G. Adams (1976). "Infantile diffuse cerebral degeneration with hepatic cirrhosis." Archives of Neurology **33**(3): 186-192.
- Kollberg, G., A. R. Moslemi, N. Darin, I. Nennesmo, I. Bjarnadottir, P. Uvebrant, E. Holme, A. Melberg, M. Tulinius and A. Oldfors (2006). "POLG1 mutations associated with progressive encephalopathy in childhood." Journal of Neuropathology and Experimental Neurology **65**(8): 758-768.
- Luft, R., D. Ikkos, G. Palmieri, L. Ernster and B. Afzelius (1962). "A case of severe hypermetabolism of nonthyroid origin with a defect in." The Journal of clinical investigation **41**: 1776-1804.

- Maranzana, E., G. Barbero, A. I. Falasca, G. Lenaz and M. L. Genova (2013). "Mitochondrial respiratory supercomplex association limits production of reactive oxygen species from Complex I." Antioxidants and Redox Signaling.
- Naviaux, R. K. and K. V. Nguyen (2004). "POLG Mutations Associated with Alpers' Syndrome and Mitochondrial DNA Depletion." Annals of Neurology **55**(5): 706-712.
- Naviaux, R. K., W. L. Nyhan, B. A. Barshop, J. Poulton, D. Markusic, N. C. Karpinski and R. H. Haas (1999). "Mitochondrial DNA polymerase γ deficiency and mtDNA depletion in a child with Alpers' syndrome." Annals of Neurology **45**(1): 54-58.
- Schaefer, A. M., R. McFarland, E. L. Blakely, L. He, R. G. Whittaker, R. W. Taylor, P. F. Chinnery and D. M. Turnbull (2008). "Prevalence of mitochondrial DNA disease in adults." Annals of Neurology **63**(1): 35-39.
- Schaller, A., D. Hahn, C. B. Jackson, I. Kern, C. Chardot, D. C. Belli, S. Gallati and J. Nuoffer (2011). "Molecular and biochemical characterisation of a novel mutation in POLG associated with Alpers syndrome." BMC Neurology **11**.
- Uusimaa, J., R. Hinttala, H. Rantala, M. Päivärinta, R. Herva, M. Røyttä, H. Soini, J. S. Moilanen, A. M. Remes, I. E. Hassinen and K. Majamaa (2008). "Homozygous W748S mutation in the POLG1 gene in patients with juvenile-onset Alpers syndrome and status epilepticus." Epilepsia **49**(6): 1038-1045.
- Wiltshire, E., G. Davidzon, S. Dimauro, H. O. Akman, L. Sadleir, L. Haas, J. Zuccollo, A. McEwen and D. R. Thorburn (2008). "Juvenile Alpers disease." Archives of Neurology **65**(1): 121-124.